ABSTRACT

Title: SUBSURFACE HETEROGENEITIES, INTERFACES AND BIODEGRADATION: DEFINING THE LIMITS ON IN SITU BIOREMEDIATION

Xin Song, Ph.D., 2005

Directed By: Associate Professor, Eric A. Seagren, Civil and Environmental Engineering

Subsurface heterogeneities and the associated interfacial processes impact *in situ* bioremediation by affecting the availability of substrates to the microorganisms. This research hypothesized that using the scales of subsurface heterogeneities as an organizational principle, a quantitative framework based on a set of dimensionless numbers could be developed to capture the effects of the competing interfacial and biokinetic processes and define the limits for successful application of *in situ* bioremediation. The overall goal of this study was to use an integrated experimental and numerical modeling approach to evaluate the developed quantitative framework under different simulated scenarios relevant to the subsurface.

Three experimental scenarios were selected to simulate field sites limited by either (1) macro-scale vertical transverse dispersion (Scenario #1), (2) micro-scale biokinetics (Scenario #2), or (3) meso-scale sorption/desorption (Scenario #3). Experiments were performed in a saturated, heterogeneous intermediate-scale flow cell (ISFC) with two layers of contrasting hydraulic conductivities and monitored the

transport of a naphthalene plume through two phases: Phase I, simulating an intrinsic biodegradation; and Phase II, simulating an engineered bioremediation, with selected system perturbations. In the first Phase II perturbation, nitrogen (N) and phosphorus (P) amendments in excess of stoichiometric requirements were made, while the second perturbation was selected based on the rate-limiting process identified via the quantitative framework. A numerical model was used to simulate the Phase I experiments and verify the independently determined mass transport and biokinetic parameters, which were then used in the dimensionless parameters of the proposed quantitative framework.

Scenario #3 was not completed due to the time constraints, but Scenarios #1 and #2 successfully demonstrated application of the quantitative framework. In Scenario #1, Phase I, vertical dispersion was identified as the overall rate-limiting process. Correspondingly, increased advection and mechanical dispersion in Phase II increased naphthalene biodegradation by ~ 2.7 times, whereas the N and P addition had no effect. In Scenario #2, Phase I, dispersion and biokinetics were identified as rate-limiting processes. Thus, in Phase II, N and P addition moderately improved biodegradation, but removal of inhibitory, high salinity conditions to improve the biokinetics increased naphthalene mass loss ~2.7 times. These results demonstrate the potential for application of the proposed quantitative framework to predict the rate-limiting process for *in situ* bioremediation and aide in the appropriate selection of any system perturbations for enhancing *in situ* bioremediation.

SUBSURFACE HETEROGENEITIES, INTERFACES AND BIODEGRADATION: DEFINING THE LIMITS ON *IN SITU* BIOREMEDIATION

By

Xin Song

Dissertation submitted to the Faculty of the Graduate School of the
University of Maryland, College Park, in partial fulfillment
of the requirements for the degree of
Doctor of Philosophy
2005

Advisory Committee:
Associate Professor Eric A. Seagren, Chair
Professor Allen P. Davis
Professor Alba Torrents
Associate Professor Karen L. Prestegaard
Assistant Professor Jennifer G. Becker

Dedication

For my parents Aifang Dai and Shurong Song, especially for my mother, who has always believed in me and who is always there for me.

Acknowledgements

It is my pleasure to take this opportunity to thank a group of people who contribute to the completion of this dissertation.

First of all, I would like to dedicate my tremendous thanks to Dr. Seagren for his guidance, encourage and patience. Without him, I would not have accomplished this work. Not only has he been invaluable in the development of my Ph.D. thesis, but it has always been a great pleasure working with him.

My appreciation goes to my other committee members as well. To Drs. Davis, Hao, Torrents, Prestegaard and Becker for spending time in reviewing this work and assisting me to complete the degree.

I would like to acknowledge my fellow graduate students Eunyoung Hong and Mark Johnson for their assistance and cooperation on this project. And Thank Jim Stagge and other undergraduates for their contribution in the lab. I would like to thank Tong Li for his advice on the FORTRAN program.

My special thanks go to Joe Penzien, who has always been very supportive in my academic development.

I owe a great deal to my best friend Naji and his family. They have always been with me in the past 5 years and support me in pursuing my Ph.D. degree. My special thanks to Naji for helping me when I needed to take samples at midnight.

Lastly, I would like to thank my mother, for her love, support and encouragement. Without her, I would not have made it this far.

Table of Contents

List of Tables

List of Figures

Chapter 1 Introduction

Organic contaminants in soils and sediments originate from a variety of anthropogenic activities. Many organic contaminants, such as benzene, toluene, ethylbenzene and xylenes (BTEX), polycyclic-aromatic hydrocarbons (PAHs), poly-chlorinated biphenyls (PCBs), methyl-tertiary butyl ether (MTBE) and tertiary-butyl alcohol (TBA), chlorinated solvents, and pesticides and herbicides have documented or suspected mutagenic and carcinogenic effects. Therefore, the fate of these compounds at contaminated sites and restoration of these sites are of high concern with respect to environmental and public health.

Bioremediation offers great potential for cleaning up environmental contaminants because: it can treat them *in situ* with little disturbance to the contaminated matrix; the contaminants can often be completely mineralized to inorganic materials (Head 1998); and bioremediation is relatively inexpensive compared to other remedial technologies such as incineration, soil washing, and pump and treat (Hughes et al. 1997; Singleton 1994). However, the wide application of this technology has been hindered because of the uncertainty of success. The success of *in situ* bioremediation is made technologically challenging by the inherently complex and heterogeneous nature of the subsurface environment (National Research Council 1993). These physical and chemical heterogeneities of the subsurface occur at several scales and affect *in situ* bioremediation by controlling the availability of nutrients and substrates that drive the microbiological processes. This is important because many field and laboratory studies suggest that a large fraction of pollutants present in the environmental systems are unavailable for

microbial degradation (Alexander 1995; Beck et al. 1995). Therefore, not understanding or accounting for the interactions between these scale-dependent physical/chemical heterogeneities and microbiological processes may reduce the effectiveness of field-scale *in situ* bioremediation. However, the interactions between these processes and *in situ* biodegradation, albeit important, are still not well understood. Indeed, reviews of field methods available for bioremediation have concluded that consideration of scale-dependent phenomena, such as mass transport and interfacial transfer mechanisms, is a prerequisite to success in the field (Sturman et al. 1995).

In order to describe subsurface heterogeneities and associated physical, chemical and microbiological processes, it is helpful to apply three scales of observation: macro-, meso- and micro-scale (Sturman et al. 1995). Advection, dispersion and geologic spatial heterogeneity are examples of macro-scale phenomena (Sturman et al. 1995). The corresponding physical scale for these phenomena ranges from $\sim 10^{-2}$ to $\sim 10^{2}$ m or even larger. The meso-scale is defined as the scale at which transport phenomena are apparent, with the exclusion of advection and mixing processes. Thus, the meso-scale phenomena include diffusion, sorption and interphase-mass transfer. Possible physical scales for meso-scale phenomena include the size of pore channels or soil particles, the characteristic diffusion length, or the dimension of microbial aggregates (10^{-5} to 10^{-2} m). The micro-scale is taken as the scale at which chemical and microbiological species exist and can be characterized independently of any transport phenomena. Examples of micro-scale features are the composition of microbial consortia and the kinetics and stoichiometry of transformation reactions. The physical scale of these phenomena is the dimension of the microbial cell, on the order of $\sim 10^{-6}$ to $\sim 10^{-5}$ m.

These scale-dependent physical and chemical heterogeneities and associated processes in the subsurface create, either directly or indirectly, interfaces between two phases, where strong contrasts in physical and chemical properties exist over short distances (centimeter to meters). The physical/chemical interface zones comprise a wide variety of types including: aqueous-solid interfaces; aqueous-nonaqueous phase liquid (NAPL) interfaces; and aqueous-aqueous interfaces. Specifically, such strong contrasts in physical and chemical properties at these interfaces control moisture nutrient fluxes and redox conditions, which, in turn, drive the distribution and activities of microbes in the subsurface, e.g., (McMahon and Chapelle 1991). For example, many organic contaminants of concern (e.g., PAHs and PCBs) are hydrophobic, resulting in low aqueous solubility and a strong tendency to sorb to the matrix of organic material in soil or to partition into oily phases at contaminated sites (Harayama 1997). Due to these chemical characteristics, the bioavailability of sorbed contaminants in natural sorbents has been an important issue in applying bioremediation technologies to remediation of contaminated sites (Willumsem and Arvin 1999).

Importantly, several of these scale-dependent, interfacial processes are occurring and impacting biodegradation simultaneously at any site. Hence, Rittmann et al. (1992) concluded that the major research needs required to facilitate bioremediation success in the field are the means to quantify mass-transfer kinetics and microbial kinetics - all of which are scale-dependent. Therefore, an integrated kinetic study of several such interfacial physicochemical mass-transfer and biokinetic processes occurring simultaneously at different scales is of significant importance in understanding the bioavailability of pollutants, which in turn impacts the effectiveness of bioremediation.

Chapter 2 Objective and Scope of Work

Despite the importance of heterogeneities in bioremediation, the impact of geochemical and hydraulic interfaces on *in situ* biodegradation is still not well understood. Because the subsurface physical, chemical, and microbiological processes and their interactions are extremely complex, it is useful to apply the scales of heterogeneity as an organizational tool and use relevant dimensionless parameters to succinctly capture the complexity of the interactions between these processes. Therefore, it is hypothesized that using the scales of subsurface heterogeneities and associated interfacial processes as the organizational principle, a quantitative framework based on a set of dimensionless numbers can be developed to capture the effects of the competing interfacial and biokinetic processes and to define the limits for the successful application of *in situ* bioremediation.

The overall goal of this research, and the larger project of which it was a part, was to develop such a quantitative framework and to evaluate its utility under different scenarios relevant to the subsurface. To accomplish this, a systematic and integrated modeling and laboratory investigation was used to evaluate the impact of a wide range of scales and magnitudes of heterogeneities on *in situ* bioremediation and the utility of the developed quantitative framework for predicting what is the overall limiting process and what engineering actions will positively impact the *in situ* biodegradation rates. This investigation had three specific major objectives.

The first objective was to develop and refine the proposed integrated quantitative framework of dimensionless numbers. A systematic comparison of the dimensionless numbers was used to integrate and compare all the phenomena

occurring at different scales of heterogeneities and to predict the overall rate-limiting process for a given environmental system. In the framework as used in this work, there are three steps. The first two steps are used to identify the slowest mass-transfer process, and the third step compares that process rate with the biokinetics to determine the overall rate-limiting process. A mathematical model, Reactive Multi-species Transport in 3-Dimensional (RT3D) Groundwater Aquifers, which mathematically describes the relationships between the processes of interest in natural subsurface systems, was used to provide a preliminary evaluation of the proposed framework.

The second objective was to design and build an intermediate-scale flow cell (ISFC) system that represented a realistic, yet experimentally tractable natural subsurface system for evaluating the physical, chemical, and microbiological processes occurring at heterogeneous interfaces, especially for aqueous-aqueous and aqueous-solid interfaces. As part of this objective, batch experiments were also conducted to measure the kinetic parameters describing groundwater flow and contaminant fate and transport in the simulated subsurface system in order to apply the quantitative framework and model the system using RT3D.

The final objective was to utilize three specially selected scenarios to evaluate the quantitative framework with both modeling and experimental investigations. The scenarios tested include cases in which either macro-scale mixing (Scenario #1), biokinetics (Scenario #2) or sorption/desorption (Scenario #3) was the rate-limiting process controlling the overall contaminant biodegradation rate and preventing formation of a biologically active zone (BAZ). These investigations were broken

down into two phases. Phase I represented biodegradation under natural conditions, as simulated in the ISFC. The results from these experiments were used to evaluate if the factors limiting the biodegradation rate under natural conditions were what was expected based on the quantitative framework. Phase II represented perturbations to the system as part of a simulated engineered *in situ* bioremediation. Engineered remedial actions involve efforts to overcome the mass-transfer and microbial limitations and create a BAZ where it is needed. Importantly, only an appropriate remedial strategy that alleviates the overall rate-limiting phenomenon will enhance the *in situ* biodegradation rate. Therefore, the results of the Phase II experiments were used to test the quantitative framework utility for predicting what, if any, engineered actions would augment the intrinsic *in situ* biodegradation.

In the next chapter (Chapter 3), background literature is reviewed with respect to the key processes relevant to this project that occur at the macro-scale (e.g., advection and dispersion), meso-scale (e.g., sorption/desorption), and micro-scale (e.g., microbial activities). Subsequent chapters review the theoretical concepts underlying this research (Chapter 4), as well as the experimental materials and methods (Chapter 5), and the results and discussion (Chapter 6). Finally, the conclusions are outlined in the last chapter (Chapter 7), along with recommendations for future work.

Chapter 3 Literature Review

As introduced in Chapter 1, the subsurface is a geologically, chemically, and microbiologically heterogeneous environment. Furthermore, the scale-dependent physical and chemical heterogeneities create various types of interfacial zones, such as aqueous-solid interfaces, aqueous-NAPL interfaces, and aqueous-aqueous interfaces. These interfaces have physical and chemical properties that are different from any one of the individual phases involved and, as a result, their presence can support a greater density, activity and/or diversity of microorganisms, which is of great concern for bioremediation.

This situation occurs because the subsurface has geological units with different chemical compositions that exist at different scales, such as strata, beds, laminae, and pores. For example, at a pore scale, different phases and different types of sedimentary organic matter may exist, creating different aqueous-solid interfaces and influencing rates of substrate flux via sorption and desorption, the rate of which can affect the microbial ecology and biodegradation rate. Therefore, accurate prediction of the transport and fate of organic solutes in groundwater requires an understanding of the controlling hydrogeologic chemical and microbiological processes and their interactions.

Thus, the subsurface should always be investigated at different scales, the scale of interest being a function of the scientific question or applied problem. For example, the most appropriate scales for studying bioremediation design and engineering include the macro-, meso- and micro-scales as discussed above and defined further below. Although these scale definitions are arbitrary, they serve as a

useful conceptual structure for approaching the engineering problem. The goal of this chapter is to review the current state of knowledge of these heterogeneities and associated interfaces and their impact on microbiological processes. For convenience, the discussion is broken down into three scales: macro-, meso-, and micro-scale.

3.1 Macro -scale heterogeneities

Macro-scale heterogeneity refers to heterogeneity at the scale of laminae, thin lenses or beds, or inclusions (scales of millimeters to 10s of centimeters thick) (Brockman and Murray 1997). At the macro-scale, mass transport via advection and dispersion can significantly impact contaminant distribution and the availability of substrates, nutrients, and electron acceptors to microorganisms (Sturman et al. 1995), which may, in turn, drive the distribution and activity of the microbes in the subsurface (Brockman and Murray 1997).

Advection refers to the movement of dissolved contaminants due to the bulk flow of groundwater, which is important in bioremediation in terms of the transport of dissolved microbial substrates. According to Darcy's law, the one dimensional volumetric flow rate, Q [L^3 T^{-1}], through a cross sectional area, A [L^2], of a porous medium can be described as (Fetter 2001),

$$\frac{Q}{A} = -K\frac{dh}{dx} \tag{3.1}$$

where: K = hydraulic conductivity, [LT^{-1}]; and dh/dx = hydraulic gradient in the direction of groundwater flow. The magnitude of K varies widely, and for a given geologic formation, is a function of a variety of physical factors, e.g., porosity, particle size and distribution, particle shape, particle arrangement, and secondary

features such as fracturing and dissolution. Using Equation 3.1, and accounting for the fact that flow only passes through the pore openings of the full cross-sectional area, the average pore-water velocity, v , can be calculated for one-dimension as,

$$v = \frac{Q}{\phi A} = -\frac{K}{\phi}\frac{dh}{dx} \tag{3.2}$$

where: ϕA = the effective area of flow, [L^2]; and ϕ = effective porosity, i.e., the percentage of interconnected pore space.

Another key subsurface process at the macro-scale that has an important role in the transport/mixing and biodegradation of contaminants is hydrodynamic dispersion. It refers to the combined effect of mechanical dispersion and molecular diffusion (Fetter, 2001). Importantly, diffusion and heterogeneity induced mechanical dispersion are the only mixing processes for solute in the deep subsurface. The mathematical description of hydrodynamic dispersion for a two-dimensional domain is,

$$\frac{\partial C}{\partial t} = D_X \frac{\partial^2 C}{\partial x^2} + D_Z \frac{\partial^2 C}{\partial z^2} \tag{3.3}$$

where: $D_X = \alpha_X v + D^*$ = longitudinal hydrodynamic dispersion coefficient, [L^2T^{-1}]; α_X = longitudinal dispersivity, [L]; $D_Z = \alpha_Z v_x + D^*$ = vertical transverse hydrodynamic dispersion coefficient, [L^2T^{-1}]; α_Z = vertical transverse dispersivity, [L]; v_x = average pore water velocity in x-direction [LT^{-1}]; and D* = effective diffusion coefficient [L^2T^{-1}]. In the following discussion, the term "dispersion" is meant the hydrodynamic dispersion.

In particular, vertical dispersion is an important process for developing zones of mixing in the subsurface (Sudicky et al. 1985). However, vertical transverse dispersion has generally been found to be a weak process in groundwater systems (Gelhar et al. 1992). Therefore, both mechanical dispersion and molecular diffusion can have a significant effect on the vertical transverse dispersion for a wide range of relevant pore water velocities because of low values of vertical transverse dispersivities. Two examples of situations in which vertical transverse dispersion is critical are: oxygen transfer across the water table, and heterogeneities in hydraulic conductivity. Theoretical and field studies, e.g., (Borden and Bedient 1986; Borden et al. 1986; Thornton et al. 2001) indicate that the vertical transverse dispersion coefficient can have a significant impact on oxygen exchange between the unsaturated and saturated zones and, thus, affect the aerobic microbial activities. Because of the weakness of the vertical dispersion process and the magnitude of the microbial oxygen demand in contaminant plumes, steep vertical oxygen gradients result, and the impact of transverse dispersion on oxygen supply is limited to relatively shallow plumes (e.g., less than about 2 to 3 m below the water table) (MacQuarrie and Sudicky 1990).

Hydraulic layer interfaces in groundwater systems resulting from heterogeneities in hydraulic conductivity, K, may be particularly important to microorganisms because interlayer mass transfer of solutes can increase the supply of limiting nutrients near the interface. For example, one key macro-scale interfacial process that can significantly impact *in situ* bioremediation is the hydraulic mixing at the interface between the contaminant plume and the "clean" groundwater, which is

induced by hydraulic conductivity heterogeneity. Indeed, Carrera (1993) comments that, "…most of the difference between the actual behavior of solutes and that predicted by the advection-dispersion equation can be attributed to the spatial variability of hydraulic conductivity".

Laboratory and modeling studies indicate that varying layers of hydraulic conductivity are an important factor affecting *in situ* biodegradation, with contaminants predominantly persisting in low hydraulic conductivity layers, e.g., (Murphy et al. 1997; Szecsody et al. 1994; Wood et al. 1994; Yang et al. 1994). For example, Szecsody et al. (1994) performed a laboratory study of the transport and biodegradation of quinoline in a two-dimensional, horizontally-stratified porous media under dual substrate limitation. Szecsody et al. (1994) found that the interlayer mass transfer resulted in arrival of substrate and oxygen 10's to 100's of hours sooner in the low-K layer near the interface compared to other locations within the low-K layer, where substrates arrived via only advection. Early arrival of substrates near the interface resulted in biodegradation of quinoline for a longer period than within layers, yielding increased growth in a 1-3 cm thick zone. Although these studies illustrate the importance of understanding processes near interfaces in subsurface systems, the data are only suggestive, as the studies were not designed to identify and quantify these mechanisms.

In addition to systems with varying layers of hydraulic conductivity, hydraulic conductivity heterogeneity can also occur at a smaller scale ($> 10^{-3}$ to < 1m) than that typically associated with measurement of "field-scale" heterogeneity. The existence of regions of small hydraulic conductivity within the flow domain creates a spatially

variable velocity field at these smaller scales. In some cases, there is a relatively minimal flow and advection in the low-conductivity domains. Due to the small advective flux, these domains act as sink/source components, with rate-limited diffusional mass transfer between the advective and nonadvective domains causing spreading of the solute front. These sink/source regions can take various forms, including the internal porosity of aggregates or porous particles, dead-end pores, the bulk matrix of fractured media, and the small conductivity micro-layers or laminae typically found in aquifers of sedimentary origin. For example, some researchers have shown that these structures can cause asymmetrical and tailed breakthrough curves and enhanced dispersion (Brusseau 1994; Brusseau and Rao 1991).

Importantly for this study, modeling and experimental studies (Murphy et al. 1997) have demonstrated that small-scale K heterogeneity combined with dual substrate limitation can result in the creation of regions of increased electron donor and electron acceptor mixing and enhanced microbial activity and growth. However, Schafer and Kinzelbach (1992), using stochastic modeling of *in situ* bioremediation, demonstrated that small scale K heterogeneity with dual substrate limitation can also decrease contaminant biodegradation, e.g., by preventing electron donor and acceptor mixing. Therefore, hydraulic conductivity heterogeneities can have significant impacts on microbial activity and biomass production, sometimes positive and sometimes negative.

3.2 Meso/pore-scale heterogeneity

Bioavailability of organic contaminants has long been identified as a major limitation to complete bioremediation of contaminated subsurface environments,

affecting clean-up time, cost, and the end-point of the process (Head 1998). In particular, the low mass-transfer rate caused by strong sorptive interactions with subsurface organic matter and intraparticle diffusion limitations is one of the main factors responsible for the low bioavailability of PAHs in subsurface systems (Brusseau et al. 1991; Guerin and Boyd 1992; Volkering 1996). In attempting to understand how sorption/desorption and biodegradation processes interactively control bioavailability, it must be considered that biodegradation of sorbed materials involves at least two rate processes: sorption/desorption and biodegradation.

Due to the field-scale spatial variability in hydraulic conductivity, it is logical to expect meso-scale reaction-related properties in the subsurface to be spatially variable as well. For example, it has been shown that spatially variable sorption can cause non-ideal transport (Brusseau 1991; Brusseau and Zachara 1993). Such physical and chemical heterogeneity at the meso/pore-scale may result in microbiological heterogeneity in terms of different microbial physiological types, or the presence or absence of microbes. The research into the bioavailability of organic pollutants as microbial substrates has largely focused on pore-scale chemical heterogeneity resulting from interfacial phenomena such as sorption to, and desorption from, sediment particles, and that is the focus here.

Contaminant sorption can have a variety of different types of effects on microbial activity. Of primary interest in this study is the impact of sorption on contaminant biodegradation. For example, if the sorption sink is significant, it can reduce the aqueous phase solute concentration. If only the substrate in solution is available for biodegradation, sorption will thus reduce the rate and extent of

biodegradation, as has been demonstrated in some studies, e.g., (Mihelcic and Luthy 1991; Miller and Alexander 1991; Rijnaarts et al. 1990). However, there has been some debate regarding the possible occurrence of direct bioavailability, whereby organisms can directly utilize the sorbed chemicals, as opposed to indirect bioavailability, in which the sorbed chemicals can only be utilized by mcrobes after desorption into the aqueous phase.

Most research addressing the issue of sorbed solute bioavailability has concluded that sorbed PAHs are not directly available for biodegradation (Smith et al. 1992). Organic polymers within the soil attract organic contaminants like PAHs via their non-polar gel structure. Once within the polymer matrix, the contaminants may bond (via covalent or hydrogen bonding) to specific sites, or may diffuse through micro-pores in the gel. It has been suggested that if such tightly bound contaminants desorb at all, it is at a rate that certainly limits biodegradation. For example, Angley et al. (1992) concluded that biodegradation of alkylbenzenes occurs only in solution and that desorption was generally diffusion-rate limited. Ogram et al. (1985) proposed three models to describe (2,4-dichlorophenoxy) acetic acid biodegradation in soil. The model that most successfully described their experimental data assumed that both attached and planktonic bacteria were capable of utilizing dissolved contaminant, but neither was able to directly degrade sorbed contaminant. The authors concluded that this was either because the contaminant may have been adsorbed sufficiently deep within the soil-organic matter matrix that bacteria were unable to reach it, or because enzymes responsible for degradation may have been incapable of attacking sorbed contaminants. In another attempt to address the question of whether desorption limits

biodegradation, Rijnaarts et al. (1990), investigated hexachlorocyclohexane biodegradation in a mixed soil system that was desorption limited. In this case, contaminant diffusion through the soil micropores was found to limit the biodegradation rate. To further investigate the effects of desorption rate on biodegradation, Fry and Istok (1994) utilized an analytical solution to the solute transport equation with rate-limited desorption and first-order decay. Their results showed that when the desorption coefficient is small relative to the degradation coefficient (desorption is the rate-limiting process), increasing the biodegradation rate any further will not improve the performance of *in situ* bioremediation. Similarly, Bouwer et al. (1994) found that naphthalene biodegradation proceeded more slowly in high organic carbon system, suggesting desorption rate limitation.

However, some researchers have concluded that enhanced biodegradation can occur, that is, the microbial utilization of a compound can occur at a rate faster than its abiotic desorption into the bulk-water phase. This requires a mechanism that facilitates degradation of sorbed chemicals. Although the mechanisms of microbial uptake that lead to such results are not precisely known, several possibilities have been proposed. One possible mechanism involves the *in situ* production of biosurfactants, which may enhance desorption of hydrocarbons from soil, e.g., (Scheibenbogen et al. 1994). A second possible mechanism is the direct utilization of chemicals by microorganisms, possibly involving direct contact between the hydrophobic cell surface and the chemicals, e.g., (Calvillo and Alexander 1996; Efroymson and Alexander 1991). Interestingly, Guerin and Boyd (1992) performed experiments using naphthalene that indicated the potential for direct uptake may be

organism specific. Thus, the uptake mechanism for the sorbed PAHs might also vary depending on the consortia present. A third possible mechanism is reduced mass transfer resistance brought about by the microorganisms being located very near the solid surface, which greatly reduces the diffusion distance from sorption site to the microorganisms, e.g., (Chang and Rittmann 1987; Harms and Zehnder 1995). Indeed, several researchers have also observed biodegradation of sorbed contaminants via attached organisms in sediments and granular activated carbon, e.g., (Speitel and DiGiano 1987), suggesting that the attached organisms may enhance contaminant concentration gradients, thereby promoting desorption directly into the biofilm.

Another possible explanation for the observation of desorption limitation in some experiments and not in others, maybe be the differences in the sorption/desorption properties of the solid phase material. For example, Brusseau (1992) was able to predict contaminant breakthrough for four different aquifer systems by representing sorption as a dual process. Specifically, sorption was modeled to be instantaneous for a portion of the aquifer material while being diffusion rate-limited for the remainder. Thus, the fraction of the sorption/desorption that is diffusion rate-limited will influence the bioavailability.

Based on these studies, the bioavailability of sorbed chemicals appears to depend on the properties of microorganisms present as well as the characteristics of the sorbents and experimental methodology. Unfortunately, variations among the studies in terms of the soil organic matter content and composition, contaminant hydrophobicity, and the length of time the contaminant had been in place, make generalization about sorptive behavior and its impact on biodegradation difficult.

A variety of conceptual and mathematical models have been developed to describe the sorption of PAHs on soils and sediments as summarized by Weber et al. (1991), among others. The sorption term can be described via equilibrium and non-equilibrium rate models. There are several different equations or models available for describing the equilibrium partitioning of a sorbate between the aqueous solution and the sorbent at a constant temperature, i.e., the sorption isotherm. This relationship between the contaminant concentrations in both phases can be described by either linear or nonlinear isotherms. The simple linear isotherm assumes that there are an infinite number of equal sites, independent of each other, available for sorption. The equation is,

$$\widetilde{C} = K_d C \tag{3.4}$$

where: C = the concentration of contaminant in the mobile phase, [ML^{-3}]; $\widetilde{C}$ = the concentration of the contaminant in the immobile phase (mass of the contaminant per unit mass of porous media), [MM^{-1}] ; and K_d = the linear partitioning coefficient, [L^3M^{-1}].

Several nonlinear isotherm models are also available, but the most common alternatives to the linear isotherm are the Langmuir isotherm,

$$\widetilde{C} = \frac{abC}{1+bC} \tag{3.5}$$

and the Freundlich isotherm:

$$\widetilde{C} = K_d C^n \tag{3.6}$$

where a, b, and n ($0<n<1$ or $n>1$) are empirical constants (Tchobanoglous and Burton 1991). In particular, the Freundlich model is frequently applied to describe sorption of organic chemicals from groundwater.

Nonequilibrium sorption conditions have also been observed under field conditions, e.g., (Brusseau and Rao 1989). There are many mathematical models that have been developed to describe the sorption/desorption process. Based on the rate characteristics, three types of models were used widely in the past research: (1) a first-order rate model; (2) a second-order rate model; and (3) a dual-resistance diffusion model.

Several investigations have applied a simple approach to describe the mass-transfer kinetics between soil and the mobile aqueous phase, with a linear driving force and a lumped first-order mass-transfer coefficient (Lapidus and Amundson 1952):

$$\frac{\rho}{\phi}\frac{\partial \widetilde{C}}{\partial t} = K_{ls}\left(C - \frac{\widetilde{C}}{K_d}\right) \tag{3.7}$$

where: ρ = the bulk density of the soil matrix, [ML^{-3}]; K_{ls} = the lumped first-order, mass-transfer rate parameter, [T^{-1}] = $a_{sa}k_{ls}/\phi S_w$, where $a_{sa} = A_{sa}/V$ = specific soil/aqueous interfacial surface area, [L^{-1}], k_{ls} = the mass-transfer-rate coefficient, [LT^{-1}]; and S_w = water saturation. This modeling approach is justified when mass-transfer is fast, i.e., when the diffusional lengths are extremely short.

The second-order model describes the sorption as a second-order process. However, this model has received only minor attention for the characterization of

sorption data in natural solid systems (Weber and Miller 1988), and is not discussed further here.

Diffusion formulations have been used widely in natural systems for nonlinear and hysteretic sorption equilibrium (Brusseau 1992; Miller 1984). The dual-resistance diffusion model describes sorption as a process of coupled mass transfer through a boundary film external to the solid particle followed by diffusion within a representative portion of the particle of itself (Weber and Miller 1988). For spherical solid particles, the intraparticle-diffusion process can be described by the following mass balance (Mulder et al. 2000; Mulder et al. 2001):

$$\frac{\partial C}{\partial t}\phi + \frac{\partial Q}{\partial t}(1-\phi)\rho_s = D_{eff}\left(\frac{\partial^2 C}{\partial r^2} + \frac{2}{r}\frac{\partial C}{\partial r}\right) \qquad (3.8)$$

where ϕ is the particle volumetric porosity (m^3/m^3), Q is the sorbed naphthalene concentration in the pores of solid particles (kg/kg), t is the time (s), ρ_s is the skeletal density of the solid phase (kg/m^3), D_{eff} is the effective diffusion coefficient through the porous matrix (m^2/s), and r is the distance from the center of the particle (m). The equation was developed based on the following assumptions: (1) the solid particles have a spherical shape, (2) the diffusion coefficient is concentration independent, and (3) local equilibrium is reached instantaneously at a certain location in the porous particle. The effective diffusion coefficient is defined as the binary diffusion coefficient of the naphthalene in dilute water solutions corrected for tortuosity and constrictivity effects imposed on this coefficient by the matrix geometry by means of a lumped matrix factor (κ) (Mulder et al. 2000; Mulder et al. 2001)

$$D_{eff} = \frac{\phi D_{AB}}{\kappa} \tag{3.9}$$

where D_{AB} is the binary diffusion coefficient of the naphthalene in water (m^2/s) and k is the dimensionless matrix factor.

In addition to intraparticle mass transfer resistance, diffusion across a stagnant liquid film surrounding the particle influences the overall transfer rate to a well mixed aqueous phase. This additional external mass transfer resistance can be modeled by assuming a linear concentration gradient across the laminar liquid film and thus defining the mass flux through the film as

$$N = \varepsilon k_l (C_{r=R} - C_b) \tag{3.10}$$

where N is the mass flux through the laminar layer ($kg/m^2/s$), k_l is the film mass transfer coefficient of naphthalene (m/s), r is the distance from the center of the particle (m), R is the particle radius, C_b is the bulk liquid naphthalene concentration (kg/m^3), and $C_{r=R}$ is the naphthalene concentration at the interface of the particle with the laminar layer (kg/m^3).

In turbulent flow reactors, a combination of film diffusion and intraparticle diffusion very often controls the sorption rate. Film diffusion may control initially; then, intraparticle transport may control after naphthalene accumulates within the pore. To determine whether film transfer or intraparticle mass transfer is limiting the overall sorption/desorption rate of naphthalene, the dimensionless Biot number is used (Mulder et al., 2000)

$$Bi = \frac{k_l R}{D_{eff}} \tag{3.11}$$

At high Biot numbers ($Bi >> 1$), film diffusion limitations can be neglected and intraparticle mass transfer is the rate-limiting step. At low Biot numbers ($Bi << 1$), the film diffusion resistances dominate the over sorption/desorption process.

In addition to the dual-resistance diffusion model, Brusseau et al. (1991) utilized another approach and assumed that the intra-organic matter diffusion was responsible for the slow desorption. Accordingly, these authors developed a bicontinuum model with two sorption domains, one with instantaneous exchange of contaminant and one in which the exchange was considered to be rate-limited. This model is known as the intra-organic matter diffusion model.

3.3 Micro-scale heterogeneities

Microbial-mediated contaminant transformation reactions occur at the micro-scale. Importantly, the stoichiometry and kinetics of microbially-mediated biodegradation are two of the key micro-scale features of interest (Sturman et al. 1995). With respect to this project, the primary focus is on the stoichiometry and kinetics of naphthalene biodegradation. Many different species of bacteria (both gram-negative and gram-positive), fungi, and algae are known to degrade PAHs, such as naphthalene. As PAHs are naturally occurring compounds, it is not surprising that many different PAH-degrading microorganisms can be found in pristine environments (Sims and Overcash 1983). Most of the microorganisms that have been isolated, however, originate from PAH-contaminated sites.

The microbial metabolism of PAHs like naphthalene has been studied extensively, e.g., (Sutherland et al. 1995). In fact, examples of bacteria, fungi, yeasts, cyanobacteria, and algae have been shown to have the enzymatic capacity to oxidize

PAHs. Because the bacterial metabolism of naphthalene under aerobic and is of importance for this research, it is reviewed here in detail. However, naphthalene degradation under anaerobic conditions is also reviewed briefly for completeness.

An overview of the specific steps in the aerobic naphthalene degradation pathway by *Pseudomonas* spp. is presented in Figure 3.1. The initial attack on an aromatic ring is usually performed by a dioxygenase, forming naphthalene *cis*-1, 2-dihydrodiol. This is then converted by a dehydrogenase into a dihydroxylated derivative, 1, 2-dihydroxynaphthalene. In the next step in the degradation pathway, a second dioxygenase oxidizes 1, 2-dihydroxynaphthalene to 2-hydroxychromene-2-carboxylic acid (HCCA). HCCA is then converted to an isomer of *trans*-o-hydroxybenzylidene pyruvic acid by an isomerase. Next, an aldolase converts the *trans*-o-hdyroxybenzylidene pyruvate to salicylaldehyde, which is converted to salicylate by salicylaldehyde dihydrogenase. The decarboxylation and hydroxylation of salicylate to catechol is then catalyzed by salicylate hydroxylase. Catechol is next transformed by catechol 2, 3-dioxygenase via *meta*-cleavage to 2-hydroxymuconic semi-aldehyde, which is further degraded to completion.

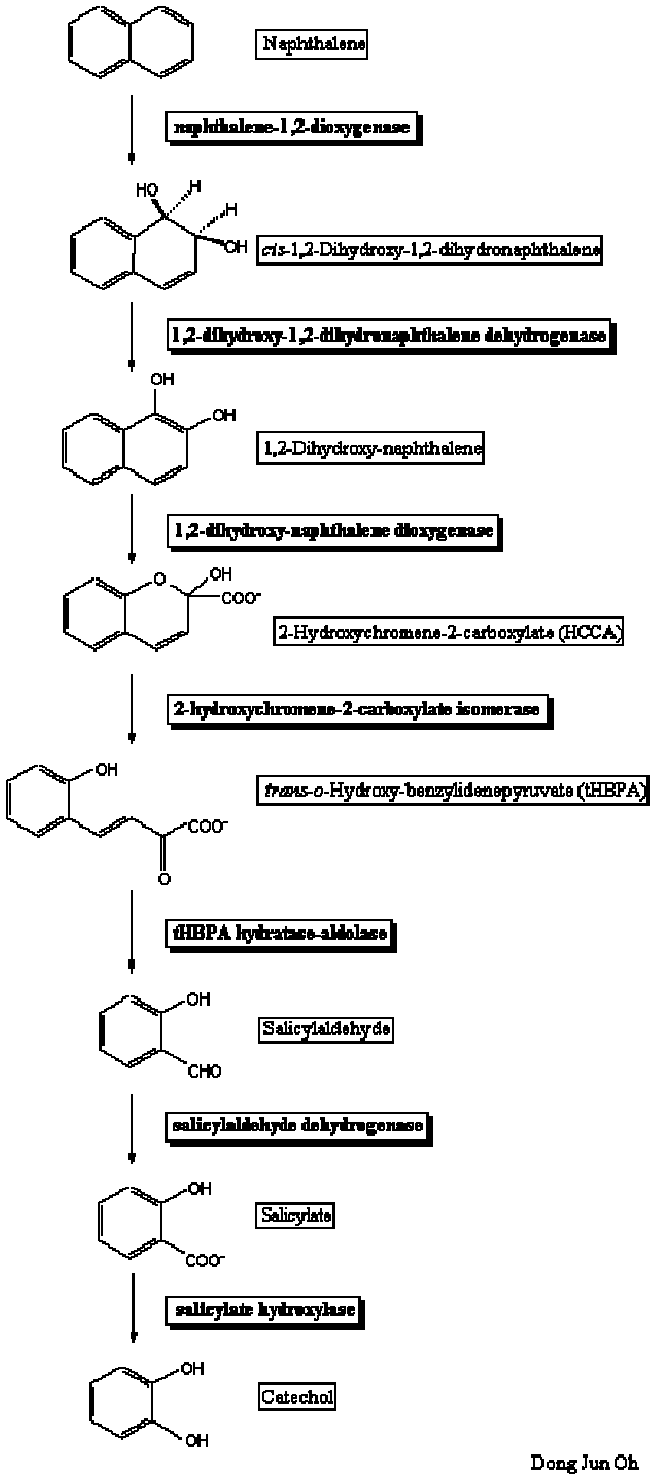

Figure 3.1 Naphthalene degradation pathway under aerobic condition (Zeng 2004)

Recent studies have also demonstrated PAH degradation under nitrate-reducing condition (Macrae and Kenneth 1998; Mihelcic and Luthy 1991; Rockne et al. 2000; Rockne and Strand 1998; Rockne and Strand 2001). For example, Rockne and Strand (2001) studied anaerobic naphthalene degradation under nitrate-reducing conditions and reported that the naphthalene degrading pure cultures they obtained were related to *Pseudomonas stutzeri* and *Vibrio pelagius*. In addition, degradation of naphthalene under methanogenic condtions has been clearly documented, as illustrated in Figure

3.2 (Grblic-Galic 1988). The methoanogenic degradation pathway for naphthalene follows a similar route to that of monoaromatic hydrocarbons, in which phenol appears to be a major intermediate. Furthermore, laboratory studies of enriched sulphidogenic consortia have shown that naphthalene is metabolized via pathways (Figure 3.3) that lead to the attachment of a carboxylic acid group to one of the aromatic ring, resulting in the formation of 2-napthonic acid (2-NA) which is further degraded by sequential ring-reduction mechanisms through 5, 6,7,8-tetrahydro-2-naphthoic acid (TH-2-NA), hexahydro-2-naphthoic acid (HH-A-NA) and decalin-2-carboxylic acid (D-2-CA) before ring cleavage (Zhang et al. 2000). Further studies are required to determine the metabolic pathways of anaerobic naphthalene mineralization. This knowledge may help to identify potential cometabolites and determine the potential for anaerobic naphthalene utilization in the environment (Rockne et al. 2000).

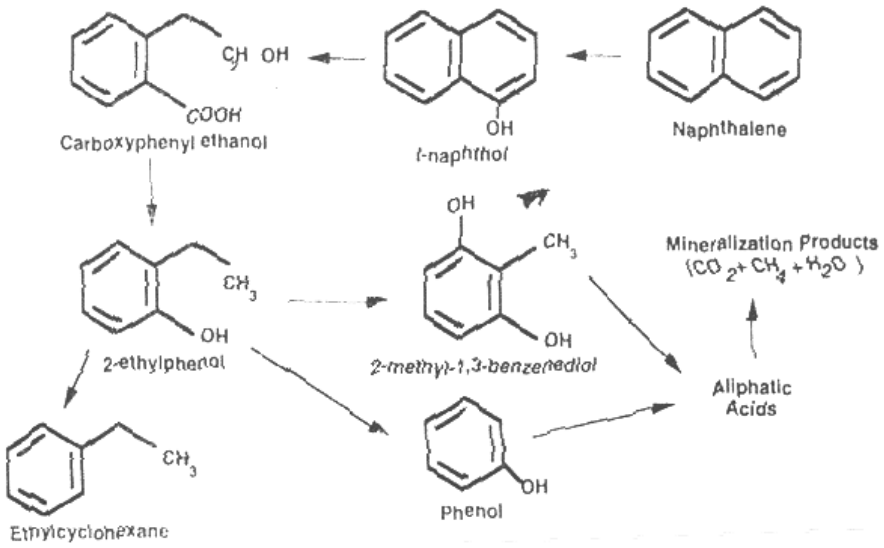

Figure 3.2 Naphthalene degradation pathway under methanogenic conditions

(Grblic-Galic 1988)

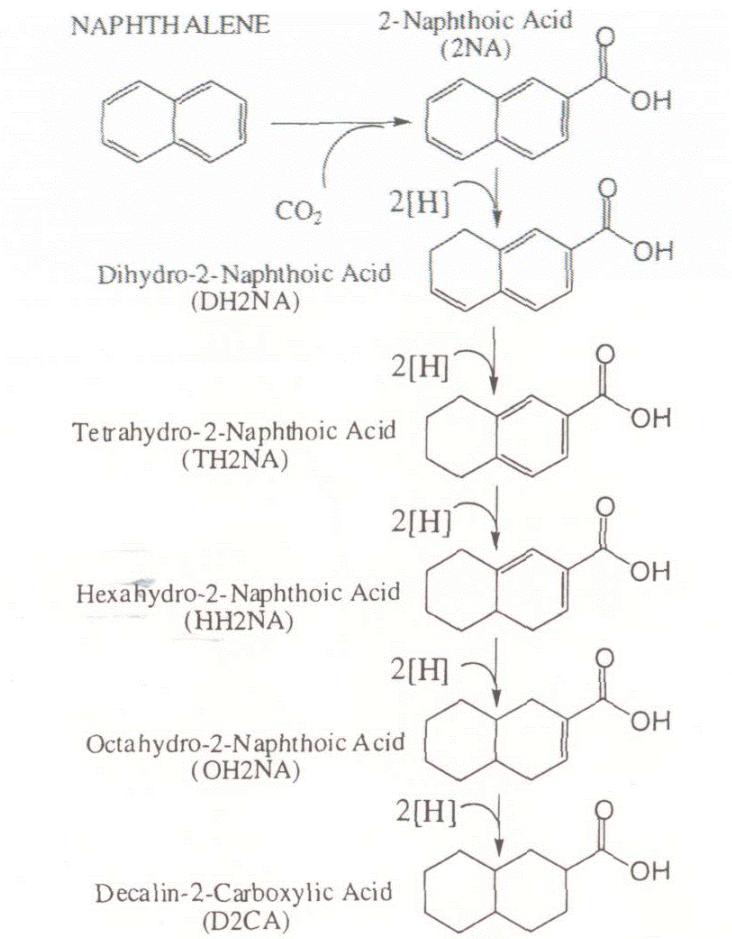

Figure 3.3 Degradative pathway of naphthalene under sulfate-reducing conditions

(Zhang et al. 2000)

Biodegradation rates in contaminated aquifers may vary due to variations in microbial species (numbers and activities), which are related to availability of nutrients and electron donors/acceptors, toxicity of contaminants, predation, and other factors. The heterogeneities in a subsurface system at the micro-scale are related to: (1) the microscopic distribution of microbes and pollutants/substrates, and (2) microbial transport. Because in this work it is assumed that microbes have already been attached to the solid phase, the discussion below focuses on the microscopic distribution of microbes and pollutants and the kinetics of PAH biodegradation under aerobic conditions.

The microscopic distributions of microbes and pollutants have been studied as well as how those distributions affect biodegradation in subsurface systems. Interestingly, soils and aquifers are desolate environments from the point of view microbes (Bosma et al. 1997), which impacts their micro-scale distribution. The average distance between colonies containing up to 100 individual cells can be estimated to be at least 100 μm based upon bacterial densities and the observation that bacteria mainly live in pores with sizes of 0.8-3 μm. On the other hand, pollutants can be present in extremely small pores. Upon entering a porous system in the subsurface, pollutants first contaminate the macropores and the particle surfaces containing relatively very few bacteria. Then, the pollutants diffuse into smaller pores where biotransformation may take place when the environmental conditions favor microbial activity. However, pollutants can also slowly diffuse into extremely small pores ($<< 1$ μm) where microorganisms are absent. Thus, pollutants and bacteria have a different microscopic distribution in contaminated subsurface materials. As a result, the

biodegradation rate and extent are affected by a number of physical-chemical processes related to substrate bioavailability such as sorption and desorption, diffusion, and dissolution, as discussed above, because it is generally assumed that the pollutants must diffuse to the bacteria before they can be taken up and degraded. Therefore, it is very necessary to study the distribution of the microorganisms and pollutants at the micro-scale, which, in turn, is influenced by the heterogeneities in natural systems.

A variety of approaches have been used to describe biodegradation kinetics in subsurface systems. Three different conceptual models have been used to describe biodegradation in the subsurface (Baveye and Valocchi 1989): (1) the strictly macroscopic model, which assumes the bacteria are immobilized and the biokinetics are a function of the macroscopic biomass and bulk fluid substrate concentrations; (2) the microcolony model, which assumes the biomass is present as small colonies growing on solid surface, and accounts for external mass transfer resistance from the bulk solution to the colony surface; and (3) the biofilm model, which assumes that the bacteria and their extracellular products are distributed as a continuous film on the solid surface, and accounts for external mass transport resistance as well as internal mass transfer resistance due to diffusion within the biofilm. Odencrantz (1991) compared the macroscopic and biofilm models for realistic groundwater conditions, and found that the two solutions converged for the organic substrate plume and biomass distribution. Therefore, the added complexity of the biofilm model (and the micro-colony model) is probably not needed for modeling the solute concentration for model groundwater scenarios. Further, the macroscopic model does not require any

assumptions regarding the spatial distribution of the biomass, nor does it require determination of biofilm parameters (Baveye and Valocchi 1989). Thus, the strictly macroscopic model was selected for this research, as described in Chapter 4.

In addition to the conceptual model, a mathematical model for the substrate utilization rate is required too. Several such models have been used including the: (1) first-order model, (2) second-order model, (3) instantaneous reaction model, and (4) Monod models. As described above, in systems with heterogeneities and the associated interfacial mass transfer processes, the resulting mixing of the limiting substrates, may cause both the electron donor and electron acceptor substrates to each limit the biokinetics. Therefore, it is necessary to describe the microbial growth and substrate utilization with an equation that accounts for dual-substrate limitation. The term dual-substrate limitation refers to a type of multiple-substrate limitation in which the electron-donor and electron-acceptor substrates together limit the overall biodegradation rate (Bae and Rittmann 1996). A commonly applied model for this case is the double Monod equation which has been utilized in the advection-dispersion transport equation to predict the fate of pollutants in the subsurface:

$$q = -q_m M\left(\frac{S}{K_S + S}\right)\left(\frac{A}{K_A + A}\right) \tag{3.12}$$

where: q_m = maximum specific substrate utilization rate, [$MM^{-1}T^{-1}$]; M = biomass concentration (pore volume basis), [ML^{-3}]; and K_S and K_A = half maximum rate constants for substrate and electron-acceptor, respectively, [ML^{-3}]. The model assumes that, if electron donor and electron acceptor are present at subsaturating

concentrations, both directly limit the overall biodegradation, and the limitation effects are multiplicative (Bae and Rittmann 1996).

It has commonly been assumed that slow biodegradation is the overall rate-limiting process for *in situ* bioremediation. In fact, biostimulation (e.g., addition of nutrients) and bioaugmentation, which are often practiced in the field, are based on the assumption that slow biokinetics are limiting the overall bioremediation (Bosma et al. 1997). In fact, many field tests have been conducted to evaluate the biostimulation and bioaugmentation effects on the overall *in situ* bioremediation and successfully demonstrated enhanced bioremediation, e.g., (Eguchi et al. 2001; Major et al. 2002; Salanitro et al. 2000). Nevertheless, in reviewing bioremediation data, Bosma et al. (1997) note that the intrinsic microbial activity (i.e., the biokinetics) actually only limited bioremediation in a few cases; in most cases, the full exploitation of the microbial biodegradation potential was prevented by mass transfer limitations.

3.4 Summary and Conclusion

As reviewed in this chapter, the physical and chemical heterogeneities of the subsurface occur at several scales and affect *in situ* bioremediation by controlling the availability of nutrients and substrates that drive the microbiological processes. There have been a significant number of studies that have focused on specific processes that affect bioremediation in the field and some definitive results have been shown. However, as summarized above, most studies have investigated *in situ* biodegradation at a single scale. For example, even in a very extensive series of studies performed at Stanford University, e.g., (Kissel et al. 1984; Rittmann and McCarty 1980), the work

only focused on mechanisms at the pore scale and was not aimed at simulating large-scale groundwater transport. Only a few experimental studies, e.g., (Murphy et al. 1997; Szecsody et al. 1994; Wood et al. 1994) and several modeling-based studies, e.g., (MacQuarrie and Sudicky 1990; Odencrantz 1991; Schafer and Kinzelbach 1992; Wood et al. 1994; Yang et al. 1994) have explicitly examined the influence on *in situ* biodegradation of several, coupled physicochemical heterogeneity factors occurring at different scales. Of course, the field studies are even more severely limited due to the complexity and financial constraints.

Clearly, the interactions between the scale-dependent physical and chemical heterogeneities, microbiological processes and *in situ* biodegradation are still not well understood. This indicates there is a "need for the process engineering approach to site remediation" that can be used to develop predictions of the effectiveness of different remedial approaches based on the information from each scale of observation (Sturman et al. 1995). In order to develop such a quantitative approach, it is necessary to study the relevant processes at a scale that represents the heterogeneity of natural systems, but on a controlled level that can be described completely. The multi-scale, multi-factor mathematical and experimental investigation at an intermediate-scale performed in this research provided a useful way to quantify the degree of heterogeneity and study the impact of coupled microbial and transport processes on *in situ* biodegradation in representative simulated subsurface systems.

Chapter 4 Theoretical Basis and Framework Development

The research hypothesis for this work was investigated using an integrated modeling and experimental approach. This Chapter's goal is to present the mathematical and theoretical framework used to investigate the research problem. First, the mathematic model used and the numerical solution techniques are presented. Then the model's governing equations are used to develop a system of dimensionless numbers and an integrated quantitative framework for identifying the overall rate-limiting process.

4.1 Mathematical Model

Reactive Transport in 3-Dimensions (RT3D), a modular computer code for simulating reactive multi-species transport in 3-dimensional groundwater aquifers (Clement 1998), was chosen as the mathematical model for evaluating the proposed quantitative framework and supporting experiments. Use of RT3D requires the groundwater flow code MODFLOW, which was developed by U.S. Geological Survey (USGS), for computing spatial and temporal variations in groundwater head distribution and flow velocities. For this research, the program used to operate the RT3D and MODFLOW codes was Visual MODFLOW (VMOD) (Version 2.8.2) (Waterloo Hydrogeologic Inc., Waterloo, Ontario, Canada). RT3D was selected for this research for several reasons. First, as a research tool, RT3D has been used for modeling several laboratory, pilot-scale and field-scale bioremediation experiments, e.g., (Clement et al. 1998; Phanikumar and McGuire 2004; Sun et al. 1999). Second, the RT3D code is unique in that it includes an implicit reaction solver that makes the

code sufficiently flexible for simulating various types of chemical and microbial reaction kinetics. Third, RT3D includes many of the processes and reactions of interest in this research. The mathematical details of the RT3D code are discussed in the following paragraphs.

4.1.1 Governing Equations

The general macroscopic advection-dispersion-reaction (ADR) equations describing the fate and transport of aqueous- and solid-phase species, respectively, in multi-dimensional saturated porous media are written as,

$$\frac{\partial C_k}{\partial t} = \frac{\partial}{\partial x_i}\left(D_{ij} \frac{\partial C_k}{\partial x_j} \right) - \frac{\partial}{\partial x_i}\left(v_i C_k\right) + \frac{q_s}{\phi} C_{sk} + r_c - r_a + r_d, \qquad \text{where k=1, 2…m} \tag{4.1}$$

and,

$$\frac{d\widetilde{C}_{im}}{dt} = \widetilde{r}_c + r_a - r_d, \text{ where im = 1, 2 … (n-m)} \tag{4.2}$$

where: n = total number of species;

m = total number of aqueous-phase (mobile) species;

im = total number of immobile species, = n-m;

x_i and x_j = distance in the direction of x_i and x_j, respectively, [L];

t = time, [T];

C_k = the aqueous-phase concentration of the k^{th} species, [ML^{-3}];

$\widetilde{C}_{im}$ = the solid-phase concentration of the im^{th} species, [MM^{-1}];

D_{ij} = hydrodynamic dispersion coefficient, [L^2T^{-1}];

v_i = the average pore water velocity, [L T^{-1}];

q_s = the volumetric flux of water per unit volume of aquifer representing sources and sinks, [T^{-1}], e.g., recharge;

C_{sk} = the concentration of species k in the source/sink water, [ML^{-3}];

r_c = the reaction rate that describes the mass of the species removed or produced per unit volume per unit time, [ML^{-3} T^{-1}];

$\tilde{r}_c$ = the reaction rate at the solid phase, [M $M^{-1}T^{-1}$];

r_a and r_d = attachment (or sorption) and detachment (or desorption) rate that describe the kinetic exchange of the transported species between aqueous and solid phases, [ML^{-3} T^{-1}];

ϕ = the soil porosity.

The processes on the right hand side of Equation 4.1 represent dispersion, advection, sources and sinks of groundwater and reactions in ground water.

The saturated groundwater flow velocities, v_i, are calculated using Darcy's law (Equation 3.2) and the hydraulic-head values that are computed by solving the three-dimensional groundwater flow model in VMOD. Thus, the flow equations used are (Zheng 1990),

$$S_s \frac{\partial h}{\partial t} = \frac{\partial}{\partial x_i}\left(K_{ii} \frac{\partial h}{\partial x_i} \right) + q_s \qquad (4.3)$$

$$v_i = -\frac{K_{ii}}{\phi} \frac{\partial h}{\partial x_i} \qquad (4.4)$$

where: h = the hydraulic head, [L];

S_s = the specific storage coefficient, [L^{-1}];

K_{ii} = the principal components of the hydraulic conductivity tensor, [L T^{-1}].

In the following subsections, the reactions rate terms pertinent to this research are discussed, followed by a description of the numerical solution technique used by RT3D.

4.1.2 Rate-Limited Sorption Reactions

Sorption mechanisms are usually described in terms of mass-transfer kinetics and the type of equilibrium isotherm, as reviewed in Chapter 3. When sorption is assumed to be rate-limited, it is necessary to track the contaminant concentrations in both mobile (groundwater) and immobile (soil) phases.

In this research, the fate and transport of a sorbing solute in the aqueous and soil phases can be predicted using the following transport equations modified from Haggerty and Gorelick's (1994) approach. First, Equation 4.1 is written with only the sorption reaction rate term, $r_a = \frac{\rho}{\phi}\frac{\partial \widetilde{C}}{\partial t}$:

$$\frac{\partial C}{\partial t} = \frac{\partial}{\partial x_i}\left(D_{ij}\frac{\partial C}{\partial x_j}\right) - \frac{\partial}{\partial x_i}\left(v_i C\right) + \frac{q_s}{\phi}C_s - \frac{\rho}{\phi}\frac{\partial \widetilde{C}}{\partial t} \qquad (4.5)$$

where the subscripts were dropped for Equation 4.1 because only one solute was of interest to this research, i.e., k = 1 and im = 1. Then, the first-order, linear driving force model (Equation 3.7) is substituted for r_a, except that the possibility of nonlinear equilibrium is incorporated using the Freundlich model (Weber and Miller 1988):

$$\frac{\rho}{\phi}\frac{\partial \widetilde{C}}{\partial t} = K_{ls}\left(C - \left(\frac{\widetilde{C}}{K_d}\right)^{\frac{1}{n}}\right) \qquad (4.6)$$

when the empirical constant, n =1, the linear isotherm equation (Equation 3.4) is integrated into the equation, and when 0<n<1 or n>1, the Freundlich isotherm (Equation 3.6) is incorporated into the equation.

Although Equation 4.5 and 4.6 are adopted for the proposed study, more complicated models, which incorporate internal (Szecsody and Bales 1989) or external (Weber and Smith 1987) mass transfer resistances, may be required to describe some systems, e.g., Equation 3.8 and 3.10, respectively. This was encountered in this work, as discussed in Chapter 6.

4.1.3 Double Monod Biodegradation Kinetic Model

Incorporating the Double Monod kinetic model (Equation 3.12) into Equation 4.1, along with the sorption reaction rate term (Equation 4.6, with n=1), gives the following governing equation for describing the fate and transport of an electron donor (a hydrocarbon, for example) in a multi-dimensional saturated porous media:

$$\frac{\partial S}{\partial t} = \frac{\partial}{\partial x_i}\left(D_{ij} \frac{\partial S}{\partial x_j} \right) - \frac{\partial}{\partial x_i}(v_i S) + \frac{q_s}{\phi}[S_s] - K_{ls}\left(S - \frac{\widetilde{S}}{K_d} \right) - q_m\left(M + \frac{\rho \widetilde{M}}{\phi} \right)\left(\frac{S}{K_S + S} \right)\left(\frac{A}{K_A + A} \right) \tag{4.7}$$

where: S = the electron donor concentration in the aqueous phase, replacing the generic term C, used earlier [ML^{-1}];

S_s = the electron donor concentration in the sources/sinks, [ML^{-3}];

M = the aqueous phase bacterial cell concentration, [ML^{-3}];

$\widetilde{M}$ = the solid-phase cell concentration (mass of bacterial cells per unit mass of porous media, [MM^{-1}];

A = the electron acceptor concentration in the aqueous phase, replacing the generic term C, used earlier [ML^{-3}];

K_S = the half-saturation coefficient for the electron donor, [ML^{-3}];

K_A = the half-saturation coefficient for the electron acceptor, [ML^{-3}];

q_m = the specific maximum electron donor utilization rate, [$MM^{-1}T^{-1}$];

The assumptions implicit in the double Monod model as implemented in Equation 4.7 are as follows:

1. The degradation reactions occur only in the aqueous phase, which is usually a conservative assumption;
2. No specific microscopic biomass structure is assumed, and diffusion limitations across biofilm are neglected, i.e., it is the strictly macroscopic model discussed in Chapter 3;
3. First-order kinetic expressions are assumed to represent the exchange of bacteria between aqueous and solid phases (Hornberger et al. 1992; Peyton et al. 1995; Taylor and Jaffe 1990), as discussed further below.
4. Permeability and porosity changes caused by the bacterial growth are ignored in the formulation (Rittmann 1993; Taylor and Jaffe 1990).

Similarly, the fate and transport of the electron acceptor (oxygen, for example) can be modeled using the following equation:

$$\frac{\partial A}{\partial t} = \frac{\partial}{\partial x_i}\left(D_{ij} \frac{\partial A}{\partial x_j} \right) - \frac{\partial}{\partial x_i}(v_i A) + \frac{q_s}{\phi} A_S - Y_{A/S} q_m \left(M + \frac{\rho \tilde{M}}{\phi} \right) \left(\frac{S}{K_S + S} \right) \left(\frac{A}{K_A + A} \right) \quad (4.8)$$

where A_s = the electron acceptor concentration in the sources/sinks, [ML^{-3}];; and $Y_{A/S}$ is the stoichiometric coefficient, relating electron acceptor consumption to utilization of the electron donor, [MM^{-1}].

In addition, the fate and transport of bacteria in the aqueous phase can be described using the equation:

$$\frac{\partial M}{\partial t} = \frac{\partial}{\partial x_i}\left(D_{ij}\frac{\partial M}{\partial x_j}\right) - \frac{\partial}{\partial x_i}\left(v_i M\right) + \frac{q_s}{\phi}M_s$$
$$- K_{att}M + \frac{K_{\det}\rho\tilde{M}}{\phi} + Y_{X/S}q_m\left(M + \frac{\rho\tilde{M}}{\phi}\right)\left(\frac{S}{K_S + S}\right)\left(\frac{A}{K_A + A}\right) - K_e M \qquad (4.9)$$

where: M_s = the bacterial concentration in the sources/sinks [ML^{-1}]; K_{att} = the bacterial attachment coefficient, [T^{-1}]; $K_{\det}$ = the bacterial detachment coefficient, [T^{-1}]; K_e = the endogenous cell death or decay coefficient, [T^{-1}]; and $Y_{X/S}$ = the true yield coefficient, [MM^{-1}].

The growth of attached-phase bacteria can be described using an ordinary differential equation:

$$\frac{d\tilde{M}}{dt} = \frac{K_{att}\phi M}{\rho} - K_{\det}\tilde{M} + Y_{X/S}q_m\tilde{M}\left(\frac{S}{K_S + S}\right)\left(\frac{A}{K_A + A}\right) - K_e\tilde{M} \qquad (4.10)$$

4.1.4 Numerical Solution Techniques

The RT3D code utilizes a standard reaction Operator-Splitting (OS) strategy to develop a general numerical solution scheme for solving the coupled partial/ordinary differential equations described above. The OS strategy is demonstrated below using Equation 4.1 as an example.

Employing the OS strategy, first the mobile species transport equation, Equation 4.1, is divided into four distinct differential equations:

the advection equation,

$$\frac{\partial C}{\partial t} = -\frac{\partial (v_i C)}{\partial x_i} \tag{4.11}$$

the dispersion equation,

$$\frac{\partial C}{\partial t} = \frac{\partial}{\partial x_i}\left(D_{ij} \frac{\partial C}{\partial x_j} \right) \tag{4.12}$$

the source/sink-mixing equation,

$$\frac{\partial C}{\partial t} = \frac{q_s}{\phi} C_s \tag{4.13}$$

and, the reaction equation,

$$\frac{dC}{dt} = r \tag{4.14}$$

where: the term r represents all possible reaction terms that appear in a typical mobile-species transport equation. In a typical immobile species equation (Equation 4.2), the advection, dispersion, and source/sink-mixing terms are zero and only the reaction term exists.

Each of the differential equations described above is solved numerically by RT3D using various solution solvers. The advection package can use either a method of characteristics (MOC), modified method of characteristics (MMOC), hybrid method of characteristics (HMOC), or an upstream finite-difference solution schemes (Zheng 1990). In this research, the MOC method was applied because it is virtually free of numerical dispersion. The dispersion and source-sink mixing packages use

explicit finite-difference approximations, while the reaction package has an improved implicit reaction solver. The logical steps involved in the numerical solution procedure are illustrated in Figure 4.1. As shown in the figure, the solution algorithm initially solves the advection, dispersion, and source-sink mixing steps for all mobile components. After solving the transport, the coupled reaction equations are solved implicitly. Use of the modular OS approach for solving the reactive transport problem facilitates representation of different contaminant transport systems through a set of pre-programmed reaction packages.

It should be noted that RT3D as included in Visual MODFLOW has the rate-limited sorption package (Equations 4.5 and 4.6) and Double Monod biokinetics (Equations 4.7-4.10) built in. However, it does not allow their simultaneous use. Therefore, in a related project, Mark Johnson (M.S. student), with assistance from Waterloo Hydrogeologic program, created a new module to add that capability to RT3D. As a result, a new reaction transport engine with the title of "University of Maryland-biokinetic model" was added to the Transport Engine Options in RT3D, which incorporates the lumped first-order mass-transfer sorption kinetics and Double-Monod biodegradation kinetics into one package, allowing their simultaneous utilization.

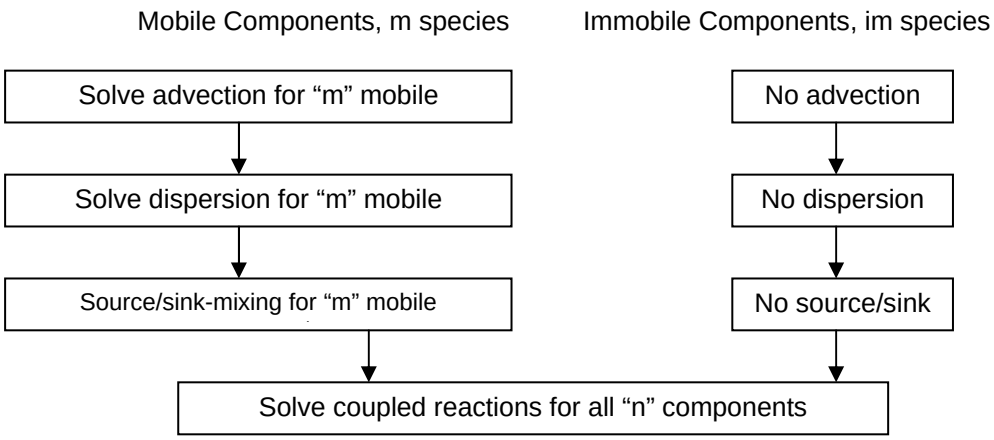

Figure 4.1 Block diagram illustrating the numerical solution scheme.

4.2 Framework Development

In previous research, the various scales of heterogeneities and associated interfacial processes have been studied extensively individually. However, in real natural systems, several of these processes occur simultaneously at different scales of heterogeneities. Nonetheless, there is one process that will limit the overall biodegradation rate given a certain combination of environmental conditions. If that limitation is significant, then the bioremediation is usually not successful (Sturman et al. 1995). In fact, Sturman et al. (1995) concluded that an assessment of the feasibility of an *in situ* bioremediation project is dominated by the need to identify and estimate the appropriate rate-controlling phenomenon.

Therefore, in order to have successful *in situ* bioremediation in the field, a systematic method is needed to identify the rate-limiting process and then the appropriate engineering action can be taken for enhancing the biodegradation rate. An integrated quantitative framework that can be used to identify the overall rate-limiting process was developed in this research (Figure 4.2), which is based on a systematic comparison of a set of dimensionless numbers. The definition of dimensionless numbers is presented in Table 4.1. The developed framework is an expansion of the one presented in Weiner et al. (1999), which was adapted from Ramasmami and Luthy (1997).

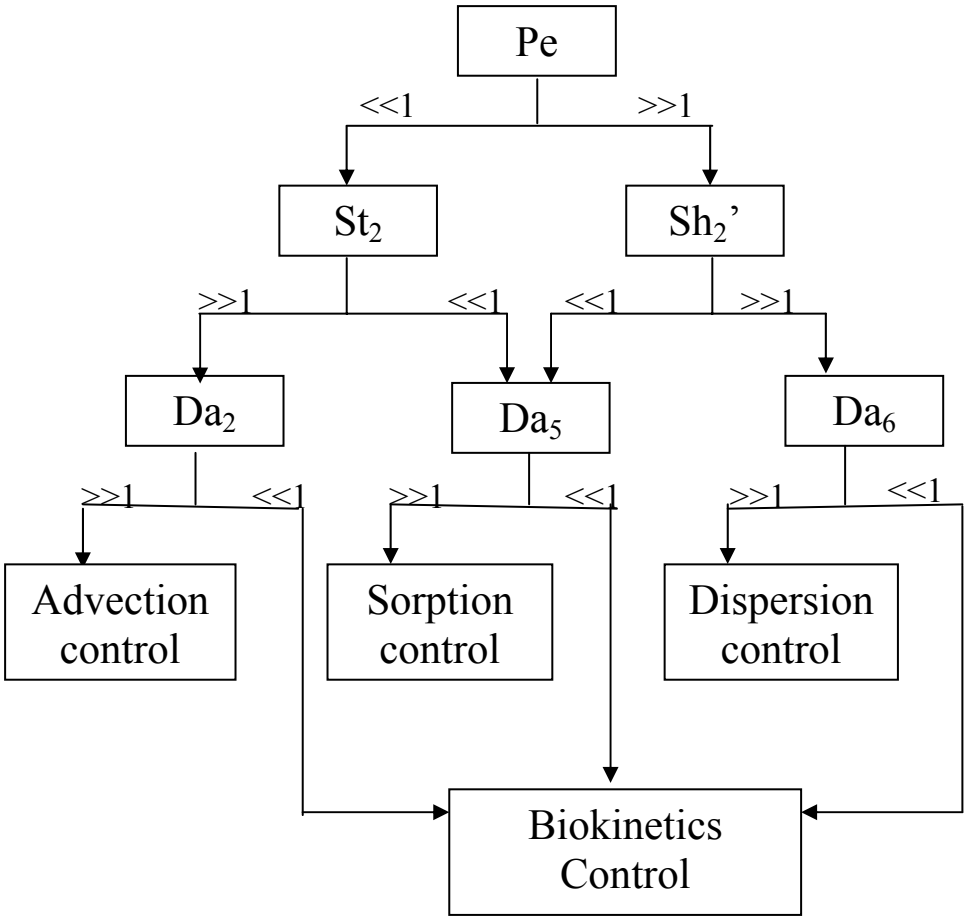

Figure 4.2 Quantitative framework for predicting the rate-limiting phenomenon.

Table 4.1 Definition of dimensionless numbers

Symbol	Meaning and Equations	Indication of rate-limiting process
Pe_l (Longitudinal Peclet No.)	=(advection rate/dispersion rate) $=\frac{q_x L}{D_x \phi S_w}=\frac{v_x L}{D_x}$	If Pe_l >>1: longitudinal dispersion limits
Pe_t (Transverse Peclet No.)	=(advection rate/dispersion rate) $=\frac{q_x L}{D_z \phi S_w}=\frac{v_x L}{D_z}$	If Pe_t >>1: transverse dispersion limits
St_1 (Stanton No. 1)	=(NAPL dissolution/advection rate) $=\frac{k_{\ln} a_{na} L}{q_x}=\frac{K_{\ln} L}{v_x}$	If St_1>>1: advection limits
St_2 (Stanton No. 2)	=(soil mass transfer rate/advection rate) $=\frac{k_{ls} a_{sa} L}{q_x}=\frac{K_{ls} L}{v_x}$	If St_2>>1: advection limits
Sh_1' (Modified Sherwood No. 1)	=(NAPL dissolution/dispersion rate) $=\frac{k_{\ln} L}{D_z} or \frac{K_{\ln} L^2}{D_z}$	If Sh_1'>>1: transverse dispersion limits
Sh_2' (Modified Sherwood No. 2)	=(soil mass transfer rate/dispersion rate) $=\frac{k_{ls} L}{D_z} or \frac{K_{ls} L^2}{D_z}$	If Sh_2'>>1: transverse dispersion limits
Da_2 (Damköhler No. 2)	= (biodegradation rate/advection rate) $=\frac{q_{\max} M_0 L}{S_0 v_x}$	If Da_2 >>1: advection limits
Da_6 (Damköhler No. 6)	= (biodegradation rate/dispersion rate) $=\frac{q_{\max} M_0 L^2}{S_0 D_z}$	If Da_6 >>1: transverse dispersion limits
Da_3 (Damköhler No. 3)	= (biodegradation rate/NAPL dissolution rate) $=\frac{Da_2}{St_1}=\frac{q_{\max} M_0}{S_0 K_{\ln}}$	If Da_3 >>1: dissolution limits
Da_5 (Damköhler No. 5)	= (biodegradation rate/soil mass transfer rate) $=\frac{Da_2}{St_2}=\frac{q_{\max} M_0}{S_0 K_{ls}}$	If Da_5 >>1: desorption limits

where: L = characteristic length, in all cases, L=aquifer thickness (Mukherji et al. 1997; Oya and Valocchi 1998); q_x = specific discharge [LT^{-1}]; v_x = average pore water velocity [LT^{-1}]; M_0 = initial biomass concentration [ML^{-3}]; S_0 = initial substrate concentration [ML^{-3}]; $k_{\ln}$ = the mass-transfer-rate coefficient between liquid and NAPL [LT^{-1}]; $a_{na} = A_{na}/V$ = specific NAPL/aqueous phase interfacial area [L^{-1}]; $K_{\ln} = a_{na} k_{\ln} / n S_w$ = the lumped mass-transfer-rate coefficient between liquid and NAPL [T^{-1}];

The dimensionless numbers in Figure 4.2 and Table 4.1 can be developed from the governing equations describing transport of contaminants presented in Section 4.1. For example, the advection and dispersion equation describing transport of an electron donor solute influenced by nonlinear kinetic sorption, nonlinear double-Monod biodegradation kinetics, and biomass growth and decay, for two-dimensional steady-state flow can be written as,

$$\frac{\partial S}{\partial t} = -\frac{\partial}{\partial x}(vS) + \frac{\partial}{\partial x}\left(D_x \frac{\partial S}{\partial x}\right) + \frac{\partial}{\partial z}\left(D_z \frac{\partial S}{\partial z}\right) - K_{ls}\left(S - \frac{\widetilde{S}}{K_d}\right) - q_m\left(M + \frac{\rho \widetilde{M}}{\phi}\right)\left(\frac{S}{K_S + S}\right)\left(\frac{A}{K_A + A}\right) \tag{4.15}$$

Equation 4.15 can be converted into dimensionless form by using the dimensionless numbers defined in Table 4.1 and the following dimensionless parameters:

$$x^* = \frac{x}{L}, \qquad z^* = \frac{z}{L}, \qquad t^* = \frac{t}{L/v_x}, \qquad S^* = \frac{S}{S_0}, \qquad \widetilde{S}^* = \frac{\widetilde{S}}{S_0}$$

$$A^* = \frac{A}{A_0}, \qquad K_S{}^* = \frac{K_S}{S_0}, \qquad K_A{}^* = \frac{A}{A_0}, \qquad \widetilde{M}^* = \frac{\rho\widetilde{M}/\phi}{\widetilde{M}_0}$$

Using this series of dimensionless parameters, results in the following equation:

$$\frac{\partial S^*}{\partial t^*} = -\frac{\partial S^*}{\partial x^*} + \frac{1}{Pe_l}\frac{\partial^2 S^*}{\partial x^{*2}} + \frac{1}{Pe_t}\frac{\partial^2 S^*}{\partial z^{*2}} - St_2\left(S^* - \widetilde{S}^*\right) - Da_2\left(\frac{S^*}{K_S{}^* + S^*}\right)\left(\frac{A^*}{K_A{}^* + A^*}\right) \tag{4.16}$$

Although not shown here, a similar dimensionless equation can be derived for the electron acceptor, as well as the biomass in aqueous and solid phases using Equations 4.8, 4.9 and 4.10. The advantage of using the dimensionless form of the equations is that the number of independent parameters in the system is minimized.

Further, the resulting dimensionless parameters succinctly capture the complexity of the system in a way that can be used in the quantitative framework presented in Figure 4.2.

The quantitative framework was used to integrate and compare the key interfacial processes that occur in contaminated natural systems and predict the rate-limiting process under certain environmental conditions. The first two steps were used to identify the slowest mass-transfer process among advection, dispersion, sorption/desorption and the third step was used to compare the slowest mass transfer process with the biokinetics to determine the overall rate-limiting process. The framework is viable for offering insight into the rate-limiting process for the overall bioremediation application as long as the dimensionless numbers are significantly smaller or larger than unity (e.g., <0.2 or >5) (Ramaswami and Luthy, 1997). If the rate-limiting process can be properly identified, then an appropriate remedial approach can be chosen to alleviate that limitation. For example, in the study of Falatko and Novak (1992), a biosurfactant was added to the influent to enhance desorption, which was the rate-limiting step for the overall biodegradation rate.

4.3 Research Approach

The integrated modeling and experimental approach for evaluating the quantitative framework and the research hypothesis was comprised of four components (as discussed in subsequent chapters, some of these components were performed in conjunction with other graduate students). First, the quantitative framework based on a set of dimensionless numbers described above was developed to evaluate the effects of different scales of heterogeneities, associated mass transfer

process, and biokinetics on *in situ* bioremediation. Second, the RT3D was chosen and utilized to perform a preliminary evaluation of the relationship between the heterogeneities, interfacial processes, and biokinetics to test the framework. Third, an intermediate-scale flow cell (ISFC) was designed and constructed, representing a realistic, yet experimentally tractable system to investigate the rate-limiting process that affects the successful application of *in situ* bioremediation. Finally, selected bioremediation scenarios were simulated in the constructed ISFC. These scenarios were designed to provide a useful evaluation of the quantitative framework. Specifically, in each of the simulated scenarios, the experimental conditions were varied such that a different single process limited the overall bioremediation rate in each case. The results of these experiments were used to evaluate the utility of the quantitative framework for defining the rate-limiting process and selecting an appropriate engineered bioremediation approach.

Specifically, three sets of experiments simulating three different scenarios were performed, with each scenario being representative of one common rate-limiting phenomenon occurring in natural subsurface systems. Each scenario had a combination of processes occurring at the macro-scale, meso-scale, and micro-scale. All these experiments were performed in a two-dimensional domain with horizontal flow and vertical (hydraulic conductivity) stratification. Different hydraulic conductivity (K) strata (i.e., a high-K layer and a low-K layer) were used because they are a relatively simple type of macro-scale heterogeneity of practical importance and because of the importance of vertical transverse dispersion as discussed in Chapter 3. Meso-scale interfacial processes were focused on sorption/desorption,

while micro-scale processes were focused on biodegradation. In all three cases, the simulated groundwater contained the model contaminant naphthalene and conservative tracer Br, along with oxygen, to be representative of field conditions. The experimental conditions were varied in such a way that only one single mass-transfer process or biokinetics limited the overall bioremediation rate in each case. The three scenarios are illustrated schematically in Table 4.2 and the corresponding dimensionless numbers are presented in Table 4.3.

Scenario #1 was performed with relatively fast aerobic biokinetics, in a porous media with relatively low sorption, resulting in macro-scale vertical transverse dispersion from the fast-K to the slow-K layer being the rate-limiting process (Figure 4.3). It was expected that the bioremediation would be limited by transverse dispersion from the fast-K layer into the slow-K layer and that the biodegradation would occur primarily at the interface between the layers where substrate mixing occurs.

Scenario #2 was designed to simulate a situation where slow biokinetics limited the overall biodegradation rate (Figure 4.4). It utilized the same porous media and sorptive characteristics as Scenario #1. The experiment was run with the same microbial culture, but with inhibited slower biokinetics, which was accomplished by adding high concentration of salt (5% of NaCl solution by w/v) as an inhibitor to reduce the water potential of the system so as to slow down the biodegradation rate (Brock 1977).

Table 4.2 Description of the flow cell experiments

Scenarios	Schematic experimental settings	Description
Scenario #1: macro-scale: transverse dispersion controls	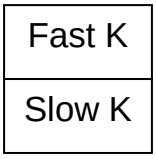	- Relatively fast biokinetics - Limited sorption - Relatively slow transverse dispersion
Scenario #2: micro-scale: biokinetics controls	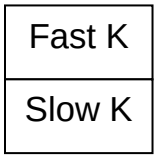	- Slow biokinetics - Limited sorption - Relatively slow transverse dispersion
Scenario #3: meso-scale: sorption/desorption controls	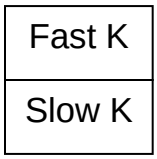	- Relatively fast biokinetics - Increased sorption - Relatively slow transverse dispersion

Table 4.3 Application of the dimensionless numbers in the quantitative framework to simulated bioremediation scenarios

Scenario description	First two-step result	Final step result
Scenario #1: transverse dispersion is the overall rate-limiting process	$Pe_t >> 1$ $Sh_2^{'} >> 1$	$Da_6 >> 1$
Scenario #2: sorption/desorption is the overall rate-limiting process	$Pe_t >> 1$ $Sh_2^{'} << 1$	$Da_5 >> 1$
Scenario #3: biokinetics is the overall rate-limiting process	$Pe_t >> 1$ $Sh_2^{'} >> 1$	$Da_6 << 1$

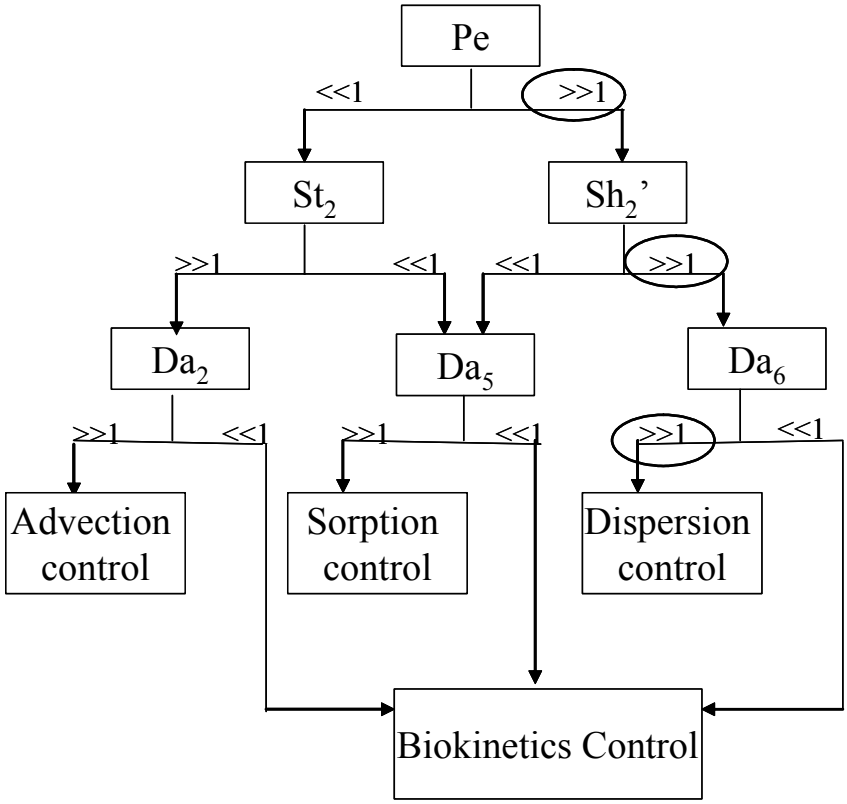

Figure 4.3 Quantitative framework for predicting the rate-limiting phenomenon

Application of the flow chart to Scenario #1 is highlighted by encircling the experimental conditions.

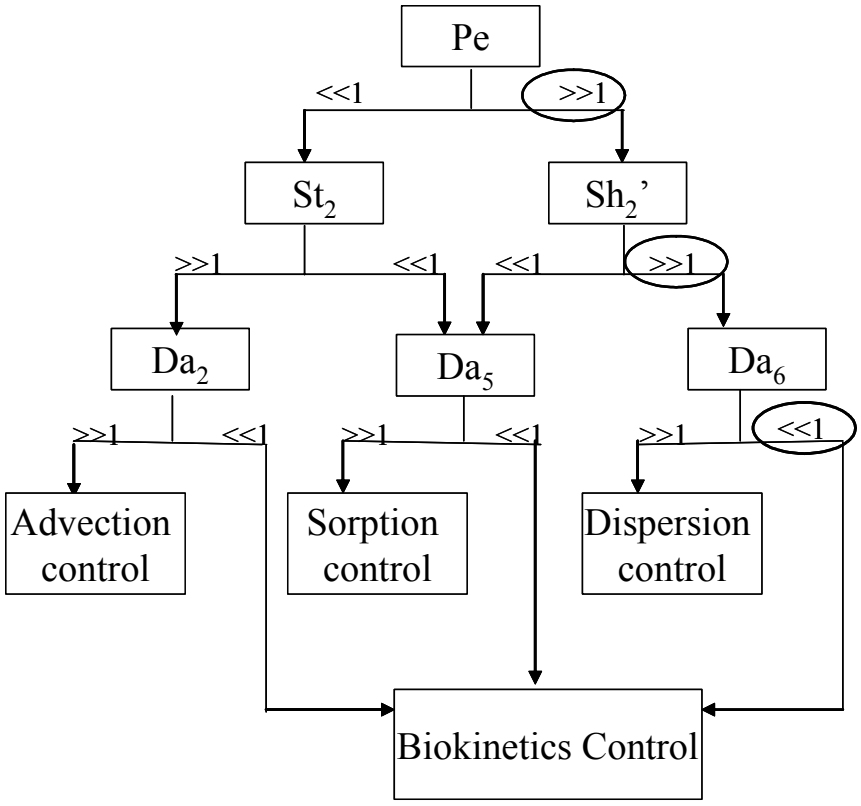

Figure 4.4 Quantitative framework for predicting the rate-limiting phenomenon

Application of the flow chart to Scenario #2 is highlighted by encircling the experimental conditions.

Finally, in Scenario #3, the influent solution, the two-layered porous media, and the biokinetics were the same as in Scenario #1, but the sorptive characteristics of the porous media were increased so that the meso-scale desorption rate was the overall rate-controlling mass-transfer process (Figure 4.5). Thus, it was expected that the overall bioremediation rate would be limited by the naphthalene sorption/desorption rate. Due to time constraints, this scenario was not implemented completely. The sorption/desorption equilibrium and kinetic studies were performed in batch experiments and parameter estimates were obtained from model fittings. However, the evaluation of this scenario in ISFC is still under investigation and will be conducted by Ms. Eunyoung Hong.

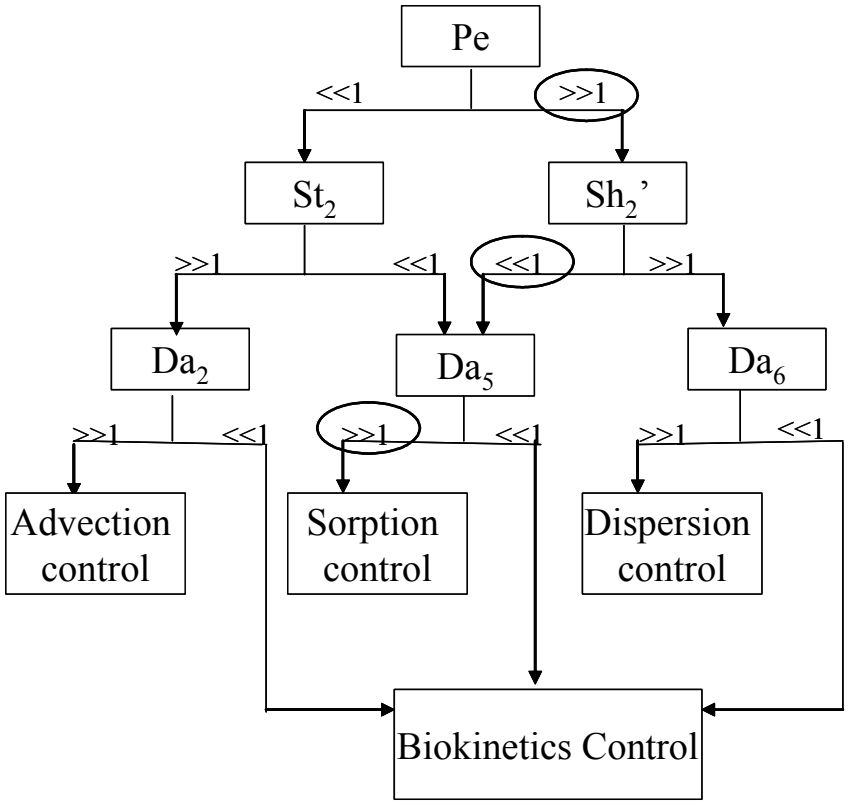

Figure 4.5 Quantitative framework for predicting the rate-limiting phenomenon

Application of the flow chart to Scenario #3 is highlighted by encircling the experimental conditions.

Chapter 5 Experimental Materials and Methods

To experimentally investigate the research hypothesis and evaluate the quantitative framework using the three experimental scenarios presented in Table 4.2, appropriate experimental materials and methods were developed and applied, as described in this chapter. First, a model contaminant was selected, an artificial groundwater was designed to be representative of natural groundwater chemistry, and a microorganism was chosen as inoculum for biodegradation. Second, an intermediate-scale flow cell (ISFC) was designed and constructed to simulate a contaminated aquifer with various scales of heterogeneities. Third, batch experiments were conducted to estimate the kinetic parameters for the physical, chemical and biological processes occurring in the simulated subsurface of the ISFC. Fourth, the bioremediation simulation experiments were carried out in the ISFC to investigate the research hypothesis. Finally, analytical methods were chosen to analyze the model contaminant concentration, tracer concentration, biomass concentration and dissolved oxygen (DO) concentration, which are summarized below.

5.1 Model Contaminant, Artificial Groundwater and Microorganism

5.1.1 Model contaminant

Naphthalene (Fisher Scientific, 99%) was selected as the test contaminant, because PAHs are a class of contaminants that has critical bioavailability issues at numerous contaminated sites (Rittmann et al. 1994), and naphthalene has often been used as a model experimental compound for PAHs, e.g., (Park et al. 2002). Although

like other PAHs naphthalene has generally poor mobility in the environment (i.e., low solubility, high sorption, low volatility), it has a sufficiently high aqueous solubility to facilitate experimentation. The properties of naphthalene are summarized in Table 5.1.

Table 5.1 Physicochemical properties of naphthalene

(Sims and Overcash 1983)

Chemical	Naphthalene ($C_{10}H_8$)
Molecular weight (g/mol)	128.2
Vapor pressure (Pa at 25°C)	10.4
Log (K_{ow})	3.37
Solubility at 30°C (mg/L)	31.7
Molecule surface area (A^2)	155

Once naphthalene was selected, an experimental concentration needed to be chosen. There were two factors that affected the selection of the naphthalene concentration: (1) the concentration should be representative of the typical concentration found at sites contaminated with naphthalene, and (2) the concentration should be high enough so the experimental trends could be followed during the course of an experiment. With respect to the first constraint, in coal tar/water system studies (Peters and Luthy 1993), an equilibrium concentration for naphthalene was measured to be 3.3 mg/L, and Kramer and Hayes (1987) measured an equilibrium aqueous concentration of 2.540 mg/L naphthalene in a No. 2 heating oil/water

system. Based on these examples, the naphthalene concentration in the research was originally chosen to be 5 mg/L as utilized in the control experiments. The concentration selected was higher than the above examples, because it was easier to study experimental trends compared to if the concentration was lower. Later, in the bioremediation simulation experiments, the naphthalene concentration was adjusted to 10 mg/L due to the fast biodegradation rate in the simulated aquifer, which necessitated that the naphthalene concentration be adjusted to make it more feasible to monitor the plume development.

Aqueous naphthalene solutions were prepared either from methanol stock solutions (sorption experiments) or N, N-Dimethylformamide (DMF, Sigma-Aldrich, 99.8%, A.C.S. reagent) (Whitman et al. 1998) stock solutions (batch respirometry experiments and bioremediation simulation experiments). The naphthalene methanol stock solutions were initially prepared by dissolving solid naphthalene in methanol. These methanolic solutions were then used to prepare the naphthalene aqueous solutions. In all cases, it was ensured that the resulting concentration of methanol in the aqueous solutions was lower than 2% by volume. It had previously shown that the presence of methanol up to 5% by volume did not modify the sorption properties of naphthalene (Appert-Collin et al. 1999). Naphthalene DMF stock solutions were prepared by using a similar technique, and following the same constraints.

5.1.2 Artificial Groundwater

A dilute mineral salt nutrient solution (MSNS) was used in the parameter estimation batch experiments and ISFC bioremediation simulation experiments to represent dilute groundwater chemistry. The MSNS was prepared in de-ionized (DI)

water as described by Murphy et al. (1997), with the mineral compositions as presented in Table 5.2.

The MSNS was prepared from three stock solutions. The macro nutrient stock solution was made by dissolving 10 mg of $FeSO_4 \cdot 7H_2O$, 200 mg of $MgSO_4 \cdot 7H_2O$, 300 mg NH_4Cl, and 60 mg $NaH_2PO_4 \cdot H_2O$ into 1 L deionized water (= final concentration $\times 100$). The trace element stock solution was made by first dissolving 50 mg each of $MnCl_2$, Na_2SeO_3, H_3BO_3, $Na_2MoO_4 \cdot 2H_2O$, $CoCl_2 \cdot 6H_2O$, $NiSO_4 \cdot 6H_2O$, $CaSO_4 \cdot 5H_2O$, and $ZnSO_4 \cdot 7H_2O$ into 1 L deionized water, from which 10 ml was taken out and diluted into 1 L with distilled water to obtain the trace stock solution (= final concentration $\times 100$). The PIPES (Sigma Chemical Co., 99%) stock buffer solution was prepared with 151.2 g PIPES dissolved into 2L deionized water, which was adjusted to pH = 6.8 with 4 N NaOH and then diluted to 2 L with deionized water (= final concentration $\times$ 25). To make MSNS, appropriate volumes of the macro nutrient stock solution, trace element stock solution and PIPES buffer solution were combined and diluted to the desired volume with deionized water. Different concentrations of naphthalene solution were then prepared in the MSNS by adding naphthalene in methanol or DMF stock solutions as needed. On at least one occasion, the pH of the effluent from the bioremediation experiments described below was measured and found to be 6.8, indicating that the buffering capacity of the MSNS was adequate.

Table 5.2 Mineral medium compositions

Macro nutrient compounds	Concentration, mg/L
$FeSO_4 \cdot 7H_2O$	0.1
$MgSO_4 \cdot 7H_2O$	2
NH_4Cl	3
Na_2HPO_4	0.6
Trace element compounds	Concentration, µg/L
$MnCl_2$	5
Na_2SeO_3	5
H_3BO_3	5
$Na_2MoO_4 \cdot 2H_2O$	5
$CoCl_2 \cdot 6H_2O$	5
$NiSO_4 \cdot 6H_2O$	5
$CaSO_4 \cdot 5H_2O$	5
$ZnSO_4 \cdot 7H_2O$	5
Buffer Solution	Concentration, mM
PIPES	10

In the MSNS, NH_4Cl and Na_2HPO_4 served as the N and P source, respectively. The overall stoichiometry for aerobic naphthalene degradation, including biomass synthesis, with ammonia as the nitrogen source, is as follows (McCarty 1987):

$$C_{10}H_8 + 6O_2 + 1.2NH_3 \Rightarrow 1.2C_5H_7O_2N + 4CO_2 + 1.6H_2O \qquad (5.1)$$

This equation was used as the stoichiometric basis for the nutrient requirement calculation. Based on stoichiometry of biological reaction of naphthalene and assuming the phosphorus required is approximately one-fifth of that for nitrogen, the mass ratio of naphthalene $C_{10}H_8$: NH_4Cl: Na_2HPO_4 for the biodegradation under aerobic conditions is 10:5:1. Therefore, for an initial naphthalene concentration of 10 mg/L, the stoichiometric amount of NH_4Cl and Na_2HPO_4 required to degrade the naphthalene are 5 mg/L and 1 mg/L, respectively. Correspondingly, the amounts of NH_4Cl and Na_2HPO_4 in the MSNS, 3 mg/L and 0.6 mg/L, respectively, meet 60% of the stoichiometric nutrient requirements for biodegradation of 10 mg/L of naphthalene.

5.1.3 Microorganism

The microbial culture used in this work was selected as part of the larger project, of which this research was a part, by Eunyoung Hong, a Ph.D. student in the Department of Civil and Environmental Engineering, University of Maryland, College Park. Based on the selection process, *Pseudomonas fluorescens* Uper-1 was chosen as the organism for these experiments, and was obtained from Dr. D.R. Lueking (Department of Biological Sciences, Michigan Technological University, Houghton, MI, USA). This organism is able to aerobically utilize naphthalene as a

sole source of carbon for growth and displays no other growth factor requirement (Whitman et al. 1998). A stock culture of Uper-1 was maintained by periodic subculture on nutrient agar in the presence of naphthalene vapor and was stored at 4 °C in a refrigerator. Batch growth of Uper-1 was routinely conducted in 50-mL side-arm flasks at 30 °C with shaking (240 rpm) in a glycerol-based basal salt medium (BSM). The BSM contained (per liter at pH 7.0): 4 g KH_2PO_4, 4 g NaH_2PO_4, 2 g $(NH_4)_2SO_4$, 0.2 g $MgSO_4 \cdot 7H_2O$, 0.001 g $CaCl_2 \cdot 2H_2O$, 0.001 g $FeSO_4 \cdot 7H_2O$, and 1.5% w/v glycerol. Batch culture growth in the side-arm flasks was monitored turbidimetrically (wavelength = 510 nm) utilizing a Spectronic 21 spectrophotometer (Bausch & Lomb).

The Uper-1 inoculum utilized for the preliminary batch respirometry experimental studies was prepared in 50 ml side-armed flasks using the following procedures. The inoculum was first grown on glycerol (ACROS, 99+ %) in MSNS as a primary culture, followed by growth on naphthalene in MSNS as a secondary culture. Five flasks were used for each batch preparation. Fifty ml of MSNS was added to each side-arm flask, two of which also contained glycerol (1.5% by volume). The flasks were closed with cotton balls, wrapped with foil paper, and autoclaved (121°C for 15 minutes).Using aseptic techniques, a Uper-1 plate culture was used to inoculate the duplicate flasks with glycerol. A third flask with MSNS only was used as a control. The three flasks were shaken in a water bath at the temperature of 30°C for about 24 hours. The absorbance was monitored to determine the phase of growth. Once the culture arrived in the late exponential phase, 0.5 ml (1%) of the primary culture was transferred into the remaining two flasks, into which filter-sterilized

naphthalene in DMF had been introduced to reach the desired concentration of 5 mg/L. These two flasks were then shaken in the same water bath for about 6 hours. Again the absorbance was monitored to assess when the culture had reached the middle of the exponential phase, at which point the culture was used as the inoculum in the preliminary respirometry studies described in Section 5.3.4.

The Uper-1 culture used for inoculating the ISFC was initially prepared in five 250 ml flasks containing autoclaved BSM, by following the same procedures as described for the batch respirometry experiments. Once the initial culture reached the late exponential phase, the prepared cells were harvested by centrifugation (12 000 x g for 10 min), and freed of residual glycerol by washing three times in BSM minus glycerol. The washed culture was then resuspended in 500 ml BSM lacking glycerol, and used to inoculate 30 L of the autoclaved MSNS artificial groundwater containing 5 mg/L naphthalene. The second culture was then incubated for 24 h at a room temperature, after which the heterotrophic plate count (HPC) was 8.5×10^{11} CFU/L. The secondary culture was used to ensure that the microorganisms had fully adapted to growth on naphthalene medium before inoculating the ISFC.

5.2 Intermediate-Scale Flow Cell (ISFC)

5.2.1 Sizing of ISFC

In this research it was very important to size the flow cell reactor in such dimensions that it could satisfactorily represent the heterogeneity in natural systems, but in a controlled way that allowed a complete description. In reviewing previous studies in the literature, there are a variety of sizes of intermediate-scale flow cell reactors that have been used for various purposes, with flow cell lengths ranging from

less than 1m to up to 10m. These flow cells are summarized in Table 5.3 in terms of their size and experimental use.

For this research, the flow cell dimensions were selected such that it is essentially a two dimensional reactor, that is, the contaminant plume is only varying in the longitudinal and vertical directions. This was done because the two-dimensionality reduced the complexity of the monitoring problem in the bioremediation simulation experiments as well as the mathematical modeling of these experiments. Therefore, the flow cell needed to be sufficiently narrow to ensure homogeneity across its width, yet wide enough to cause negligible wall effects for the contaminant migration. In the study of Klotz et al. (1980), they found that in order to be able to neglect boundary disturbances, the relationship between the average grain diameter, d_{50} and the column diameter, d_c, must meet the following relationship: $d_c \geq 25\ d_{50}$. The maximum sand size d_{50} (for the coarse sand) in our experiment is 1.2 mm. Therefore, the flow cell diameter needs be larger than 3 cm. On the other hand, the flow cell should be narrow enough to eliminate significant effects of dispersion in the horizontal transverse direction. In order to study the dispersion effect in the horizontal transverse direction, model simulations were made using RT3D in a three dimensional scenario and it was verified that the transverse dispersion is negligible with a width of 10 cm. Based on the d_c calculation, the model simulations, and the values from the literature, a flow cell width of 10 cm was selected. This selection was somewhat conservative, but reasonable considering that, some operations, such as sampling, would be more challenging with a narrower width.

Table 5.3 Summary from literature study of flow cells and their applications

Authors	Flow cell size (length ×height ×width)	Purpose of study
Bath et al. (2001)	10 m ×1.2 m ×0.06 m	To investigate the flow and transport in a two-dimensional intermediate-scale, heterogeneous medium
Silliman and Dunlap (2001)	1.6 m ×0.67 m ×0.094 m	To study a bacterial transport in porous media
Murphy and Ginn (1997)	1 m ×0.2 m ×0.1 m	To investigate the influence of physical heterogeneity on microbial degradation and distribution in porous media
Pearce et al. (1994)	0.75 m×0.37 m×0.21m	To evaluate the dissolution of tricholorethylene (TCE) and trichloroethane (TCA) pools in saturated subsurface systems
Szecsody et al. (1994)	1 m ×0.2 m × 0.1 m	To study the transport and biodegradation of quinoline in horizontally stratified porous media
Voudrias and Yeh (1993)	1 m ×0.3 m ×0.2 m	To evaluate dissolution of a toluene pool under constant and variable hydraulic gradients with implications for aquifer remediation

In addition to the appropriate selection of the flow cell width, the flow cell longitudinal and vertical dimensions were also very important factors. As for the longitudinal dimension, it was important to select a length that would allow subsequent bioremediation simulation experiments to be run for a significant length of time during which interlayer mass transfer could be observed before the flow cell boundaries were encountered by the plume. This allowed for the study of the contaminant plume and associated chemical and microbiological gradients through the whole length of the flow cell. With respect to the vertical dimension, the same constraints held as in the longitudinal direction. In addition, it was very important to have enough space in the vertical direction to create the desired K heterogeneity.

Based on the constraints described above and the literature review, different flow cell sizes were tested using RT3D in VMOD. With regard to the length, because

of space limitations in the laboratory, flow cell lengths on the order of 10 m, such as used by Bath et al. (2001) were not feasible. Therefore, based on the laboratory space constraints, lengths of 1 m, 1.2 m, and 1.5 m were chosen for model simulations of the transport of a step input of conservative tracer in the flow cell. The results demonstrated that there were no real significance differences among these three lengths. The only difference was that the longer the flow cell, the longer was the time required for the solute plume to reach the end of the flow cell. Correspondingly, the time to reach steady state was also different in each case. Based on these model runs, and assuming an observation period of about one-week's length during the transitory phase of each experiment would be sufficient for adequate data collection, a flow cell length of 1.2 meter was selected.

The flow cell heights chosen for testing in the modeling simulations were 0.2 m and 0.3 m, based on the literature review. Based on model simulations, a height of 0.3 m was selected over 0.2 m, because of the greater flexibility with 0.3 m. For example, with a height of 0.3 m, the bottom, low-K layer, could be set as deep as 0.2 m, which provided more space for the observation of dispersion. In addition, with the height of 0.3 m, it is be more convenient to set up multiple layers to simulate more complex heterogeneities in future experimental studies using the flow cell.

In summary, based on the literature study and model simulations, the dimensions for the flow cell were selected to be 1.2 meter long (horizontal direction, x coordinate), 0.3 meter high (vertical transverse direction, z coordinate), and 0.1 meter wide (horizontal transverse direction, y coordinate).

5.2.2 Flow Cell Material

After sizing the flow cell, the next step was the design and construction of the flow cell reactor. A schematic of the basic design of the reactor assembly is presented in Figure 5.1. The flow cell was designed to simulate a heterogeneous sand aquifer, with the groundwater flow represented by the water pumped through the reactor.

The walls, bottom, and the lid were made from untempered glass (Glass Distributors Inc., Bladensburg, MD, USA). Glass has been a very common choice in previous similar studies, e.g., (Voudrias and Yeh 1994; Whelan et al. 1994). There were at least two reasons for the selection of glass: (1) it allows visual observation of the reactor, and (2) glass is a hydrophilic surface, which prevents the preferential wetting and spreading of hydrophobic organics. Untempered glass was chosen so that it would not shatter when holes for sampling needles, influent fittings and effluent fittings were drilled. A glass thickness of $\frac{1}{2}$" was chosen based on literature review and consultation with professionals from Glass Distributors Inc.. The dimensions of the glass plates used are as follows: two side wall plates $52\frac{1}{4}$" long $\times 16\frac{3}{4}$" wide; two end wall plates $16\frac{3}{4}$" long $\times$ 5" wide; one top plate $52\frac{1}{4}$" long $\times$ 5" wide; and one bottom plate $53\frac{1}{4}$" long $\times$ 5" wide (Item 1, Appendix A).

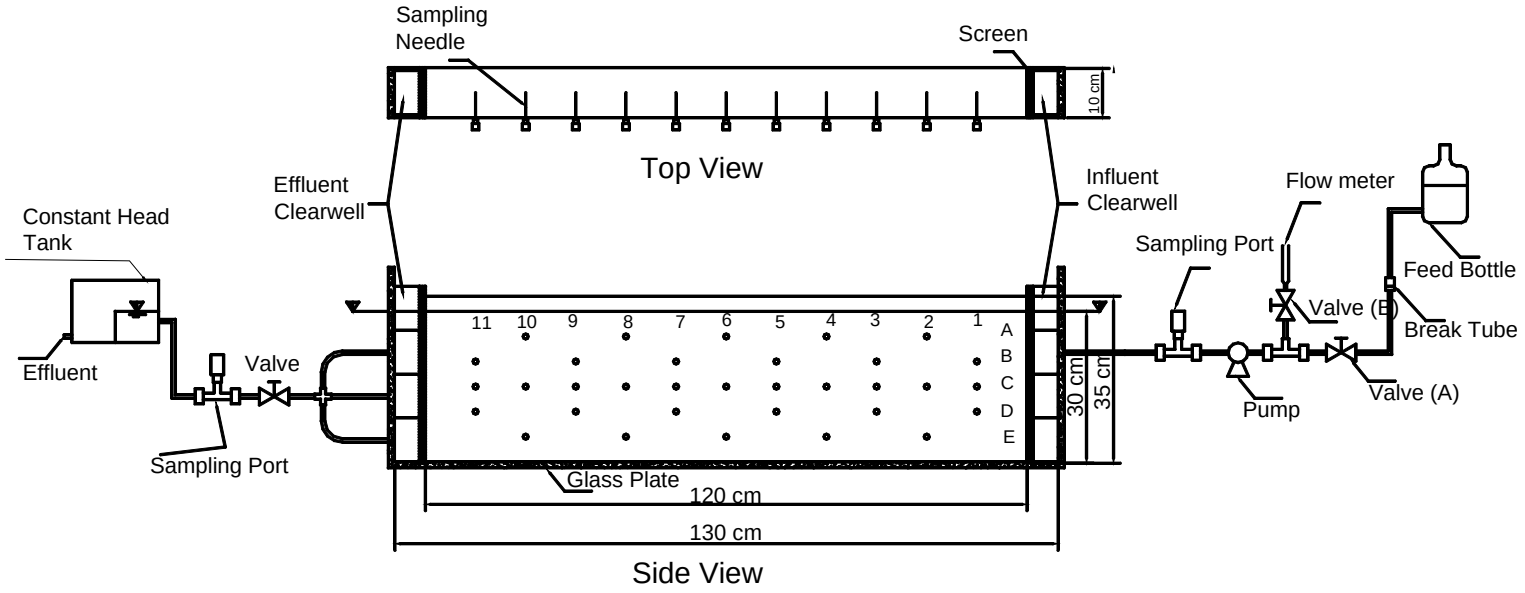

Figure 5.1 Schematic diagram of experimental aquifer assembly with influent and effluent appurtenances, and sampling port identification.

To support the weight of the filled flow cell reactor and ensure the integrity of the glass flow cell, it was necessary to provide a support structure. This structure had two components. First, an aluminum frame was selected for supporting the reactor walls. An aluminum frame provided a strong support structure, yet allowed flexibility in fabrication. Second, because of the large size and heavy weight of the flow cell when filled with the porous media, it would be very difficult to move the flow cell in the laboratory. In order to solve this problem and provide increased flexibility and ease of operation during experiments, the aluminum frame was attached to an aluminum cart. The cart was made of 3.8 cm$\times$0.3 cm aluminum strips with overall dimensions of 6' (L) $\times$16" (W) $\times$33" (H), which supported a top surface made from a piece of 6' (L) $\times$16" (W) $\times$ $\frac{1}{4}$" (Thickness) aluminum sheet. Four thermoplastic Rubber Wheels (Item 2, Appendix A) with brakes (Item 3, Appendix A) were installed on the cart so that it can be easily moved around in the laboratory, or held in place.

5.2.3 Inlet and Outlet Assemblies

The flow cell was equipped with vertical clearwells at the influent and effluent ends, which created medium zone of 1.2 m in length and functioned to provide an even distribution of the inflow and outflow across the sand. To form the clearwells and contain the sand, stainless-steel screens were installed in the flow cell. The screens were made out of stainless-steel to provide chemical resistance, with dimensions of 10 cm wide and 35 cm high. The screens were positioned the correct distance from the end walls to create the desired size of clearwells, which were nominally 5 cm long (Figure 5.1). In designing the screens, two requirements had to

be met. One, the screens should distribute the inflow and outflow evenly. Two, the screens had to contain the sand. Most designs used by other researchers, e.g., (Pearce et al. 1994; Voudrias and Yeh 1994; Whelan et al. 1994) have used an 80-mesh stainless-steel wire cloth (mesh opening = 177 μm) to provide the permeable screen. However, in this study, a very fine sand (d_{10} = 0.15 mm) was used to create the hydraulic conductivity heterogeneity; therefore, a 150-mesh stainless-steel wire cloth (mesh opening = 66 μm) was chosen to form the screens (Item 4, Appendix A). The screens were fabricated in the Clark School of Engineering machine shop by Mr. Bernie LaFrance. The wire cloth was sandwiched in between two single one-piece frames fabricated from stainless steel (Item 5, Appendix A), and the assembly was held together using 24 stainless steel bolts. Eleven of the bolts were chosen to be longer than the others to position the screens the correct distance from the end walls. The bolts were secured with nuts (Item 6, Appendix A). In addition, two hex nuts were placed at each end of the longer bolts to provide a larger area to set against the walls.

Another key aspect of designing the inlet and outlet assemblies was the selection of appropriate influent and effluent tubing and fittings for providing the flow to and from the influent and effluent clearwells, respectively. Because both the influent and effluent contained simulated groundwater with the naphthalene model contaminant, it was important that all the parts be made of a material that was resistant to the contaminant. Teflon was selected to meet the requirement and all tubing and fittings mentioned below are made of Teflon unless noted otherwise. For the influent flow, a Teflon bulkhead Union (Item 7, Appendix A) and white Teflon

washer (Item 8, Appendix A) were used to connect the influent tubing (Item 9, Appendix A) to the influent clearwell. The union had a compression fitting into which the $\frac{3}{8}$" O.D. Teflon influent tubing was inserted. Next, a reducing union (Item 10, Appendix A) was used to change from the $\frac{3}{8}$" O.D. Teflon tubing into $\frac{1}{4}$" Teflon tubing (Item 11, Appendix A) because of connection convenience. An influent sampling port was then installed in the influent flow line. The sampling port consisted of a branch tee (Item 12, Appendix A) and a Mininert valve (Item 13, Appendix A). Next, a Masterflex® L/S® PTFE-tubing pump (Item 14, Appendix A) was installed upstream of the sampling port, to control the simulated groundwater flow. Finally, a simple flow-meter was installed upstream of the sampling port, between the feed bottle and the pump. The flow meter was constructed using a branch tee (Item 12, Appendix A) inserted into the influent line, with one valve (valve A) (Item 15, Appendix A) installed in the upstream line, and one valve (valve B) in the branch line. In addition, there is a 20 ml glass pipette installed in the branch line. A schematic of the flow-meter is shown in Figure 5.2. During normal flow cell operation, the valve B was closed. However, to measure the flow rate, valve B was opened and the feed solution was allowed to fill the flow meter pipette. The valve A was then closed and the flow rate was determined by measuring the time required to pump a certain volume of solution from the pipette. After measuring the flow rate, valve A was opened and valve B was closed.

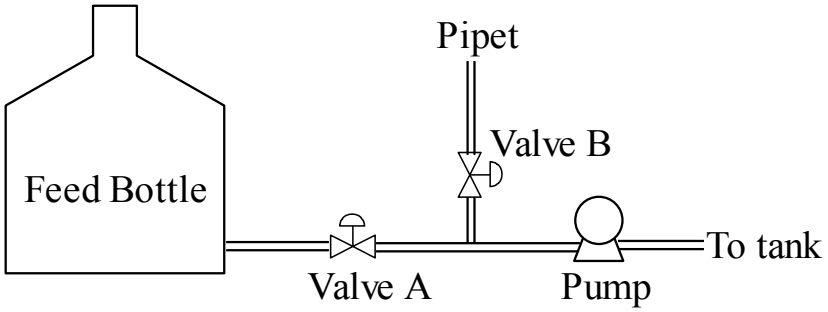

Figure 5.2 Schematic of in-line flow meter.

The effluent flow system involved an assembly of three $\frac{1}{4}$" O.D. Teflon tubes (Item 11, Appendix A) leaving the effluent clearwell at different elevations to form a single mixed effluent stream (Figure 5.1). The three outlets were placed 10 cm, 17.5 cm and 25 cm above the bottom of the flow cell, respectively. This effluent system yielded representative, vertically-averaged effluent concentrations. Three bulkhead unions (Item 16, Appendix A) and white Teflon washers (Item 17, Appendix A) were used to connect the tubing and clearwell. These three effluent tubing lines were brought together in a union cross (Item 18, Appendix A). The effluent line then continued as a single line to a valve (Item 15, Appendix A), which allowed the flow leaving the flow cell to be stopped, and then to a sampling port, the same as described for the influent line, which allowed sampling of the flow cell effluent. The union cross and the sampling valve were held by three-prong clamps on the same support stand. The effluent continued to a constant-head reservoir, which could be raised or lowered to set the hydraulic head at required elevation to create the desired flow (Figure 5.1). The effluent tubing was connected to the constant-head reservoir by a male pipe adapter (Item 19, Appendix A). The constant-head reservoir was placed on a support stand to facilitate its upward and downward movement for adjusting the water-level in the flow cell. From the constant-head reservoir, the effluent flowed through a long segment of $1/4$"O.D. Teflon tubing that led into an activated carbon trap (Barnstead/Thermolyne, Dubuque, IA U.S.A.), which was used to sorb the naphthalene remaining in effluent. Subsequently, the effluent line was drained into a sink.

The dimensions of the adjustable constant-head reservoir were 8" (L) ×5" (W) ×4"(H), and it was constructed from 0.23" thick sheet of Extruded acrylic sheet (Item 20, Appendix A). The constant-head tank was also fabricated in the Clark School of Engineering machine shop by Mr. Bernie LaFrance. The constant-head tank was designed as a closed system to minimize the release of volatized naphthalene into the laboratory. Inside the constant-head tank, there was a 2.5" high barrier wall that formed a water basin at the influent end of the tank, the water surface of which defined the water level in the flow cell. Threads were drilled in the influent wall, effluent wall and top cover into which previously described male pipe adapters (Item 19, Appendix A) were screwed. The influent and effluent pipe adapters were used to connect the constant-head reservoir to the effluent tubing. The pipe adapter in the top cover was used to connect to an activated-carbon tube. This arrangement kept the pressure in the constant-head at atmospheric pressure, while permitting capture of any volatized naphthalene.

5.2.4 ISFC Construction

The glass plates for the flow cell wall were purchased and cut to size by Glass Distributors Inc. (Bladensburg, MD, USA). In addition, holes of appropriate size for the chosen influent and effluent fittings were drilled through the glass by Glass Distributors Inc. as well. The influent hole was $\frac{5}{8}$" diameter, and the three effluent holes were $\frac{1}{2}$" diameter. The holes for the sampling needles were drilled with a diameter of $\frac{1}{8}$", which was the smallest hole that the glass shop could drill.

After the glass was cut and drilled, the next step was to bond the plates together to build up the flow cell. The glass plates were bonded with silicone caulk (Item 21, Appendix A). Three persons were required to perform the assembly given the size and weight of the glass plates. During the assembly, the stainless-steel end screens were used as a guide to correctly place the sidewalls. After the finishing the assembly, the flow cell was left to dry for 48 hours.

After the flow cell was dried, all the excessive caulking was removed using a razor blade. Then, several water leakage tests were run. To do this, the needle holes were temporarily closed by silicone caulking (Item 21, Appendix A) and the influent and effluent fittings were put in place and sealed with silicone caulking. The flow cell was then filled with water to test for leakage. In the initial test, there were quite a few leaks detected. Therefore, more silicone caulking was placed along the inner edges of the flow cell to close the leaks, and provide a better seal. Another leakage test was then conducted and was 100% successful. At this point, the screens were put in place, and silicone caulking was used to close the small gap between the screen frame edge and the glass wall to prevent sand grains from slipping around the screen into the clearwells. A third water leakage test was carried out at this point and successfully demonstrated no leaks.

The final step was to construct and install the aluminum frame around the flow cell for structural support and ease of handling. The aluminum frame, which was also constructed in the Clark School of Engineering machine shop by Mr. Bernie LaFrance, was made such that it did not touch the glass flow cell. Instead, a 5 mm gap

was left open between the glass and the frame. The gap was filled with rubber pads that held the flow cell tightly in place.

5.2.5 Pore Water Sampling Ports Installation

A two-dimensional network of $\frac{1}{8}$"sampling ports was drilled in the front glass wall, as discussed above. The positions and labels of the sampling ports are shown schematically in Figure 5.1 as well. The locations of the ports were selected on the basis of the designs used in previous studies found in the literature and economic considerations. The nominal distance between ports in a horizontal row was 10 cm and the distance between each row of ports in the vertical direction was 5 cm. Stainless-steel, Luer-lock, 18-gauge hypodermic needles (Item 22, Appendix A) were used to create the sampling ports. The needles were originally 4" long, but were cut down to a length of $2\frac{9}{16}$"in order that the end could be positioned at the center of the flow cell. The needles were inserted into the holes drilled in the glass and fixed in place. The major difficulty in this process was to locate the sampling needles exactly in place through the drilled holes, with the needle tip at the center of the flow cell in the desired vertical and horizontal location. This was made more challenging by the fact that the drilled holes ($\frac{1}{8}$" diameter) were much larger than the needle diameter (0.022" O.D.)

To assist in precisely locating the needle tips, a balsa wood (Specialized Balsa Wood, Loveland, CO, USA) board was fashioned that had pin holes punched through it that were located to match the center of the holes on the front glass wall. The board was fabricated in such a way that when it was placed in the flow cell, the needles

passed through the center of glass holes, and then through the holes on the board, with the needle tips just reaching to the opposite side of the board, at which point the needle tips were located at the center of the flow cell. When the needles were properly located, a small amount of 5-minute Epoxy caulking was first put in the holes in the glass wall to position the needles because Epoxy caulking can dry and harden quickly. Then, silicone caulking was used to seal the needles in place by filling the holes in the front glass. When the silicone caulking dried sufficiently, the balsa wood board was gently removed. After being fixed in place, the Luer hubs of the needles were plugged with removable Teflon Mininert sampling valves (Item 23, Appendix A).

A schematic of the flow cell's front glass wall showing the placement of each sampling needle is presented in Figure 5.3. Each needle location is referenced by a letter for its row and a number for its column, which were used to label each sampling location. The exact position of each needle tip was measured after the installation of the sampling needles. Each needle tip location is defined by an x- and a z- value, as measured from the inside lower corner of the screen on the influent side. The locations are listed in Table 5.4. A photograph of the glass flow cell with the screens, sampling ports, and aluminum frame and cart in place is presented in Figure 5.4.

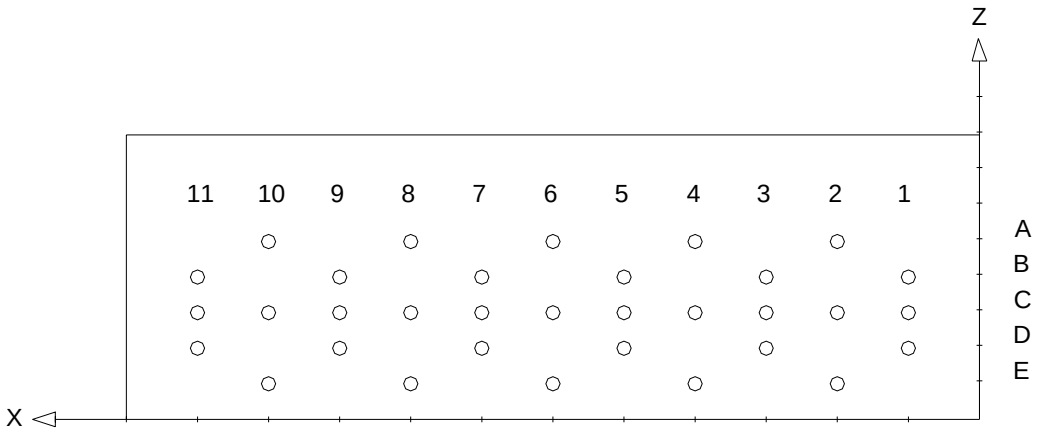

Figure 5.3 Placement of Sampling Needles.

Table 5.4 Placement points of the sampling needle tips

Needle No.	X location (cm)	Z location (cm)
B1	15.5	21.3
C1	15.5	15.9
D1	15.5	10.5
A2	25.6	26.7
C2	25.6	16
E2	25.6	5.1
B3	35.7	21.3
C3	35.7	16
D3	35.7	10.5
A4	45.9	26.7
C4	45.9	16
E4	45.9	5.1
B5	56.0	21.2
C5	56.0	15.8
D5	56.0	10.5
A6	66.2	26.7
C6	66.2	15.8
E6	66.2	5.1
B7	76.3	21.2
C7	76.3	15.8
D7	76.3	10.5
A8	86.5	26.7
C8	86.5	15.8
E8	86.5	5.0
B9	96.6	21.1
C9	96.6	15.9
D9	96.6	10.5
A10	106.7	26.6
C10	106.7	15.7
E10	106.7	5.0
B11	116.8	21.1
C11	116.8	15.6
D11	116.8	10.2

Figure 5.4 Glass ISFC with screens, sampling ports, and aluminum frame and cart.

5.2.6 Sand Selection, Characterization and Packing

To simulate macro-scale heterogeneities, the sand flow cell reactor used in these experiments was set up with two layers of sand with differing hydraulic conductivities. Therefore, a variety of sands were evaluated for possible use in this study as the simulated aquifer media. The two sands ultimately selected for use in this research were: (1) Mystic White II from U.S. Silica Company (Berkeley Springs, WV, USA), and (2) Filtersil sand from Unimin Corporation (New Canaan, CT, USA). Specifically, Mystic White II was selected for use in the fast-K layer and Filtersil sand was chosen to be used in the low-K layer. These sands were selected because of the difference between their hydraulic conductivities, as discussed below, which was sufficient to create a model aquifer with the stratified hydraulic conductivity heterogeneity required for this study. The coarse sand and fine sand have d_{10} values of 0.8 mm and 0.15mm, respectively, based on data provided by the manufactures. The bulk density, particle density and porosity of each type of sand in the experimental aquifer were determined as discussed in the Parameter Estimation Experiments Section (5.3.2 Porous Media Density and Porosity). In addition, the following properties were determined by Agri Analysis, Inc. (Leola, PA USA) for the Mystic White II sand after it was prepared as described below. The cation exchange capacity (CEC) = 0.3, percentage of organic matter = 0.4%.

Prior to their emplacement in the flow cell, the sands were prepared following the procedures of Murphy et al. (1997). First, trace contaminants were removed from sand by washing with 0.25 M NaOH for 12 hours, followed by 0.25 M HNO_3 for 12

hours. Then, after thorough rinsing with deionized water until the pH reached approximately 7, the sands were autoclaved.

Based on the literature, both dry, e.g., (Oliviera et al. 1996) and wet packing, e.g. (Pearce et al. 1994; Voudrias and Yeh 1994; Whelan et al. 1994) methods have been used in previous sand-tank laboratory experiments. Oliviera et al. (1996) studied the packing of sands for the production of homogeneous porous media and concluded that a dry packing consisting of the deposition of sequential 0.2-cm layers, each followed by compaction with a metal pestle, or a wet packing while vibrating columns, are the best options. In either operation, the sand was always poured or sprinkled in small batches to prevent the preferential deposition of large grained material. Furthermore, the sand was always deposited from a height of 0.5 cm to prevent heap formation. Neither of these techniques could be applied in this research exactly as described: the dry packing technique could not be used because of the interference to the pestle by the sampling methods, and no method of vibrating the flow cell was available for the wet packing method. However, in some previous research studies (Pearce et al. 1994; Voudrias and Yeh 1994; Whelan et al. 1994), another wet packing method was applied for packing the flow cells. In preliminary experiments by these authors, small slugs of a methylene blue dye injected at different places in the aquifer showed that the flow was uniform without field variations introduced by the packing procedure.

Therefore, the same packing technique used by Voudrias and his coworkers was adopted to pack the sands into the ISFC. Specifically, the ISFC was filled with sand by applying about 0.5 kg at a time with a beaker, under a water head of 5 cm

maximum. Sand was always poured through ≤ 5cm of water in order to prevent entrapment of air bubbles and reduce sand stratification. The same sequence of water addition and deposition of 5-cm sand layers was repeated until the entire aquifer was formed, with the water level always maintained above the top of the sand. The ISFC was filled with fine sand to a level of 15 cm, followed by another 15 cm of coarse sand. After the aquifer was formed, it was flushed with DI water for three days. Then the water level was lowered 3 cm, thereby creating a capillary fringe zone of ~ 3cm, which was controlled by the adjustable constant-head reservoir. The top of the sand was covered with a sheet of aluminum foil to minimize volatilization from, and spilling of undesired materials or chemicals into, the simulated aquifer. The ISFC was at that point ready to be utilized in the bioremediation experimental investigation.

5.3 Parameter Estimation Experiments

In past studies of heterogeneous systems, a rarely stated underlying assumption of scaling up in engineered bioremediation is that the heterogeneity can be explicitly represented, with parameter values that are measured in batch and/or column studies producing accurate flow and mass transport results at a larger scale. An improved understanding of how measured hydraulic and transport parameter values relate to *in situ* values is needed to examine this assumption, however, the same assumption was inherent in this work. Specifically, to describe the controlled heterogeneous experiments in the ISFC, and the associated detailed observations of flow and transport, it was necessary to have the following parameter estimates: hydraulic conductivity, bulk and particle densities, porosity, dispersivity, biokinetics, and sorption/desorption equilibrium and kinetics.

5.3.1 Hydraulic Conductivity

There are three commonly used methods for hydraulic conductivity, K, measurement: field tests, laboratory tests, and empirical and semi-empirical methods based on grain diameters and grain size distributions. Of most interest here are the laboratory testing techniques, which typically include the constant head and falling head methods. Of these, the constant head method was employed in these experiments to measure the saturated hydraulic conductivity. Prior to the hydraulic conductivity experiment, the sands were treated following the procedures from (Murphy et al. 1997), as previous described in Section 5.2.6.

The hydraulic conductivities of the sands were measured by the constant-head method using a gradient ratio permeameter (Figure 5.5). The method requires setting up a cylindrical clear permeameter with a soil sample (in this case sand) of length L and cross-sectional area A, and passing water through the system by applying differential heads, H. Measurements of the differential heads with steady a flow rate, Q, were taken at different time intervals to determine hydraulic conductivity by applying the following equation, derived from Darcy's law,

$$K = \frac{QL}{AH} \tag{5.2}$$

where K = hydraulic conductivity, [LT^{-1}]; L = length of sample, [L]; A = cross-sectional area of sample, [L^2]; Q = outflow rate, [$L^3\ T^{-1}$]; H = fluid head difference across the sample, [L]. The major pieces of equipment required for performing the constant head test are illustrated in Figure 5.6, and include the permeameter, two constant water head devices (one mounted on a jack stand adjustable and one stationary), and manometer boards.

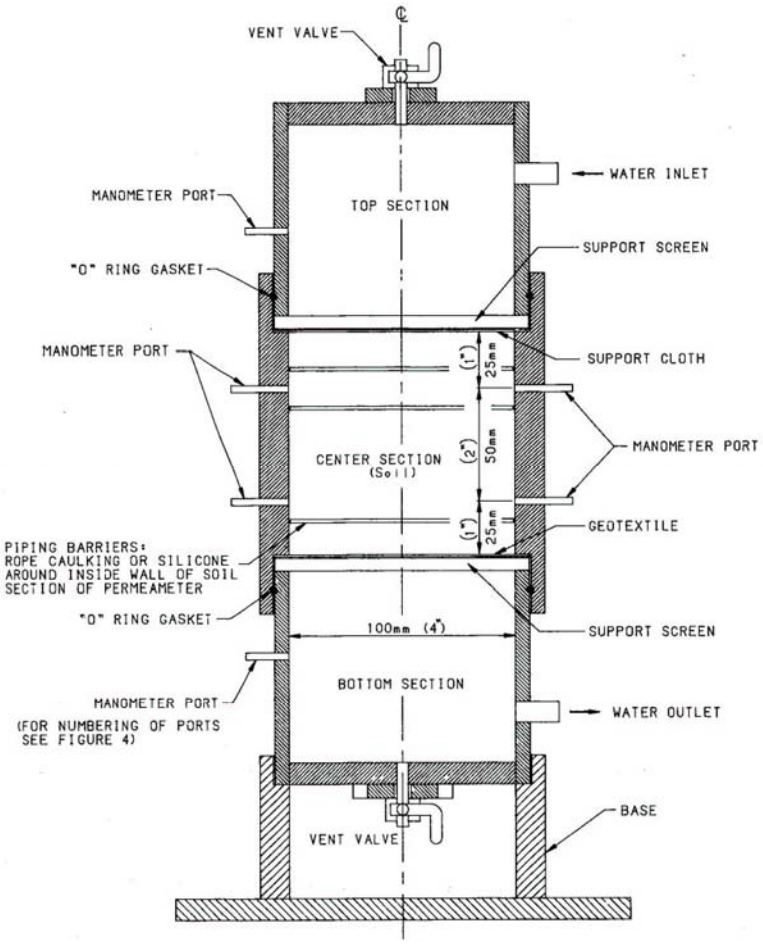

Figure 5.5 Schematic of the permeameter for the constant head method (ASTM-D2434 2000).

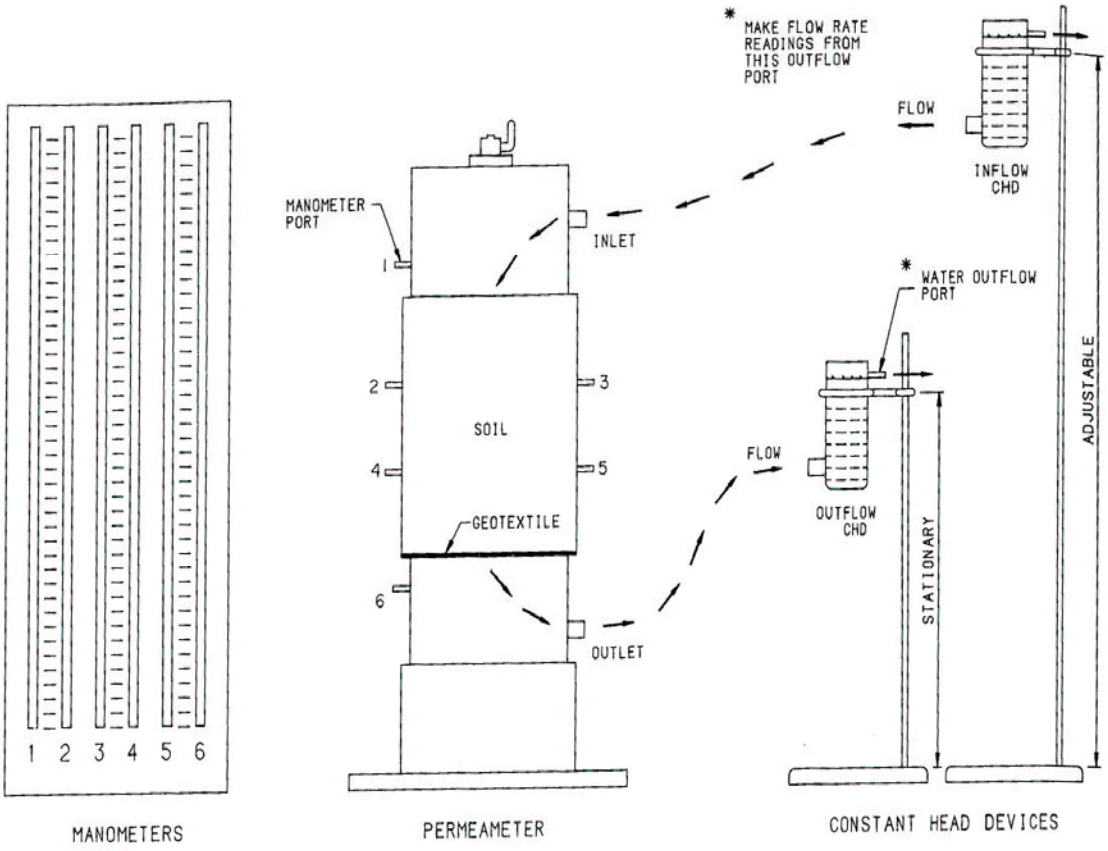

Figure 5.6 Schematic of the permeameter set up for the constant head method. (ASTM-D2434 2000)

The specific steps in performing the constant head test were as follows, beginning with sand placement. First, before sand placement, the center section of the permeameter was weighed on a scale. In the second step, the sand was placed above the support cloth to a total depth of 110 mm. The final depth of sand should be approximately 100 mm, which was checked after completion of the experiment. During placement, the clean sand was poured carefully into the permeameter with a maximum drop of soil no greater than 25 mm. No consolidation procedure was utilized. A sand leveler was used to remove any excess sand. Third, the weight of the center section was taken again for determination of the bulk density, which provided an indicator of how close the packing of the sand in permeameter was close to that of ISFC.

Permeameter assembly followed the sand placement. First, the support screen and the bottom section of the permeameter were aligned and inserted into the center section. When the bottom was secured, the permeameter was positioned into the holding stand. The sand was now compressed from 110mm to 100 mm. Subsequently, the inflow and outflow constant head devices were connected to their corresponding permeameter ports (Figure 5.6) with plastic tubing. Specifically, the outflow device was attached to the bottom permeameter port and the inflow device was attached to the top permeameter port. All of the manometer tubes were then connected to their corresponding permeameter manometer port, and all over-flow tubes to their corresponding outlet ports.

Following the permeameter assembly, the next step was to saturate the system. To accomplish this, a piece of long tubing with very small I.D. was inserted

into the bottom section of the permeameter through the tubing used to connect the water outlet and the outflow constant head device, until one end of the tubing reached the ceiling of the bottom section, with the other end extruding out the outflow constant head device and into the air. Next, the top vent valve on the permeameter was opened and the permeameter water outlet was closed off. The permeameter was then backfilled with water through the outflow constant head device. The air trapped in the system were sucked out via the small I.D. tubing through the open end for about 5 minutes until all air bubbles were removed from the system. The top vent valve on the permeameter was then clamped off and the system was allowed to stand overnight in a no-flow static condition to ensure complete saturation of water. After the saturation of the system, a recorded volume, V, of the outflow water was then collected in a container over a time period, to calculate the flow rate, Q ($=V/t$) at the applied differential heads. The tests were performed in duplicate for each sand to investigate the effect of any variability in the packing sand.

5.3.2 Porous Media Density and Porosity

The bulk density, ρ_b, and particle density, ρ_p, were determined experimentally for the Mystic White II sand and the Filtersil sand. Both sands were dried at 104°C in the oven for 24 hours before the density experiments.

The bulk density was determined in two ways: (1) batch experiment in 100 ml graduate cylinders; and (2) experimental estimation while packing the ISFC. First, in the batch experiment, each type of sand was added to about the 20 ml mark of a 100 ml graduate cylinder. The sand was compacted by tapping the cylinder base on the

palm of the hand. Following that, about 20 ml more of the sand was added and compacted as above. The steps were repeated until 80 to 100 ml of the sand was in the cylinder. The sand volume was recorded (ml) and the weight was measured. The experiments were carried out in triplicate. The bulk density was calculated using the equation of bulk density, ρ_b = (mass of dry sand / total volume of sand and air). Second, when the sands were packed into the ISFC, the mass of sand added was measured for the Mystic White II and Filtersil sands. The bulk density was then calculated by dividing the weight of each type of sand by half of the porous media volume of the ISFC.

The particle density was measured using a water-displacement technique (Blake and Hartge 1986). First, the mass of an empty flask was measured. Then, twenty five grams of dried sand was measured out, placed in the flask using a funnel, and the mass of the flask containing the sand was weighed. The mass of sand was doubled checked by deducting the mass of empty flask from the mass of flask with sand. Subsequently, about 50 ml of DI water was added in the flask. The sand/water mixture was brought to a gentle boil by placing the flask on a hot plate to ensure complete air bubble removal. The flask was then removed from the heat and allowed to cool. The flask was capped and allowed to sit for 24 hours. After 24 hours, the cap was removed and the flask was filled with DI water so that the bottom of the meniscus was at the 100 ml line. The 100 ml-sand/water mixture was then weighed in the flask, and the temperature was recorded using a thermometer. The mass of water was calculated by deducting the mass of flask with sand from the mass of sand/water mixture. The volume of water was obtained from the mass of water by using the

appropriate density of water at the experimental temperature, while the volume of sand was found by taking 100 ml minus the volume of water. Finally, the particle density was obtained using the equation of particle density, ρ_p = (mass of dry sand / volume of sand particles (air removed)).

Once the bulk density and particle density were obtained for the Mystic White II and the Filtersil sands, the porosity, n, was calculated by the equation,

$$\phi = 1 - \frac{\rho_b}{\rho_p} \tag{5.3}$$

5.3.3 Dispersivity

With regard to dispersivity, three different dispersivities were evaluated: (1) vertical transverse dispersivity (α_z) within the two layers, (2) the longitudinal dispersivity (α_x) within the two layers, and (3) the interlayer mass transfer (α_z'). A continuous point-source tracer study method that was adapted from Robbins (1989) was chosen to estimate the transverse dispersivity and longitudinal dispersivity within each layer. The interlayer mass transfer coefficient was estimated in the control experiments which are discussed in a later section (5.4.1 Control Experiments).

The basic approach of the continuous point-source tracer technique was as follows. First, a continuous injection of the conservative tracer was started via a sampling needle inserted to the centerline of each layer. The tracer concentration variations were then monitored with time at a down gradient sampling port at the same vertical location as the injection port. Prior to, and during, tracer injection,

simulated groundwater was flowing through the flow cell at a constant average pore water velocity, v_x, in the longitudinal direction.

The first step in performing these tracer studies was the selection of non-reactive tracer, which should be transported through the water system in a manner similar to the item of interest. A good tracer should be a stable substance, show no reactivity with the system components, and must have reliably quantitative detection at low concentrations (Behrens 1986). Based on these characteristics, two non-reactive tracers were selected for use in these experiments: bromide (Br) and fluorescein.

The non-reactive tracer initially used in the experiments was chosen to be potassium bromide (KBr), with mercury chloride ($HgCl_2$) added at a concentration of 400 mg/L to inhibit microbial activities in the flow cell. Bromide was chosen as the conservative tracer because it had been used extensively, e.g., (Bath et al. 2001) and the presence of mercury chloride as an inhibitor did not interfere with its measurement. The tracer injection solution concentration, C_0, was selected to be 0.1 M KBr, to maximize the tracer breakthrough concentrations, while avoiding density-induced flow effects. The concentrations of Br in samples taken from sampling port were quantified by ion chromatography (IC). However, after running three tracer studies with potassium bromide, the IC instrument was non-functional and the repair process was lengthy. Therefore, it was necessary to select an alternative tracer.

The second non-reactive tracer used was the organic compound fluorescein (sodium salt). Fluorescein is an excellent tracer because it is easy to detect and can be measured using either its strong fluorescence or highly absorptive character (Klonis

and Sawyer 1996). Compared to absorbance methods, fluorescence sensitivity is tens to thousands times better. Therefore, fluorescence was utilized to measure the fluorescein tracer concentration in this study. The other advantages of fluorescein include its low sorption tendency (Behrens 1986) and its relatively low temperature exponent (Feuerstein and Selleck 1963). The disadvantages are its pH sensitivity and its photochemical instability. However, Smith and Pretorius (2002) demonstrated that conservative behavior of fluorescein is possible if one correctly evaluates the system parameters. For example, Smith and Pretorius (2002) noted that for optimum results, pH should be between 6 ~ 10. They further concluded that the test area and samples must be protected from bright light when using fluorescein as a tracer so that the fluorescein can be used quantitatively. The simplest way to block light is to perform the test at night and to store samples in the dark.

For this study, the fluorescein dye solution (C_0 = 10 mg/L) and bulk feed solution were made using sodium bicarbonate-sodium carbonate in deionized water buffer solution (0.0138 M $NaHCO_3$, 0.012 M Na_2CO_3, pH = 10), with $AgNO_3$ added as a biocide. The experiment was set up as closely as possible to the approach described by Robbins (1989). This method involves three important factors: (1) the bulk flow of the reactor, (2) continuous point source injection of a known concentration of tracer, and (3) continuous sampling at a point downgradient of the point source. An average pore water velocity of 9 m/d was used in Robins' study (1989), which corresponded to a bulk flow rate of 75 ml/min for the reactor used in this study. However, the Teflon pump described Section 5.2.3 has a maximum flow rate of 65 ml/min. Therefore, for this study, a flow rate of 60 ml/min was selected,

corresponding to average pore water velocities of approximately 10 m/d and 0.75 m/d in the high-K and low-K layers, respectively.

The tracer point source injection was provided using a Harvard Apparatus Syringe Pump Model 22. To perform the injection, a 5-ml plastic syringe filled with tracer solution, which was connected via Tygon tubing to a stainless-steel microtube, was set in the syringe pump. The stainless-steel microtube was inserted through one of the sampling needles (B3 for the coarse sand in the high-K layer, and D3 for the fine sand in the low-K layer) in such a way that its tip matched the sampling needle tip location. Before the steel microtube was inserted into the sampling needle, it was ensured that the tracer solution reached the end of the microtube. The tracer injection was then begun, at a flow-rate, Q_n, of 0.05 ml/min, which was selected so as to not disturb the flow in the flow cell and was utilized successfully by Schicke (1996).

After the tracer injection began, samples were taken through a sampling needle (B3 for the coarse sand in the high-K layer, and D3 for the fine sand in the low-K layer), that was 20.2 cm downgradient of the injection needle at the same vertical location. The proper selection of the sampling location is an important factor to get valid results for dispersivity. Specific requirements have been described in detail by Robbins (1989). In addition, the sampling flow rate, Q_{sample}, should be a small fraction of the bulk flow so that the flow disturbances can be neglected. In the high-K layer, the sampling flow rate of less than 1.15 ml/min was achieved by opening the Mininert valve at sampling port B3, which corresponded to less than 2% of the bulk flow rate. In a low-K layer, the samples were taken using a pump (Gilson Miniplus 2, Vilier-le-Bell, France) at a flow rate of 0.7 ml/min to ensure negligible

disturbance to the slow flow in the low-K layer. In both layers, sample volumes of 2 ml were collected. To correct for the time difference between when the samples were taken and when the solution entered the sampling needle, a calculation based on the sampling flow rate and microtube diameter was performed to determine the time delay between when the tracer reached the needle tip and when it exited the Mininert valve. In this way, the "actual" sampling times were obtained by the subtracting the delay time from the original sampling times. The general experimental conditions for these tracer studies are summarized in Table 5.5.

Table 5.5 Point-source tracer experimental operational conditions

Fluorescein Experiments	Bulk flow rate (ml/min)	Sampling flow rate (ml/min)	injection flow rate Q (ml/min)	Concentration C_0 (mg/L)
High-K layer (a)	60	1.15	0.05	10
High-K layer (b)	60	1.15	0.05	10
High-K layer (c)	60	1.15	0.05	10
Low-K layer (a)	60	0.7	0.05	10
Low-K layer (b)	60	0.7	0.05	14
Low-K layer (c)	60	0.7	0.05	22
Low-K layer (d)	60	0.7	0.05	22

For each layer, the steady-state tracer concentration, C', at the sampling location was calculated by averaging the sample concentrations after they became constant. The vertical transverse hydrodynamic dispersion coefficient, D_z, was then calculated from an analytical expression, which assumes that the horizontal and vertical transverse dispersivities are equal (Robbins, 1989):

$$D_z = \left(C_0 Q\right) \Big/ 4\pi x C' \tag{5.4}$$

where: C_0 = the injection concentration; Q = the tracer injection rate; and x = the distance between the tracer injection port and the sampling port. The vertical transverse dispersivity (α_z) was calculated using,

$$D_z = D^* + \alpha_z v_x^{\,n} \tag{5.5}$$

where D^* is the effective coefficient of molecular diffusion in the porous medium, v_x is the average interstitial velocity, and n is 1.0 (Rose, 1977). In the experimental design, v_x was selected to be sufficiently large that molecular diffusion was negligible compared to mechanical dispersion, so that $\alpha_z = D_z \Big/ v_x$.

Longitudinal dispersivities were determined by using the tracer breakthrough curve at the sampling port, and the following equation (Robbins 1989):

$$\frac{C}{C'} = \frac{1}{2}\left(erfc\left(\frac{\left(x - v_x t\right)}{\left(2\left(D_x t\right)^{1/2}\right)} \right) \right) \tag{5.6}$$

where C = the tracer concentration measured down gradient at distance x over time, t, until steady state is achieved, and D_x is the longitudinal hydrodynamic dispersion coefficient. Only α_x and D_x are unknown in Equation 5.6. Therefore, the best-fit

values for v_x and D_x were obtained by using non-linear regression to fit Equation 5.6 to the experimental breakthrough curves.

The non-linear regression was performed using a FORTRAN program "trafit3d" (Schicke 1996), which calculates the sum of the squares of either the absolute or relative residuals between the normalized experimental conservative tracer data and the normalized flux-averaged concentration calculated using the continuous point source model at steady state as described by Robbins (1989) and gives as an output of the best fit longitudinal hydrodynamic dispersion coefficient, the average pore-water velocity and the porosity (Appendix 2). In this research, the absolute non-linear regression was utilized. The best fit v_x and D_x parameters are obtained using a modified Levenberg-Marquardt method to minimize the sums of the squares of the residuals between the observed and calculated concentrations. The longitudinal dispersivity (α_x) was calculated using,

$$D_x = D^* + \alpha_x v_x^{\,n} \qquad (5.7)$$

As in the determination of α_z, v_x was selected to be sufficiently large that molecular diffusion was negligible compared to mechanical dispersion, so that $\alpha_x = D_x / v_x$.

5.3.4 Biodegradation Kinetics

Microbial kinetic parameters for growth of Uper-1 on naphthalene were estimated in batch experiments conducted in support of the simulated bioremediation experiments in ISFC. Some of these experiments were performed in conjunction with, or by, Ms. Eunyoung Hong. Biokinetic parameters are commonly measured in batch systems using suspended cells in a liquid medium. One of the advantages of this

approach is that mass-transfer limitations are minimized. Another key advantage of batch tests is the ease of performing the test and the quickness with which the test can be done (Grady Jr. et al. 1996). However, Monod kinetic parameters estimated using non-steady-state batch analysis are subject to large uncertainties. These uncertainties are a function of the initial experimental conditions, the values of parameters, the type and magnitude of the measurement errors, and the number of samples (Liu and Zachara, 2001).

Due to the large uncertainties related to the kinetic parameters estimation, careful manipulation of experimental conditions was required to reduce the correlations between the Monod parameters, thereby allowing for the estimation of unique parameters with the lowest degree of uncertainty. Liu and Zachara (2001) found that the correlation and relative standard deviations of Monod parameters are a function of a few dimensionless variables involving the initial substrate concentration, S_0 , and the initial biomass concentration, X_0. Analysis of these dimensionless variables allowed for identification of the optimal experimental conditions for estimation of unique and accurate Monod kinetic parameters.

For the purpose of this research, the concentrations of naphthalene and biomass were expressed as chemical oxygen demand (COD). Thus, all mass-related parameters, such as K_s and the yield coefficient, Y , were expressed as mg/L as COD and units of biomass COD formed per unit of naphthalene COD removed, respectively. Grady and co-workers define kinetic parameters obtained with a high S_0 to X_0 ratio (e.g., $S_0 / X_0 > 20$, both as COD) as the "intrinsic" kinetics, that is, the

maximum capability of the culture (Grady Jr. et al. 1996). On the other hand, "extant" biokinetics, which represent the capability of the culture in the source reactor from which it was obtained are determined with a low S_0/X_0 (e.g., $S_0/X_0 < 0.025$, both as COD) (Grady Jr. et al. 1996).

In this work, preliminary batch biokinetics determinations were performed under intrinsic and extant conditions using batch culture of Uper-1 as the inoculum. In addition, batch experiments were also carried out to estimate the biodegradation kinetics for the biomass in the flow cell once the ISFC experiments were started. It was originally planned to perform these experiments under extant conditions. However, the cell concentration collected from the effluent samples was very low, which made it impossible to set up the required low S_0/X_0. Therefore, the batch experiments utilizing the cell culture from the effluent samples were all set up with a high S_0/X_0 to represent the "intrinsic" biokinetics in the flow cell. This approach worked for the Scenario #1 Phase I sample. However, during Scenario #2 Phase I, with inhibited biodegradation, no usable data were obtained using the ISFC effluent inoculum under intrinsic conditions, as discussed in Chapter 6. Therefore, it was necessary to use the results of an "extant" kinetics study with the primary culture Uper-1 inhibited by high salinity to obtain the kinetic parameters for Scenario #2 Phase I.

In the kinetic parameters study, respirometry (Challenge AER-200, Aerobic/Anaerobic respirometer system, Challenge Environmental Systems, Inc.) was used to estimate the kinetic parameters of aerobic naphthalene biodegradation by

Uper-1. The basis for batch respirometry is the balanced equation for microbial growth that links substrate consumption, biomass growth, microbial product formation and oxygen uptake (Smets et al. 2001):

$$S + -(1-Y)O_u \Leftrightarrow YX + Y_P P \qquad (5.8)$$

where, S is the instantaneous substrate concentration (M/L^3), Y is the true biomass yield coefficient (M/M), O_u is the accumulative oxygen uptake (M/L^3), X is the instantaneous biomass concentration, Y_p is the product yield coefficient (M/M), and P is instantaneous microbial product concentration (M/L^3).

During a batch growth assay using respirometry, time-series profiles for oxygen uptake are obtained. In this study, the true biomass yield coefficient, Y, was calculated directly from the raw oxygen accumulative uptake profile using the formula (and assuming Y_p = 0 mg P COD/ mg S COD (Brown et al. 1990)):

$$Y = 1 - \frac{O_{uplateau}}{S_0} - Y_p \qquad (5.9)$$

where $O_{uplateau}$ is the oxygen accumulative uptake at the beginning of the plateau in the respirogram, indicative of the substrate exhaustion. The kinetic parameters (μ_m, K_S) were estimated by fitting the experimentally measured oxygen data to the Monod kinetic model for a batch culture using nonlinear parameter estimation techniques (Smets et al. 2001), as discussed further below.

The inoculum for the preliminary estimates of the intrinsic biokinetics of Uper-1 was prepared by following the protocol described in Section 5.1.3 Microorganism. Thus, the cells utilized were extensively adapted to late exponential phase growth. Before the inoculum was transferred into the respirometer vessels, it

was harvested by centrifugation (12 000 x g for 10 min), freed of residual glycerol and naphthalene by resuspension and washing (three times) in MSNS. The inoculum for the "intrinsic biokinetics" of Uper-1 in the ISFC was aseptically collected from the ISFC effluent during various experimental phases of selected bioremediation simulation experiments.

The same basic procedure was followed in all of the respirometry studies, whatever the source of the inoculum. First, the respirometer vessels and Teflon-coated stir bars were washed with Alconox solution. Then, each respirometer vessel was filled with 555 mL artificial groundwater (MSNS), leaving 550 mL after autoclaving. This operation was calibrated in triplicate before the preparation. The respirometer vessels were then autoclaved at 121°C for 15 minutes.

A naphthalene solution of 10,000 mg/L in DMF was prepared in advance. An aliquot of 1 ml of this naphthalene in DMF solution was taken by a syringe with Teflon filter. A small amount of the solution was pushed through to rinse the filter. Then a volume of 0.55 ml of the filter-sterilized stock solution was spiked into each respirometer vessel. The nominal target concentration was 10 mg/L in the 550 ml solutions, which was confirmed by analyzing the samples taken at this point for naphthalene by either gas chromatography (GC) or spectrofluophotometry. The theoretical concentration of COD in 10 mg/L naphthalene solution is 30 mg/L. In order to ensure that substantial microbial growth occurred during the biokinetic assay, the COD of the seed culture was measured and the volume of seed culture added into the vessels was adjusted as appropriate to give a S_0/X_0 ratio either >> 20 or << 0.025 to meet the requirement of desired biokinetic parameter assay.

After inoculation, the autoclaved CO_2 traps were filled with about 5 ml KOH solution (45% by weight), which had been filtered-sterilized (0.2 μm filter). The KOH traps were then aseptically inserted into the prepared respirometer vessels and capped snugly. The vessels were placed on the Challenge MS58-300 magnetic stirrer base in the constant temperature water batch (24°C). The stirring speed was adjusted so as to produce a vortex that extended from the gas-liquid interface down to the stirring bar. A sterile 20-gage needle was inserted through the septum momentarily to vent the vessel in order to equalize the pressure prior to the test. The operation was repeated to ensure the pressure inside all the vessels that were connected to flow cells had equilibrated with the pressure outside of vessels. The sterile needles attached to the tubing connected to each of the oxygen flow cells were inserted into the septa of the vessels at an angle of 45°. The needle tips were carefully adjusted to ensure free flow of oxygen by preventing the needle tip from contacting the vessel wall or the KOH trap holders. The oxygen cylinder was then opened and the oxygen flow rate was set up at approximately 3 bubbles /second.

After confirming that the software was set up properly, a trial run was started to test the communication between the vessels and respirometer. A 10-ml syringe and 20-gage needle were used to withdraw headspace gas from each respirometer vessel until one or two bubbles passed through the respective flow cell. The counts were checked to make sure that they were registered on the computer monitor. At this point, the trial data were deleted by resetting the system counters and timers and data acquisition was initiated. Subsequently, the oxygen uptake rate and oxygen uptake accumulation were followed during the experimental run.

Replicate vessels containing the inoculum vessels were set up along with the duplicate control vessels for each respirometry experiment. The preliminary respirometry experiments were run with inoculum from the batch primary culture. In addition, experiments were also performed using as an inoculum from the cells in effluent sample collected during Scenario #1 Phase I and Phase II simulated bioremediation experiments, as well as the cells in effluent samples collected during Scenario #2 Phase I simulated bioremediation experiments.

The parameters in the nonlinear Monod rate expressions were estimated by nonlinear methods. The algorithms in Microsoft Excel (Version 2002) add-in Solver were first utilized to solve the non-linear optimization of the sum of squared errors (SSE), which was evaluated by taking a measured oxygen uptake value, subtracting the model predicted value from it, squaring the difference, and adding that value to a running total (Smets et al. 2001). However, it was difficult to obtain a reasonable K_s value based on this non-linear optimization method, which usually resulted in the fitted K_s equaling the upper constraint. Therefore, ultimately a FORTRAN program "Nvolma", which was obtained from Prof. Barth F. Smets (Technical University of Denmark) and originally developed at Clemson University, was used to perform the biokinetic parameter estimation (Appendix 3). This program fits a curve to batch oxygen uptake data using Monod or Andrews kinetics to describe the removal of a non-volatile substrate. The best fit values for the parameters μ_m and K_s are found using a least sum of squares estimator to determine the best fit for a given set of experimental data. The complex search routine of Box (Kuester and Mize 1973) is used to find the best fit. Initial estimates of μ_m and K_s for the fitting program were

obtained from the oxygen uptake data by following the procedures of Brown et al. (1990).

5.3.5 Sorption/Desorption Equilibrium and Kinetics

To accomplish Scenario #3, the sorptive characteristics of the two-layered porous media used in Scenario #1 and Scenario #2 needed to be increased so that the meso-scale desorption rate was the overall rate controlling mass-transfer process. The overall goal in creating Scenario #3 was to develop a synthetic system that modeled a real subsurface system, yet possessed defined quantitative physicochemical parameters. Obviously, the physicochemical properties of the model system should be similar to actual subsurface systems so that the results can be translated into realistic systems. There were two major concerns with the synthetic system. First, the modified porous media system needed to possess a strong sorptive capacity so that the sorption/desorption would limit the overall bioremediation rate. Second, it was important that the modification to the porous media not significantly alter the hydraulic conductivities of the system, nor alter the amount or the nature of the surface area available for microbial attachment and growth for Scenario #3 compared to Scenario #1 and 2.

The original idea was to increase the sorptive capacity of the porous media by using the protocol of Szecsody and Bales (1989) to create a thin, patchy surface coating of organosilanes, including aliphatic-chain groups (C_1, C_8, and C_{18}) and an aliphatic chain terminating in a phenyl group, on the silica sand. However, the idea was abandoned because of the health hazards and potential for laboratory damage posed by organosilanes (J. Szecsody, personal communication).

Three other alternatives were evaluated in batch sorption experiments, which fell into two categories of synthetic sorbent systems: (1) modification of the sand surface to increase the sorption capacity, and (2) mixing sand with a certain amount of a synthetic sorbent. Two of the alternatives tested for the preparation of a synthetic model soil were in the first category--2,2,4,6,6,8,8-heptamethylnonane (HMN) and surfactant coated sands-- and one was in the second category-- mixing sand with Amberlite Resins. The investigation of these three options is described in detail in the following subsections.

In these experimental studies, all of the apparatus used consisted of borosilicate glass where possible, or Teflon, which demonstrated negligible sorption of naphthalene. These experiments consisted of two general types: rate investigation and equilibrium isotherm studies. The rate studies were designed to assess the effect of time on the partitioning of naphthalene and sorption/desorption kinetics. The equilibrium isotherm studies were designed to evaluate the partitioning coefficient of naphthalene onto the modified synthetic sorbents. In order to select a synthetic sorbent with a strong sorptive capacity, as characterized by the partitioning coefficient, K_d , sorption isotherm experiments were generally conducted first, followed by the rate studies, if sorbent was considered promising.

5.3.5.1 Unmodified Sand Sorption

As the first step in the sorption kinetics study, the sorption isotherm of naphthalene on unmodified Mystic White II coarse sand was investigated. Naphthalene solutions of 5, 4, 3, 2, 1 and 0.5 mg/L were prepared and added to 40 ml amber vials along with 1 g of sand. All the vials were then tumbled on a rotary shaker

(RKVS, Appropriate Technical Resources, Inc., Laurel, MD USA) 124 hours to ensure that the aqueous-solid equilibrium was reached. The aqueous equilibrium naphthalene concentrations were determined using the spectrofluorophotometer. The sorbed naphthalene was obtained by the concentration difference method (Burris and Antworth 1992).

5.3.5.2 HMN-Coated sand sorption

The first option evaluated was to increase the sand sorptive capacity by coating HMN onto the surface of the sand, and thereby simulate the sorption of PAHs onto organic matter in the subsurface. HMN was selected because of its high fluidity, which allowed a very homogeneous coating on the sand (Appert-Collin et al. 1999). To prepare the sand, it was coated with 0.5% HMN (weight fraction) and then air dried for 48 hours before use.

The preliminary naphthalene sorption isotherm was accomplished by placing 1 g of HMN-Coated sand in each of twenty 40-ml borosilicate vials. Then 40 ml of naphthalene solution in MSNS with varying initial concentrations (0.5 mg/L, 1 mg/L, 2 mg/L, 3 mg/L, 5 mg/L, 10 mg/L, 12.5 mg/L, 15 mg/L and 20 mg/L) was added to duplicate sets of vials. In addition, duplicate blank samples were prepared without HMN-Coated sand to determine the naphthalene loss due to sorption to the vials or vaporization. All the vials were then tumbled on a end-over-end shaker for 48 hrs to minimize mass transfer limitations. All steps were performed aseptically. After 48 hrs, 2 ml of equilibrium solution was taken from each vial and subjected to liquid-liquid extraction and analysis by gas chromatography (GC) as described in the Analytical Methods Section. The aqueous phase concentrations measured were then used to calculate the solid-phase concentrations by difference. The equilibrium solid-

phase concentration data were presented as a function of the equilibrium liquid-phase concentrations to analyze the sorption isotherm.

5.3.5.3 Surfactant-coated sand sorption

The second option tested, the use of cationic surfactants to enhance the sorptive capacity of the sand, was investigated very carefully. The surfactant-coated sand sorption study was conducted with the help of James Stagge, an undergraduate Honors student in Civil and Environmental Department, University of Maryland. Cationic surfactants have been used successfully by other researchers to enhance organic contaminant sorption onto sand, e.g., (Brown and Burris 1996; Sheng et al. 1998; Wang et al. 2001). In particular, the cationic surfactants cetylpyridinium chloride (CPC) and cetyltrimethylammonium bromide (CTAB or HDTMA) have been the most widely used cationic surfactants for this purpose. Therefore, they were studied for the feasibility of their use in this research. The CPC was chosen over CTAB because of its greater affinity for natural materials (Kibbey and Hayes 1993), although the latter has been used more often in the surfactant research field.

There were three steps in the evaluation of sorption of naphthalene onto CPC-coated sand. First, it was necessary to evaluate the equilibrium time for CPC sorption onto the sand. This was accomplished by mixing a group of 28 samples for different time intervals. Each sample contained 40 ml of 30 μM CPC solution and 1.2 g of Mystic White II coarse sand in 40 ml amber vials. The pH and ionic strength in these samples were varied. Specifically, in addition to a blank, for every mixing time intervals, there were four subsets of samples: Groups 1 and 2 had pH=7 and NaCl = 0.0 and 0.05 M, respectively, and Groups 3 and 4 had pH=9 and $CaCl_2$ = 0.0 and 0.05

M, respectively. The vials were mixed on the end-to-end shaker for 4, 8, 12, 24, 36, and 48 hours. At each sampling point, four samples, one from each group, were sacrificed and the final CPC concentrations were determined using spectrophotometry (Shimadzu, UV160A). Sorbed CPC concentrations were determined by difference. It was shown that CPC sorption onto sand reached equilibrium within 14 hours. Therefore, a mixing time of 24 hours was used subsequently to ensure the sorption equilibrium of CPC onto the sand. A pH value of 9 was experimentally determined to be the most appropriate for the CPC coating.

Second, a CPC sorption isotherm experiment was conducted to determine how much CPC could be coated onto sand and the best experimental conditions for preparing the CPC-coated sand. Specifically, the preliminary CPC sorption isotherm experiment was carried out using duplicate vials containing 1g of Mystic White II coarse sand and 170, 102, 34, 23.8, 17, 10.2, 3.4, and 1.7 mg/L CPC solution prepared in DI water, with the pH adjusted to 9 using 0.1 N NaOH. The samples were then rotated at 25°C for 48 h to reach equilibrium. After equilibration, the samples were centrifuged, filtered (Acrodisc 0.2 μm PTFE filter), and the concentrations of CPC in samples were measured. The sorbed concentration was determined by difference.

Finally, naphthalene sorption onto CPC-coated sand was studied to determine whether the sorption/desorption process could limit the overall rate of bioremediation when naphthalene sorbed to the coated sand. The CPC-coated sand for the naphthalene sorption test was prepared in a 1L bottle, using 18 g of Mystic White II coarse sand with a CPC solution of 34 mg/L $=1\times10^{-4}$ M (as discussed further below,

it was determined that the critical micelle concentration (CMC) for CPC for the conditions used in this study was between 1×10^{-4} and 3×10^{-4} M) and pH value of 9. The mixture was mixed on a horizontal shaker table for 48 hours, at which time a sample was taken to determine the final aqueous concentration and, thereby, sorbed CPC concentration. The sand sample was then drained and oven dried at 110 °C for 3 days. One gram samples of the dried CPC-coated sand were added to 40 ml amber vials, followed by addition of naphthalene solutions with the same concentrations as in the sorption onto unmodified sand experiment (Section 5.3.5.1). Vials were rotated end-over-end for 124 hours, centrifuged (1500 rpm for 10 min), and the aqueous phase filtered (Acrodisc 0.2 μm PTFE filter) and analyzed by spectrophotometry. The sorbed naphthalene concentration was determined by difference.

5.3.5.4 Mixing sands with Amberlite resins

The third option considered for modifying the sorptive properties of the porous media sand involved mixing the porous media sand with a relatively small amount of a commercially available Amberlite resin. Amberlite resins have been shown to be a good sorption sink based on the partitioning coefficient (Guerin and Boyd 1997; Mulder et al. 2000). Initially, XAD-2 (Supelco, Bellefonte, PA, USA) was chosen because it can be used to simulate both the strong sorption of organic matter and intraparticle diffusion-limited sorption (Mulder et al. 2000). Importantly for this project, Guerin and Boyd (1997) demonstrated that reversible sorption of naphthalene to XAD-2 resin allowed it to be desorbed and mineralized by two microbial strains. Thus, use of XAD-2 was a promising candidate for Scenario #3, especially if enhanced desorption could be achieved with the utilization of (bio)

surfactant, which, would in turn, enhance the biodegradation. The physical properties of XAD-2 are presented in Table 5.6.

Table 5.6 Physical properties of Amberlite resins XAD-2 and XAD-7

Name	Average pore diameter (Å)	Specific surface area (m^2/g)	Skeletal density (kg/m^3)	Porosity
XAD-2	90	300	640	0.41
XAD-7	90	450	1240	0.55

Preliminary sorption isotherm experiments were conducted to observe the sorption behavior of naphthalene with XAD-2 in the simulated groundwater system. Ten naphthalene in MSNS solutions with concentrations of 0.5 mg/L, 1 mg/L, 2 mg/L, 3 mg/L, 5 mg/L, 10 mg/L, 12.5 mg/L, 17.5 mg/L and 20 mg/L, were prepared. First, 5.0 mg autoclaved XAD-2 was placed in each of the 40-ml borosilicate amber vials using tweezers. Next, 40 ml of each naphthalene solution was introduced into duplicate vials. All vials were then capped and shaken at an average room temperature of 24ºC for a sufficiently long period (approximately 136 hours) to ensure that sorption equilibrium was attained. The analysis procedures are the same as those described for the previous sorption isotherm experimental investigations.

As discussed below, the sorption capacity of XAD-2 was demonstrated to be very promising for Scenario #3. However, there was one concern with regard to the application of XAD-2: the skeleton density. The density of XAD-2 is significantly lower than that of either of the two types of sands used in the ISFC (Table 5.6), which at a minimum may lead to a problem of the XAD-2 floating out of the sand and might result in a change in the physical properties of simulated aquifer. Therefore, XAD-7

was chosen as the next alternative to evaluate because it had a similar sorption capacity as XAD-2, yet more attractive physical properties, in particular a skeletal density of 1240 kg/m^3, which was more similar to the particle densities of the sands used in this research. Thus, compared to XAD-2, it was more promising that the mixing of XAD-7 resin with sand would not affect the flow cell hydraulics significantly. Therefore, further efforts were focused on the investigating sorption/desorption of XAD-7.

The sorption isotherm experiments of XAD-7 were conducted following the same procedures as described above for XAD-2. Specifically, two sorption isotherms for naphthalene sorption onto XAD-7 were investigated, one in which the XAD-7 was mixed with fine sand and the other in which the XAD-7 was mixed with the coarse sand, which how XAD-7 was eventually incorporated Scenario #3, as discussed below. To do this, 30 mg XAD-7 were mixed 270 mg of either fine sand or coarse sand, which resulted in the synthetic model soil having an Amber resin content of 10% by weight.

Based on the determined partition coefficient, XAD-7 also has a strong affinity for sorbing naphthalene from solution. Thus, it was decided that the XAD-7/coarse sand mixture would be selected for meeting the desired criteria in creating the increased sorptive characteristics. Therefore, further sorption/desorption kinetics experiments were performed using XAD-7. The kinetic experiments were carried out in completely mixed batch reactors (CMBRs) following the bottle-point rate procedure described by Weber and Miller (1988).

The bottle-point rate experiments were performed by preparing 28 identical 40-ml borosilicate amber vials, each containing 40 ml of naphthalene solution (nominal concentration = 5 mg/L) and 30 mg XAD-7. Once set up, the vials were shaken on a end-to-end shaker to maintain completely mixed conditions. Subsequently, duplicate reactors and a solution blank were removed from the shaker at selected intervals (ranging from 1h to 192 h). The samples from these vials were then analyzed for the naphthalene aqueous concentration and the data were used to obtain serial data for sorbed naphthalene as a function of time by difference. The data collected from these bottle-point rate studies were used to evaluate the rate of sorption and the time required to reach the equilibrium.

Scenario #3 represented a system in which the meso-scale desorption rate was to be the overall rate limiting process. It was important to investigate the desorption rate of the XAD-7/sand mixture to ensure that the slow desorption rate was limiting the overall rate of bioremediation. Therefore, a bottle-rate experiment was also conducted to evaluate the desorption kinetics. First, twenty identical 40-ml borosilicate amber vials were prepared, each containing 40 ml of naphthalene solution (C_0 = 20 mg/L) and 30 mg XAD-7. The vials were then shaken on a rotary shaker for 48 hours to ensure that the equilibrium was reached. Second, the naphthalene concentrations were measured to determine the amount of naphthalene sorbed onto XAD-7 in each vial. Third, the naphthalene solutions were decanted, being careful not to lose any XAD-7. Fourth, the vials were filled with 40 ml of fresh MSNS, which was free of naphthalene. Finally, the vials were shaken on the rotary shaker and duplicate vials were removed from the shaker at selected intervals (intervals

ranging 1h to 52 h). Naphthalene aqueous concentrations were analyzed and the data were used to obtain serial rate data for desorption as a function of time.

As discussed in the sorption/desorption literature review, many models have been developed to describe sorption/desorption kinetics of with porous media. A dual-resistance model proposed by Crittenden et al. (1986), the batch pore surface diffusion model (BPSDM) for describing solute transport in a soil system, was utilized to obtain the sorption/desorption kinetic parameters. The model incorporates the following mechanisms: (1) axial dispersion and diffusions; (2) film transfer resistance to mass transport from the mobile to the stationary phase; (3) local sorption equilibrium; and (4) surface and pore diffusion as intraparticle mass transport mechanisms. Thus, it incorporates film, pore and surface diffusion mass transfer coefficients.The BPSDM model was obtained from Dr. D.W. Hand (Michigan Technological University, Houghton, MI).

In Scenario #3 Phase IIB, an engineered perturbation was needed to increase the limting desorption rate of naphthalene and, thereby, increase the biodegradation rate. Based on a review of the literature, a biosurfactant was chosen for this purpose over a synthetic surfactant. Biosurfactants are advantageous compared to synthetic compounds for use in soil remediation because biosurfactants are natural compounds that will have a low environmental effect. Thus, complete removal after treatment may not be necessary. In addition, *in situ* production may also be possible, e.g., (Desai and Banat 1997). To be effective for enhancing the removal of sorbed contaminants, a biosurfactant should have high solubilizing properties, should be

water soluble, and should not strongly adsorb to soil. On the basis of these criteria, a rhamnolipid biosurfactant was selected for the study.

In particular, a rhamnolipid biosurfactant was selected because: (1) it is a glycolipid, which is the most commonly isolated type of biosurfactant; and (2) members of the genus *Pseudomonas*, which produce various rhamnolipids, are common soil microorganisms (Zhang and Miller 1992). The specific rhamnolipid selected was the Jeneil Biosurfactant Company (Sankville, WI) product JBR425. The two major rhamnolipid components present in the rhamnolipid solution are monorhamnolipid (α -L-rhamnopyranosyl-β-hydroxydecanoyl-β-hydroxydecanoate) and dirhamnolipid (2-O-α-L-Rhamnopyranosyl-α -L-rhamnopyranosyl-β-hydroxydecanoyl-β-hydroxydecanoate). The mono- to di-rhamnolipid ratio is of 1:1, with molecular weights of 504 and 650, respectively. The critical micelle concentration of this biosurfactant is 0.037 mM (Gu and Chang 2001).

Due to the time limitations, the investigation of enhanced desorption of naphthalene from XAD-7 by biosurfactant was not completed during this work. Therefore, that study will be performed by Ms. Eunyoung Hong.

5.4 Bioremediation Simulation Experiments

As discussed in Chapter 4, three different bioremediation scenarios were simulated in the ISFC to represent different combinations of natural rate-limiting phenomena in subsurface systems. Each scenario was conducted in two phases: Phase I, intrinsic biodegradation, and Phase II, engineered bioremediation, with selected system perturbations, as discussed further below. However, after performing the point-source concentration tracer studies and before inoculating the flow cell and

conducting the bioremediation simulation experiments, several control experiments were first done in the ISFC to demonstrate that effects observed in subsequent experiments after inoculation were due to microbial activity, not physicochemical changes in the system. The control experiments were originally designed to replicate the Scenario #1 experiments, but without microbial activity. Although the design of the Scenario #1 experiments was altered from a continuous injection of naphthalene in MSNS in the control experiments to a pulse of contaminated artificial groundwater in the actual Scenario #1 bioremediation simulation experiments that were performed, several key pieces of information were still obtained. In particular, these experiments were useful for developing sampling techniques, evaluating interlayer dispersivity, and demonstrating the effect of the Phase II system perturbation in the absence of microbial activity in Scenario #1. In the following subsections, the control experiments are described, followed by a description of the general procedures followed during the bioremediation simulation experiments and explanation of the methodology used for simulation Scenarios #1, 2, and 3.

5.4.1 Control Experiments

5.4.1.1 Phase I: Intrinsic Control Experiments

The control experiment for Scenario #1 was conducted for three purposes: (1) to develop and refine the techniques to be used in the full simulated bioremediation experiments; (2) to determine the interlayer dispersivity because of the importance of understanding processes near interfaces in the subsurface environment; and (3) to evaluate the effects of naphthalene mass loss in the ISFC via volatilization, or sorption onto the silicone caulking.

In the Phase I control experiments, the ISFC was filled with filter-sterilized MSNS before starting. Subsequently, filter-sterilized MSNS with naphthalene (~5 mg/L) was pumped into the ISFC continuously at a rate of 6 ml/min. The general microbial inhibitor, diluted acid-free formaldehyde in PIPES buffer solution, was added at a concentration of 0.04% (by weight) to inhibit microbial growth (Brock 1977; Trevor 1996). The flow rate was monitored and adjusted appropriately throughout the experiment to ensure that it did not fluctuate too much either due to the Teflon pump tubing wearing out or accidental mistakes in setting up the Masterflex® L/S® PTFE-tubing pump. In only one case was it necessary to adjust the pump back to 6 ml/min due to a slight slowing down because of worn out tubing.

During this experiment, and all of the other ISFC experiments, the movement of the contaminant plume was followed by monitoring the naphthalene in the pore water and effluent. In the case of the control experiments, monitoring was continued until a steady state condition was reached with respect to naphthalene plume development. The pore water samples were used to obtain breakthrough curve data at selected locations. Therefore, it was necessary to develop sampling techniques and locations.

Designing the sampling approach in the ISFC experiments in general was very challenging because of the small volume of water present within the flow cell combined with the minimal volumetric fluxes moving through the flow cell. Thus, withdrawal of significant quantities of water was impossible without significantly affecting the flow field (Silliman et al. 1998). In a compromise between minimizing flow disturbance and having sufficient sample for analysis, the sampling volume was

selected to be 1ml, which required some adjustment in analytical protocols (e.g., the naphthalene analysis using GC, see below). Samples were withdrawn from sampling ports with a syringe pump (Harvard Apparatus, Model number 55-2226) using gas-tight glass syringes attached to the Mininert valve of the ports via a Teflon tubing set (1/16" OD). The pore-water sampling rates were set at 250 μL/min and 50 μL/min for the high-K layer and low-K layer, respectively. The samples from both influent and effluent sampling ports were taken manually, using a gas-tight glass syringe (Hamilton Series 1000 Gastight Syringe, Fisher Scientific) at a rate that was as slow as possible. These sampling flow rates were chosen carefully to be less than 5% of the bulk flow rate in order to be small enough to not interfere with the bulk flow in the flow cell. These sampling techniques provided the capability for complete chemical analysis of the pore fluid withdrawn from the flow cell, but limited the number of samples that could be withdrawn both temporally and spatially based on minimizing the impact of the sampling on the flow field, which, in turn, made the arrangement of the sampling schedule challenging during ISFC experiments.

In order to obtain the contaminant breakthrough curve data, the selection of sampling times and locations was of primary importance. Samples from the inlet flow line, the outlet flow line, and selected pore-water sampling ports were taken at intervals of hours early in the ISFC experiments and days at later times. The pore-water sampling ports selected for monitoring during Phase I control experiment were A4, C4, E4, B9, C9 and D9. The sampling ports A4, C4, B9 and C9 were sampled more intensely than the others during the early period of each experiment, because the plume in the high-K layer developed much faster than that in the low-K layer. On the

other hand, the sampling ports E2 and D9 were monitored more intensely during the later period of each experiment because at that point the plume was mainly developing in the low-K layer. The effluent sampling port was sampled at the same time interval as the influent sampling port, which was taken every time the pore-water samples were withdrawn.

The interlayer dispersivity was obtained by calibrating the control experimental breakthrough curves from D9. The experimental results were simulated using RT3D in VMOD and the interlayer dispersivity was adjusted by trial-and-error to fit the data of the initial mass pulse from interlayer mass transfer.

5.4.1.2 Phase IIA: Nutrients Addition Control Experiments

As part of the control experiments for Scenario #1, a control perturbation experiment was also conduced. Numerous studies have been published on the effects on pollutant biodegradation rates in response to nutrient supplements. The results have been controversial, with some studies reporting they observed stimulated degradation with the addition of nitrogen and/or phosphorous (Alexander 1994), while others observed that the degradation rate was unaffected by the added nutrients or may actually have declined relative to controls (Johnson and Scow 1999; Manilal and Alexander 1991). Despite the continuing debate over the effect of nutrient supplements for bioremediation in the field, the addition of excess N and/or P has been a common remedial strategy. For this reason, in Phase IIA of all the experimental scenarios, the first "engineered" perturbation received was the addition of N and P in excess of the stoichiometric requirement. Similar to many field observations, this perturbation was not expected to be effective in the experimental scenarios, because another factor other than nutrient levels was ultimately most

limiting the biodegradation rate. Therefore, the effects of addition of excess N and/or P were investigated in a control experiment, too. To perform this component of the control experiment, 6 times the stoichiometric requirement (Equation 5.1) for N and P were applied in the simulated groundwater. This control experiment was performed once, following the same protocol as described in the Phase I control experiment.

5.4.1.3 Phase IIB: Engineered Control Experiments

In the second engineered perturbation experiment of Scenario #1, Phase IIB, advection was increased to increase transverse dispersion, being careful not to increase advection so much that it started to limit the biodegradation rate by dilution. Therefore, the effect of increasing flow rate was examined in the control experiment as well. In order to determine the appropriate flow rate that would have a significant effect on transverse dispersion, but at the same time be experimentally feasible, a simulation was run using RT3D VMOD. Based on the modeling simulation, the flow rate was doubled to meet the above criteria. This control experiment with the increased flow rate was performed once for 24 hours, following the general procedures of Phase I control experiment.

5.4.2 General Bioremediation Simulation Experimental Procedures

5.4.2.1 ISFC preparation and Inoculation

When the ISFC was originally set up before the control experiments, all components of the influent feed line – tubings, connections, and feed bottles – were sterilized by autoclaving. All feed solutions were then filter (Membrane filters, 0.25 μm, Schleicher & Schuell, Dassel Germany) sterilized during addition to the feed bottle. In addition, before the start of bioremediation simulation experiments, the

ISFC, pump, tubing and connection parts were treated with 3 pore volume of the formaldehyde solution (0.04% by weight) in PIPES buffer solution to inhibit microbial activity (Brock 1977; Trevor 1996). The ISFC was then allowed to sit stagnant for 3 days to assure complete microbial inhibition. To confirm complete microbial inhibition, the microbial populations in the flow cell effluent were estimated using the heterotrophic plate count (HPC) method. Subsequently, the system was rinsed with 3 pore volumes of filter sterilized MSNS to prepare for inoculation. Solutions, glassware and other materials used in the ISFC bioremediation simulation experiments were also sterilized by autoclaving for 20 min.

After flushing with filter-sterilized MSNS, the ISFC was inoculated with the chosen microorganism Uper-1. The 30L (~ 2 pore volumes) of inoculated MSNS were then pumped through the ISFC for inoculation. To maximize microbial attachment, the ISFC was subsequently allowed to stand for 24 hours before the initiation of experiment. Following that, samples were taken from A2 and E2 for HPC to determine the biomass concentration in aqueous phase.

The inoculation of ISFC had to be performed a second time later during the simulated bioremediation experiments. Specifically, following the excess addition of N and P in the Phase IIA experiments in Scenario #1 and #2, algae growth occurred in the high-K layer and the interface between the high-K and low-K layers, which affected the ISFC physicochemical and biological conditions. As the result, the ISFC was treated using a disinfectant prepared from household bleach and Alconox detergent (Barkley and Richardson 1994). The household bleach was diluted 100 times, containing 525 mg/L of available chlorine, with 0.7% of Alconox detergent

added. One pore volume of prepared disinfectant solution was first pumped through to disinfect the ISFC. Then, 3 pore volumes of filter-sterilized MSNS were pumped into the ISFC to flush out the residual disinfectant solution. Following that, 3 pore volumes of formaldehyde (4%) (Trevor 1996) were pumped through the ISFC to ensure complete microbial inhibition. Finally, the ISFC was rinsed with 3 pore volumes of filter-sterilized MSNS to prepare for the inoculation. The ISFC was inoculated again following the same procedure as described above.

5.4.2.2 General ISFC Operation

Although the experimental conditions were different for each bioremediation simulation scenario, the general sampling plan and data analysis were the same. To quantify the processes controlling bioremediation and the process interactions, the nonreactive tracer (Br), naphthalene and dissolved oxygen (DO) concentration were monitored within the high-K layer (A2 and B7), within the low-K layer (D1, E2 and D7), at the sand layer interface (C2 and C7), and in the influent and effluent. Samples of ~ 1 ml were withdrawn from these sampling ports following the same procedures as described in the control experiments. The aqueous microbial numbers were also quantified using HPC within both layers (A2 and E2) as well between the sand layer interface (C2) and in the effluent. Although most of the microbial biomass was probably associated with the porous media, changes in the attached biomass should be reflected in changes in the microbial biomass in solution.

A temporal moment data analysis was utilized in this research for interpreting the breakthrough curve data from the bioremediation simulation experiments, e.g., (Kent et al. 1994). The zeroth moment is defined as the area under the breakthrough curve, which was calculated utilizing the linear trapezoidal integration. In this

research, the zeroth moment analysis was performed using the areas under the naphthalene and Br breakthrough curves, A_{naph} and A_{Br}, respectively, after different horizontal flow distances, at selected sampling ports. The ratio of A_{naph}/A_{Br} was utilized for comparison between experimental Phase I and Phase II because the effect of dispersion on the naphthalene concentration could be eliminated by normalizing to A_{Br}. In addition, the average pore-water velocity at each port was determined by dividing the Br travel distance by the estimated average travel time.

As described further below, bioremediation Scenarios #1 and #2 were simulated in the ISFC. The experiments were broken down into two phases, similar to the control experiments. Phase I represented intrinsic biodegradation under natural conditions, as described in each scenario. Each scenario was designed such that a particular process (e.g., a physical-chemical mass transfer process or biokinetics) was the overall rate-limiting process controlling the overall bioremediation rate. The results of the Phase I experiments were used to evaluate if the limitations on biodegradation under intrinsic conditions were what was expected. Specifically, the experimental results from the ISFC were modeled using RT3D in VMOD and the independent parameter estimates to confirm that the parameter estimates successfully described the system. Then, the parameter estimates were used in the quantitative framework to identify the rate-limiting process. The Phase II experiments then represented perturbations to the system as part of an engineered bioremediation. The successful perturbation was expected to be one selected based on the overall rate-limiting phenomenon and how the remedial strategy affected it.

5.4.3 Scenario #1: Dispersion-Limited Biodegradation

The experimental conditions for Scenario #1 were selected to simulate a field scenario with relatively fast biokinetics in porous media with low sorption, making macro-scale transverse vertical dispersion from the fast-K layer to the slow-K layer the overall rate-limiting process. Therefore, this scenario represents a key macro-scale interfacial process that can significantly impact *in situ* bioremediation, i.e., the hydraulic mixing at the interface of a dissolved contaminant plume and the "clean" groundwater, which is induced by subsurface hydraulic conductivity heterogeneities. To experimentally set up this scenario, the two-layer, low sorptive capacity porous media and microorganism Uper-1 were used as described in Sections 5.2.6 and 5.1.3, respectively.

5.4.3.1 Phase I: Intrinsic Biodegradation

Phase I represented intrinsic biodegradation under natural conditions for which vertical transverse dispersion was the overall rate-limiting process. The MSNS with naphthalene (~ 10 mg/L) and Br (~ 120 mg/L) was pumped into the ISFC for 48 hours at a flow rate of 3 ml/min to simulate a pulse input of contaminant. This was followed by an input of MSNS alone at the same flow rate until the end of the experiment. The flow rate used in these experiments was half of that in control experiment, because: (1) it reduced the amount of feeding solutions needed to run the experiments, and (2) it ensured that the flow rate increase in Phase IIB be significant enough to alleviate the transverse dispersion limitation. This experiment was performed in triplicate. However, Br was not added in the first experiment. Therefore, the Br data obtained from the second experiment was utilized in the moment analysis. As described in Section 5.4.2.1, the ISFC had to be disinfected and re-inoculated

following the same procedures as during the initial inoculation. Therefore, to ensure the system was under the same conditions, the baseline Phase I experiment was performed a third time.

In order to investigate the naphthalene plume development and distribution in the ISFC, a plume contour plot was desired. To obtain the data required for a complete plume contour plot, it was necessary to capture the plume contour in both layers, which meant that the selection of sampling ports and the sampling schedule had to be very accurate. If the sampling timing was too early, there was a possibility that the plume in the low-K layer had not developed sufficiently to reach the first column of sampling ports. However, if the sampling time was too late, it was possible that the plume front in the high-K layer could have exited the ISFC before sampling was completed. With respect to the sampling ports, it was also important to choose the appropriate locations. On one hand, sampling as many ports as possible would have provided the most complete description of the plume contours. On the other hand, sampling many ports was not desirable because it could contribute to changes in the plume due to interferences with the simulated groundwater flow. Therefore, special attention was paid to the design of the sampling approach for the plume contour. Based on practicing and preliminary predictions using model simulations in RT3D in VMOD , the following sampling ports- C1, D1, C2, E2, C5, C6, C7, C8, A10, C10, B11, and C11-were sampled in addition to those sampled for the breakthrough curve analysis at 48 hours, immediately after the pulse input was halted.

This plume contour investigation was not performed in Phase I (1) because that was the first bioremediation simulation experiment performed, and it was not

possible to complete the labor and time consuming plume contour sampling. Instead, the contour investigation was practiced in the experiment Phase I (2). However, because of the intense sampling schedule, it was very challenging to take samples from sufficient sampling ports at one "snapshot" to produce the desired contour plot. Furthermore, the plume contour plot was only a qualitative technique to evaluate the experimental results. Therefore, this practice was abandoned in the later bioremediation simulation experiments.

5.4.3.2 Phase IIA: Nutrient Enhanced Biodegradation

The first perturbation represented the commonly applied engineered remedial practice in the field, in which N and P in excess of the stoichiometric requirement were added to enhance the biodegradation rate. Therefore, the experiment was repeated as described for Phase I except that 2.5 times of the N and P stoichiometric requirements for 10 mg/L of naphthalene was used in the input MSNS. The Phase IIA experiment was performed only once to minimize the algae problems caused by the excess addition of N and P nutrients.

5.4.3.3 Phase IIB: Engineered Biodegradation

The second perturbation represented a manipulation to the system as part of an engineered bioremediation that was selected based on the identification of rate-limiting process using the system parameters confirmed in Phase I and the quantitative framework in Figure 4.3. As discussed below, it was determined based on the framework that dispersion was the overall rate-limiting process. Therefore, the flow rate was increased to a level of three times that in Phase I, to increase the advection rate and thereby the dispersion (Equation 5.5), especially the interlayer transverse dispersion between the high-K layer and low-K layer. It was expected that

the increased transverse dispersion would increase the spreading of the naphthalene in the vertical direction and allow more mixing with the DO, thus increasing the biodegradation rate and the overall rate of bioremediation. In order to compare the results between Phase I and Phase II, the pulse input time was reduced to 16 hours to ensure that the naphthalene mass pumped into the ISFC was the same as in Phase I. This experiment was conducted twice to ensure the results were reproducible.

5.4.4 Scenario #2: Biodegradation-Limited Biodegradation

Scenario #2 was designed to simulate a field scenario in which slow-biokinetics would limit the overall bioremediation rate. Experimentally, the same porous media and sorptive characteristics were utilized in Scenario #2 as those of Scenario #1, i.e. layered heterogeneity and very limited sorption/desorption. In addition, the same microbial culture, Uper-1 was used. However, the biodegradation rate was inhibited so that the slower biokinetics limited the overall bioremediation rate.

There were two criteria used in the selection of inhibition method: (1) the inhibition needed to be significant enough such that the biokinetics were the overall rate-limiting process; and (2) the bacteria needed to be able to resume the original activity once the inhibitor was removed from the ISFC to facilitate experiment replication. There are a wide range of inhibition methods available, as summarized by Brock (1977). In general, there are three categories of general inhibitors: (1) chemical agents, such as formaldehyde (4%) (Trevor 1996), mercuric bichloride (100 μg/ml or 10 μg/ml), streptomycin sulfate (100 μg/ml), sodium azide (1000 μg/ml), novobiocin (100 μg/ml) and hydrochloric acid (0.1N); (2) temperature as an inhibitor; and (3)

water potential as an inhibitor, which includes a variety of solutes such as NaCl, alcohols, sugars, urea, etc. In all cases, it is very necessary to assume that the utilized inhibitor has no effect on the biological reactions.

Different options for inhibiting the biodegradation rate were investigated using batch respirometry experiments. This work was done by Ms. Eunyoung Hong. Ultimately, it was decided to inhibit the microbes by applying a high salt concentration (NaCl) (Brock 1977). Thus, this scenario represented bioremediation of a saline, hydrocarbon contaminated subsurface. This is actually an important problem in many areas, e.g., due to oil exploration and processing (Rhykerd et al. 1995; Riis et al. 2003). If salinity levels are sufficiently high to inhibit biodegradation, one option for enhancing bioremediation was to add water to reduce the salinity.

5.4.4.1 Phase I: Intrinsic Biodegradation

Phase I represented intrinsic biodegradation in a high salinity, hydrocarbon contaminated subsurface system for which slow-biokinetics were the overall rate-limiting process. . The MSNS with naphthalene (~ 10 mg/L), Br (~ 120 mg/L) and NaCl (2.5% by weight) was pumped into the ISFC for 48 hours at a flow rate of 3 ml/min to simulate a pulse input of contaminant, which was followed by an input of MSNS with NaCl at the same flow rate until the end of the experiment. This experiment was performed in duplicate.

5.4.4.2 Phase IIA: Nutrient Enhanced Biodegradation

As in Scenario #1 Phase IIA, N and P in excess of the stoichiometric requirement were added in an effort to enhance the biodegradation rate, as commonly applied in field-scale remedial actions. Therefore, the experiment was repeated with

the high salinity as in Phase I except that 2.5 times of the N and P stoichiometric requirements were used in the input MSNS.

5.4.4.3 Phase IIB: Engineered Biodegradation

As discussed below, in Scenario #2, it was determined based on the quantitative framework and system parameters that biodegradation was the overall rate-limiting process. Therefore, the biokinetics were increased to alleviate the limitation and, thus, enhance the overall rate of bioremediation. Experimentally this was accomplished by the removal of the high concentration of salt to speed up the biodegradation rate. Once the salt was eliminated from the MSNS feeding solution, the biomass theoretically resumed to their original activity and the engineered bioremediation experiment was conducted. Therefore, the experimental settings for Phase IIB were the same as those of Scenario #1 Phase I experiments and the results were compared with those from Scenario #1 Phase I. As discussed below, it was verified that the results from Scenario #2 Phase IIB were very similar to those obtained from the Scenario #1 Phase I bioremediation experiments. As a result, the engineered bioremediation simulation of Scenario #2 Phase IIB was only performed once and the duplicate experiments in Scenario #1 Phase I were utilized as the replicate experiments.

5.4.5 Scenario #3: Sorption-Limited Biodegradation

Scenario #3 represented a system in which the meso-scale desorption rate was the overall rate limiting process. Therefore, the influent solution, two-layered porous media and biokinetics was kept the same as in Scenario #1, but the sorptive characteristics of the porous media were altered. Specifically, the experiment was set

up in such a way that a naphthalene-loaded XAD-7/coarse sand mixture was the contamination source, such that the aqueous phase concentration in equilibrium with the sorbed source was initially approximately 10 mg/L. In order to minimize the disturbance to the ISFC, this sorbed contaminant source zone was incorporated by installing a new stainless-steel screen in the influent clearwell, which was located 1 cm away from the influent side wall, leaving ~ 4 cm of space between the two stainless-steel screens. The naphthalene-loaded XAD-7/coarse sand mixture was packed in the space between the two stainless-steel screens, following the same wet packing method as used in the construction of the ISFC. The MSNS was then pumped into the ISFC and the plume development was monitored, as described above.

A moment analysis was to be performed for this scenario as well. However, to obtain the non-reactive tracer data, a separate control experiment was to be conducted with sodium azide as a microbial inhibitor so that naphthalene desorbing from the source zone could be used as the tracer. This was necessary because Br could not be loaded onto XAD-7/coarse sand mixture in the same way as naphthalene. Due to time constraints, these experiments will be completed by Ms. Eunyoung Hong and are not reported on further here.

5.5 Analytical Methods

5.5.1 Naphthalene Analysis

5.5.1.1 Gas Chromatography

5.5.1.1.1 Liquid-Liquid Hexane Extraction

A liquid-liquid hexane extraction method was used to prepare aqueous samples for naphthalene analysis by gas chromatography (GC). GC grade hexane (Fisher Scientific, 99%) was used as the extraction solvent. An internal standard was used for the GC analysis in order to reduce possible errors in the analysis resulting from manual injection of the samples. Specifically, acenaphthene (Acros Chemicals, 99.9%) in methanol was used as the internal standard.

For each analysis, 2 mL of aqueous samples was transferred into 8-mL amber vials with screw caps and Teflon-lined septa (Fisher Scientific) in order to prevent possible photolytic decomposition of naphthalene, which was light sensitive (APHA, 1995). After sample transfer, 10 μL of a 500 mg/L acenaphthene in methanol internal standard solution was spiked into the sample inserting a Hamilton Gastight syringe into the sample vial through the septum in the vial cap. After addition of internal standard, the vial was shaken by hand vigorously for 1 minute to mix the solutions. Following mixing, 1 mL of hexane was injected into the vial. During the injection, a 22-gauge needle was also inserted through the septum of the vial to relieve any pressure that may build up due to the hexane injection. The vial was then shaken vigorously again for 10 minutes using a mechanical horizontal shaker (Eperback Corporation, Ann Arbor, Michigan, U.S.A.). After shaking, the sample vial sat

stagnant for 10 minutes to allow the two liquid phases to separate. Subsequently, the GC measurement was performed on the extract within 3 days after extraction, as described below. When the samples could not be analyzed immediately, they were stored in a refrigerator at 4°C to reduce any chance of volatilization and biological degradation that might occur before analysis (APHA et al. 1995)

5.5.1.1.2 Solid-Liquid Hexane Extraction

A solid-liquid hexane extraction method was used to analyze naphthalene concentration that was sorbed on the solid phase of interest, e.g., XAD-2, XAD-7 or sand. As with the liquid-liquid extraction, GC grade hexane (Fisher Scientific, 99%) was used as the extraction solvent.

For solid-phase sample extraction, the wet weight of the solid phase sample was measured, followed by transfer into an 8-ml amber vial that had been autoclaved. Next, 8 mL of hexane was added to each vial, after which the vials were shaken for 45 minutes using a rotating shaker. Unlike the operation in liquid-liquid extraction method, no internal standard was used. After shaking, the hexane extract was directly injected into the GC to measure the naphthalene concentration, as described below. As with the aqueous samples, the GC measurement was performed within 3 days after extraction unless the samples could not be analyzed immediately, in which case they were stored in a refrigerator at 4°C to reduce any chance of volatilization and biological degradation that might occur before analysis.

The moisture content of solid sample was determined at the same time as the naphthalene analysis by drying a subsample of the wet solid phase material in a

104°C oven until a constant weight was reached (e.g., 24 hours was found to be sufficient for XAD-2). The weight difference between the wet and dried subsamples was used to calculate the moisture content. In addition, the dry weight of solid sample was later used to calculate the sorbed naphthalene concentration.

5.5.1.1.3 Gas Chromatography Analysis

Analysis of the naphthalene concentration in the hexane extracts was performed using a Hewlett Packard (HP) gas chromatograph (GC) Model 6890 with a flame ionization detector (FID). The software Chemstation (version 6.03) was used for analysis and integration of the output signal from the GC. The column installed was the HP-5, which is a cross-linked 5% phenyl/methyl siloxane column with a length of 30 m, an internal diameter of 0.32 mm, and a film thickness of 0.25 μm. The GC system and operating conditions used in analysis of naphthalene and acenaphthene were the same as used by Seagren and Moore (2003), which were adapted from a HP method (David et al. 1993) for polynuclear aromatic hydrocarbon (PAH) analysis in hexane. A summary of the GC operating conditions for the method is shown in Table 5.7. The mode of operation used was splitless injection and the septum purge time was 0.75 minutes. With these operating conditions, the retention times for naphthalene and acenaphthene were 6.1 and 7.9 minutes respectively. Therefore, all runs were stopped at 9 minutes.

Table 5.7 Operation parameters for GC analysis

Gas flow rates	Carrier Gas	Helium
	Septum Purge	60 mL/min
	Column Flow rate	8.2 mL/min
	Makeup Gas (Nitrogen)	45 mL/min
	Flame Oxidant (Air)	400 mL/min
	Flame Combustible (Hydrogen)	40 mL/min
Oven	Initial Temperature	30 °C
	Initial Hold Time	2 min
	Temperature Gradient	25°C
	Hold Time	1 min
	Final Temperature	205 °C
Injector	Temperature	250 °C
Detector	Temperature	300 °C

A sample volume of 1 μL was manually injected using a 10 μL Hewlett Packard analytical syringe. Before injection of each sample, the syringe was rinsed with the sample 3 times. After each injection, the syringe was washed with hexane 3 times. All injections were made in duplicate for each sample to ensure good reproducibility.

This GC analysis was calibrated with a 1mg/L naphthalene standard sample on daily basis. A new calibration curve was prepared with both standard solutions of naphthalene and acenaphthene in hexane when the GC conditions were changed due to septa change, gas change, or any other possible maintenance. The calibration curves were obtained from the relationship between the peak area from the GC response and the concentration of the standard solution. The standard solutions of naphthalene in hexane were obtained by first making a standard 50 mg/L stock solution of naphthalene-in-hexane, which was then serially diluted to concentrations of 25, 10, 5, 1, and 0.1 mg/L. The standard solutions of acenaphthene were prepared in the same manner. These standard solutions were stored in 8-mL amber vials with Teflon septa, and kept at 4ºC when not in use in order to reduce any volatilization or biodegradation that may occur during storage. To produce the standard curves, three 1-μL injections were made from each standard vial using Hewlett Packard standard 10-μL syringes. The average, standard deviation, and coefficient of variation of the peak areas for the triplicate injections of both naphthalene- and acenaphthene-in-hexane as a function of concentration were obtained, and calibration curves for peak area versus concentration of the standard solutions were produced using an absolute

least square linear regression. The concentrations of samples were then obtained by inputting the peak area to the linear regression equation from the calibration curve.

By using the internal standard in the aqueous samples, it was possible to calculate the aqueous naphthalene concentration using measurements that were known accurately (e.g., V_{is} , the volume of internal standard; V_{sam} , the volume of aqueous sample), or for which the uncertainty could be quantified (e.g., $NAPH_{hex}$ and $ACEN_{hex}$, the concentrations of naphthalene and acenaphthene measured by GC in the hexane extract). Thus, the aqueous concentration of naphthalene $NAPH_{aq}$ could be calculated with the following equation (Seagren and Moore 2003):

$$NAPH_{aq} = \frac{NAPH_{hex}}{ACEN_{hex}}\left(\frac{V_{is}}{V_{sam}}\right)ACEN_{is} \qquad (5.10)$$

where $ACEN_{is}$ = the known concentration of the internal standard solution, 500 mg/L.

A MDL study was performed for the aqueous concentration of naphthalene analysis using GC. It was determined the MDL for naphthalene analysis by GC method was 0.1 mg/L.

For the solid-phase samples, the naphthalene concentration determined in the hexane extract by GC analysis was multiplied by the volume of hexane, to give the mass of naphthalene in the known volume of hexane that was used for extraction. Then, the solid phase naphthalene concentration on the solid sample (mg naphthalene/dry g solid sample) was determined by dividing the mass of naphthalene extracted by the dry weight of solid sample.

5.5.1.2 Spectrofluophotometry

A spectrofluorophotometer (Shimadzu, RF5301 PC) method was utilized an alternative to measure the naphthalene concentration. In the naphthalene analysis, the excitation wavelength and emission wavelength utilized were 273 nm and 336 nm, respectively.

2 ml sample was transferred into the cuvette (Shimadzu, cell fluorimeter, 10 mm, Silica). The volume of 2 ml was experimentally determined to be large enough not to interfere with the fluorescein or naphthalene analysis, yet small enough not to disturb the flow in the ISFC while taking samples from it. The cuvette was put into the holder and the reading of concentration was recorded. After each sample measurement, the cuvette was washed with DI water 3 times, followed by washing with acetone once. A Vakuwash® cell washer (Bel-art Products, Pequannock, NJ USA) was used to accelerate the drying process of cuvette. The naphthalene analysis was conducted as soon as the samples were collected to minimize the loss due to vaporization.

Naphthalene intensity readings were converted to naphthalene concentration using standard curves. To prepare a standard curve, a naphthalene stock solution of 20 mg/L was made first, and standards at 15, 12.5, 10, 7.5, 5, 2.5, 1, 0.5, 0.1 mg/L were made by serial dilution. A multi-point working curve was utilized in the standard curve preparation, which was quantified by a third order of curve equation. The detection limit for the aqueous naphthalene analysis was reported to be 0.4 ppb (Famisan and Brusseau 2003; Mulder et al. 2000).

It is possible that intermediates formed during naphthalene biodegradation at occurred in the bioremediation simulation experiments might have interfered with the

naphthalene fluorescence measurements. However, on several occasions, naphthalene measurements of effluent samples using the spectrofluophotometry method were compared to the measurements using the GC and found to be comparable.

5.5.2 Non Reactive Tracer Analysis

5.5.2.1 Fluorescein

The spectrofluorophotometer (Shimadzu, RF5301 PC) method was utilized to measure the tracer fluorescein concentration. To measure the fluorescein, the excitation wavelength and emission wavelength were set up at 440 nm and 514 nm, respectively. The fluorescein samples were analyzed immediately after each tracer experiment due to its sensitivity to light. Fluorescein intensity readings were converted to fluorescein concentration using standard curves. To prepare a standard curve, a fluorescein stock solution of 50 mg/L was made first, and standards at 20, 10, 5, 2, 0.5, 0.1, 0.05 and 0.01 mg/L were made by serial dilution. The specific operation and calibration procedures were followed as described in Section 5.5.1.2.

5.5.2.2 Bromide (Br)

5.5.2.2.1 Bromide Probe

Bromide concentration in pore water samples obtained from bioremediation simulation experiments was measured using an Orion 94-35 Bromide Electrode (Thermo Electron Corporation, Beverly, MA), connected to an ion meter Orion Model 520A. The Orion double junction reference electrode 90-02 was utilized along with Orion 94-35. Filling solutions were added to inner chamber and outer chamber each time before using the electrode. A 5 M $NaNO_3$ solution was prepared as the

ionic strength adjustor (ISA) to ensure all samples having a constant background ionic strength.

Pore water samples taken from ISFC, which were analyzed for naphthalene concentration using a spectrofluorophotometer immediately after taking the samples, as described above, were subsequently poured from the cuvette back to the amber vial for storage in the refrigerator. Then, after the completion of each bioremediation simulation experiment, all the pore water samples were analyzed for the Br concentration. To perform the analysis, a 1 ml sample was taken using pipette, transferred into a 50-ml volumetric flask and then diluted to 50 ml using DI water. The diluted sample was next transferred into a 100-ml beaker, and 0.5 ml ISA solution added to adjust the ionic strength. The diluted solution was stirred thoroughly at a moderate speed. The electrodes were rinsed with DI water, blotted dry and placed into the beaker containing the diluted sample. When a stable reading was displayed, the mV value was recorded.

mV readings were converted to Br concentration in the diluted samples using standard curves. To make standard curves, a 1000 mg/L KBr standard solution was made by dissolving 1.488 g of KBr in 1L of DI water. Standards at 100, 75, 50, 25, 10, 5, 0.5 mg/L were made by serial dilution. Several standard curves of mV versus logBr concentration were prepared and the linear regression was performed to fit these data. In Scenario #2, a high salinity was utilized to inhibit the biodegradation. Different standard curves were prepared with the employed high salinity in standard solutions following the above procedures. The bromide concentration in pore water sample was then calculated by multiply the diluted sample concentration with the

dilution factor. The detection limit for the bromide probe was reported 0.4 ppm from the manufacture's manual.

5.5.2.2.2 Ion Chromatography

Bromide samples from tracer studies were originally analyzed using a Dionex DX-100 ion chromatograph with a Dionex AS4 column. The samples were filtered with 0.2 μm syringe filter. A solution of 1.2 mM sodium carbonate/2.8 mM sodium bicarbonate was employed as the eluent. The concentration of Br was determined against the standard curve prepared with KBr (Fisher Scientific) in DI water. The standard solutions were made using the technique as described in the above section.

5.5.3 CPC Analysis

In the surfactant-coated sand study, the CPC aqueous samples were analyzed using UV-vis Spectrophotometry. Specifically, a spectrophotometer (Shimadzu, UV160U) was used at the wavelength of 258 nm with 2 ml aqueous samples for analysis. The CPC samples were diluted appropriately to ensure the diluted concentration fall into the concentration range of standard solutions before the analysis. The absorbance readings were converted to CPC concentrations in the diluted samples using standard curves. To make standard curves, a CPC standard stock solution of 0.2 mM was made. Standards at 0.1, 0.05 and 0.01 mM were made by serial dilution. The linear regression was performed to fit the standard curve.

5.5.4 Chemical Oxygen Demand (COD) Test

In the biodegradation kinetic study, the initial and final substrate concentration and biomass concentration were express as COD. Therefore, COD tests

were conducted before the respirometry experiments to determine the ratio of S_0/X_0.

The dichromate reactor digestion method was used, with Hach's COD digestion regent vials (Sample concentration of 0~1500 mg/L). The vials contain the pre-measured reagents, including catalysts and chloride compensator. The COD reactor was turned on in advance to preheat to 150 °C. Two ml of inoculum sample was pipetted into vials. The outside of COD vials was rinsed with deionized water and wiped clean with a paper towel. A blank was prepared by substituting 2.00 ml deionized water for the sample. The vials were then incubated in the reactor for 2 hours to assure complete digestion. The reactor was turned off and the vials were cooled. The measurement was made either with the spectrophotometer at 620 nm or by titration.

COD calibration curves were prepared by digestion of dilutions from a 1000-mg/L stock solution of potassium acid phthalate (KHP). The stock solution was made by diluting 850 mg of dried (105°C, overnight) KHP in 1000 mL deionized water. COD analyses were performed following procedures from manufacture instructions (Hach Chemical Co., Loveland, CO). The selected COD vials are accurate over a range of 0-1500 mg COD/L with a typical method detection limit of 12 mg COD/L provided by the supplier's manual.

5.5.5 Dissolved Oxygen

Dissolved oxygen (DO) was determined utilizing an oxygen microelectrode (Microelectrodes, Inc., Bedford, NH USA), connected to an OM-4 oxygen meter. The measurement was taken during the bioremediation simulation experiments by

opening the Minert valve attached on the sampling port and inserting the tubing connected to the microelectrode flow cell into the outlet of the valve. About 0.1 ml pore water samples were then withdrawn into the flow-through chamber using a 1mL syringe. The oxygen percentage was recorded by the OM-4 meter and later converted into mg/L using the following equation:

$$S = (a/22.414) \times ((760 - p)/760) \times (r\%/100) \times 32000 \qquad (5.11)$$

where S = solubility of gas in mg per liter; a = absorption coefficient of gas at temperature; p = vapor pressure of water at temperature; and r% = actually reading in percent of oxygen.

The microelectrode was calibrated by a two-point calibrating using ambient air as well as in a sample with zero DO. The calibration with ambient air was performed whenever the microelectrode was used during the experiments. The calibration with a sample of zero DO was carried out once a week. The sample with zero DO was prepared by adding excess sodium sulfite, Na_2SO_3, and a trace of cobalt chloride, $CoCl_2$, to bring DO to zero (APHA et al. 1995). The relative accuracy of microelectrode was reported ±0.04 mg/L at 24°C by the manufacture.

5.5.6 Heterotrophic Plate Count (HPC)

During bioremediation experiments, the microbial populations in the porous media were estimated using the heterotrophic plate count(s) (HPC) to monitor the microbial number in the pore water, which, in turn, indicated the microbial biomass associated with porous media. The experimental procedures used in this method was adapted from Standard Method 9215 (APHA et al. 1995).

Petri dishes for the HPC were prepared using sterilized disposable petri dishes (VWR, No. 25384-070) and commercially available R2A agar (Difco, No. DF1826-17). Nine grams of R2A agar were added to 500 mL of deionized water and the solution was mixed and heated for complete dissolution. The R2A medium was autoclaved for 15 minutes at 121°C and cooled to about 45°C to 50°C for the proper amount of surface moisture and easy handling. Then, the agar medium was aseptically poured into the bottom of the sterile plates. Once the agar solidified, the plates were placed in a sealed bag and stored at 4°C in the refrigerator. The plates were predried in an incubator at 30°C for 24 hours before use to provide sufficient water loss from the surface of the agar. Throughout the plate preparation procedure and all following steps, aseptic techniques were used, and all of the equipment used (e.g., test tubes with caps, dilution bottles, pipette tips, and filter papers) were autoclaved before use.

Dilution water for diluting the aqueous samples was made with phosphate and magnesium chloride stock solutions (APHA et al. 1995). The stock phosphate buffer solution was made by dissolving 34.0 g of KH_2PO_4 in 500 mL deionized water, adjusting the pH to 7.2 ± 0.5 using 1 N NaOH, and diluting to 1 L with deionized water. The $MgCl_2$ stock solution was prepared by dissolving 81.1 g of $MgCl_2 \cdot 6H_2O$ in deionized water and diluting to 1 L. The final dilution water was made by adding 1.25 mL stock phosphate solution and 5.0 mL $MgCl_2$ stock solution and diluting to 1 L distilled water.

One mL of aqueous sample and 9 mL of dilution water were aseptically placed into a sterile dilution test tube and shaken for 30 seconds vigorously using a

mini vortexer (VWR Scientific Products), establishing a 10^{-1} dilution. The sample solution was further diluted by transferring 0.1 mL of sample from the first test tube into a second test tube containing 9.9 mL of dilution water, to produce a 10^{-3} solution. The same procedures were followed to obtain a series of test tubes with a range of sample dilutions. Subsequently, taking 1 mL or 0.1 mL of each suspension and transferring it to the agar plate established the desired dilution, or a one order of magnitude lower dilution, respectively. For example, if 1 mL and 0.1 mL of solution from the 10^{-3} dilution test tube are introduced to plates, the dilutions are 10^{-3} and 10^{-4}, respectively. The series of dilution steps performed is summarized in Figure 5.7.

After aseptically pipetting 1 mL or 0.1 mL of solution from each test tube onto the agar plates, the solution was distributed over the agar surface using a flame-sterilized bent glass rod while rotating the plate. The R2A agar plates for each dilution were prepared in duplicate. Subsequently, the edges of R2A agar plates were wrapped with Parafilm, and the plates were inverted and incubated at ~30°C for 48 hours. After incubation, plates having 30 to 300 colonies were considered in determining the plate count (APHA et al., 1995). All colonies in plates with appropriate range were counted. When counting was delayed, the plates were temporarily stored at 4°C. If the number of colonies per plate far exceeded 300, the result was recorded as "too numerous to count" (TNTC). The bacterial count per milliliter (colony-forming units (CFU)/mL) was computed by following equation:

$$CFU\ /\ mL = \frac{colonies\ \ counted}{actual\ \ volume\ \ of\ \ sample\ \ in\ dish, mL} \tag{5.12}$$

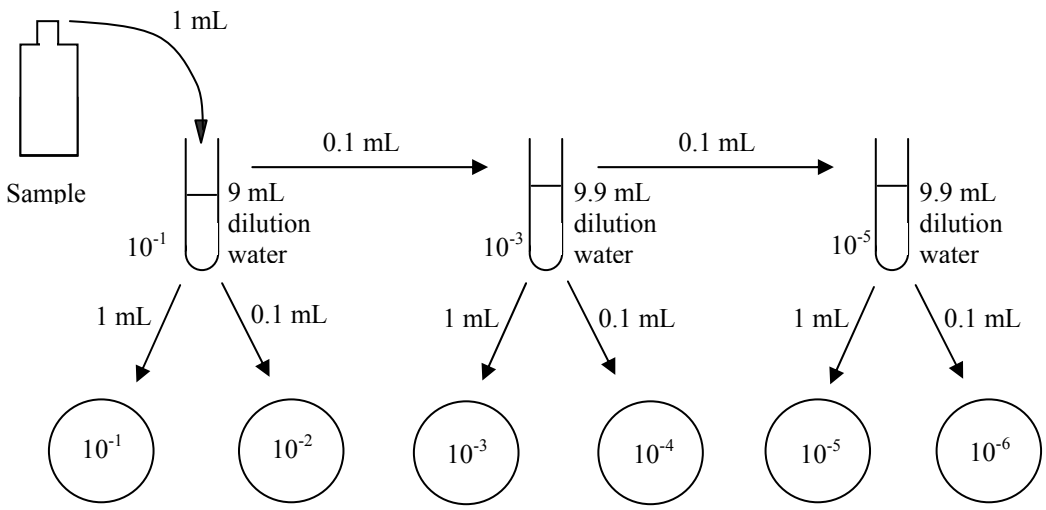

Figure 5.7 Sample dilution steps used for microbial plate counts.

Chapter 6 Results and Discussion

This chapter presents and discusses the results of the integrated modeling and experimental evaluation of the research hypothesis and quantitative framework. First, the results of parameter estimation experiments are presented. Next, the results of the control experiments are described and analyzed. Finally, the results from the Scenario #1 and Scenario #2 bioremediation simulation experiments are reported and evaluated. For each scenario, the Phase I data and parameter estimates are used to demonstrate the application of the quantitative framework to predict the rate-limiting process. Then a qualitative and quantitative comparison of the Phase I and Phase II data is used to investigate whether the appropriate perturbation to the system predicted based on the quantitative framework had the expected effect.

6.1 Parameter Estimation Experiments

6.1.1 Hydraulic Conductivity

The hydraulic conductivities determined for the Mystic White II Sand and Filtersil Sand using the constant head method and Equation 5.2 are given in Table 6.1. The order of magnitude of these K-values is reasonable based on representative values for different sands (Domenico and Schwartz 1998), which range from 9×10^{-7}-6×10^{-3} m/s for coarse sand to 2×10^{-7}- 2×10^{-4} m/s for fine sand. Furthermore, the hydraulic conductivity in the high-K layer (Mystic White II) sand was approximately 7 times larger than in the low-K layer (Filtersil) sand, which was close to the goal of a factor 10 times difference.

Table 6.1 Physical properties for Mystic White II and Filtersil sands

Sand	Properties				
	d_{10} (mm)[1]	K (m/s)[2]	ρ_b (kg/m^3)	ρ_p (kg/m^3)	ϕ
Mystic White II	0.8	0.0040 $\pm$ 0.0001	1415	2655	0.47
Filtersil	0.15	0.00065 $\pm$ 0.00008	1813	2788	0.35

[1] Source: manufacture,
[2] Average $\pm$ standard deviation for duplicate measurements.

6.1.2 Porous Media Density and Porosity

The results of the bulk density, ρ_b, and particle density, ρ_p, are summarized in Table 6.1. The particle density for Mystic White II sand reported by the supplier is 2650 kg/m^3, which is essentially the same as determined in this work and indicates that the techniques utilized in this research were able to accurately estimate the particle densities. The bulk density results presented were obtained during the packing of the ISFC. The order of magnitude of the bulk densities is reasonable compared to values reported in the literature for sands of a similar size (Pearce et al. 1994; Whelan et al. 1994). The porosity data that were obtained using the particle and bulk density values in Equation 5.3 are also presented in Table 6.1. These values fall into the reported porosity range of 0.31-0.46 for coarse sand and 0.26-0.53 for fine sand (Davis 1969; Schwartz and Zhang 2002), which further verifies that the techniques used to determine the bulk and particle densities were appropriate.

6.1.3 Dispersivity

As discussed in Section 5.3.3, the tracer study was conducted first with Br and then changed to fluorescein because of analytical difficulties. However, due to the sensitivity of fluorescein to light, there were some concerns as to whether the fluorescein would behave conservatively in the ISFC. Therefore, the breakthrough from a fluorescein tracer experiment was initially compared with that from a Br tracer experiment (Figure 6.1). Based on this comparison, it was confirmed that the techniques used in these tracer studies ensured that fluorescein was conservative.

The point-source tracer (fluorescein) experimental results are illustrated in Figures 6.2 and 6.3 for the high-K layer and low-K layer, respectively. The absolute least-square regressions for each concentration breakthrough curve are also included, which were obtained by using the FORTRAN program, "trafit3d", with the best fit estimates for the v_x and D_x values. The optimization routines always converged to the same solution from different initial v_x and D_x guesses, indicating that the obtained parameters were unique. A visual appraisal of the experimental data and the regression curves reveals a close match and indicates that the test data could be closely approximated by the FORTRAN program. The best-fit estimates for the parameter v_x and D_x obtained using the non-linear regression are listed in Table 6.2, along with the values for α_x, which were calculated by ignoring the molecular diffusion and assuming $\alpha_x = D_x / v_x$. The average longitudinal dispersivities calculated from the replicate experiments and used in RT3D and VMOD are presented in Table 6.3.

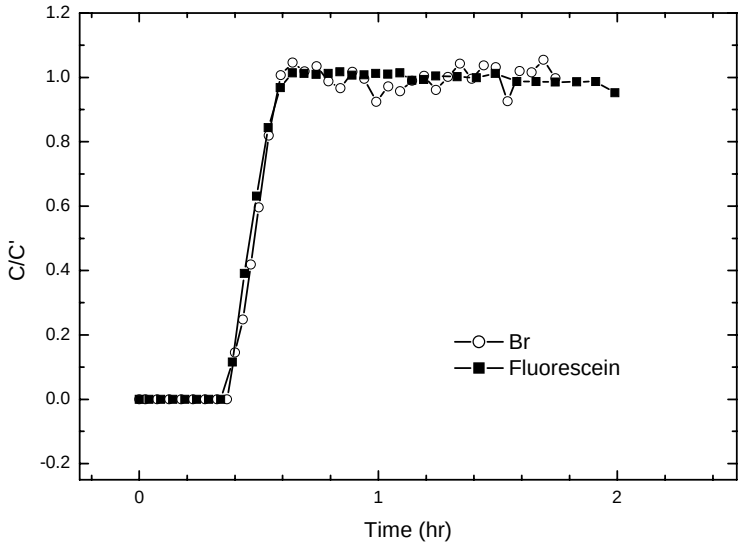

Figure 6.1 Comparison between breakthrough curves at sampling port B3 for the Br and fluorescein tracer experiments.

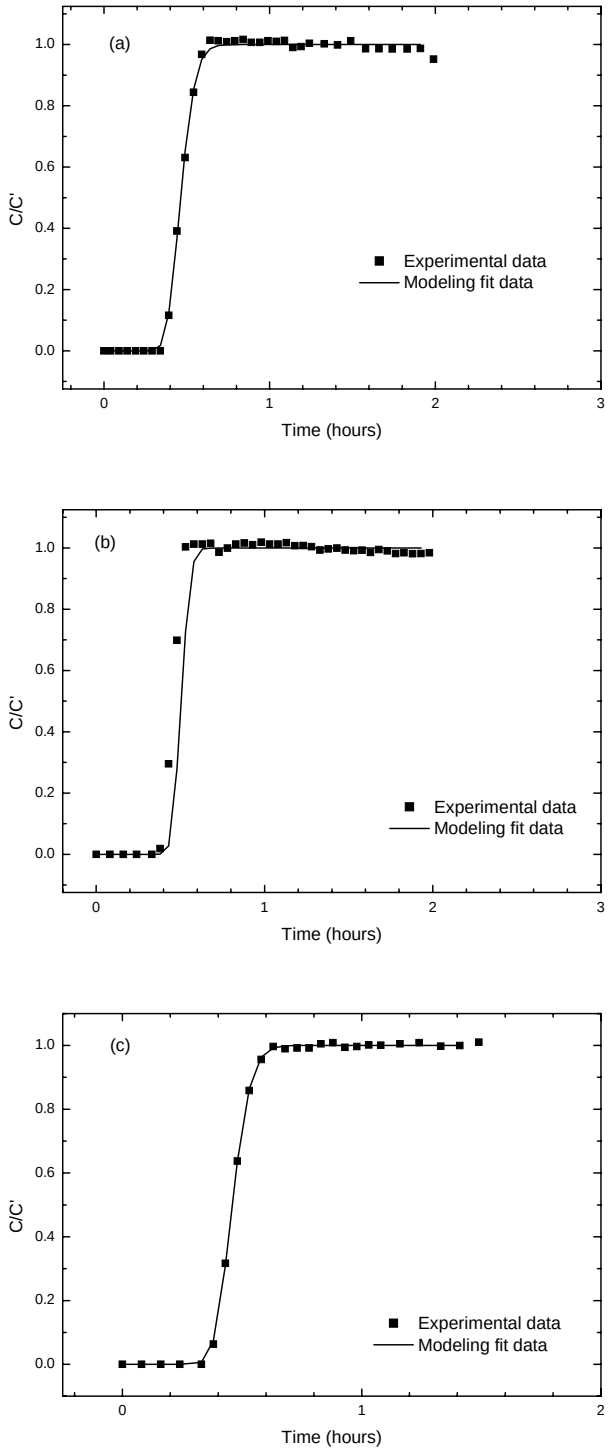

Figure 6.2 Breakthrough curves from continuous point source fluorescein experimental data along with the model fitting data in the high-K layer. Graphs (a), (b) and (c) are data from triplicate experiments.

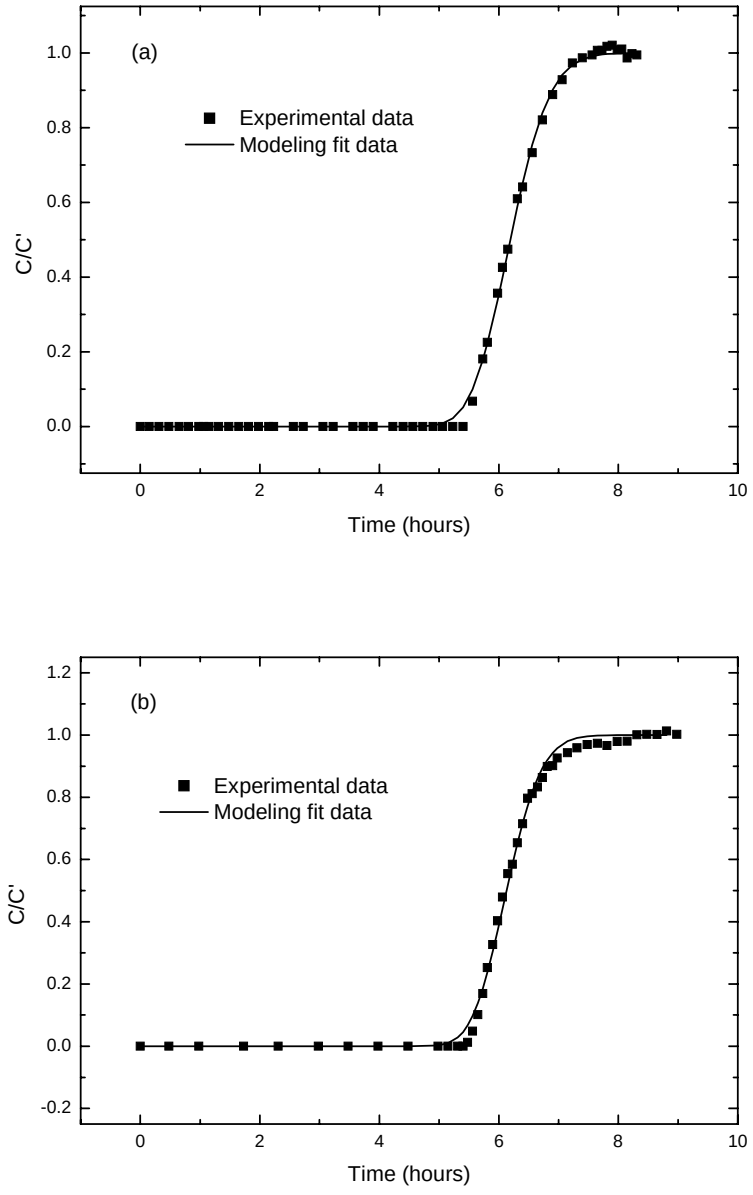

Figure 6.3 Breakthrough curves from continuous point source fluorescein experimental data along with the model fitting data in the low-K layer. Graphs (a), (b), (c) and (d) are data from replicate experiments.

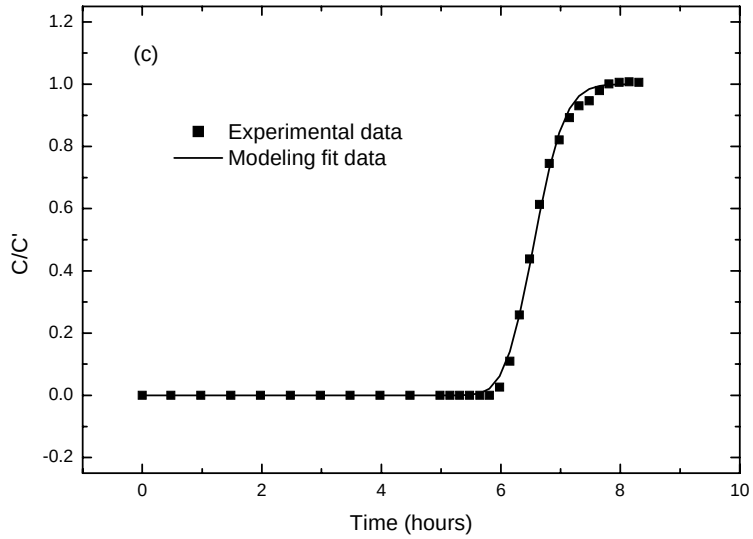

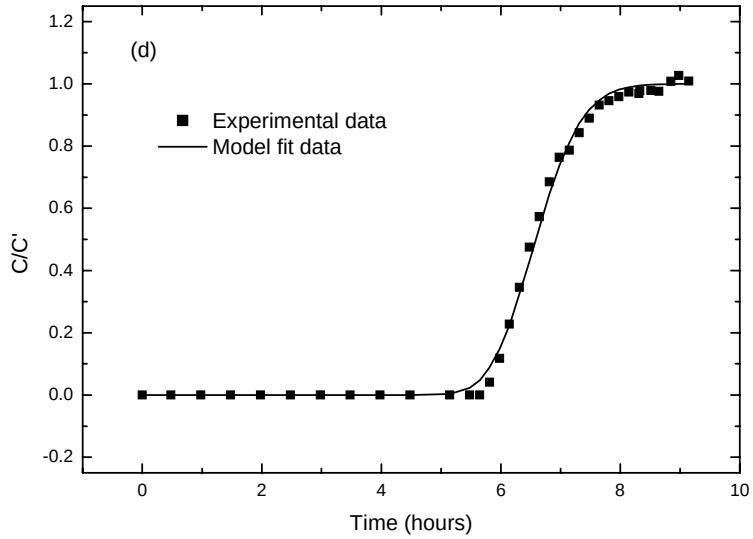

Figure 6.3 Continued

Table 6.2 FORTRAN "trafit3d" calibration results for the longitudinal dispersion

	Velocity (cm/hr)[1]	D_x (cm^2/hr)[1]	α_x (cm)[2]
High-K (a)	43.23	9.34	0. 22
High-K (b)	39.69	2.72	0. 07
High-K (c)	43.58	7.53	0. 17
Low-K (a)	3.23	0.23	0. 07
Low-K (b)	3.26	0.18	0. 06
Low-K (c)	3.05	0.11	0. 04
Low-K (d)	3.04	0.26	0.08

[1] Fitted value.
[2] Calculated value.

Table 6.3 Summary of non-reactive tracer results

	α_x (m) [1]	α_z (m) [1]	α_x / α_z
High-K Layer (0.8mm)	0.0015 ± 0.00070	7.6E-5 ± 9.7E-6	20
Low-K Layer (0.15mm)	0.0006 ± 0.0002	0.002 ± 0.001	0.3

[1] Average ± standard deviation for three measurements in the high-K layer and four measurements in the low-K layer.

Once v_x and D_x were estimated, the assumption that the experimental flow rates were large enough for D_x to be dominated by mechanical dispersion was confirmed in the two layers. First, based on Equation 5.7 and assuming an effective diffusion coefficient for fluorescein of 0.0104 cm^2/hr (Seagren 1994), the relative error of over estimation introduced by ignoring the molecular diffusion effect was approximately 2.9 % in the high-K layer and 1.8 % for the low-K layer. Second,

based on Rumer's (1962) study D_x is dominated by mechanical dispersion for Reynolds number $\mathrm{Re} > 10^{-3}$ (where $\mathrm{Re} = v_x d_{50} / \nu$, with d_{50} =50% grain size, and ν =kinematic viscosity). Using $\nu = 1.003 \times 10^{-6} m^2 / s$ at 20°C (Metcalf & Eddy Inc. 1991), d_{50} =1.2mm and $v_x = 1.2 \times 10^{-4} m/s$ (Table 6.2), and d_{50} =0.3mm and $v_x = 8.74 \times 10^{-6} m/s$ (Table 6.2), for Mystic White II sand in high-K layer and Filtersil sand in low-K layer, respectively, the Re numbers equals 0.14 for Mystic White II sand and 2.6×10^{-3} for the Filtersil sand. Both of these values are greater than 10^{-3} and also indicate that the approximation $D_x = \alpha_x v_x$ is appropriate.

The vertical transverse dispersion coefficient, D_z, was calculated using Equation 5.4. The tracer injection concentration, C_0, tracer injection rate, Q, and the steady-state tracer concentration, C', used in the equation are summarized in Table 6.4. The steady-state tracer concentration at the sampling location, C', was calculated by averaging the sample concentrations after they remain relatively constant (See Figure 6.2 and 6.3). When there was a question whether or not a sample concentration should be included in average, the Q test (Fritz and Schenk 1979), which uses the range to determine if a questionable result should be rejected for small sample numbers (n=3-10), was used with a 95% confidence to decide whether the value should be used in the average or not. The final value required for Equation 5.4, the distance between the tip of the injection needle and the tip of the sampling needle, x, was estimated to be 20.2 cm. The obtained D_z and α_z values are presented in Table 6.4 as well. α_z was calculated by assuming the effect of molecular diffusion was

Table 6.4 Vertical transverse dispersivities calculation summarization table

Tracer Fluorescein	Injection flow rate, Q (ml/min) [1]	Injection concentration, C_0 (mg/L) [1]	Steady-state concentration, C' (mg/L) [2]	Velocity, v_x (cm/hr) [3]	D_z (cm^2/hr) [2]	α_z (cm) [2]
High-K (a)	0.05	10	0.32	43.23	0.3696	0.0086
High-K (b)	0.05	10	0.35	39.69	0.3400	0.0076
High-K (c)	0.05	10	0.41	43.58	0.2933	0.0067
Low-K (a)	0.05	10	0.09	3.23	1.2877	0.4
Low-K (b)	0.05	14	0.63	3.26	0.2648	0.08
Low-K (c)	0.05	22	0.72	3.05	0.3657	0.12
Low-K (d)	0.05	22	0.48	3.04	0.5475	0.18

[1] Experimentally determined,
[2] Calculated value.

negligible, so $\alpha_z = D_z / v_x$. Using Equation 5.5, and applying the effective molecular diffusion coefficient for fluorescein in porous media, $D^* = 0.0104$ cm^2/hr (Seagren 1994), the relative error of over estimation introduced by ignoring the molecular diffusion effect was approximately 8% in the high-K layer and less than 2% for the low-K layer. The average vertical transverse dispersivities based on the replicate experiment, and later used in the RT3D/VMOD model predications, are summarized in Table 6.3.

Values of dispersivity generally appear to be dependent on the techniques utilized in testing or observation (Gelhar et al. 1992). The dispersivity values have been determined in a number of studies, e.g., (Gelhar et al. 1992; Pearce et al. 1994; Robbins 1989; Seagren et al. 1994; Szecsody et al. 1994; Voudrias and Yeh 1994). These studies provided a range of longitudinal dispersivity values from 10^{-4} m to 10^{-3} m. A rule of thumb is that α_x should be of the same order of magnitude as the mean grain size (Rumer 1962). This rule holds for the experimental values obtained in this research, as shown in Table 6.3. The values of transverse dispersivities from the above literature studies ranged from 10^{-5} m to 10^{-4} m, although most were between $1 \times 10^{-5}$and 8×10^{-5}m. The transverse dispersivity in the high-K layer is reasonable compared to the literature values. However, the dispersivity value in the low-K layer is relatively high in this study, because α_x is generally one order of magnitude higher than α_z, and in this layer α_x / α_z <1. A similar observation was made for the fine silica sand by Szecsody et al., (1994), who obtained an α_x / α_z =3. It is speculated that the

loosely packed fine sand in the low-K layer in the vertical direction may contribute to the high α_Z value. Other references who packed sand tanks in a similar manner, e.g., (Pearce et al. 1994; Voudrias and Yeh 1994; Whelan et al. 1994), also had relatively high α_z value, although not as high as found in this work. Nonetheless, these experimental values are reproducible and describe the ISFC simulated aquifer well, as demonstrated in the Section 6.2 Bioremediation Simulation Experiments. Therefore, they were utilized in the quantitative framework to define the rate-limiting process for the designed bioremediation simulation experiments.

6.1.4 Biodegradation Kinetics

As described in Section 5.4.3, careful manipulation of the batch respirometry experimental conditions, such as initial S_0/X_0 ratio, was necessary in order to reduce the correlations between Monod parameters and allow for the estimation of unique parameters with the lowest degree of uncertainty. The initial substrate concentration S_0, initial biomass concentration X_0, and S_0/X_0 are listed in Table 6.5 for the three kinetics experiments used in the data analysis of this work. These three experimental runs utilized three different inocula as follows: (1) an inoculum from the Uper-1 primary culture, (2) an inoculum aseptically collected from the ISFC effluent during the Scenario #1 Phase I experiment, and (3) an inoculum from the Uper-1 primary

Table 6.5 Biokinetic parameters for respirometry experiments

Cell Sources	Primary culture in MSNS (1)	Scenario #1 Phase I effluent (2)	Primary culture in MSNS with high salinity (3)
Initial substrate, S_0 [1] (mg/L as COD)	30	30	30
Initial biomass, X_0 [2] (mg/L as COD)	0.6	0.5	320
S_0 / X_0	50	60	0.09
Yield Coefficient, Y (mg biomass / mg naphthalene) [3]	1.12	0.34	1.27
μ_{max} (/hr), initial estimate	0.050	0.050	0.004
μ_{max} (1/hr), best-fit	0.015	0.060	0.001
K_S (mg/L), initial estimate	4.0	5.3	2.0
K_S (mg/L), best-fit	5.0	8.0	1.7

[1] Based on measured naphthalene concentration and 3 mg COD/mg naphthalene.
[2] Measured COD.
[3] Calculated using Equation 5.9.

culture in MSNS with high salinity to represent the slow biokinetics in Scenario #2 Phase I. The initial S_0/X_0 ratios for experimental runs (1) and (2) were set up to be 50 and 60, respectively, to obtain the "intrinsic" kinetics, which represented the maximum capabilities of the Uper-1 primary culture and the culture in the ISFC effluent. For experimental run (3), the S_0/X_0 ratio of 0.09 was achieved, indicating the biokinetics obtained were neither intrinsic nor extant (Grady Jr. et al. 1996). Unfortunately, this experiment, which was performed in MSNS with high salinity (5% w/v as used in Scenario #2 Phase I), was the only data set available for quantifying the effect of high salinity on the biokinetics of Uper-1. Respirometry experiments using an inoculum collected from the ISFC effluent during Scenario #2 Phase I, which had the high salinity, were conducted under intrinsic conditions as well, just as in Scenario #1 Phase II. However, although there was a long lag phase, apparently due to the high salinity, the culture always eventually exhibited biokinetics comparable to the uninhibited cells in the Scenario #1 Phase I effluent. These biokinetics were inconsistent with Uper-1's performance in the ISFC with high salinity. Therefore, the slow biokinetics were estimated using the inoculum from the Uper-1 primary culture inhibited with high salinity experiment (Run 3). Finally, a respirometry experiment using an inoculum collected from Scenario #1 Phase II was also conducted once, but resulted in an invalid data set based on the technique for initial parameter estimates described below. Therefore, only the above mentioned three experimental results are reported.

Before performing the nonlinear parameter estimation using the FORTRAN program "nvolma", some initial work was required. First, before the raw data could be used for parameter estimation, some clean-up of the data was required. Specifically, in the plot of cumulative oxygen uptake, there were instances in which lags existed before initiation of oxygen uptake. The points recorded during the lag phase were removed from the data set because the models employed do not account for a lag phase.

Second, initial estimates of the yield coefficient, Y, maximum specific growth rate, μ_m, and half-saturation constant, K_s, were required. The initial estimates of the yield coefficients were calculated from the oxygen consumption at the plateau of the accumulated oxygen uptake profile (e.g., Figure 6.5) by using Equation 5.9 and are summarized in Table 6.5 for the respirometry experiments with the three different sources of initial inoculum. Based on the work of Brown, et al. (1990), these initial estimates of the yield coefficients were just used as the final parameter values.

Although the determination of the final $\mu_{\max}$ and K_S values were accomplished by nonlinear parameter estimation using the FORTRAN routine, good initial guesses were necessary to make the search progress more efficient and to perform the search in the appropriate range in order to obtain the best fit. Thus, it was desirable to have a reliable technique to make initial estimates, which could also be used to examine whether the data sets were satisfactory for parameter estimation. Therefore, the techniques utilized by Brown et al. (1990) were employed in this study, which proved to be very valuable during initial parameter estimation, as described below.

In the initial estimate technique employed, it is assumed that the biomass concentration in a batch reactor increases at a rate that is first order with respect to biomass concentration during growth conditions in which endogenous metabolism and biomass decay may be neglected, which holds for this respirometry study. Thus, a plot of dX / dt vs. X will have a constant positive slope equal to the specific growth rate, μ, until something becomes limiting in a reactor (Kono and Asai 1969). In addition, for a batch reactor, dX / dt is proportional to the rate of oxygen uptake, dO_u / dt, whereas X is proportional to the cumulative oxygen uptake, O_u (Dand et al. 1989). Thus, a plot of dO_u / dt vs. O_u will exhibit the same characteristics as a plot of dX / dt vs. X, with a slope equal to μ. Therefore, a routine was created in a Microsoft Excel spreadsheet that used the cumulative oxygen uptake data to calculate the rate of oxygen uptake as a function of time, $\Delta O_u / \Delta t$, for successive data points. Then those data were used to make a plot a four point running average of dO_u / dt versus the cumulative oxygen uptake, O_u (Brown et al. 1990). A typical plot for a valid data set (Run 2) is shown in Figure 6.4.

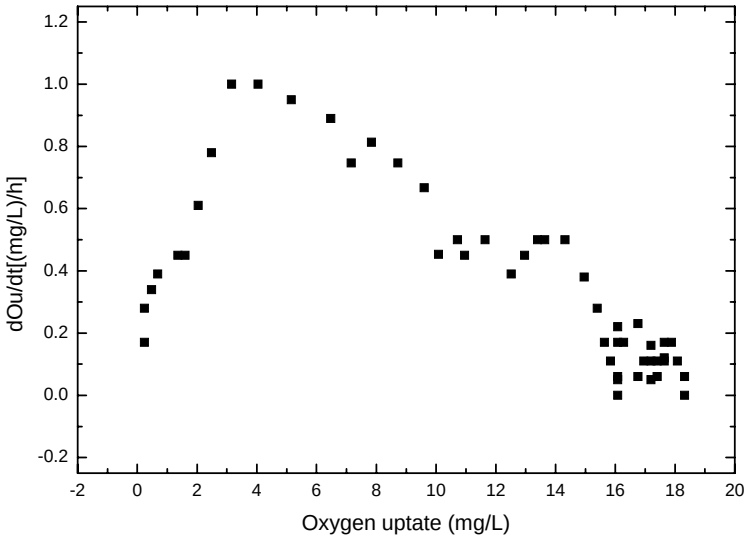

Figure 6.4 Typical plot of the rate of oxygen uptake vs. the cumulative oxygen uptake for a valid data set (Run 2) (an inoculum collected from the ISFC effluent during Scenario #1 Phase I).

In the Monod kinetics, the values of μ can then be obtained from the calculated oxygen update rates $\Delta O_u / \Delta t$ using (Brown et al. 1990):

$$\mu = \frac{(dO_u / dt)_t}{(X_0 / Y)(1 - Y_p - Y) + (O_u)_t} \tag{6.1}$$

The calculated μ values were then plotted as a function of oxygen uptake. Based on that point, the initial estimate of $\mu_{\max}$ was easily obtained as the maximum observed value of μ. Because K_S is the substrate concentration corresponding to $\mu =$ $0.5\,\mu_{\max}$, an initial estimate can obtained from the equation (Brown et al. 1990):

$$K_s = S_0 - \frac{O_{uh}}{1 - Y_p - Y} \tag{6.2}$$

where O_{uh} is the oxygen uptake associated with $\mu = 0.5\,\mu_{\max}$. The initial estimates for $\mu_{\max}$ and K_S made based on this approach are summarized in Table 6.5, along with the final parameter estimation results. These biokinetic parameters were obtained by fitting a single oxygen cumulative curve, although 2 or 3 vessels were set up for each run. The model results using the best fit parameters are demonstrated in Figure 6.5, along with the laboratory cumulative oxygen uptake profile.

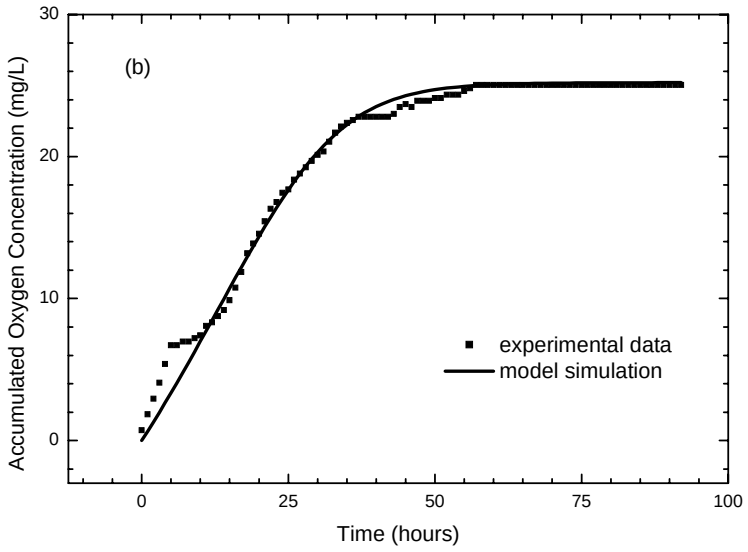

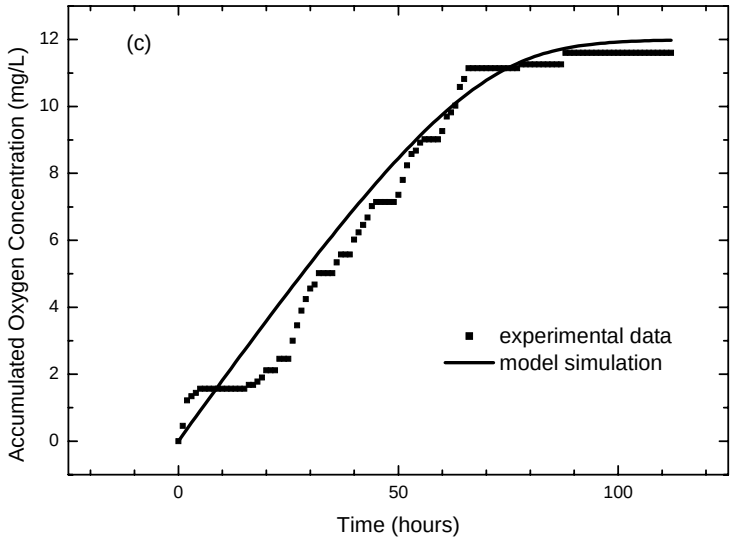

Figure 6.5 Cumulative oxygen uptake profiles during respirometry batch growth with Uper-1 from different cell sources: (a) an inoculum from the Uper-1 primary culture, (b) an inoculum aseptically collected from the ISFC effluent during the Scenario #1 Phase I experiment, and (c) an inoculum from the Uper-1 primary culture in MSNS with high salinity.

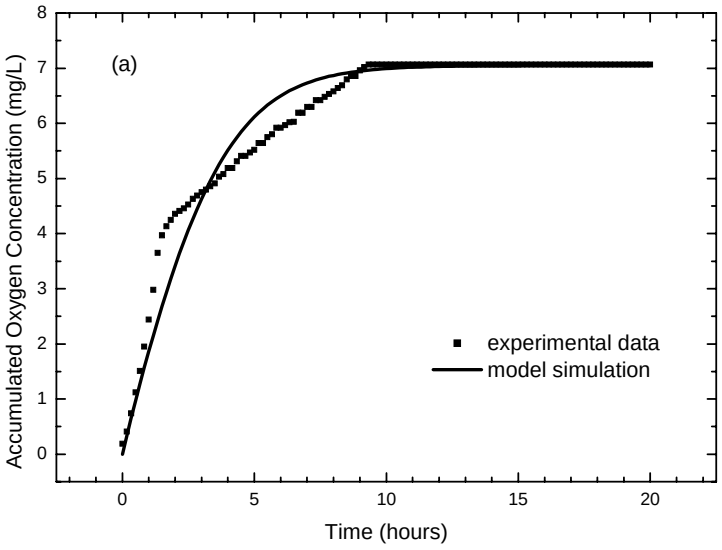

Figure 6.5 Continued

The calculated yield coefficients in Table 6.5 are consistent with yield values reported in the literature for naphthalene, which range from 0.25 -1.2 (Ghoshal and Luthy 1998; Volkering et al. 1993; Woozinski and Johnson 1968). However, it was surprising that the yield coefficient with the high salinity inhibition (1.26) was higher than the one obtained without inhibition (0.34). This might be due to the source of inoculum, because the Y values obtained using the primary culture (with or without inhibition) are similar to each other, whereas the value calculated using inoculum from Scenario #1 Phase I effluent is much lower. Alternatively, it could be that the nutrient levels were reduced in the effluent sample, which reduced the yield. The final μ_{max} estimation of 0.06 hr^{-1} (1.44 d^{-1}) obtained using the inoculum collected from Scenario #1 Phase I effluent is comparable to the literature values of 0.7-1.2 d^{-1} by Goshal et al. (1996), 1.6 d^{-1} by Goshal and Luthy (1998)and 7.9 d^{-1} by Volkering et al. (1993). The μ_{max} value obtained from primary culture with high salinity for Scenario #2 is fairly reasonable considering the inhibitory effect of the high salinity, which is expected to slow down the specific growth rate. Interestingly, the intrinsic biokinetics, i.e., the maximum capability of the isolated culture growing aerobically on naphthalene measured with the Uper-1 primary culture was estimated to be only 0.015 hr^{-1} (0.36 d^{-1}), which is lower than the value obtained from the Scenario #1 Phase I effluent experiments. Nonetheless, this value was not utilized in the evaluation of the quantitative framework. The K_S values are in the same order of magnitude as reported in the literature for naphthalene, which range from 0.02-3.4 mg/L (Ghoshal and Luthy 1998; Ghoshal et al. 1996; Volkering et al. 1993). Therefore, the kinetic coefficients appear reasonable and the values obtained with the

Scenario #1 Phase I effluent and the primary culture in MSNS with high salinity were used in the dimensionless number analysis.

6.1.5 Sorption/Desorption Equilibrium and Kinetics

6.1.5.1 Unmodified Sand Sorption

The naphthalene sorption isotherm for the unmodified coarse sand provided a baseline to compare with the sorption capacity of modified sands in the later experiments. The equilibrium solid-phase concentration data as a function of the equilibrium liquid-phase concentrations are presented in the naphthalene sorption isotherm plot in Figure 6.6. The partitioning coefficient, K_d, was obtained by fitting the experimental data with the linear sorption isotherm model. As expected given the relatively low organic content of the coarse sand, the unmodified coarse sand shows relatively low sorption capacity, as verified by the partitioning coefficient of 0.0031 L/g sand. It was assumed that the partitioning coefficient for the unmodified fine sand was comparable considering the similar properties for both sands, such as the negligible organic content. Given the low sorption levels on the unmodified coarse sand, the sorption/desorption kinetics were not determined, but were assumed to be very fast.

6.1.5.2 HMN-Coated Sand Sorption

The results of the HMN-coated sand sorption isotherm experiments are shown in Figure 6.7, and suggest a linear relationship between the experimental sorbed and aqueous phase equilibrium concentration data. Applying the linear isotherm model, the partitioning coefficients, K_d, are 0.010 L/g and 0.016 L/g for the HMN-Coated Mystic White II coarse sand and Filtersil fine sand, respectively.

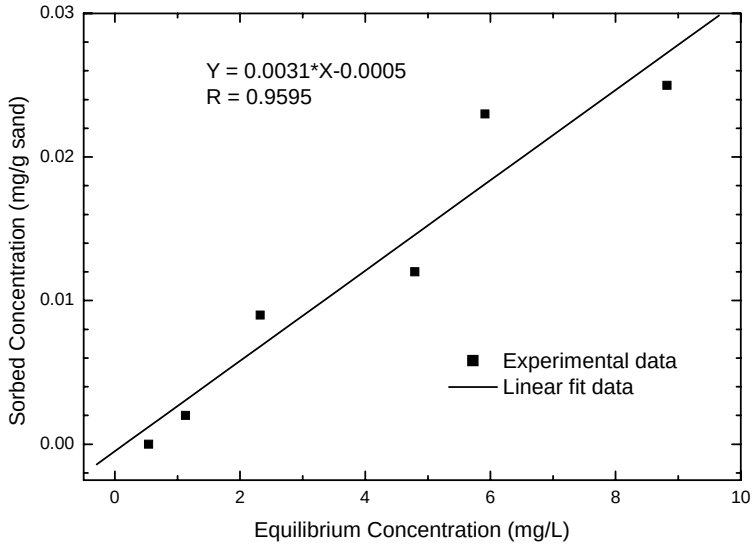

Figure 6.6 Naphthalene sorption isotherm onto unmodified coarse sand.

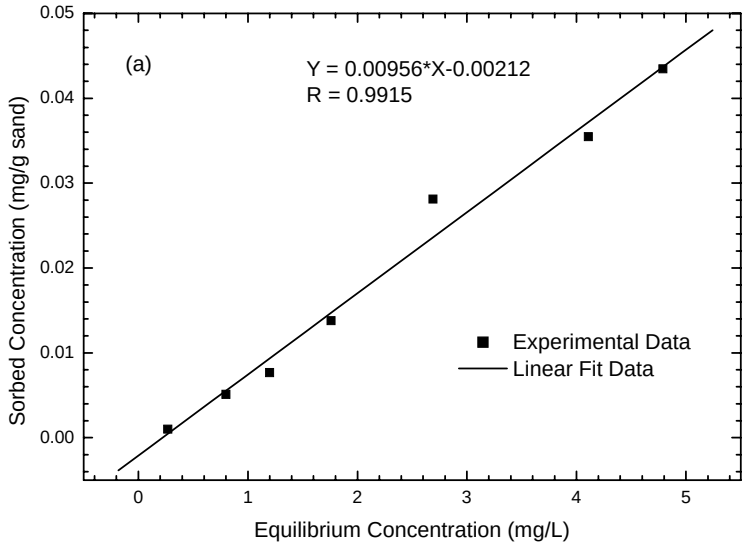

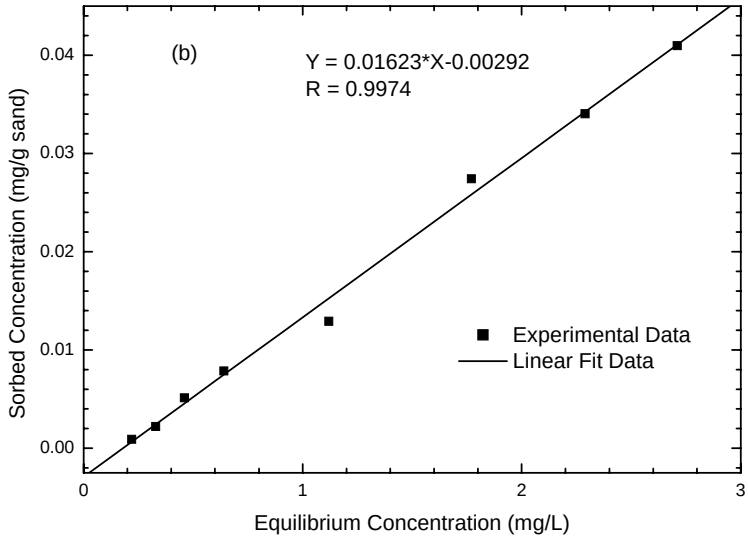

Figure 6.7 Naphthalene sorption isotherms onto HMN-Coated sands: (a) HMN-Coated Mystic White II coarse sand, and (b) HMN-Coated Filtersil fine sand.

The partitioning coefficients for HMN-coated sands are fairly high compared to the values of 8×10^{-5} and 1.7×10^{-4} L/g reported for two types of sands by Appert-Collin et al., (1999). Compared to the sorption capacity of unmodified sand, the increases in the partitioning coefficients with the HMN coating are 3.2 and 5.2 times for the Mystic White II and Filtersil sands, respectively (assuming $K_d = 0.0031$ L/g for both sands). Although the increase in the partitioning coefficients is fairly significant due to the very low sorption capacity of the unmodified sands, most of the naphthalene still remained in the aqueous phase, as demonstrated by the equilibrium aqueous naphthalene concentrations. As discussed in Section 5.3.5, one of the major concerns regarding the modified porous media system was that the modified system should possess a strong sorptive capacity, yet slow desorption rate, so that the sorption/desorption rate would limit the overall bioremediation rate. Therefore, there was concern that the sorption capacity of the HMN-coated sands did not increase enough compared to the unmodified sand to meet the above requirement. Furthermore, Appert-Collin et al., (1999) showed that the desorption rate of naphthalene from HMN-coated sand was relatively fast, which did not meet the requirement that the desorption rate should be the overall rate-limiting process for *in situ* bioremediation. Therefore, the idea of coating sand with HMN was abandoned for the utilization in this project, and no sorption/desorption kinetic experiments were performed.

6.1.5.3 Surfactant (CPC)-coated sand sorption

The major factor that affects the capacity of sand to sorb a surfactant coating is the cation exchange capacity (CEC). Although the CEC value for Mystic White II coarse sand was determined with Agri Analysis, Inc., it was measured again when the CEC value for the Filtersil sand needed to be determined. The CEC value for the Mystic White II and the Filtersil sands were determined to be 0.1-0.3 meq/g by the Maryland Cooperative Extension Soil Testing Lab (University of Maryland, College Park, MD USA). These low values suggest that this approach may be challenging, although others have reported success applying surfactant coatings to sandy aquifer materials, e.g.,(Kibbey and Hayes 1993).

In the investigation of CPC-coated sand sorption, the operational conditions that promoted the best surfactant coating results were determined and found to be pH=9, when the aqueous phase was DI water. It was also shown that CPC sorption onto sand reached equilibrium within 14 hours. Therefore, a mixing time of 24 hours was used subsequently to ensure the sorption equilibrium of CPC onto the sand.

Critical micelle concentration (CMC) is another key factor that affects the coating of CPC on the sand. Kibbey and Hayes (1993) reported the CMC for CPC to be 4.4×10^{-5} M at 0.1 M ionic strength and 25°C. However, in general, the CMC values are subject to large changes depending on factors such as temperature, ionic strength and pH. It was estimated that the CMC for CPC for the conditions used in this study was between 1×10^{-4} and 3×10^{-4} M by examining the CPC aqueous solutions. When the CPC concentrations were greater than 1×10^{-4} M, no CPC was sorbed on the sand, suggesting the formation of micelles, which interfered with the

coating of CPC and measurement of CPC by spectrophotometer. Therefore, the CPC sorption isotherm was conducted with CPC concentrations lower than 1×10^{-4} M. The CPC partitioning coefficient was determined to be 0.02 L/g under the experimental conditions, which is much lower than the value of 16 L/g reported by (Kibbey and Hayes 1993) for CPC-coated silica, probably due to the low CEC value of the coarse sand used in this study.

The naphthalene sorption isotherm onto the CPC-coated Mystic White II coarse sand is shown in Figure 6.8. Again the data appeared to be linear and a linear isotherm model was applied. The partitioning coefficient (K_d) was determined to be 0.0064 L/g. This represents an increase in the value of twice over the unmodified sand, but it is still relatively low, suggesting very little naphthalene sorbed on the CPC-coated sand, consistent with the limited amount of CPC coating on the sand. As with the HMN-Coated sands, a synthetic model soil with such limited sorption capacity could not sorb enough naphthalene to meet the requirement of Scenario #3, which disqualified the CPC-coated sand as a candidate for the synthetic model soil. Therefore, no further study was conducted with CPC-coated Filtersil sand because of its even lower CEC, and no sorption/desorption kinetics experiments were performed.

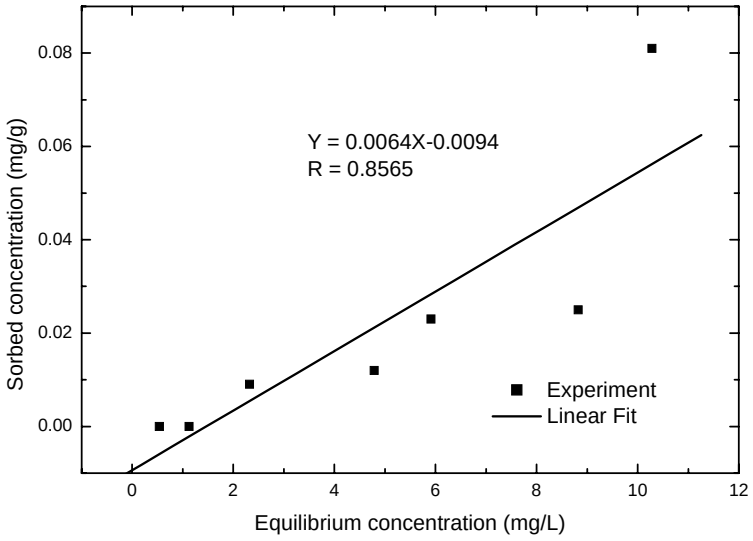

Figure 6.8 Naphthalene sorption isotherms onto CPC-coated Mystic White II sand.

6.1.5.4 Mixing sands with Amberlite Resins

The naphthalene sorption onto Amberlite resin XAD-2 was investigated first and the resulting isotherm data are presented in Figure 6.9. These data showed that XAD-2 had a significant sorption capacity for naphthalene. A comparison of sorption isotherm models revealed that the XAD-2 data could be described using the Freundlich equation. Therefore, the best fit of the Freundlich equation to the experimental data by the linear regression of log (Q) versus log (C) is shown along with the experimental data in Figure 6.9, and the resulting Freundlich equation constants are given in Table 6.6. Guerin and Boyd (1997) reported a K_d value of 13.6 L/g for the naphthalene sorption isotherm on XAD-2, which is in the same order of magnitude of the value obtained in this study, although smaller. Nonetheless, both the partitioning coefficients suggest that the sorption capacity of XAD-2 for naphthalene is very large.

Table 6.6 Freundlich constants for sorption of naphthalene from XAD-2

Material	K_f $(mg^{1-1/n} \cdot L^n \cdot g^{-1})$	n
XAD-2	56	0.46

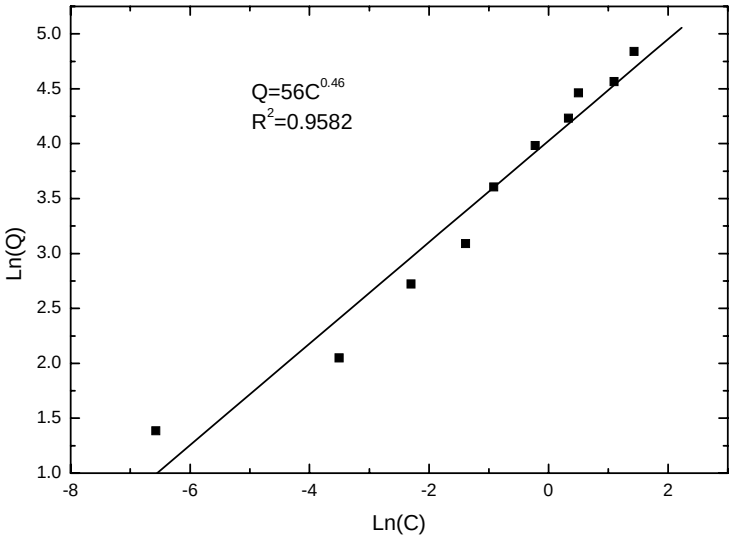

Figure 6.9 Naphthalene sorption isotherm onto XAD-2.

Although it was demonstrated that XAD-2 has a large sorption capacity for naphthalene, there was concern that the naphthalene desorption rate from XAD-2 would be extremely slow (based on an approximate evaluation of XAD-2 properties such as pore size and polarity), which would make the experimental operation in Scenario #3 infeasible if it took too long to monitor the desorption process. In addition, as described previously, in Section 5.3.5, another major concern about the synthetic sorption system is that the modification to the porous media should not significantly alter the hydraulic conductivities of the two-layer ISFC system, nor should they alter the amount or the nature of the surface area available for microbial attachment and growth. However, the skeleton density of XAD-2 is 640 kg/m^3, which is significantly lower than the particle densities of both Mystic White II coarse sand and Filtersil fine sand (Table 6.1). As a result, there was some concern regarding the potential for floating of XAD-2 in the synthetic sorption system. Therefore, XAD-7 (Alltech, USA) was chosen as an alternative to evaluate. Although it has lower sorption capacity for naphthalene compared to XAD-2, the partitioning coefficient was expected to sufficiently high to ensure that enough naphthalene could be sorbed on the XAD-7. In addition, XAD-7 possesses more attractive physical properties, such as a density of 1240 kg/m^3, which is more similar to the sands used in ISFC. Therefore, it was decided that, compared to XAD-2, the mixing of XAD-7 resin with sand was less likely to affect the hydraulics in the ISFC significantly. Therefore, all further efforts were focused on the sorption/desorption of XAD-7.

The experimental data for the naphthalene sorption isotherm using XAD-7 is presented in Figure 6.10, and the naphthalene sorption isotherms onto mixtures of

XAD-7 with Mystic White II coarse sand and the Filtersil fine sand are presented in Figure 6.11 and 6.12, respectively. In all cases, the data were fit with the linear isotherm model. Two observations can be made with regard to the naphthalene sorption isotherms on XAD-7. One, the partition coefficient of naphthalene on XAD-7 was 3.9 L/g, based on the linear sorption model, which was much higher than the value reported by Mulder et al. (2000). In their study, the naphthalene sorption isotherm on XAD-7 was described by the Freundlich isotherm model, with the K_d and n values of 1.93 L^{3n}/g^n and 0.69, respectively. This difference is speculated to be possibly due to the fact that in Mulder et al. (2000) study, the XAD-7 was sieved and the resulting size fractions were utilized, whereas the XAD-7 was utilized without any sieving pretreatment in this study. Two, as summarized in Table 6.7, the partition coefficients for the mixtures of XAD-7 with Mystic White II coarse sand and Filtersil fine are less than for XAD-7 alone, which suggests that the presence of the sand interferes with the contact between the naphthalene and XAD-7, resulting in the decreased sorption capacity.

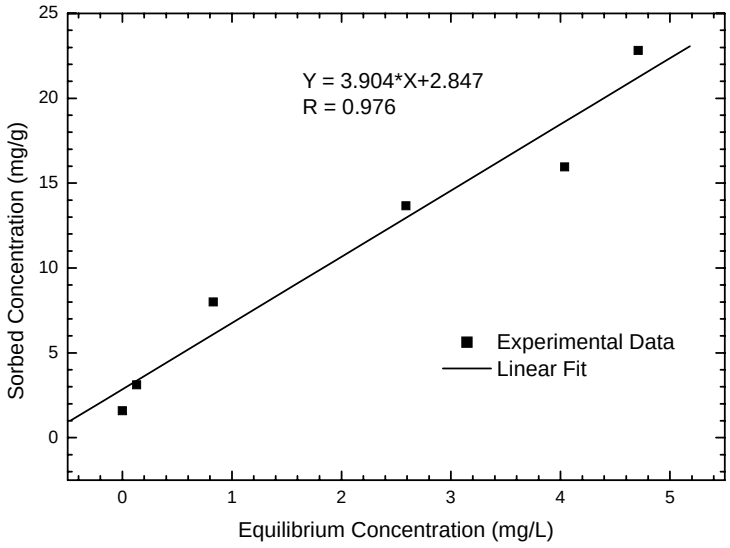

Figure 6.10 Naphthalene sorption isotherm onto XAD-7.

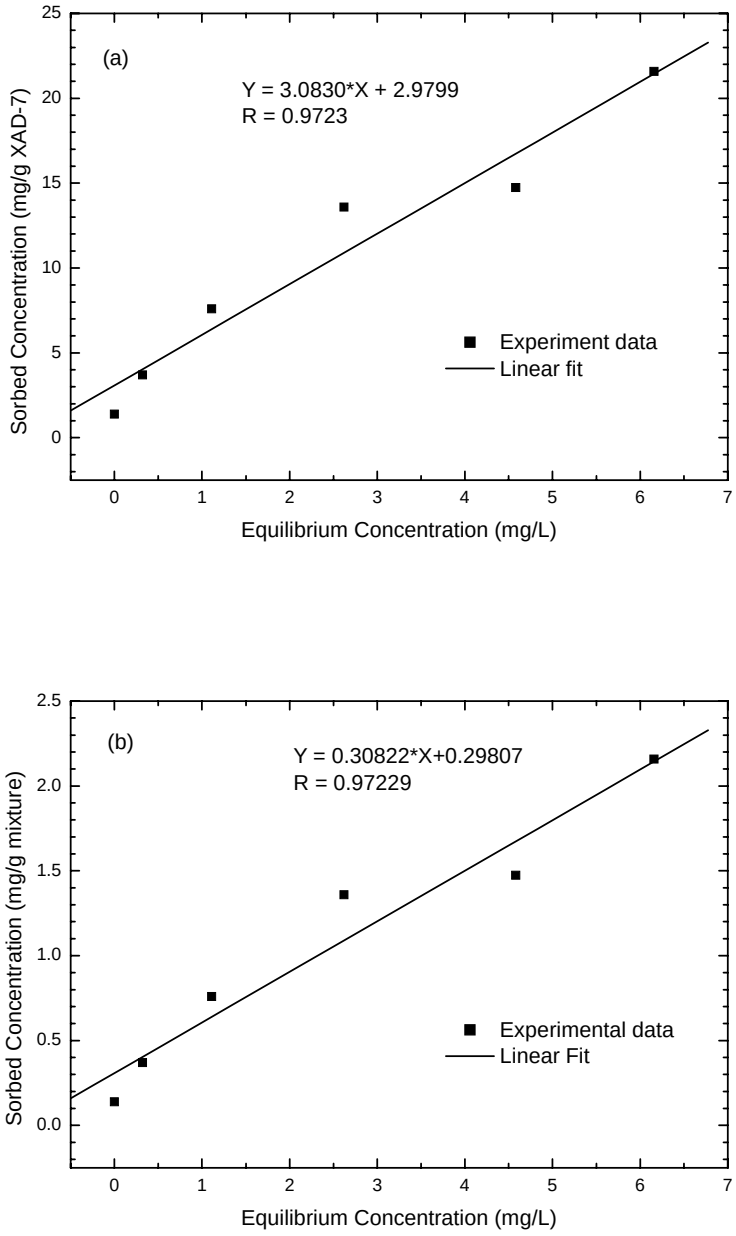

Figure 6.11 Naphthalene sorption isotherms onto the mixture of Mystic White II coarse sand and XAD-7 (10% w/w of XAD-7): (a) Sorbed concentration based on the XAD-7 mass; and (b) Sorbed concentration based on the mass of the mixture of XAD-7 with Mystic White II coarse sand.

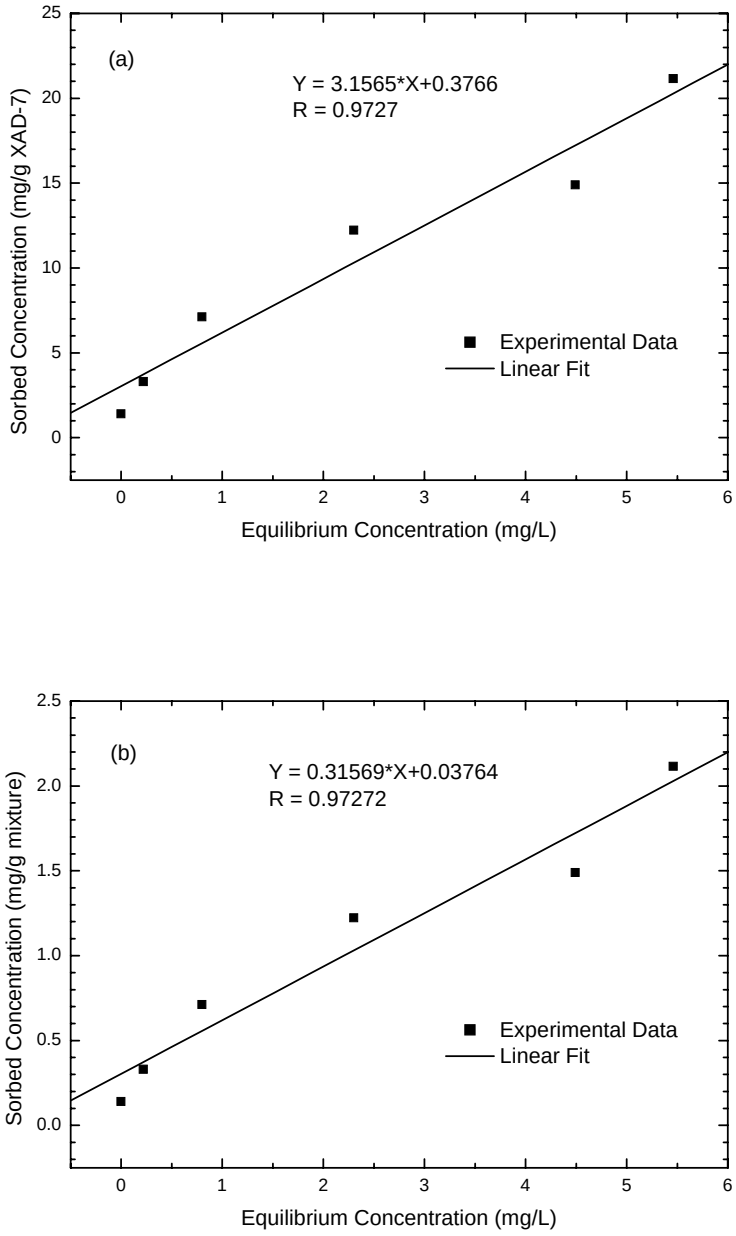

Figure 6.12 Naphthalene sorption isotherms onto the mixture of Filtersil fine sand and XAD-7 (10% w/w of XAD-7): (a) Sorbed concentration based on the XAD-7 mass; and (b) Sorbed concentration based on the mass of the mixture of XAD-7 with Filtersil fine sand.

Table 6.7 Partition coefficient of naphthalene onto XAD-7

Sample	Partition coefficient, K_d (L/g XAD-7)
XAD-7	3.904
Mixture of XAD-7 (10% w/w) with Mystic White coarse sand	3.083
Mixture of XAD-7 (10% w/w) with Filtersil fine sand	3.157

Once the properties describing the sorption equilibrium for naphthalene on XAD-7 had been quantified, the next step was to quantify the sorption/desorption kinetics. The sorption/desorption kinetic parameters were estimated using a nonlinear minimization procedure with the dual resistance CMBR model (Equation 3.8). Figures 6.13 and 6.14 present the experimental results of the sorption and desorption rate studies, respectively, along with the model nonlinear regression. These results indicated that the sorption/desorption process exhibited a phased behavior, proceeding with a rapid initial rate that was followed by a slower rate, which required as long as several days to approach equilibrium. The sensitivity analysis performed for the dual resistance model demonstrated that the film transfer rate may be estimated from the sorption rate at early values of time, while surface diffusivity usually controls the rate of sorption after long periods of time (Mulder et al. 2001). This observation was applicable to the stirred CMBR data of this study

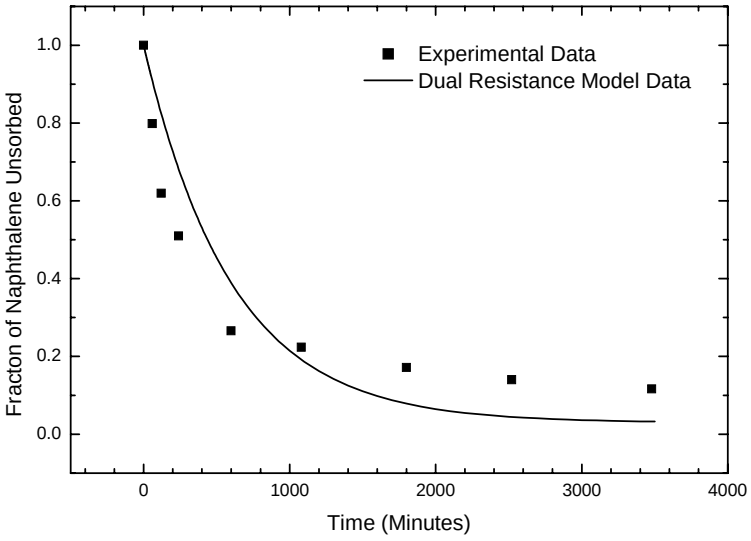

Figure 6.13 Naphthalene sorption kinetics onto a mixture of coarse sand XAD-7.

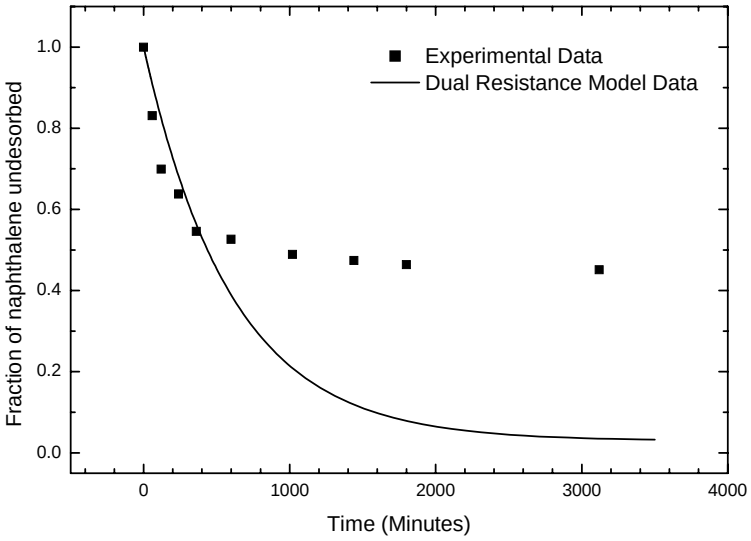

Figure 6.14 Naphthalene desorption kinetics from a mixture of preloaded coarse sand and XAD-7.

In the sorption kinetic study, the best fit model parameters for the dual-resistance CMBR model were 9×10^{-4} cm/s and 1.3×10^{-8} cm^2/s for the film transfer coefficient and intraparticle diffusion coefficient, respectively, whereas in the desorption study, these two values for the film transfer coefficient and intraparticle diffusion coefficient were 2×10^{-4} cm/s and 1.3×10^{-8} cm^2/s, respectively. These values were obtained by fitting the CMBR model with both kinetic experimental data. The sorption rate model provided reasonable reproduction of the observed laboratory sorption data (Figure 6.13). However, the desorption rate model prediction did not reproduce the observed experimental data well at the later stage of the desorption process (Figure 6.14). Based on these experimental observations, it was speculated that there was a fraction of residual naphthalene that either desorbed only at an extremely slow rate, or did not desorb from XAD-7 at all, indicating that a fraction of naphthalene sorbed onto XAD-7 was irreversible.

As discussed in Section 3.2, at high Biot numbers ($Bi >> 1$), film diffusion limitations can be neglected and intraparticle mass transfer is the rate-limiting step. In this study, the surface- and pore- based Biot number is 5.4×10^{5}, which indicates that the intraparticle mass transfer is the rate-limiting process for the naphthalene sorption/desorption process. Therefore, the intraparticle diffusion coefficient was estimated to be the representative kinetic rate parameter with a value of 1.3×10^{-8} cm^2/s, which would be adjusted by the radius of the particle, R, to be utilized in the quantitative framework for the simulated bioremediation experiment Scenario #3. The intraparticle effective diffusion coefficient of 1.3×10^{-8} cm^2/s determined in this work is about 400 times smaller than the value of 5.29×10^{-6} cm^2/s reported by Mulder et al.

(2000). Again, as discussed above with regard to the discrepancies in sorption isotherm results between this experiment and Mulder et al. (2000), the different XAD-7 particle size fractions may have also contributed to the observed kinetic differences. Furthermore, there were differences in the rotational speeds in the two studies, which affect the Reynolds numbers, and thereby affect the sorption/desorption kinetics (Mulder et al. 2000).

6.2 *Bioremediation Simulation Control Experiments*

These control experiments were originally designed to replicate the conditions in the Scenario #1 bioremediation simulation experiments, but without biological activities. However, the control experiments were performed with a step input of a naphthalene plume, as was the original experimental plan, whereas the actual Scenario #1 experiments were conducted with a pulse input of a naphthalene plume to enhance the importance of dispersion. Nevertheless, although not exact replicates of the Scenario #1 conditions, the control experiments were still useful and informative as described below.

6.2.1 Phase I: Intrinsic Control Experiments

The Phase I intrinsic control experiments were conducted twice. The representative operational flow rate and naphthalene concentration obtained from the influent sampling port as a function of time are presented in Figure 6.15 (a) and (b), respectively. It is clearly shown that the flow rate was consistent during the experiment. The naphthalene concentration was slightly higher (~5.6 mg/L) than the desired concentration of 5 mg/L at the early stage of the experiment, and then dropped to ~ 4.3 mg/L, presumably due to the volatilization into the headspace in the feeding bottle. The naphthalene concentration was quickly adjusted back to 5 mg/L by adding more fresh naphthalene solution of ~ 6 mg/L into the feeding bottle. Nonetheless, the average naphthalene sample concentration in the influent was 5.0 mg/L during the Phase I experiment.

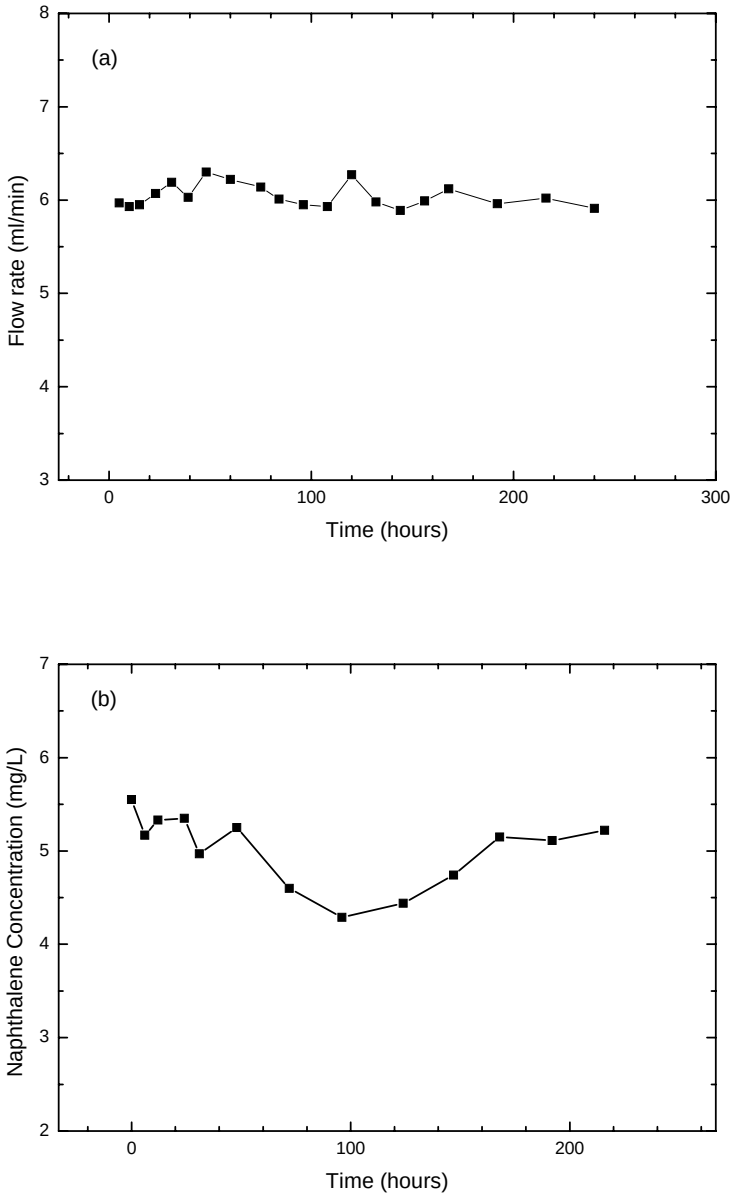

Figure 6.15 Operational conditions for Phase I control experiment: (a) flow rate; and (b) naphthalene concentration from the influent sampling port.

Representative Phase I breakthrough curves for naphthalene, normalized by its average sample concentrations in the influent (5.0 mg/L), are presented as a function of time for sampling ports A4, C4, E4, B9, C9 and D9 in Figure 6.16. These data are typical of the results obtained during the Phase I ISFC control experiments. The RT3D in VMOD simulation results for the normalized naphthalene concentrations are presented along with the experimental data, with the naphthalene concentrations normalized by average influent concentration as well. The physical and chemical kinetic parameters used in the RT3D simulation are summarized in Table 6.8. No biokinetic reaction was simulated in the RT3D numeric transport engine for these experiments, which were performed before inoculation of the ISFC.

As shown in the breakthrough curves from A4 and B9 (Figure 6.16 (a) and (b)) in the high-K layer, the naphthalene concentration arrived and reached the steady state in a very early stage of the experiment due to the fast velocity. In comparison, naphthalene concentration arrived at the steady state much later in the low-K layer because of the much slower flow rate (Figure 6.16 (e) and (f)). The experimental naphthalene concentration was slightly lower than the model simulated concentration in the high-K layer sampling ports (Figure 6.16 (a) and (b)), possibly due to the minor volatilization of naphthalene into the unsaturated zone and the overlying headspace in the ISFC, although the concentration did eventually reach the predicted value. The "tailing" in the breakthrough curves at A4 and B9 has been commonly observed by others, e.g., (Miller and Weber 1988). On the other hand at E4, the experimental concentration never quite reached the predicted concentration, probably due to the sorption to the silicone caulking.

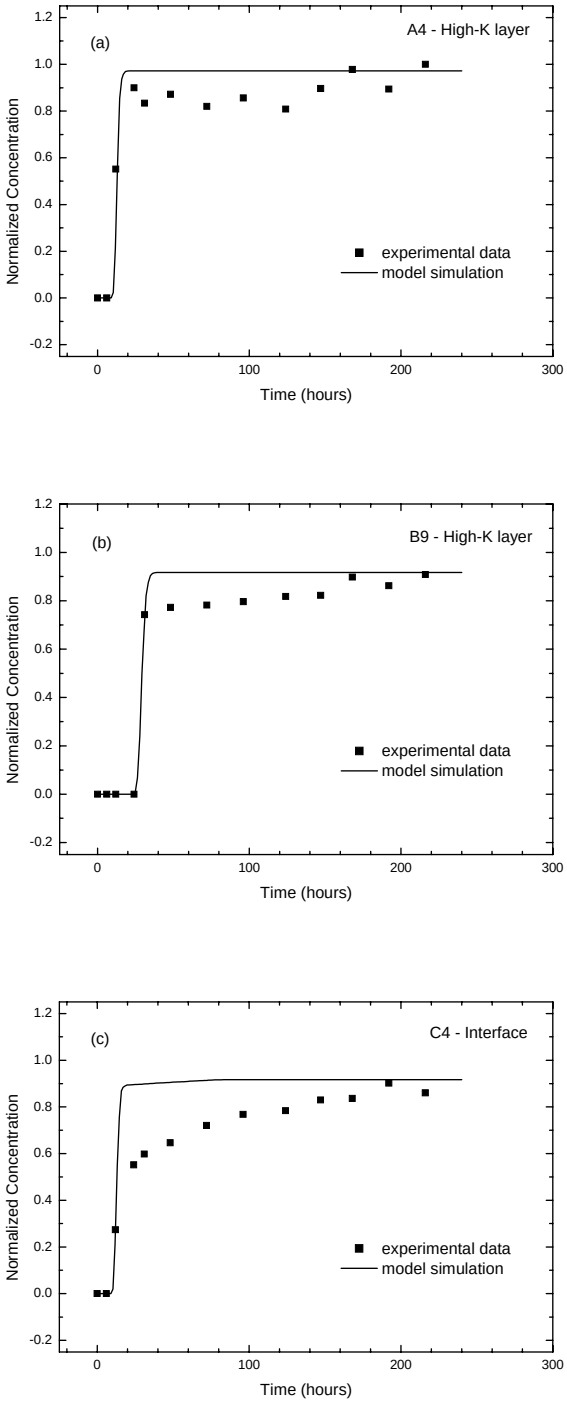

Figure 6.16 Example breakthrough curves from the Phase I control experiment for sampling ports: (a) A4, (b) B9, (c) C4 (d) C9, (e) E4 and (f) D9. Each graph shows the experimental naphthalene concentration along with the RT3D model prediction.

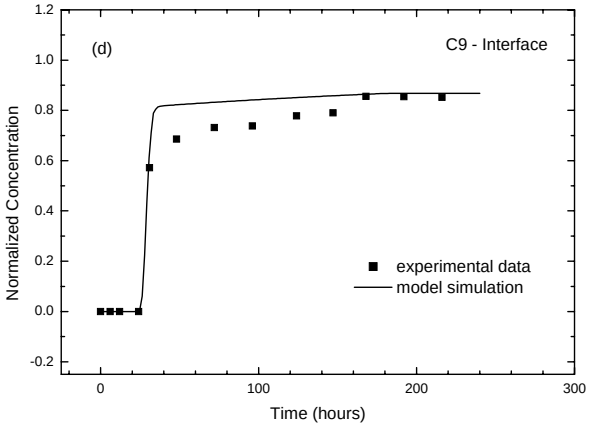

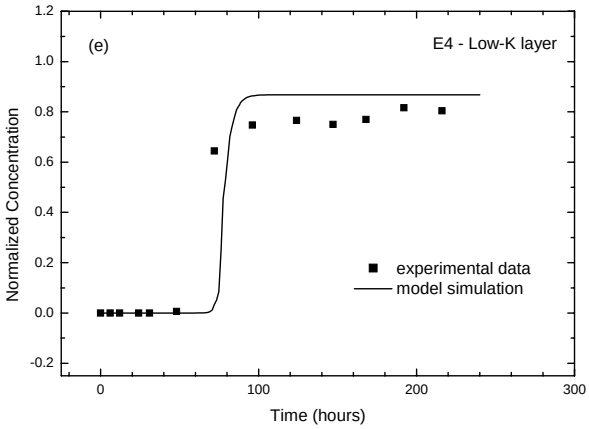

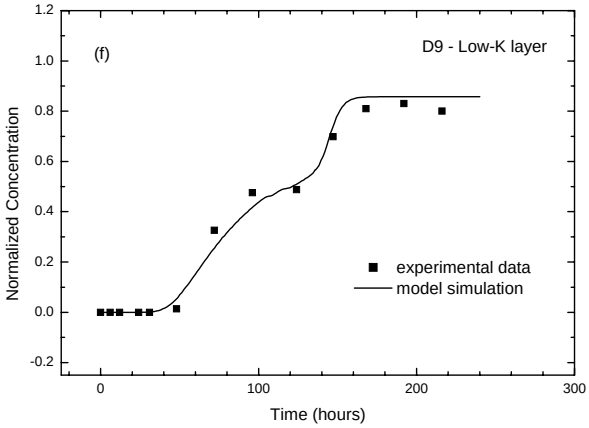

Figure 6.16 Continued

Table 6.8 Hydro-geological parameters utilized in RT3D simulation

Hydro-geological parameters		
Term	Coarse Layer	Fine Layer
Hydraulic Conductivity, K_x (m/s)	0.004	0.00065
Longitudinal Dispersivity, α_x (m)	0.0015	0.0006
Vertical Transverse Dispersivity, α_z (m)	7.6 E-5	0.002
Effective Diffusion Coefficient, D^* (m^2/hr)[1]	6.5 E-7	5.8 E-7
Interlayer dispersivity, α_z' (m)[2]	0.05	

[1] $D^* = \tau D_m$, where the aqueous diffusion coefficient D_m is calculated using the equation by Wilke and Chang (Welty et al. 1984), τ is estimated as $\tau = \phi^{1/3}$ (Schwartz and Zhang 2002),

[2] Used for model prediction at sampling port C4 and C9.

As was observed by Szecsody et al. (1994) in their laboratory with stratified porous media, the data presented in Figure 6.16 (f) for sampling ports D9 demonstrate that the interlayer mass transfer produced two stages of tracer breakthrough: an initial pulse resulting from transverse mass transfer from the high-K layer, followed by a mass pulse from the advective-dispersive movement in the low-K layer. The interlayer transverse dispersivity near the interface, α_Z', was initially modeled using RT3D/VMOD with the dispersivities determined within each layer. Then it was adjusted by trial and error based on a visual appraisal to obtain the best fit the data of initial mass pulse from interlayer mass transfer. Based on the calibration, the interlayer mass transfer coefficient was estimated to be 0.05 m. This is an order of magnitude larger than the interlayer dispersivity value of 0.003 m estimated by Szecsody et al. (1994). Nevertheless, the naphthalene broke through more slowly at

sampling port C4 and C9 than was predicted by the model simulation using the estimated α_Z' value (Figure 6.16 (c) and (d)), suggesting that the interlayer dispersion coefficient fitted using the port D9 data might actually be underestimated.

Szecsody et al. (1994) discussed several possible explanations for the observation of increased dispersivity at the interface in a low contrast (high-K/low-K=6) system. A possible reason is that the interface may be a transitional zone, and as fluid travels back and forth across the interface, tortuosity increases and α_x and α_z become somewhat larger. Some experimental artifacts may also contribute to the increased interlayer dispersivity, including: (1) irregular packing at the interface, (2) flow not being parallel to layers, or (3) acquisition of samples from near the interface. However, all these three factors were carefully considered either when packing the ISFC or taking samples during bioremediation simulated experiments to minimize these effects on the simulated aquifer system. Therefore, it was speculated that the interface being a transitional zone, rather than the experimental artifacts, might contribute to the increased interlayer dispersivity in this work.

6.2.2 Phase IIA: Nutrients Enhanced Control Experiments

The Phase IIA control experiment was performed two times following the same procedures as in Phase I, but with the input of additional N and P to the MSNS media. To achieve this, the N and P content of the MSNS media was increase to 5 times of the original concentration, resulting in N and P addition equal to 6 times the stoichiometric requirement for 5 mg/L naphthalene (Equation 5.1). The results of a representative nutrient addition experiment are presented in Figure 6.17 for sampling ports B9, C9 and D9. The Phase I naphthalene concentration data are included as well

for comparison purposes. Clearly, the nutrient addition did not have any effect on the concentration of naphthalene in the ISFC, as expected. Indeed, the results from Phase I and IIA are very similar and indicative of the reproducibility of these experiments.

6.2.3 Phase IIB: Engineered Control Experiments

In Phase IIB of the control experiments, the flow rate was doubled to increase the dispersion rate and simulate the alternative perturbation to be used in Scenario #1. The data from this experiment are also presented in Figure 6.17 for sampling ports B9, C9 and D9. These data show no significant effect on the steady-state naphthalene concentration in response to the increased advection and discussion, as was expected once the plume front had passed through the tank, because there was no biodegradation occurring in the system.

6.2.4 Summary and Conclusion

The independently determined hydrogeologic parameters (K and α) summarized in Table 6.8 and used in RT3D/VMOD were able to accurately describe the experimental data and verified the use of these parameters for modeling of bioremediation simulation experiments. There were some discrepancies, but these could be explained.

The data demonstrated the interlayer mass transfer phenomena and were used to fit the interlayer mass transfer coefficient, α_z'. There was no biodegradation of naphthalene in the ISFC prior to inoculation, and, as expected, the naphthalene transport in the ISFC was not changed when an excess of N and P were added or when the flow rate was increased.

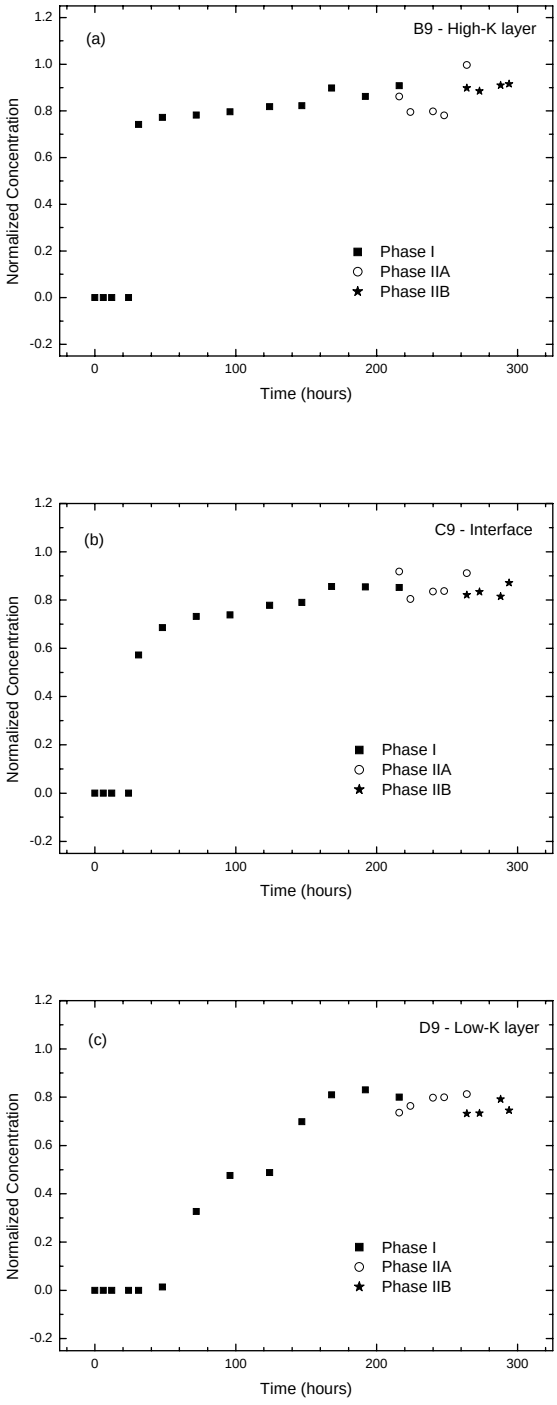

Figure 6.17 Example breakthrough curves from Phase II control experiment for sampling ports: (a) B9, (b) C9 and (d) D9. Each graph shows the naphthalene data from Phase IIA, Phase IIB and Phase I for comparison.

6.3 *Bioremediation Simulation Experiments, Scenario #1: Dispersion-Limited Scenario*

As discussed in Section 5.4.3, Scenario #1 Phase I was performed to simulate the intrinsic biodegradation under natural conditions for which vertical transverse dispersion was the overall rate-limiting process. In Phase IIA, the first perturbation received by the system was adding N and P in excess of the stoichiometric requirements in an attempt to enhance the biodegradation rate. In Phase IIB, the flow rate was increased to a level of three times that in Phase I, to increase the dispersion, especially the interlayer transverse dispersion between the high-K layer and low-K layer. The results from these simulated bioremediation experiments were presented and discussed as follows.

6.3.1 Phase I: Intrinsic Biodegradation

As described in Section 5.4.3.1, the naphthalene and Br in MSNS were pumped into the ISFC continuously for 48 hours, followed by MSNS only for the rest of experimental run. The Phase I experiment was performed twice (Phase I (1) and (2)). However, as described in Section 5.4.2.1, the ISFC was disinfected after the Scenario #1 experiments and Scenario #2 Phase IIA (Nutrients Enhanced Biodegradation), due to the algal growth that resulted from the addition of excess N and P. Therefore, the ISFC was inoculated again following the same inoculation procedure as utilized the first time. In order to verify that the results were reproducible after the reinoculation, the Phase I experiment was conducted one more time (Phase I (3)). This experiment was also the Scenario #2 Phase II experiment,

because the same experimental conditions were required and employed. Therefore, the results of Scenario #1 Phase I and Scenario #2 Phase II were combined as replicate results in the following discussion.

In order to compare the results between different phases and different scenarios, the Br, naphthalene and DO concentrations were normalized. The naphthalene and Br concentrations in the sampling ports and effluent were normalized by their average sample concentrations in the influent, whereas the DO concentrations in the sampling ports and effluent were normalized by dividing by the DO concentration in influent taken at the same sampling time to eliminate the effect of the temperature and atmospheric pressure. In the following results and discussion, the same normalization techniques were always utilized.

The influent curves for the experimental Br, naphthalene and DO data, are shown in Figure 6.18 (a). The normalized effluent Br, naphthalene and DO data are presented in Figure 6.18 (b). For comparison purposes, the normalized Br and naphthalene data in the influent are also plotted in Figure 6.18 (b). As shown clearly in Figure 6.18 (a), the influent Br and naphthalene concentrations in the pulse input are fairly steady. With respect to the effluent data in Figure 6.18, the naphthalene concentration is much reduced compared to the Br concentration. The fact that the DO concentration in effluent was approximately 50% of that in the influent indicates that the naphthalene loss was due to the consumption of naphthalene via biodegradation.

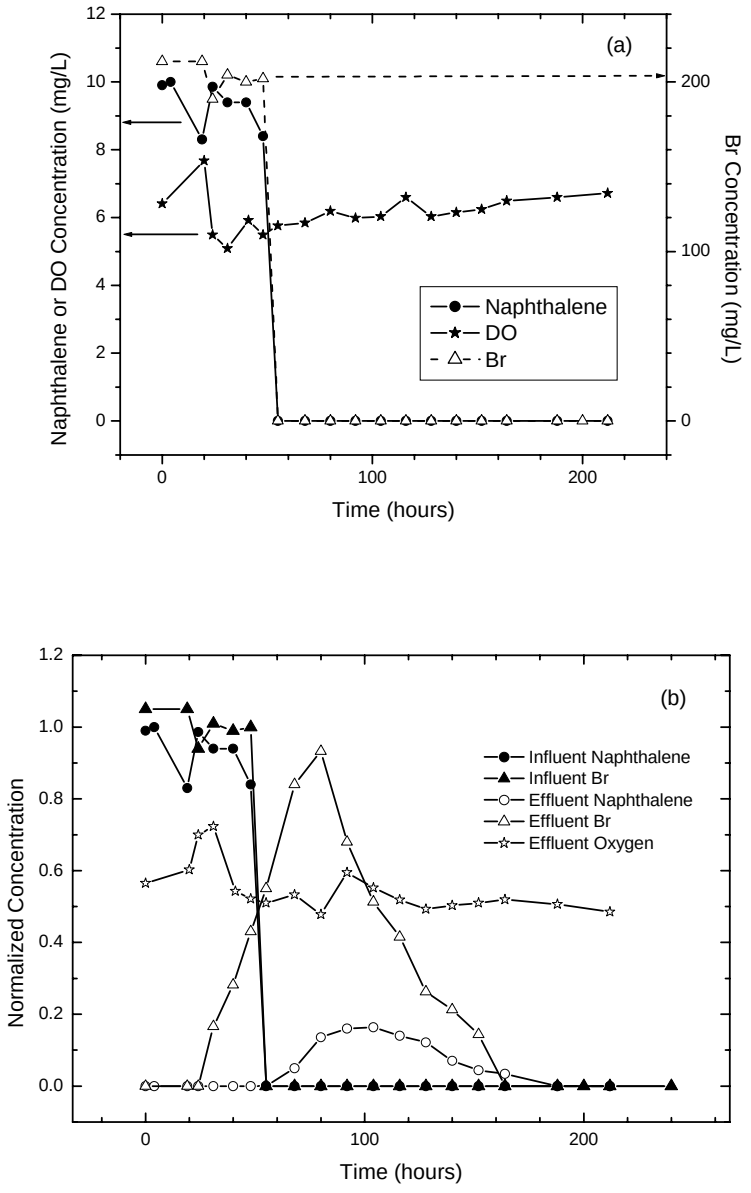

Figure 6.18 Breakthrough curves for influent and effluent from the Phase I (2): (a) Naphthalene, Br and DO concentration in the influent and (b) Normalized naphthalene and Br in the influent and effluent, and normalized DO in the effluent.

As discussed in Section 5.4.3.1, a "snapshot" contour sampling round was also performed in Phase I (2). Therefore, a contour plot was obtained to provide for visual inspection and subjective comparison of the experimental results and RT3D model simulation. To accomplish this, the output file was first exported for the selected time period of 48 hours from RT3D, and manipulated using Surfer® (Version 6.0, developed by Golden software, Inc.), to create a plume contour plot based on the model data set. Then, the experimental data recorded for all the sampling port samples taken at 48 hours were incorporated into the plot for visual comparison.

Specifically, the first step in creating a contour plot within Surfer® using the model simulation data was to "grid" the contour framework, which consisted of inputting the model grid spacing and dimensions into Surfer® Shan and Stephens (1994) provided a recommended approach for the gridding process to ensure that the actual grid spacing from the numerical model was imported into Surfer® and used for the subsequent contour development. Then, the contour plot was generated by interpolating the spatial distribution using the dataset of known points exported from the numerical model. The method used in this work was kriging, which is commonly used in contouring, e.g., (Anderson and Woessner 1992). The created contour plot for Phase I (2) at 48 hours is shown in Figure 6.19. The contour plot is presented with the longitudinal distance (0.0-1.2 m) along the x-axis and the transverse vertical distance (0.0-0.3 m) along the z-axis.

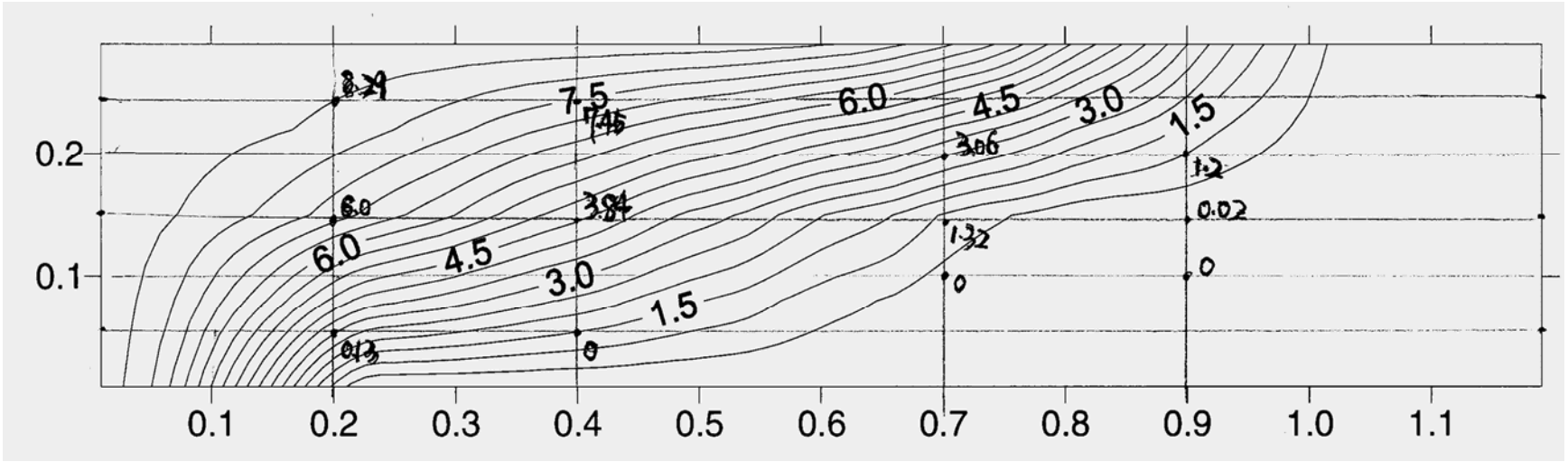

Figure 6.19 Contour plot of naphthalene plume at 48 hours for Scenario #1 Phase I (2).

Two observations can be made based on a visual comparison of the experimental data with the model simulation data. One, in general, the model simulation results matched the experimental data well, except for the data in the slow-K layer, suggesting the hydro-geological and biological parameters utilized in RT3D model simulation were reasonable. Two, as shown in the plot, the contour lines along the interface between the two layers are spread out wider than within each layer, because the interlayer dispersion coefficient is greater than those within each layer.

Representative Phase I breakthrough curves for Br, naphthalene and DO are presented as a function of time for sampling ports A2, B7, C2, C7, D1 and E2 in Figure 6.20. These data are typical of the results obtained during the Phase I ISFC experiments for Scenario #1. The RT3D in VMOD simulation results for the normalized concentrations are presented along with the experimental data, with each species normalized in the same way as described for the experimental data.

The hydro-geological parameters summarized in Table 6.8 were utilized in the RT3D simulation. In addition, the biological kinetic parameters employed are summarized in Table 6.9. All of the parameters were independently estimated as described earlier in this chapter, with the exception of the half-saturation constant for the electron acceptor for oxygen, K_A, which was taken from the literature.

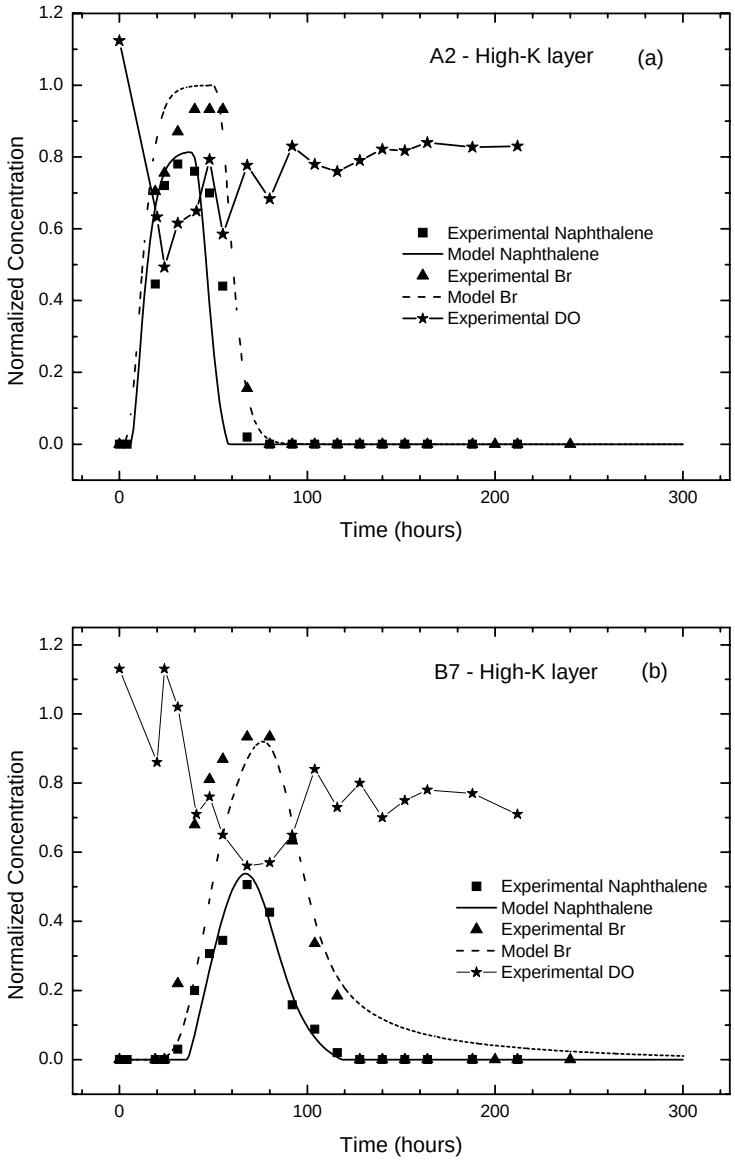

Figure 6.20 Example breakthrough curves from the Phase I (2) experiment for sampling ports: (a) A2, (b) B7, (c) C2 and (d) C7, (e) D1 and (f) E2. Each graph shows Br tracer, naphthalene, and DO data, as well as the RT3D predictions for Br and naphthalene.

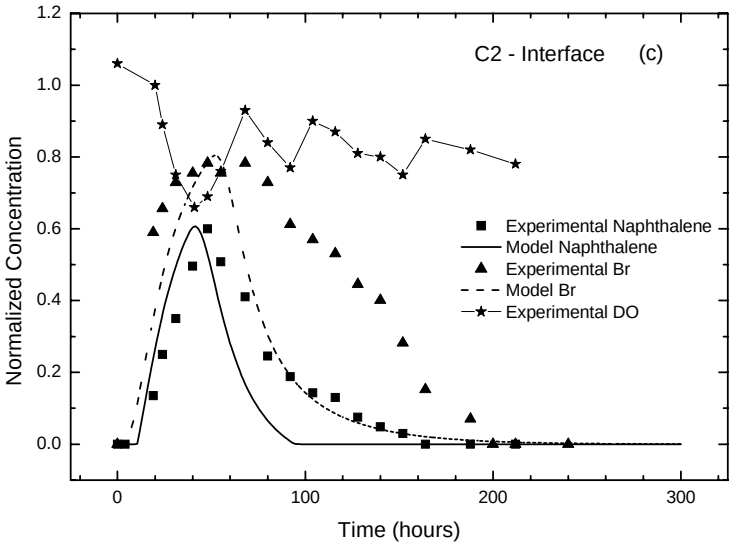

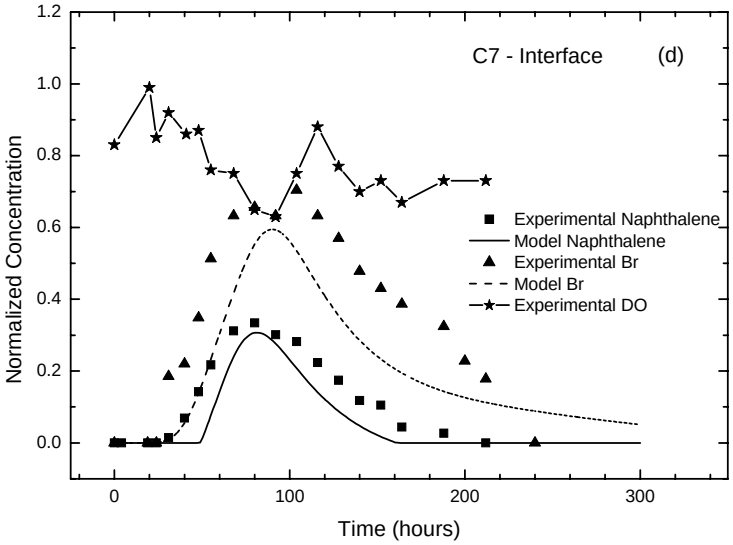

Figure 6.20 Continued

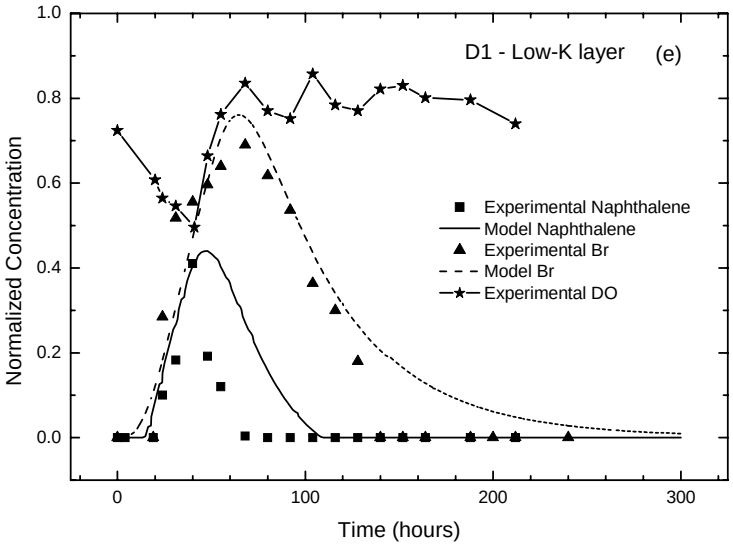

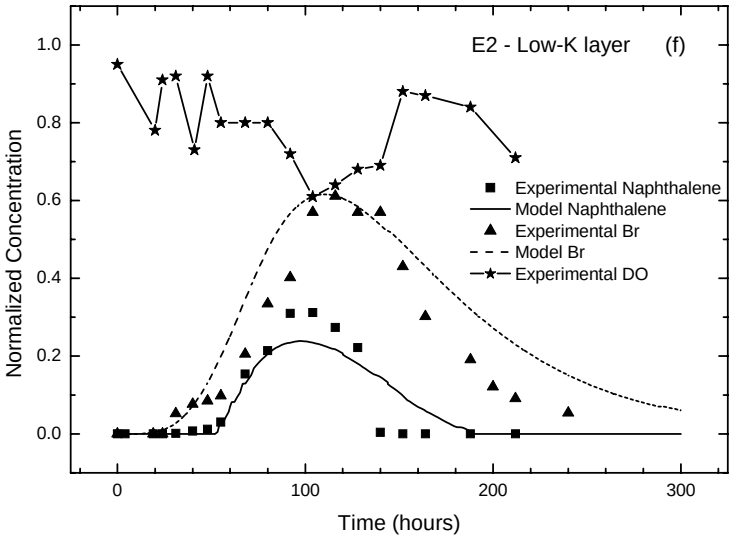

Figure 6.20 Continued

Table 6.9 Biological parameters utilized in RT3D simulation for Scenario #1

Biological parameters	
Model parameters	Values
Initial microbial concentration, M_0	0.8 mg/L
Measured initial oxygen background concentration, A_0	3.5 mg/L
Maximum specific substrate utilization rate, q_m	0.18 /hr
Monod half-saturation constant for naphthalene, K_S	8 mg/L
Monod half-saturation constant for oxygen, K_A	0.1 mg/L[(1)]
Biomass produced per unit of naphthalene utilized, $Y_{X/S}$	0.34
Oxygen used per unit of naphthalene utilized, $Y_{A/S}$	3[(2)]

(1) Literature value from Wilson et al. (1997).
(2) Calculated value based on stoichiometry, ignoring biomass synthesis.

The initial biomass concentration was estimated based on the HPC data. The HPC values of samples taken from the inoculum and sampling ports A2 and E2 after inoculation are 8.5 x 10^{11} and 8 x 10^8 CFU/L, respectively, resulting in a ~ 99.9% of attachment of biomass onto the sands, which verifies the assumption that most bacteria are on the solid phase (Harvey et al. 1984). Based on the biomass concentration of 8 x 10^8 CFU/L from sampling ports, and assuming an individual cell weight of 9.5 x 10^{-13} g (Ghoshal and Luthy 1998), the initial aqueous microbial concentration in the ISFC was estimated to be approximately 0.8 mg/L on a pore volume basis, which was also equivalent to 0.27 mg dry wt/kg sand in the high-K layer and 0.15 mg dry wt/kg sand in the low-K layer, respectively, on a solid phase basis computed from $M_0\phi / \rho_b$ (Clement et al. 1998). These values are similar to the median value of 0.2 mg dry wt/kg soil used by MacQuarrie and Sudicky (1990). The

initial biomass concentration was based on the HPC obtained from samples taken immediately after inoculation. Therefore, strictly speaking, it is only appropriate for the first experiment run. However, it was used as an estimate for all experiments, because it was not possible to sample the solid phase during the experiments. This approximation appeared to be reasonable given that the aqueous phase microbial counts did not change appreciably during these experiments.

Several general trends can be observed from/in the breakthrough curves from Figure 6.20. One, naphthalene and Br breakthrough occurred at an earlier stage of the experiment in the high-K layer, compared to the low-K layer, as expected (e.g., compare sampling ports A2 and E2). Further, the naphthalene/Br pulse arrived at sampling locations near/at interface earlier than at sampling locations "deeper" in the low-K layer (e.g., compare sampling ports C2 and E2), due to the interlayer mass transfer. This phenomenon was also observed by Szecsody et al. (1994) in their laboratory study of the transport and biodegradation of quinoline in a two-dimensional horizontally stratified porous media under dual substrate limitation. Two, at all sampling ports, the normalized naphthalene concentration is lower than that of Br due to the biodegradation of naphthalene. Correspondingly, as the plume passed a port, the oxygen concentration decreased rapidly, presumably due to the aerobic biodegradation of the naphthalene, reaching a minimum value at a time that corresponds to the time of the highest concentration of naphthalene passing the sampling port. Subsequently, the oxygen concentration increased as the naphthalene available for biodegradation decreased. Three, as the naphthalene plume moved through the ISFC, further loss due to biodegradation occurred. For example, the

normalized naphthalene concentration at C7 is lower relative to that of Br compared to C2 due to the further biodegradation of naphthalene downgradient.

The aqueous heterotrophic plate count data were relatively consistent with time at sampling ports A2, C2, E2 and in the effluent (Figure 6.21). However, the data did show that the microbial biomass tended to increase slightly when the naphthalene plume passed the port and decreased slowly as the naphthalene traveled further downgradient, e.g., see the sampling port A2 data especially.

In general, the simulated naphthalene and Br results match the experimental study values well in the high- (e.g., A2 and B7) and low-K (e.g., D1 and E2) layers, which verifies the utilization of the independent transport and biodegradation parameter estimates. However, at the interface between high- and low-K layers, there are some discrepancies between the observed and simulated data in sampling port C2 and C7, in particular for Br. As shown in C2 (Figure 6.19 (c)) and C7 (Figure 6.19 (d)), the experimental Br data spread out wider than the RT3D model simulation Br data, which indicates an underestimation of interlayer dispersivity, as discussed earlier. Interestingly, the underestimation of the interlayer dispersivity had less of an effect on the naphthalene model predictions, which are much closer to the experimental data at ports C2 and C7 than for Br. As discussed further below, this can be explained by the fact that the naphthalene biokinetics were much faster than the dispersion rate, even at the interface; therefore, the naphthalene model predictions are dominated by the biodegradation rate, not the dispersion rate. Importantly, as observed by Szecsody et al. (1994), the early arrival of naphthalene near the interface due to the interlayer mass transfer resulted in biodegradation of naphthalene

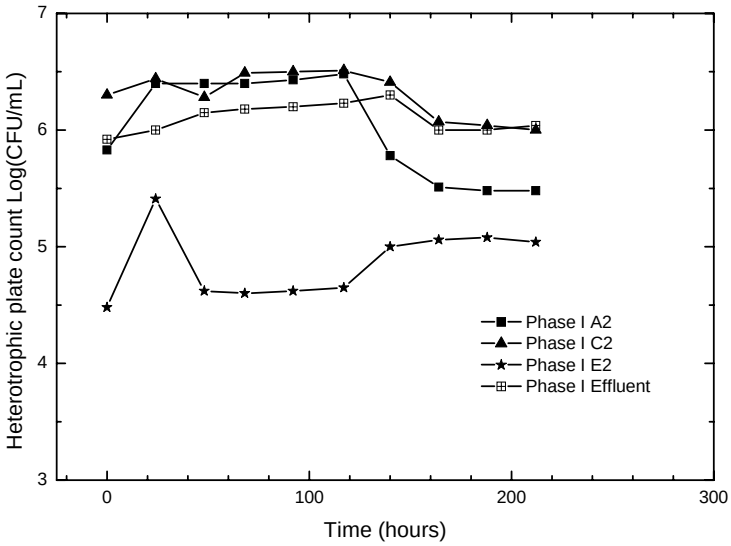

Figure 6.21 Aqueous heterotrophic plate count data at sampling ports A2, C2, E2 and Effluent for Phase I (2).

for a longer time than within the layers, e.g., compare C2 with A2 and E2, and C7 with B7.

To quantify the magnitude of naphthalene loss due to biodegradation, a moment analysis was performed as described in Chapter 5. The moment analysis results for the Phase I replicate data are presented in Table 6.11. First, velocities in each layer were computed from the individual breakthrough curves, using sampling port B7 for high-K layer and E2 for low-K layer. The calculated values vary slightly among different replicates, which could be due to the slow development of biomass distributed in the flow cell over time (Taylor and Jaffe 1990). Consistent with the K values, which varied by a factor of 7, velocities in the high-K layer were ~ 9 times greater than in the low-K layer. Second, the zeroth moment analysis was used to quantify naphthalene biodegradation. This analysis was necessary because examining biodegradation by just comparing the peak concentrations at different sampling ports, as was done above, is insufficient, due to the fact that dispersion will also reduce the peak concentration over time and distance even though the total mass remains the same. To eliminate this dispersion effect and quantify the loss due to biodegradation, the quantitative analysis was based on the areas under the Br and naphthalene breakthrough curves, A_{Br} and A_{naph}, respectively, which represent the total mass of each species detected after different horizontal flow distances. Specifically, by using the ratio of A_{naph}/A_{Br} for comparison within an experiment and between experimental Phases I and II, the effect of dispersion on naphthalene concentration can be eliminated by normalizing to A_{Br}. Further, comparison from replicate experiments and between experimental Phases I and II is improved by normalizing to A_{Br} and

eliminating effects like differences in the pulses, or advection and dispersion between experiments.

The moment analysis was focused on sampling ports C2 and C7 because of the importance of interlayer mass transfer and the resulting increased biodegradation, as discussed above. Several key observations can be made based on the moment analysis summarized in Table 6.10. One, significant biodegradation of naphthalene (43-76%) removal occurred in Phase I by the time the plume reached sampling port C2. The largest removal of naphthalene by C2 occurred in Phase I (1), which was the first experiment performed after inoculating the ISFC. Given that the inoculum was pumped from the inlet, it is speculated that there was a high biomass concentration between the inlet and C2. Two, the extent of biodegradation increased with increasing distance, as demonstrated by the decrease in value of A_{naph}/A_{Br} from C2 to C7. For the triplicate experiments, the average naphthalene mass loss between C2 and C7 due to biodegradation (A_{naph}/A_{Br} (C2) - A_{naph}/A_{Br} (C7)) is 8%, which provides the baseline for comparison with the impact of the engineered biodegradation perturbations in Phase II. Although this value is relatively small, it was reproducible (Table 6.11). Finally, following the moment of the naphthalene plume further downgradient, almost all of the naphthalene was removed in the low-K layer via biodegradation by the time the plume exited the flow cell based on the fact that no naphthalene was detected at port D7, while the naphthalene removal in the both layers due to biodegradation, coupled with the dilution by the low-K layer flow resulted in a total removal across the tank of about 80% (1-A_{naph}/A_{Br} (Effluent)).

Table 6.10 Moment analysis summarization for Scenario #1

Experiment Run	High-K layer (m/d) / Low-K layer (m/d)	A_{naph}/A_{Br} (C2)	A_{naph}/A_{Br} (C7)	A_{naph}/A_{Br}(C2) - A_{naph}/A_{Br}(C7)	A_{naph}/A_{Br} (Effluent)
Phase I (1)	0.30 / 0.035	0.24	0.18	0.06	0.16
Phase I (2)	0.30 / 0.035	0.40	0.32	0.09	0.21
Phase I (3)	0.28 / 0.03	0.57	0.48	0.09	0.20
Phase IIA	0.26 / 0.029	0.33	0.23	0.10	0.20
Phase IIB (1)	0.75 / 0.17	0.58	0.39	0.19	0.17
Phase IIB (2)	0.75 / 0.17	0.78	0.54	0.24	0.26

To verify that dispersion was the overall rate-limiting process for the system under the Phase I conditions, the quantitative framework in Figure 4.3 was applied using the parameter estimates in Table 6.8 and 6.9, and other system parameters as summarized in Table 6.11. The calculated dimensionless numbers are presented in Table 6.12. Note that the second rate comparison using the modified Sherwood No. 2, Sh_2', could not be quantitatively made because there was minimal sorption of naphthalene to the sands. Therefore, the sorption mass transfer rate was assumed to be infinite compared to the transverse dispersion rate. Based on the quantitative comparison in Table 6.13, dispersion was identified as the overall rate-limiting process. Therefore, based on the quantitative framework, it was a *priori* predicted that the best approach to stimulate biodegradation would be increasing advection and, thereby, increasing the overall rate-limiting mass transfer process, transverse mechanical dispersion. For this approach to work, it was important that vertical transverse dispersion be controlled by mechanical dispersion. For the high-K layer, $\alpha_z v_x / D^*$=1.4 and for the low-K layer, $\alpha_z v_x / D^*$=4.7; therefore mechanical dispersion is dominant in both layers and this approach should work.

Table 6.11 Parameters for quantitative framework evaluation for Scenario #1

Parameters	High-K layer	Low-K layer
Characteristic length, L, m (=vertical thickness of model aquifer)	0.3	0.3
Average pore water velocity, v_x, m/d	0.293	0.033
Vertical transverse dispersivity, α_Z, m	7.6E-5	0.002
Aqueous molecular diffusion coefficient, D_m, m^2/d	2E-5	2E-5
Tortuosity of the medium, τ	0.78	0.70
Effective molecular diffusion coefficient, D*, m^2/d [1]	1.56E-5	1.4E-5
Yield coefficient, $Y_{x/s}$, mg biomass /mg naphthalene [2]	0.34	0.34
Maximum specific substrate utilization rate, $q_{\max} = \mu_{\max} / Y_{x/s}$, 1/d	4.24	4.24
Initial biomass concentration, M_0, mg biomass/L	0.8	0.8
Initial naphthalene substrate concentration, S_0, mg/L	9.3	9.3

[1] $D^* = \tau D_m$, where D_m is calculated using the equation by Wilke and Chang (Welty et al. 1984), and τ is estimated as $\tau = \phi^{1/3}$ (Schwartz and Zhang 2002).

[2] Conversion factors: 1 mg naphthalene is equivalent to 3mg naphthalene COD and 1 mg biomass is equivalent to 1.42 mg biomass COD based on the stoichiometric equation.

Table 6.12 Quantitative framework used to identify the rate-limiting process

Symbol	High-K Layer	Low-K Layer
Pe_t (Transverse Peclet No.) $= \frac{v_x L}{D_z}$	Pe_t = 2325 >>1: transverse dispersion limits	Pe_t = 124>>1: transverse dispersion limits
Sh_2' (Modified Sherwood No. 2) $= \frac{K_{ls} L^2}{D_z}$	$Sh_2' = \infty >> 1$: transverse dispersion limits	
Da_6 (Damköhler No. 6) $= \frac{q_{max} M_0 L^2}{S_0 D_z}$	Da_6 = 875 >>1: transverse dispersion limits	Da_6 = 410>>1: transverse dispersion limits

6.3.2 Phase IIA: Nutrient Enhanced Biodegradation

Before the predicted appropriate perturbation was investigated, the commonly practiced approach of attempting to enhance *in situ* biodegradation in the field via addition of excess of N and P was tested. To achieve this, the N and P content of the MSNS media was increase to 5 times of the original concentration, resulting in N and P additions equal to 3 times the stoichiometric requirement for 10 mg/L naphthalene. In all other respects, the experimental conditions were the same as in Phase I. The influent curves for the experimental Br, naphthalene and DO data, are shown in Figure 6.22 (a). The normalized effluent Br, naphthalene and DO data are presented in Figure 6.22 (b). For comparison purposes, the normalized Br and naphthalene data in the influent are also plotted in Figure 6.22 (b). In this experiment, at one point the naphthalene concentration in the pulse input dropped to about 80% of the average concentration, which was adjusted quickly back to the desired concentration (~10

mg/L) by feeding more naphthalene solution with higher concentrations (~12 mg/L). The normalized Br concentration, on the other hand, was very steady in the pulse input. As in Phase I, the coupled losses of naphthalene and DO across the ISFC indicate biodegradation occurred in the tank.

The results of N and P addition experiment, which was performed once, are presented in Figure 6.23 in the form of breakthrough curves at ports B7, E2, C2 and C7. For comparison purposes, the Phase I naphthalene data are include as well. In addition, the HPC data for Phase IIA are presented in Figure 6.24. The aqueous heterotrophic plate count data were relatively consistent with time at sampling ports A2, C2, E2 and in the effluent, as in the Phase I (2) experiment. The microbial biomass tended to decrease at the end of experiment for all 4 sampling ports, indicating less naphthalene was available.

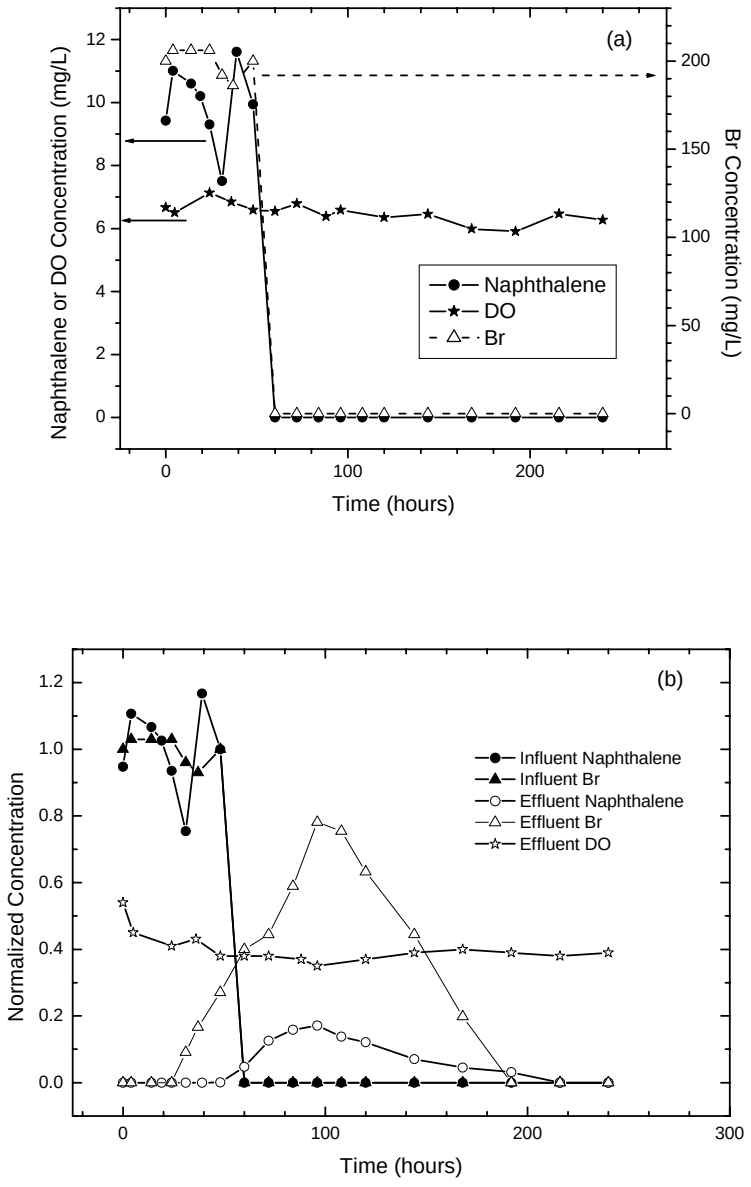

Figure 6.22 Breakthrough curves for influent and effluent from the Phase IIA: (a) Naphthalene, Br and DO concentration in the influent and (b) Normalized naphthalene and Br in the influent and effluent, and normalized DO in the effluent.

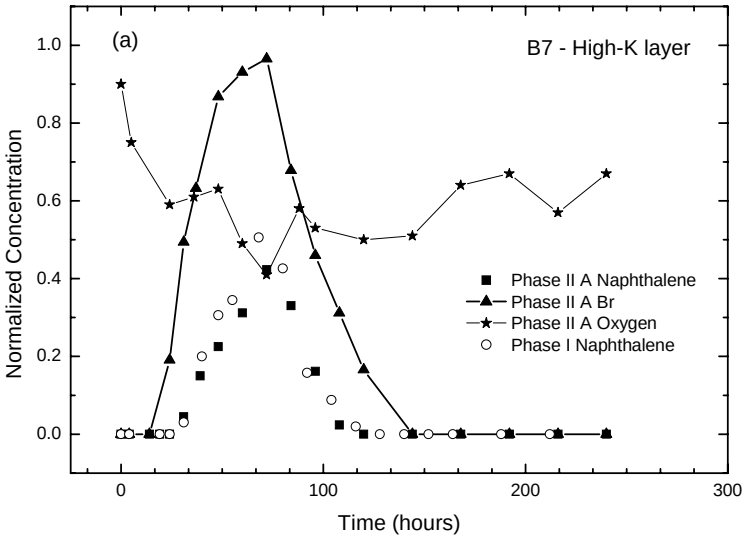

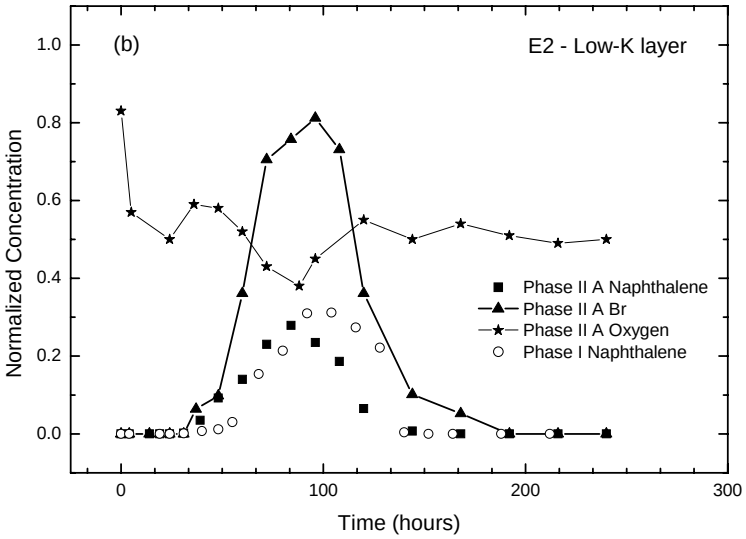

Figure 6.23 Example breakthrough curves from Phase IIA experiment for sampling ports: (a) B7, (b) E2, (c) C2 and (d) C7. Each graph shows Br tracer data, naphthalene data, dissolved oxygen (DO) data and naphthalene data from Phase I (2) for comparison.

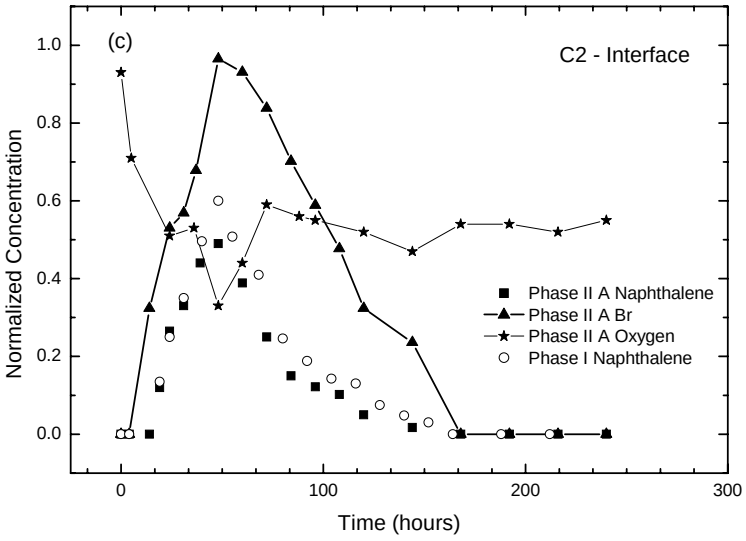

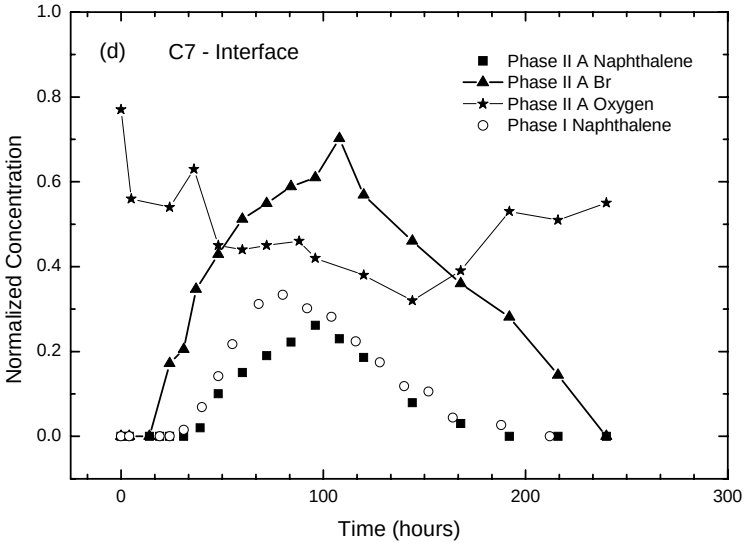

Figure 6.23 Continued

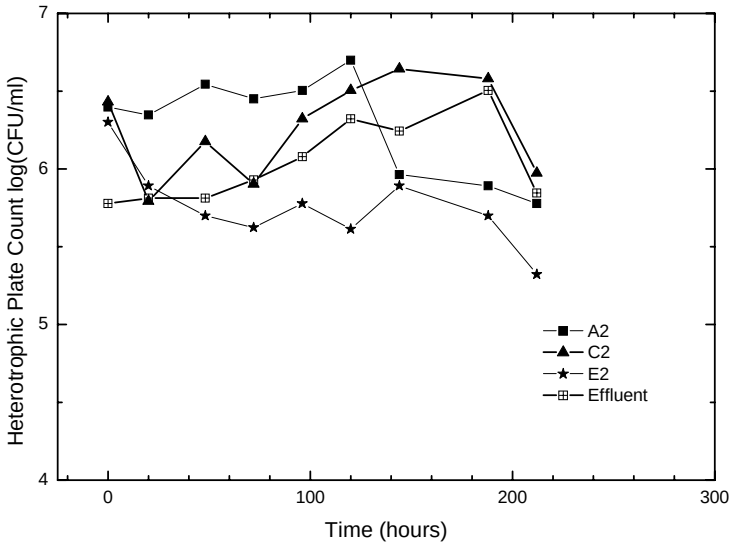

Figure 6.24 Aqueous heterotrophic plate count data at sampling ports A2, C2, E2 and Effluent for Phase IIA

With regard to the concentration trends for Br, naphthalene and DO, they are very similar to those in Phase I experiments. As in Phase I, the naphthalene concentration was reduced relative to Br, and the DO concentration decreased when the naphthalene broke through. The naphthalene concentration was slightly lower in Phase IIA than that in the Phase I, as expected considering that the N and P concentrations in the original MSNS artificial groundwater are 60% the stoichiometric amount required (Equation 5.1) for the biodegradation of naphthalene with a nominal concentration of 10 mg/L. However, the overall amount of biodegradation was very similar to Phase I, as demonstrated by the moment analysis in Table 6.10. Although the Phase IIA experiment was only performed once, the naphthalene mass loss due to biodegradation during the transport between C2 and C7 was 10%, which is very close to the average naphthalene loss of 8% in the Phase I replicates. This outcome is not surprising because the rate-limiting process in the scenario is dispersion, as determined by the quantitative framework, not biokinetics due to the nutrients limitation. Therefore, a more appropriate approach is needed to alleviate the overall rate-limiting process so as to enhance the overall bioremediation rate. This was investigated in Phase IIB.

6.3.3 Phase IIB: Engineered Biodegradation

As discussed above, the engineered perturbation that was expected to be successful for this scenario was increasing the groundwater flow rate so as to increase the rate of transverse mixing between the two layers, alleviating the overall-rate limiting process of transverse dispersion, and thereby stimulating contaminant degradation and growth. Therefore, the Phase IIB experiments were conducted in the same way as in Phase I, except that (1) the bulk flow rate was increased 3 times, resulting in an ~ 2.6 increase in v_x (Table 6.10); and (2) the pulse input time was reduced to 16 hours. The influent naphthalene, Br, and DO are presented in Figure 6.25 (a), along with the normalized naphthalene and Br data for influent and effluent, and normalized DO for the effluent only in Figure 6.25 (b), for the Phase IIB (2) experiment. In this case, the influent naphthalene and Br were relatively consistent during the pulse input. The effluent Br concentration was reduced compared to Phase I, due to the increased dispersion. Qualitatively, the normalized effluent DO and naphthalene concentrations appear to be reduced compared to Phase I, suggesting increased biodegradation across the tank.

Examples of the Phase IIB (2) normalized breakthrough curve data are presented in Figure 6.26 for sampling ports B7, C2, C7, E2 and D7. The Phase I (2) naphthalene breakthrough data are also presented as a point of comparison. In addition, the HPC data for Phase IIB are presented in Figure 6.27.

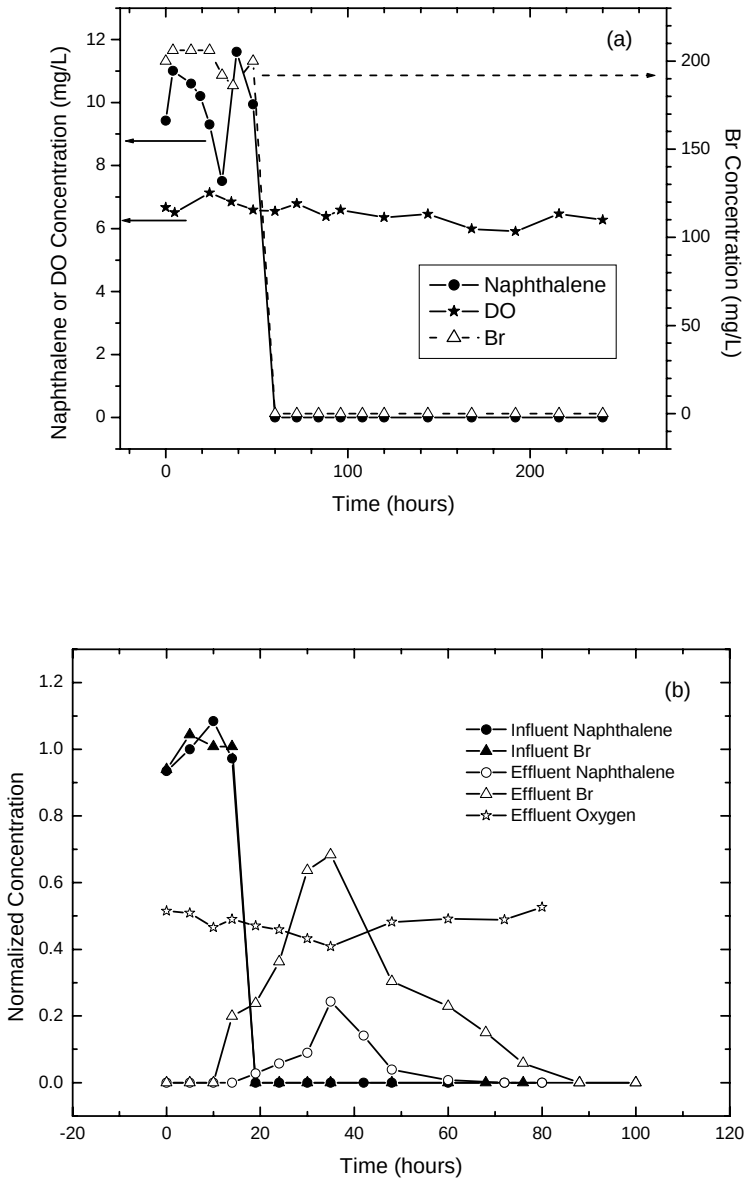

Figure 6.25 Breakthrough curves for influent and effluent from the Phase IIB (2): (a) Naphthalene, Br and DO concentration in the influent and (b) Normalized naphthalene and Br in the influent and effluent, and normalized DO in the effluent.

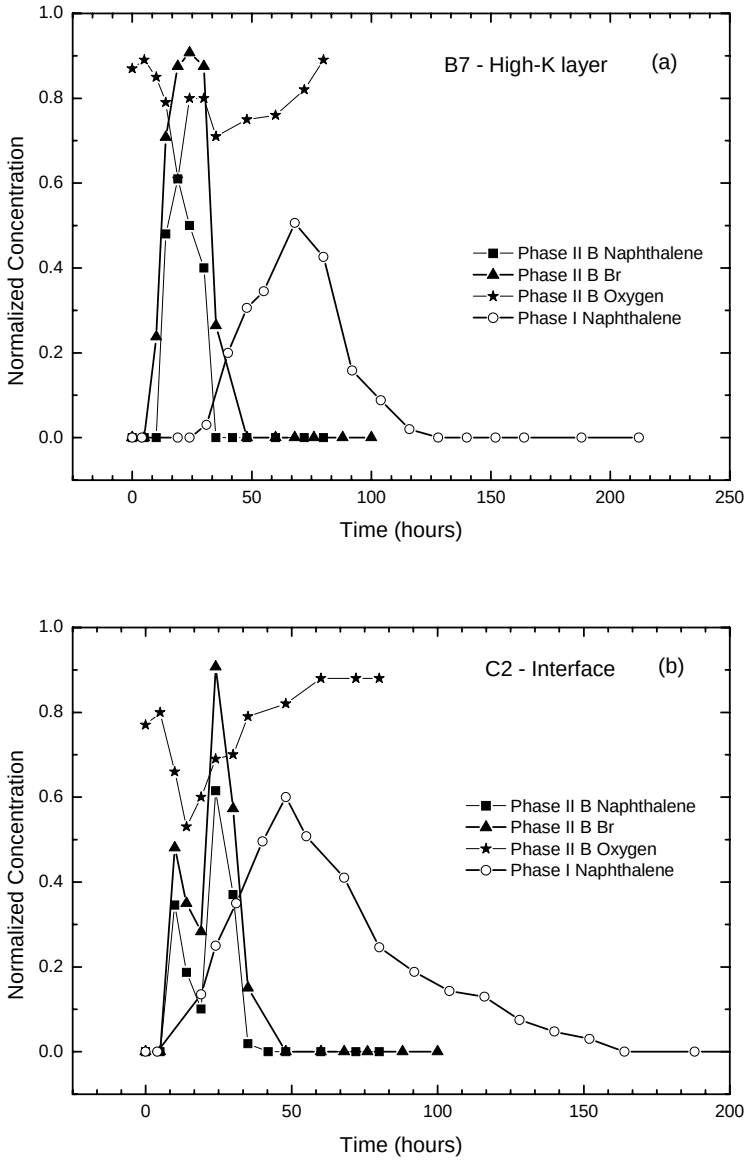

Figure 6.26 Example breakthrough curves from Phase IIB (2) experiment for sampling ports: (a) B7, (b) E2, (c) C2, (d) C7 and (e) D7. Each graph shows Br tracer data, naphthalene data and DO data along with naphthalene data from Phase I for comparison.

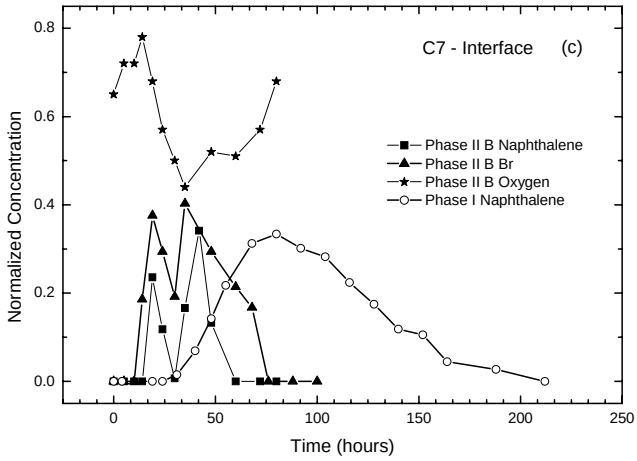

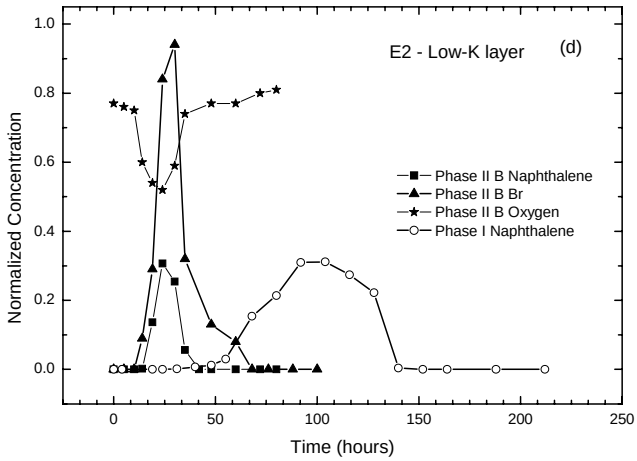

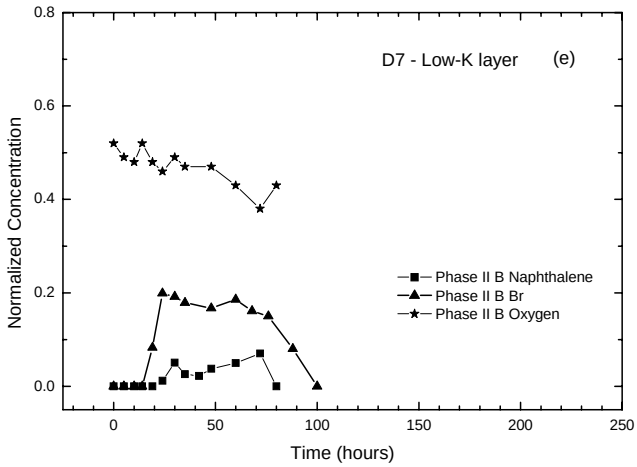

Figure 6.26 Continued

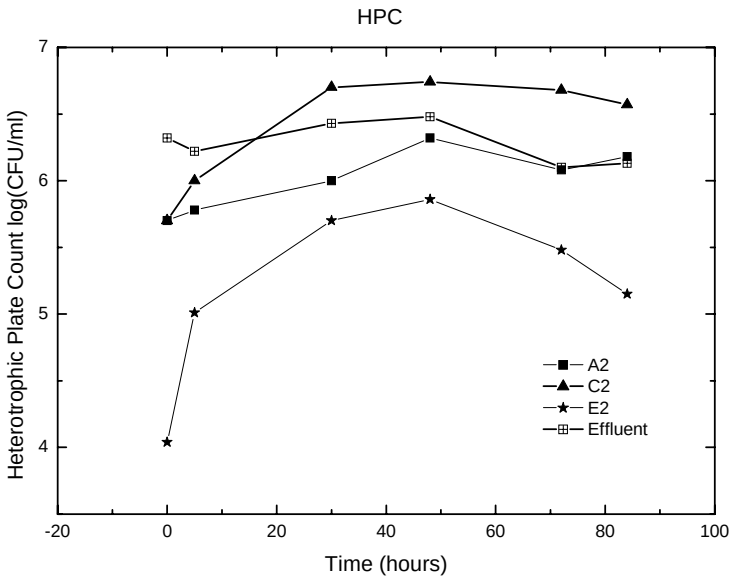

Figure 6.27 Aqueous heterotrophic plate count data at sampling ports A2, C2, E2 and Effluent for Phase IIB (2).

These data illustrate the general effects of increased advection and the resulting increased longitudinal, transverse and interlayer dispersion on the system. One, due to the increased flow rate, the naphthalene and Br broke through earlier than in the Phase I experiment, as expected. This can clearly be seen by comparing the Phase I and Phase IIB naphthalene or Br breakthrough curves. Two, as a result of increased interlayer dispersion, there are actually two breakthroughs shown at the layer interface sampling ports C2 and C7: an initial mass pulse of naphthalene, Br and possibly oxygen due to the interlayer dispersion from the high-K layer, and a second mass peak resulting from advection in the low-K layer. This effect was also observed at sampling port D7 (Figure 6.26 (e)). No naphthalene was detected at sampling port in D7 in Phase I, because the naphthalene in the low-K layer was completely degraded before it reached the D7 sampling port. However, due to the increased advection in the low-K layer as well as increased dispersion from the high-K layer into the low-K layer, two breakthroughs occurred in D7 as well.

Following similar trends as in Phase I, the aqueous heterotrophic plate count data were relatively consistent with time at sampling ports A2, C2, E2 and in the effluent (Figure 6.27). However, the data did show that the microbial biomass tended to increase slightly when the naphthalene plume passed the port and decreased slowly as the naphthalene traveled further downgradient, which was illustrated in all 4 sampling ports.

It is speculated that the increased dispersion at the edge of the plume within the layers, and at the interface of the different K layers, increased the microbial biomass access to the DO and naphthalene, resulting in more biodegradation. For

example, as the plume moved through the high-K layer, there would have been increased mixing with the DO containing water in the low-K ahead of the plume in the that layer. This is demonstrated by the moment analysis in Table 6.10, which shows the naphthalene loss between C2 and C7 due to biodegradation was ≈ 2.7 times greater in Phase IIB compared to Phase I, representing a significant enhancement in biodegradation. The magnitude of the increase in biodegradation between C2 and C7 is equivalent in magnitude to the increase in v_x. That correspondence is consistent with the hypothesis that the increase in biodegradation was due to the increased supply and mixing of DO. Specifically, the flux of oxygen into the ISFC is quantified by $Cv_x\phi$, which would increase proportional to the increase in v_x. Similarly, the increase in mechanical dispersion ($\alpha_z v_x$) would also be proportional to the increase in v_x. However, the naphthalene mass loss by port C2 was reduced compared to Phase I, presumably due to the reduced contact time between the plume and the biomass in that part of the tank.

However, it is important to note that although the increase in advection resulted in an increase in naphthalene plume degradation, the plume did travel further downgradient in a given time frame than in Phase I, as discussed above. For example, as shown in Figure 6.26 (b), it took 25 hours for naphthalene to break through in Sampling port E2 in Phase IIB (increased flow rate), while it took 90 hours for the naphthalene to do so in Phase I. Therefore, as discussed by MacQuarrie and Sudicky (1990), if the position of the naphthalene plume is more important than the time required for substantial mass loss, then the remediation of naphthalene with high-velocity flow may be of more concern, even though it experiences faster mass loss.

The general observations made in this research are consistent with those of Johnson (2004), who performed a model simulation of a dispersion-limited Scenario similar to that investigated in this Scenario #1, although under different initial conditions. In Johnson's (2004) simulation, dispersion was identified as the rate-limiting process for the baseline Phase I, based on application of the quantitative framework in Figure 4.4. The enhanced biodegradation of Phase II was implemented by numerically increasing the advection rate about 6 times. As in this work, through an increase in the rate of advection, the transverse dispersion and, thus, the mixing between the dissolved contaminant plume and "clean" groundwater was increased and the overall bioremediation rate was enhanced. This was verified by a total mass balance estimation for the domain, which quantified an overall greater decrease in the total mass for enhanced biodegradation (Phase IIB), with greater advection and, therefore, increased dispersion. However, it is important to note that although the naphthalene plume degraded at a more rapid rate with increased advection, it did travel further in a given time frame, as observed experimentally in this work. Therefore, as discussed above, if the plume location is more important in a given situation than the time needed for substantial mass loss, increasing advection rate might be a concern (MacQuarrie and Sudicky 1990).

6.3.4 Summary and Conclusion

The hydraulic mixing at the interface of the dissolved contaminant plume and "clean" groundwater that is induced by subsurface hydraulic conductivity heterogeneities, is a key interfacial process that has been observed to impact *in situ* bioremediation (Barker et al. 1987; MacIntyre et al. 1993; Molz and Widdowson 1988; Sutton and Barker 1985). Further, laboratory (Szecsody et al. 1994) and modeling (MacQuarrie and Sudicky 1990; Odencrantz 1991; Wood et al. 1994; Yang et al. 1994) studies have demonstrated increased microbial activity and, thus, enhanced biodegradation near the two-layer interface where hydraulic mixing between waters carrying different substrates occurs due to vertical transverse dispersion. Therefore, in Scenario 1, the experimental conditions were established such that the dimensionless numbers were as follows, $Pe_T >> 1$, $Sh'_2 >> 1$ and $Da_6 >> 1$. Correspondingly, the vertical transverse dispersion was successfully identified experimentally as the overall rate-limiting process based on the quantitative framework. Based on this analysis, increased advection, and thereby increased vertical transverse dispersion was selected as the appropriate system perturbation and was observed to increase the biodegradation of naphthalene by ~ 2.7 times. Specifically, the increased flow rate (3 times), increased the vertical transverse dispersion, which probably resulted in a greater mixing of electron donor (naphthalene) and electron acceptor (oxygen) across the interface and, thus, an enhanced amount and rate of biodegradation.

6.4 *Bioremediation Simulation Experiments, Scenario #2: Biodegradation-Limited Scenario*

As discussed in Section 5.4.4, Scenario #2 Phase I was performed to simulate a field scenario in which slow-biokinetics would limit the overall bioremediation rate. As in Scenario #1, N and P in excess of the stoichiometric requirement were added to enhance the biodegradation rate in Phase IIA. In Phase IIB, the biokinetics were increased by the removal of the high concentration of salt to alleviate the limitation, and, thus, enhance the overall biodegradation rate. In this Scenario, the excess of nutrient addition experiment (Phase IIA) was performed first, which resulted in the above mentioned algal problem. Therefore, the ISFC was disinfected and reinoculated right after the Phase IIA experiment. Following the reinoculation, the Phase IIB experiment was conducted to ensure the reproducibility of the ISFC compared to Scenario #1 Phase I experiments. Finally, the duplicated Phase I experiments were performed with high salinity. The results from these simulated bioremediation experiments are presented and discussed below.

6.4.1 Phase I: Intrinsic Biodegradation

As in Phase I of Scenario #1, the naphthalene and Br pulse was pumped into the ISFC for 48 hours, but in this case the MSNS had a high salinity as did the MSNS pumped in after the pulse. The influent curves for the experimental Br, naphthalene and DO data, are shown in Figure 6.18 (a) for Phase I (2), and the normalized Br and naphthalene data for the influent and effluent sampling ports, along with the DO data for the effluent, are shown in Figure 6.28 (b).

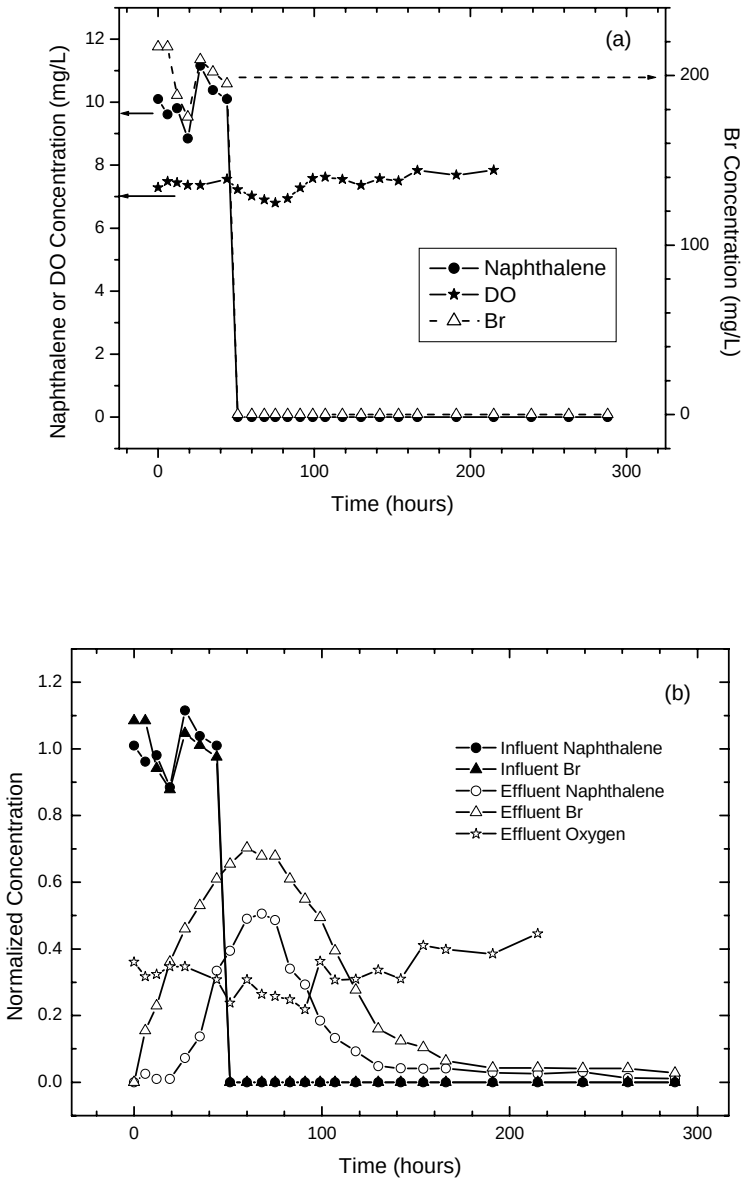

Figure 6.28 Breakthrough curves for influent and effluent from the Phase I (2): (a) Naphthalene, Br and DO concentration in the influent and (b) Normalized naphthalene and Br in the influent and effluent, and normalized DO in the effluent.

The influent Br and naphthalene concentrations in the pulse were relatively consistent. Comparing the influent and effluent in Phase I of Scenario #2 to the difference between those curves in Phase I (2) of Scenario #1 (Figure 6.18), it is clear that the amount of biodegradation was significantly reduced by the salinity. However, the DO in the effluent was still quite reduced.

Representative Phase I (2) breakthrough curves for Br, naphthalene and DO, are presented as a function of time for sampling ports B7, C2, C7, D1 and E2 in Figure 6.29. The RT3D in VMOD simulation results for the normalized naphthalene and Br concentrations are presented along with the experimental data as well. The hydro-geological parameters and the biological kinetic parameters employed in RT3D simulations are summarized in Tables 6.9 and 6.13, respectively.

Table 6.13 Parameters utilized in RT3D simulation for Scenario #2

Biological parameters	
Model parameters	Values
Initial microbial concentration, M_0	0.8 mg/L
Measured initial oxygen background concentration, A_0	3.5 mg/L
Maximum specific substrate utilization rate, q_m	7.89E-4/hr
Monod half-saturation constant for naphthalene, K_S	1.7 mg/L
Monod half-saturation constant for oxygen, K_A	0.1 mg/L[(1)]
Biomass produced per unit of naphthalene utilized, $Y_{X/S}$	1.27
Oxygen used per unit of naphthalene utilized, $Y_{A/S}$	3[(2)]

(1) Literature value from Wilson et al. (1997).
(2) Calculated value based on stoichiometry, ignoring biomass synthesis.

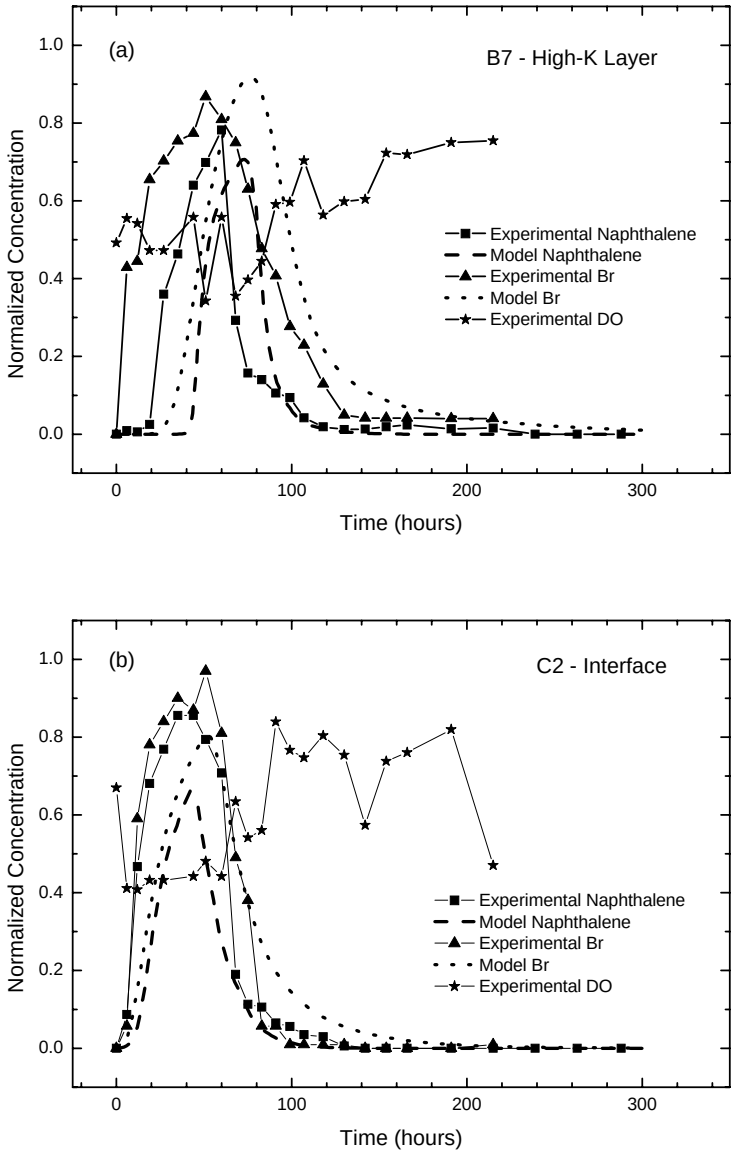

Figure 6.29 Example breakthrough curves from the Phase I (2) experiment for sampling ports: (a) B7, (b) C2, (c) C7, (d) D1 and (e) E2. Each graph shows Br tracer, naphthalene, RT3D fitting data for Br and naphthalene, and DO data.

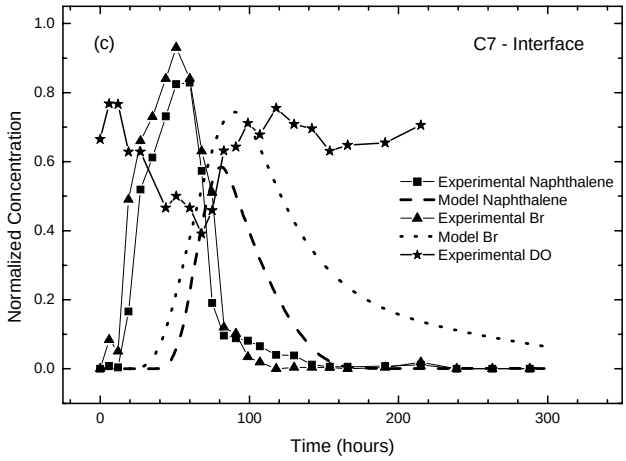

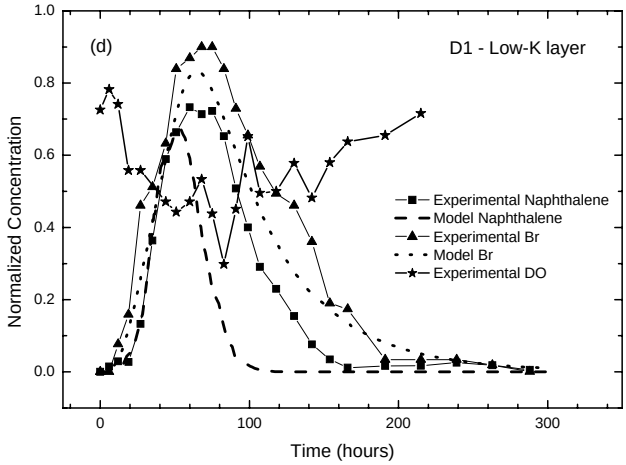

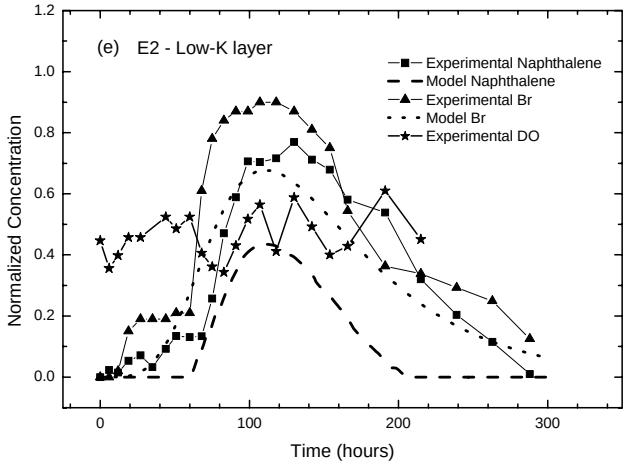

Figure 6.29 Continued

Several general observations were made based on the breakthrough curves presented in Figure 6.29. One, naphthalene and Br breakthrough occurred at an earlier stage of the experiment in the high-K layer, compared to the low-K layer, as expected and observed in Scenario #1 (e.g., compare port B7 and E2). Two, at all sampling ports, but in particular in the high-K layer (Sampling port B7) and at the interface between the two layers (Sampling ports C2 and C7), the normalized naphthalene concentration is only slightly lower than that of Br due to the very slow, inhibited biodegradation of naphthalene. Three, the normalized naphthalene concentration is similar to that of Br at C2 and C7, indicating little biodegradation of naphthalene occurred moving downgradient. Importantly, as the plume passed a port, the oxygen concentrations for B7 and E2 fluctuated, while those for C2, C7 and D1, decreased while the naphthalene plume passed the port, presumably due to the biodegradative consumption of the naphthalene, suggesting that the little biodegradation that did occur was primarily at or near to the interface between the two layers where naphthalene and oxygen mixed well, which was demonstrated in Scenario #1.

The aqueous heterotrophic plate count data were relatively consistent at sampling ports A2, C2, E2 and Effluent (Figure 6.30). However, the biomass concentration tended to decrease at all sampled ports, consistent with the inhibited microbial activity and, thus, decreased biomass, which further supports the assumption that a relatively small amount of biodegradation of naphthalene occurred for Phase I.

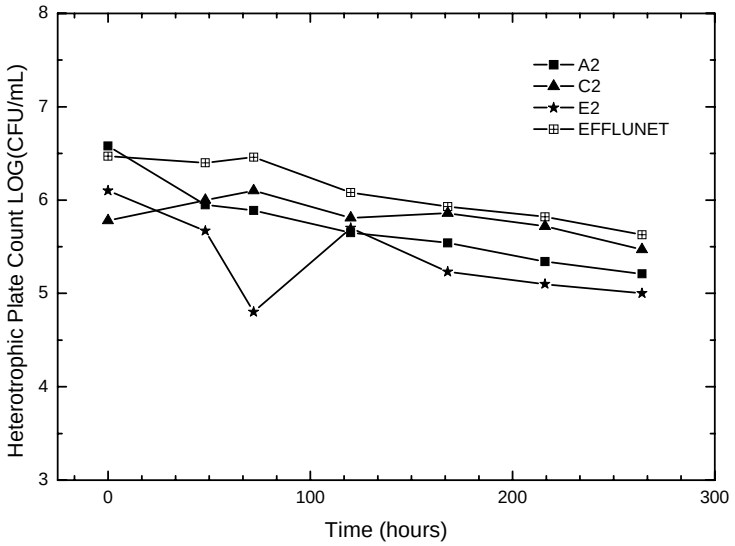

Figure 6.30 Aqueous heterotrophic plate count data at sampling ports A2, C2, E2 and Effluent for Phase I (2).

The simulated naphthalene and Br results using RT3D/VMOD describe general trends in the experimental data for the high- and low-K layers. However, there are some discrepancies between the observed and simulated data. First, the naphthalene and Br pulses broke through earlier in the experiment than predicted by the RT3D simulation at sampling ports B7 and C7 (Figure 6.29 (a) and (c)). Two factors were speculated to have contributed to this observation: (1) more water was forced to flow through rows B and C because of clogging of sampling port A2 that occurred when starting the experimental operation for Scenario #2, and thus the flow rate at rows B and C was increased, which in turn resulted in the earlier breakthrough of Br and naphthalene plume; and (2) the hydro-geological parameters were evolving slowly during the experimental operation due to the biomass development in the ISFC (Taylor and Jaffe 1990). Second, as shown in C2 and C7 (Figure 6.29 (b) and (c)), the experimental Br and naphthalene spread out wider than the RT3D model simulation data, indicating an underestimation of interlayer dispersivity, as observed in the control and Scenario #1 experiments. Note that in this experiment, due to the reduced biokinetics, the effect of dispersion on Br and naphthalene was similar, unlike Scenario #1 Phase I in which the biokinetics effects dominated over dispersion for naphthalene. Finally, the peak Br and naphthalene breakthrough concentration data from experiments are almost all greater than those values obtained from RT3D model simulation. This suggests in the case of naphthalene an underestimation of the inhibition effect of high salinity on the biodegradation rate (i.e., an overestimation of the rate of biodegradation). Furthermore, based on the Br data, it suggests an overestimation of dispersion in general, except at sampling port B7 in the high-K

layer. Nonetheless, given that the independent parameter estimates utilized in RT3D model simulation resulted in a reasonable general description of the experimental trends, they were used in the quantitative framework evaluation.

The magnitude of naphthalene loss due to biodegradation for the Phase I data was quantified by the moment analysis, the results of which are presented in Table 6.14. Several key statements can be made based on the moment analysis results. One, as occurred in Scenario #1, the velocities computed from individual breakthrough curves varied slightly among different replicates, probably due to the slow development of biomass distributed in the flow cell (Taylor and Jaffe 1990). Two, much less biodegradation of naphthalene occurred in these experiments by the time the pulse reached sampling port C2 (14-18%) compared to in Phase I of Scenario #1 (43-76%). Three, the extent of biodegradation increased only slightly with increasing distance as demonstrated by the decrease in value of A_{naph}/A_{Br} from C2 to C7, which verifies the inhibited biodegradation. The average naphthalene mass loss between C2 and C7 due to biodegradation (A_{naph}/A_{Br} (C2) - A_{naph}/A_{Br} (C7)) is only 3% for the duplicate experiments, which provides the baseline for comparison with the impact of the engineered biodegradation perturbations in Phase II. Finally, following the moment of the naphthalene plume further downgradient, an average of only 48% of the naphthalene was removed via biodegradation by the time the plume exited the flow cell, with an average of 52% of naphthalene remaining in the effluent. In comparison, there was a total removal by biodegradation of ~80% in Phase I of Scenario #1. Clearly, these data indicate that biodegradation was inhibited under the Scenario #2 Phase I conditions

Table 6.14 Moment analysis summarization for Scenario #2

	High-K layer (m/d) / Low-K layer (m/d)	A_{naph}/A_{Br} (C2)	A_{naph}/A_{Br} (C7)	A_{naph}/A_{Br}(C2) - A_{naph}/A_{Br}(C7)	A_{naph}/A_{Br} (Effluent)
Phase I (1)	0.285 / 0.045	0.86	0.83	0.03	0.57
Phase I (2)	0.30 / 0.045	0.82	0.79	0.03	0.47
Phase IIA	0.293 / 0.04	0.66	0.61	0.05	0.33
Phase IIB (1) [1]	0.30 / 0.035	0.24	0.18	0.06	0.16
Phase IIB (2) [2]	0.30 / 0.035	0.40	0.32	0.09	0.21
Phase IIB (3) [3]	0.28 / 0.03	0.57	0.48	0.09	0.20

[1] Same as Scenario #1 Phase I (1) experiment,
[2] Same as Scenario #1 Phase I (2) experiment,
[3] Same as Scenario #1 Phase I (3) experiment.

Following the approach of Scenario #1, to verify that slow biodegradation was the overall rate-limiting process for the system, the quantitative framework in Figure 4.4 was applied using the parameter values in Table 6.8 and 6.14, and other system parameters as summarized in Table 6.15. The calculated dimensionless numbers are presented in Table 6.16. Again as discussed in Scenario #1, the sorption mass transfer rate was assumed to be infinite compared to the transverse dispersion rate. Based on the quantitative comparison in Table 6.16, biokinetics and transverse vertical dispersion were identified as the overall rate-limiting processes. Therefore, it was decided to stimulate overall bioremediation by increasing the slow biokinetics (MacQuarrie and Sudicky 1990), given that the effect of increasing dispersion had already been investigated in Scenario #1.

Table 6.15 Parameters for quantitative framework evaluation for Scenario #2

Parameters	High-K layer	Low-K layer
Characteristic length, L, m (=Vertical thickness of model aquifer)	0.3	0.3
Average pore water velocity, v_x, m/d	0.293	0.033
Vertical transverse dispersivity, α_Z, m	7.6E-5	0.002
Aqueous molecular diffusion coefficient, D_m, m^2/d	2E-5	2E-5
Tortuosity of the medium, τ	0.78	0.70
Effective molecular diffusion coefficient, D*, m^2/d [1]	1.56E-5	1.4E-5
Yield coefficient, $Y_{x/s}$, mg biomass /mg naphthalene [2]	1.27	1.27
Maximum specific substrate utilization rate, $q_{\max} = \mu_{\max} / Y_{x/s}$, 1/d	0.019	0.019
Initial biomass concentration, M_0, mg biomass/L	0.8	0.8
Initial naphthalene substrate concentration, S_0, mg/L	10.0	10.0

[1] $D^* = \tau D_m$, where D_m is calculated using the equation by Wilke and Chang (Welty et al. 1984), τ is estimated as $\tau = \phi^{1/3}$ (Schwartz and Zhang 2002).

[2] Conversion factors: 1 mg naphthalene is equivalent to 3mg naphthalene COD and 1 mg biomass is equivalent to 1.42 mg biomass COD based on the stoichiometric equation.

Table 6.16 Quantitative framework used to identify the rate-limiting process

Symbol	High-K Layer	Low-K Layer
Pe_t (Transverse Peclet No.) $= \frac{v_x L}{D_z}$	Pe_t = 2325 >>1: transverse dispersion limits	Pe_t = 124 >>1: transverse dispersion limits
Sh_2' (Modified Sherwood No. 2) $= \frac{K_{ls} L^2}{D_z}$	$Sh_2' = \infty >> 1$: transverse dispersion limits	
Da_6 (Damköhler No. 6) $= \frac{q_{max} M_0 L^2}{S_0 D_z}$	Da_6 = 0.2<3.6<5: both dispersion and biokinetics limits	Da_6 = 0.2<1.8<5: both dispersion and biokinetics limits

6.4.2 Phase IIA: Nutrient Enhanced Biodegradation

Before the predicted appropriate perturbation was investigated, the addition of excess of N and P was tested in Phase IIA, which was performed once. As in Scenario #1, the N and P content of the MSNS was increased to 3 times the stoichiometric requirement for 10 mg/L naphthalene. The influent data and the normalized influent and effluent data are given in Figure 6.31 (a) and (b) respectively. The resulting breakthrough curves for Br, naphthalene and DO are presented in Figure 6.32. For comparison purposes, the Phase I (2) naphthalene data are plotted in Figure 6.32 as well. There are both similarities and differences between the results of Phase I and Phase IIA. With regard to the similarities, the general concentration trends for Br, naphthalene and DO, for Phase IIA, are very similar to those in Phase I experiments: the naphthalene concentration was reduced somewhat relative to Br, and the DO concentration decreased when the naphthalene broke through.

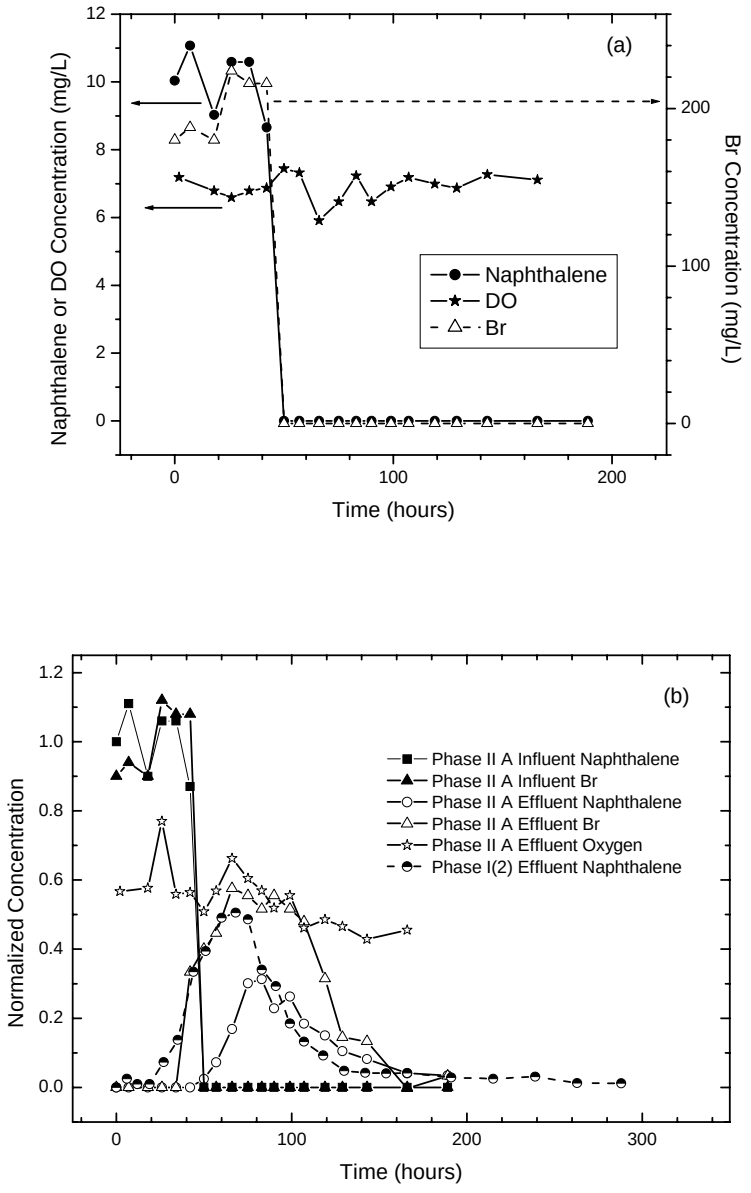

Figure 6.31 Breakthrough curves for influent and effluent from the Phase IIA: (a) Naphthalene, Br and DO concentration in the influent and (b) Normalized naphthalene and Br in the influent and effluent, and normalized DO in the effluent.

.

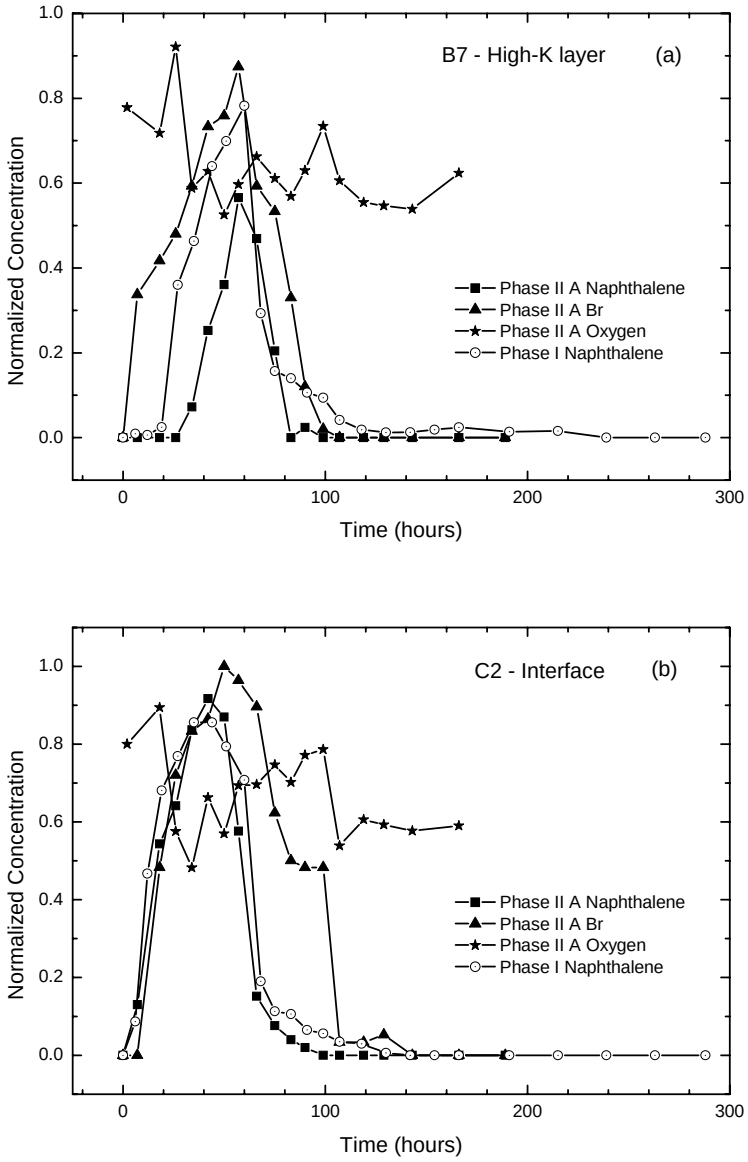

Figure 6.32 Example breakthrough curves from Phase IIA experiment for sampling ports: (a) B7, (b) C2, (c) C7, (d) D1 and (e) E2. Each graph shows Br tracer data, naphthalene data, DO data and naphthalene data from Phase I (2) for comparison.

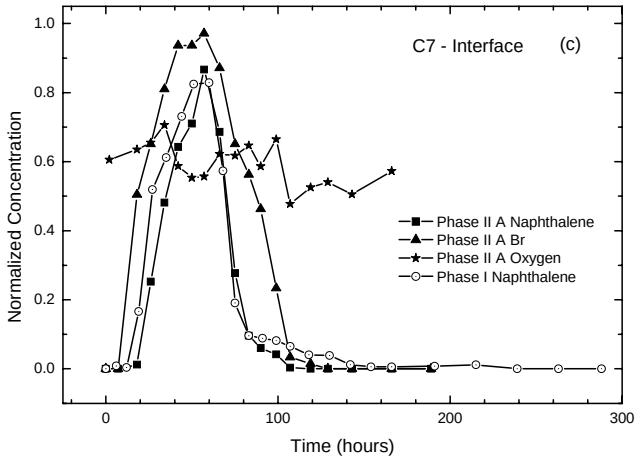

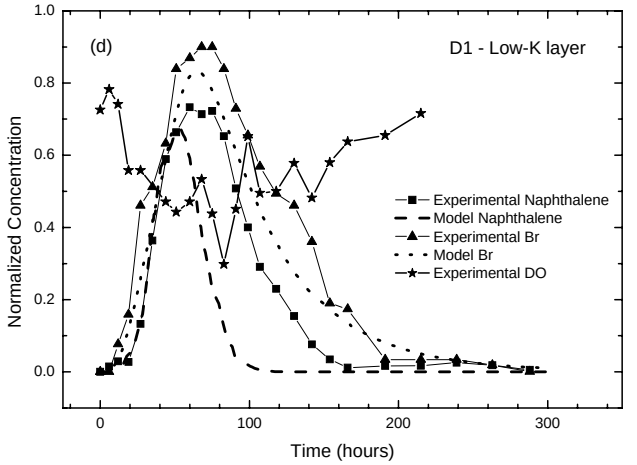

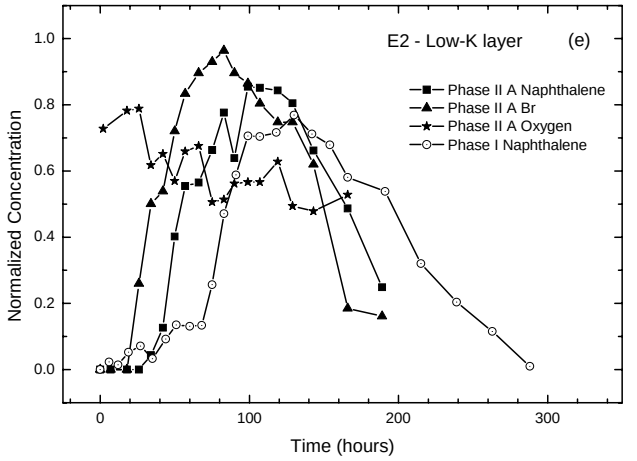

Figure 6.32 Continued

With respect to the differences, when compared to the values in Phase I experiments, although the naphthalene concentrations were similar in the two sets of experiments at sampling ports C2 and C7, they were lower in Phase IIA at sampling B7 (high-K layer) and higher in Phase IIA at D1 and E2 (low-K layer). This phenomenon was speculated to be due to differences that resulted from replicate operations. As described in Section 5.1.3, there were clogging problems after the run of Phase IIA of Scenario #2 due to the algae growth in the ISFC, which resulted from the addition of excess N and P. As a result, the simulated aquifer in the ISFC was disinfected and reinoculated again, which may have contributed to some of the differences that occurred between the Phase IIA and the Phase I experiments of Scenario #2, although they were performed under the same experimental conditions except for the nutrient concentrations. However, although the naphthalene removal was not greater at all sampling ports, the overall amount of bioremediation was improved in Phase IIA compared to Phase I, as demonstrated by the moment analysis in Table 6.14. Although the Phase IIA experiment was only performed once, the naphthalene mass loss due to biodegradation by the time the pulse reached sampling port C2 increased from less than 20% in Phase I to over 30% in Phase IIA. In addition, during the transport between C2 and C7 the loss due to biodegradation was 5%, which represented an increase of 2% compared to the Phase I average naphthalene loss. Furthermore, the naphthalene remaining in the effluent was reduced to 33%, indicating an increase of 19% in naphthalene removal compared to Phase I. The outcome of increased biodegradation is not surprising considering that the N and P concentrations in the original MSNS artificial groundwater were 60% of the

stoichiometric amount required for the biodegradation of naphthalene with a concentration of 10 mg/L. Thus, it is speculated that under the biokinetics limited conditions, as determined by the quantitative framework, the added N and P nutrients enhanced the inhibited biodegradation and resulted in a moderate increase in the biokinetics rate. However, the removal of naphthalene due to biodegradation in Phase IIA did not reach that observed in Phase I of Scenario #1 (the same conditions without high salinity), because the slow biokinetics was also a result of the high salts concentration, not only due to the nutrients limitation. Therefore, it was expected the overall rate of bioremediation could be further enhanced if an appropriate approach was implemented to alleviate the rate-limiting process of slow biokinetics, which was investigated in Phase IIB.

The trend in the aqueous heterotrophic plate count concentrations at sampling ports A2, C2 and Effluent were relatively consistent (Figure 6.33). In all cases, the HPC tended to decrease until the peak of the naphthalene pulse had passed, after which the cell counts increased again. This was especially accentuated with sampling port E2 (Figure 6.33). The HPC concentrations at sampling port E2 decreased rapidly, apparently due to the shortage of naphthalene substrate and then increased slowly once the naphthalene arrived at the sampling port.

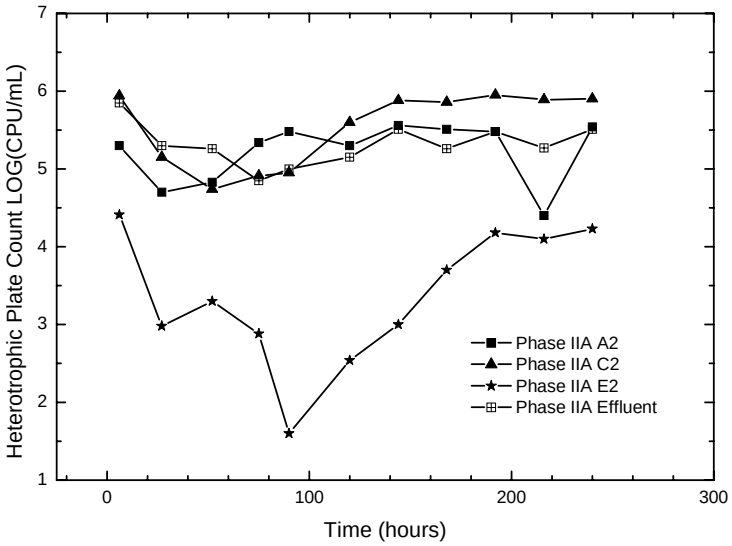

Figure 6.33 Aqueous HPC at sampling ports A2, C2, E2 and Effluent for Phase IIA.

6.4.3 Phase IIB: Engineered Biodegradation

As discussed above, an engineered perturbation that was expected to be successful for Scenario #2 was increasing the biokinetics so as to alleviate the overall-rate limiting process and stimulate the biodegradation rate. Therefore, all experiments were conducted under the same conditions as Phase I except that the high salinity was removed. In practical terms, this change could represent the reduction of salinity below inhibitory levels by addition of water (Riis et al. 2003). Because the conditions for Phase I of Scenario #2 without salinity are the same as Scenario #1 Phase I, two of those experiments (Scenario #1 Phase I (1) and (2)) were used as replicates for comparison to the Scenario #2 Phase IIB (3) experiment, which was performed after the reinoculation, yet before the salt addition.

The influent data and the normalized influent and effluent data for Phase IIB (2) (also Phase I (2) of Scenario #1) are shown in Figure 6.34 (a) and (b), respectively. The influent Br and naphthalene concentrations were relatively steady, with some slight fluctuations during the pulse input. The effluent naphthalene concentrations were reduced compared to the Phase I (2) data presented, which coupled with the reduced DO in the effluent indicates increased naphthalene biodegradation had occurred. The aqueous heterotrophic plate count data were relatively consistent with time at sampling ports A2, C2, E2 and in the effluent (Figure 6.17).

Examples of the Phase IIB (2) breakthrough curve data are presented in Figure 6.35 for sampling ports B7, C2, C7, D1 and E2, which illustrate the general effects of increased biokinetics effects on the system. For comparison purposes, the Phase I (2)

naphthalene breakthrough data are shown as well. Several observations can be made by comparing the Phase IIB and Phase I data. One, with the exception of D1, the naphthalene and Br concentrations broke through later in the Phase IIB experiment than in Phase I (2), especially at ports C7 and E2. This was probably because of the biomass development in the ISFC and the differences that resulted from reinoculation of ISFC, as discussed in Phase IIA. Two, due to the increased biokinetics, the normalized naphthalene concentration in Phase IIB was much lower than that of Phase I. Importantly, the effect of increased biokinetics on the overall bioremediation is quantified by the moment analysis in Table 6.14. This is seen in the increased loss of naphthalene due to biodegradation by the time at which the naphthalene pulse reached sampling port C2 (43-76% removal in Phase IIB compared to 34% in Phase IIA and 14-18% in Phase I). In addition, the naphthalene loss between C2 and C7 due to biodegradation was ≈ 2.7 times greater in Phase IIB compared to Phase I and 1.6 times greater than Phase IIA, representing a significant enhancement in biodegradation. This result is further verified by the moment analysis in the effluent, which had only an average of 19% of naphthalene remaining in the effluent when the plume exited the ISFC in Phase IIB, while there was 52% of naphthalene remaining in the effluent in Phase I, and 33% in Phase IIA.

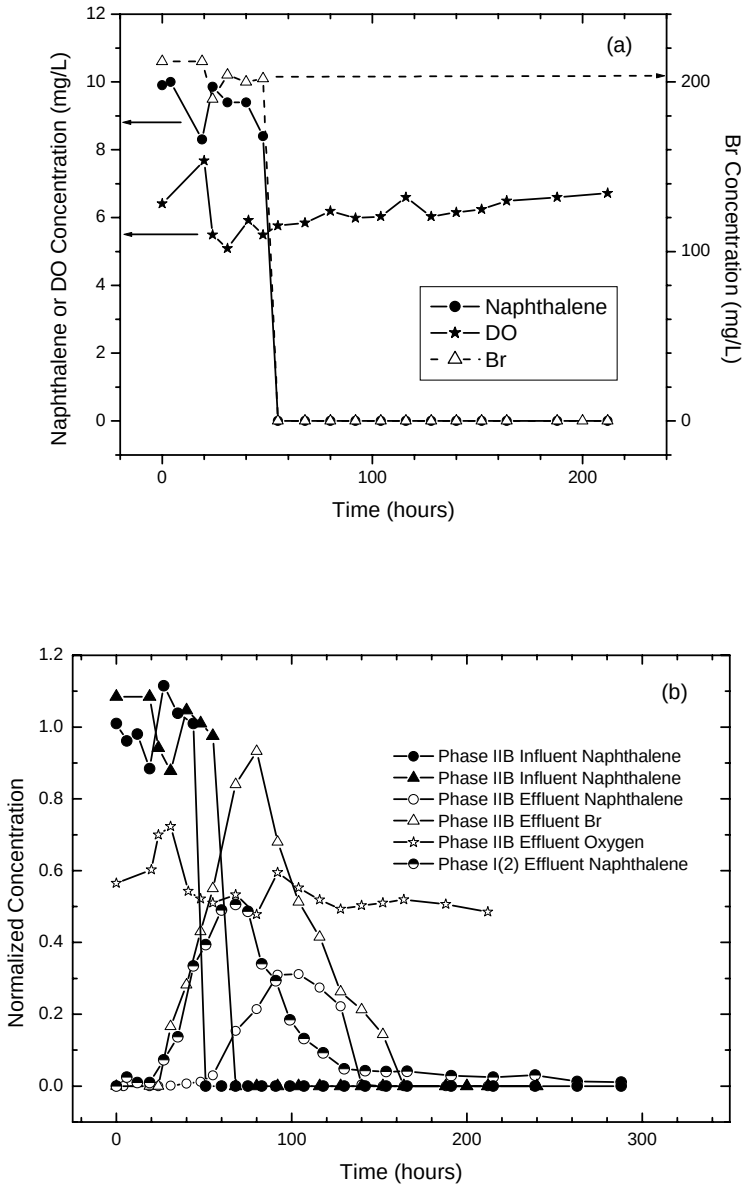

Figure 6.34 Breakthrough curves for influent and effluent from the Phase IIB (2): (a) Naphthalene, Br and DO concentration in the influent and (b) Normalized naphthalene and Br in the influent and effluent, and normalized DO in the effluent.

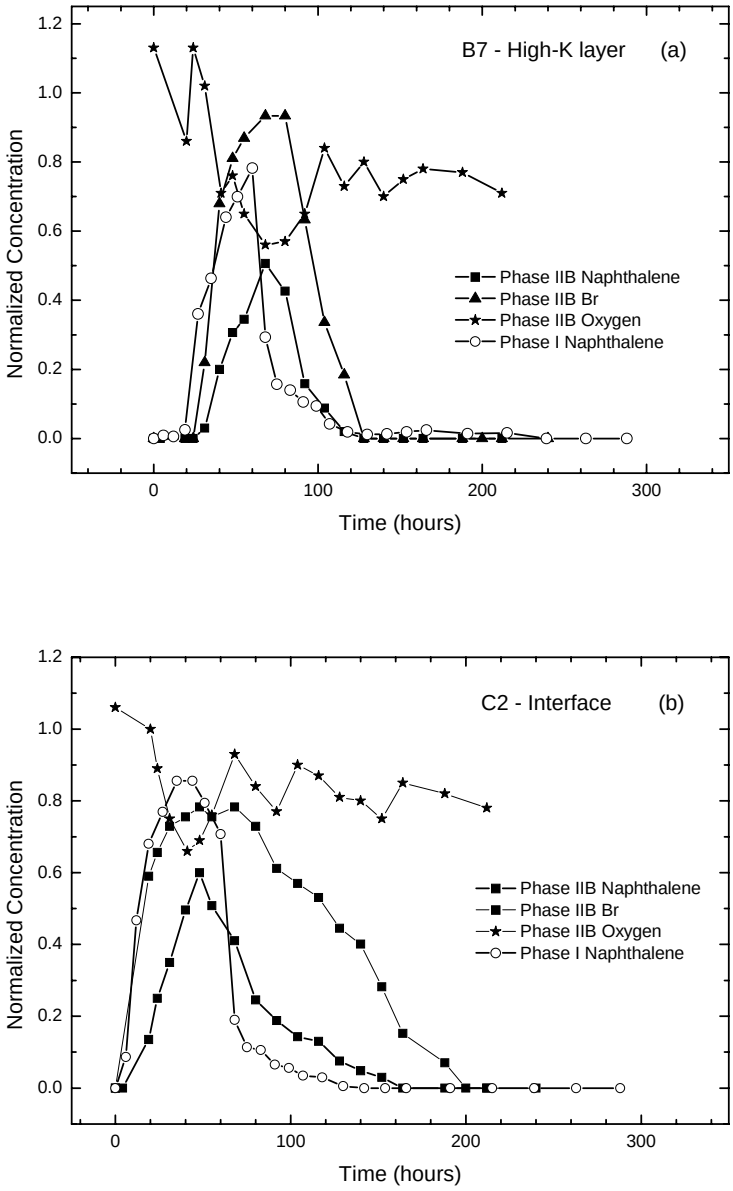

Figure 6.35 Example breakthrough curves from Phase IIB (2) experiment for sampling ports: (a) B7, (b) C2, (c) C7, (d) D1, (e) E2 and (f) Effluent. Each graph shows Br tracer data, naphthalene data and DO data along with naphthalene data from Phase I (2) for comparison.

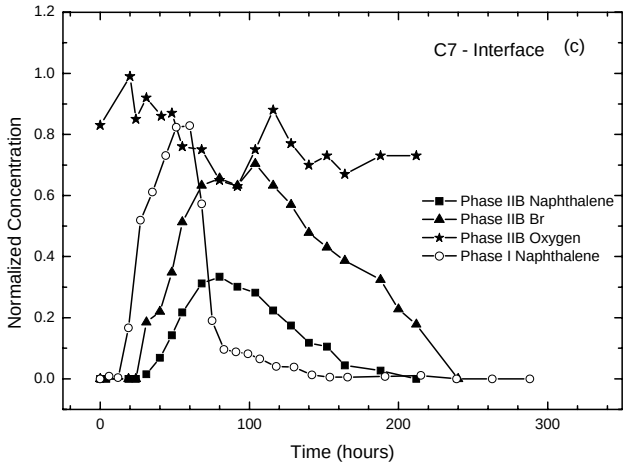

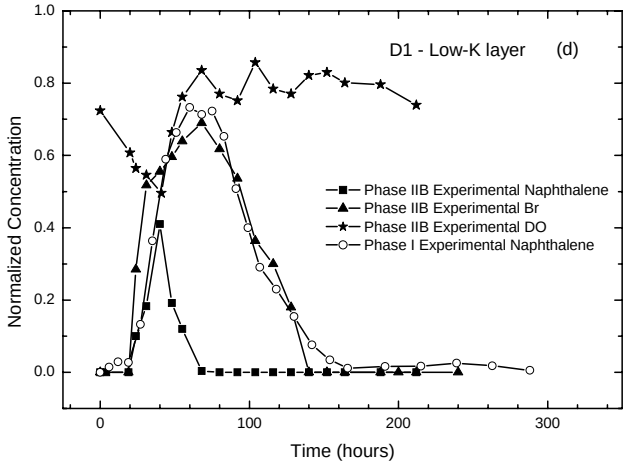

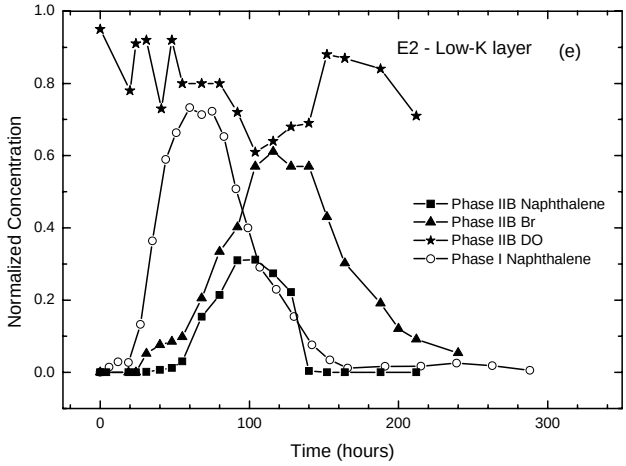

Figure 6.35 Continued

The Phase IIB (3) was the only replicate of Phase IIB performed after reinoculation the ISFC. The data sets for Phase IIB (3) are presented in Figure 6.36, 6.37 and 6.38 to illustrate that the experimental results were comparable to those obtained before reinoculation. As in Phase IIB (2), the influent data, normalized influent and effluent data, breakthrough curves for sampling ports B7, C2, C7, D1, E2 and Effluents, along with the HPC data for sampling ports A2, C2, E2 and Effluents are shown. In general, similar breakthrough trends were observed in Phase IIB (3), as in Phase IIB (2). However, there were some discrepancies between Phase IIB (2) and Phase IIB (3) when compared to the results from Phase I (2). First, there was more oxygen loss in most sampling ports due to the naphthalene biodegradation consumption in Phase IIB (3) than in Phase IIB (2). The oxygen concentration in Phase IIB (3) dropped to ~ 40% of the influent concentration, but the decrease in Phase IIB (2) only reached ~ 50-60% of the influent oxygen concentration. This was especially accentuated with sampling port E2 (Figure 6.37 (f)), at which the oxygen concentration decreased to 0 mg/L. This observation further supported the enhanced biodegradation because of the removal of salt. Interestingly, both the Br and naphthalene broke through much later in Phase IIB (3) than in Phase I (2) at sampling ports from low-K layer (sampling ports D1 and E2), especially at sampling port E2, for some unknown reasons . This observation only occurred in Phase IIB (3) once during all these experiments. Despite the above discussed discrepancies, the same conclusions could be made based on the moment analysis (Table 6.14).

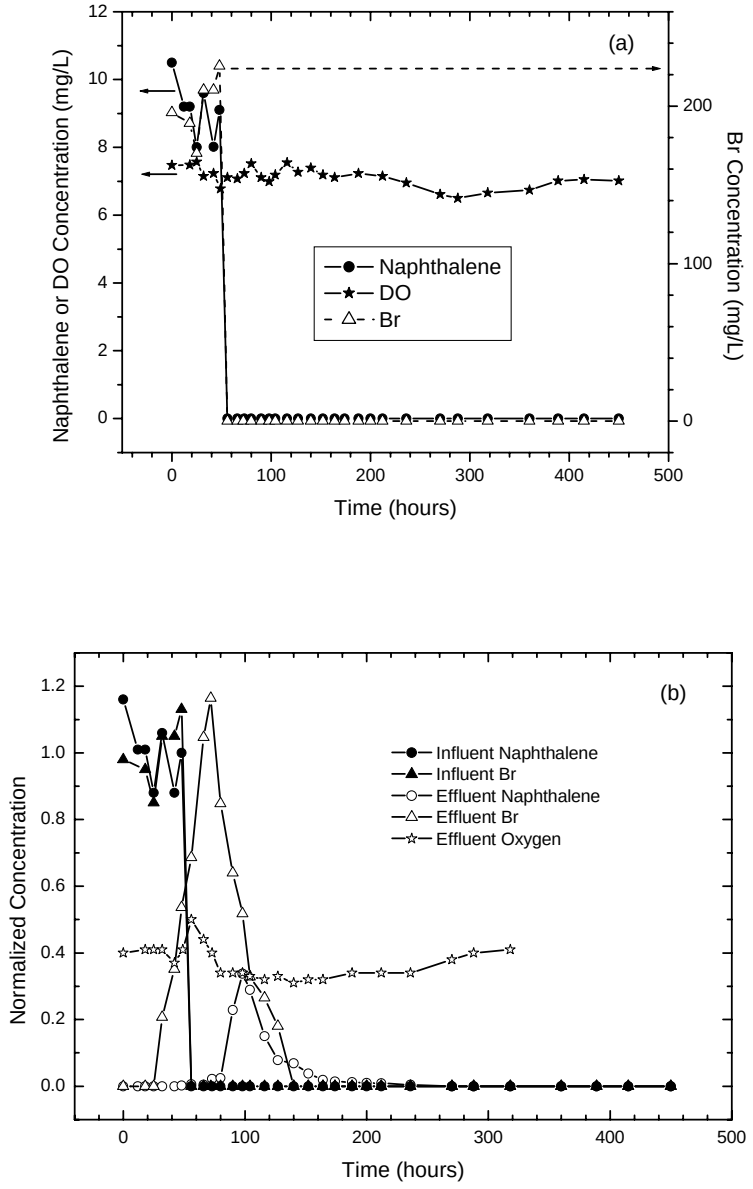

Figure 6.36 Breakthrough curves for influent and effluent from the Phase IIB (3): (a) Naphthalene, Br and DO concentration in the influent and (b) Normalized naphthalene and Br in the influent and effluent, and normalized DO in the effluent

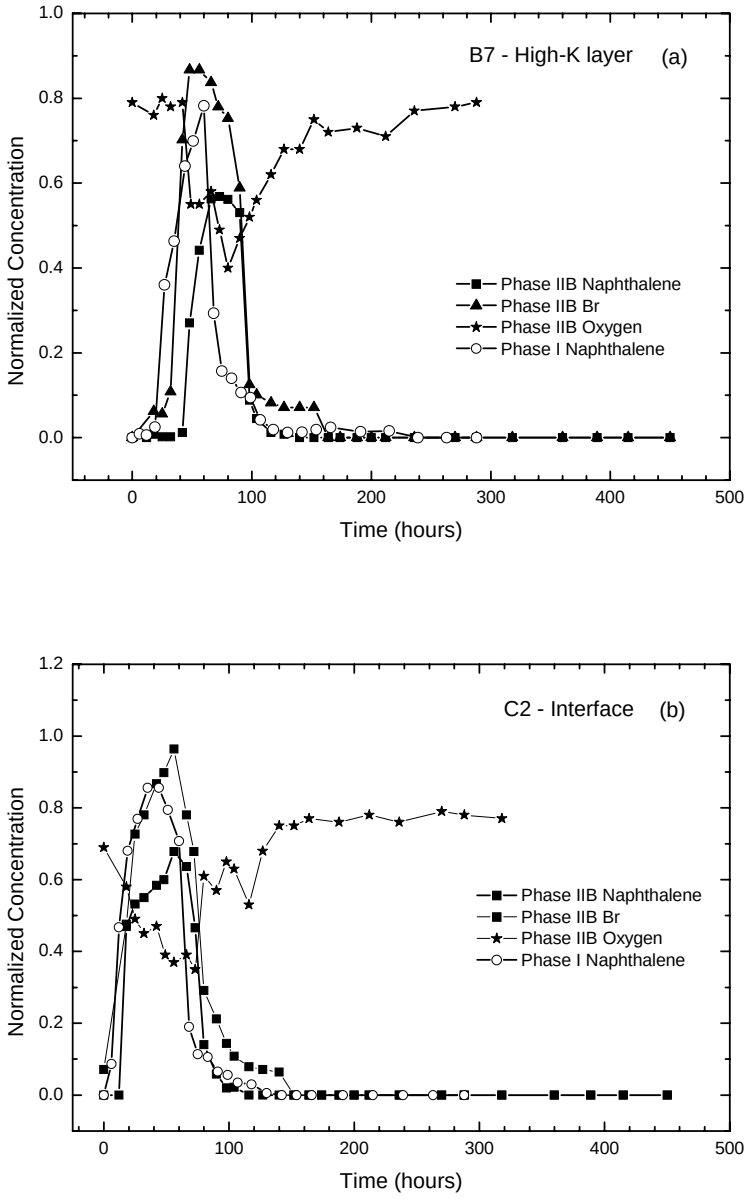

Figure 6.37 Example breakthrough curves from Phase IIB (3) experiment for sampling ports: (a) B7, (b) C2, (c) C7, (d) D1, (e) E2 and (f) Effluent. Each graph shows Br tracer data, naphthalene data and DO data along with naphthalene data from Phase I (2) for comparison.

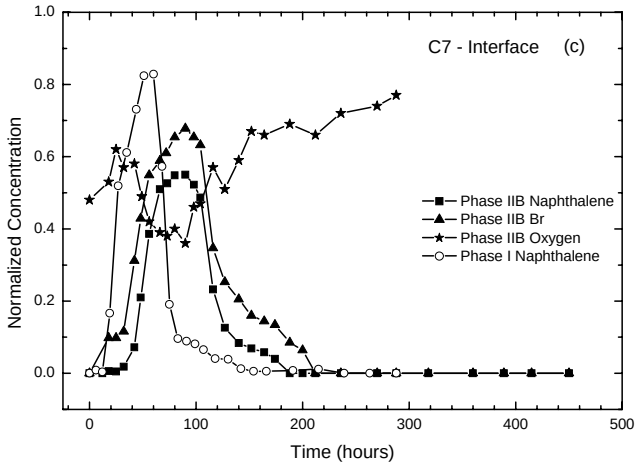

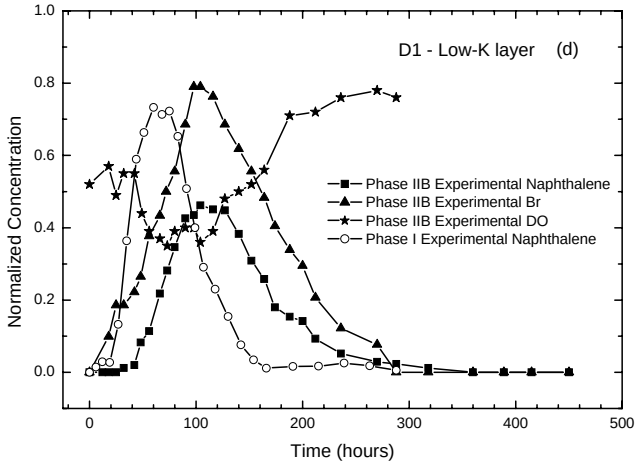

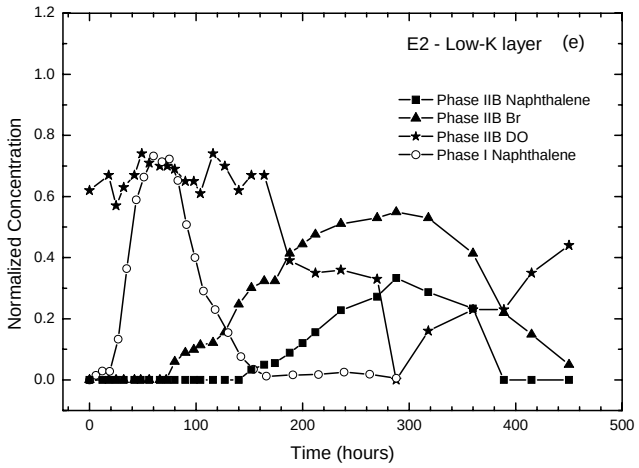

Figure 6.37 Continued

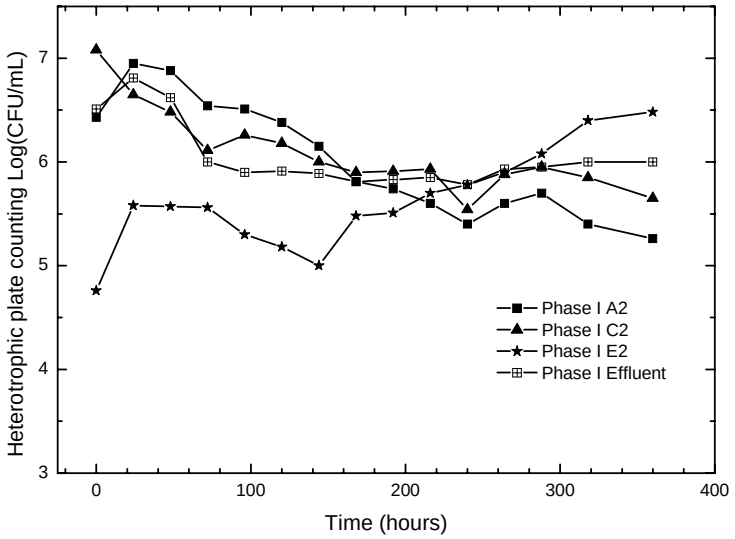

Figure 6.38 Aqueous heterotrophic plate count data at sampling ports A2, C2, E2 and Effluent for Phase IIB (3).

The general observations made in this research are consistent with those of Johnson (2004), who performed a model simulation of a biokinetics-limited Scenario similar to that investigated in this work. In Johnson's (2004) simulation, the biokinetics limited case of Phase I was simulated by reduced kinetics under denitrifying conditions and the enhanced biodegradation of Phase II was implemented by greater biokinetics under aerobic conditions. As in this work, there was a high-K layer overlying a low-K layer and a pulse of naphthalene entered the domain. Specifically, the overall biodegradation was enhanced due to the increased biokinetics, i.e., the greater specific substrate utilization rate. This was verified by a total mass balance estimation in the domain, which quantified that the initial removal rate of naphthalene was significantly greater early in the model simulation 0.980 mg/d of enhanced biodegradation (Phase IIB) compared to in the baseline biodegradation (Phase I) (0.492 mg/d). This observation was explained by the initial proximity of the electron donor substrate (naphthalene) to the electron acceptor along the injection front and, thus, the increased utilization rate in the enhanced phase (Phase IIB). Furthermore, the enhanced degradation was confirmed by a review of the electron acceptor mass data. The electron acceptor (nitrate) under the slow biokinetics (Phase I) increased due to the mass loading from the injection front, although experiencing a mass loss due to the advection and dispersion out of the domain. However, the electron acceptor mass data (oxygen) under the fast biokinetics conditions (Phase IIB) decreased significantly due to the greater consumption of naphthalene biodegradation.

Finally, as noted in Section 6.4.1, based on the quantitative framework analysis, both biokinetics and vertical transverse dispersion were predicted to be the rate-limiting

processes under the conditions of Scenario #2 Phase I. This conclusion is supported the results of Scenario #2 combined with the results of Scenario #1. In Scenario #2, removing the biokinetics limitation due to the high salinity resulted in an increase in the removal of naphthalene via biodegradation between C2 and C7 from 3% removal in Phase I to 8% removal in Phase IIB. The conditions of Phase IIB of Scenario #2 were equivalent to those of Scenario #1 Phase I. Alleviating the dispersion limitation in Scenario #1 by increasing the advection and, thereby, dispersion, resulted in an increase in the removal of naphthalene via biodegradation between ports C2 and C7 of 8% in Phase I to approximately 22 % in Phase II. Therefore, these data demonstrate successful application of the quantitative framework in a situation where more than process was overall rate-limiting.

6.4.4 Summary and Conclusion

In general, it has been stated that the biodegradation kinetics of easily degraded organic contaminants do not control the mass loss rates observed in groundwater bioremediation (Bosma et al. 1997). Rather, it is often the rate of advective transport and dispersive mixing (macro-scale) of the contaminants and other substrates (e.g., DO) and the sorption (meso-scale) of the organics that have a greater influence on the actual mass loss by biodegradation (MacQuarrie and Sudicky 1990). However, the conditions in this scenario represented a case with slow biokinetics, e.g., due to inhibitory conditions or difficult-to-biodegrade organic contaminants. For the experimental conditions of Scenario #2 Phase I, with high salinity, the slow biokinetics were successfully identified as the one of the overall rate-limiting processes, based on the system parameter estimates and application of the quantitative framework of dimensionless numbers. Removal of the

high salinity in Phase IIB illustrated that the kinetics of biodegradation have a strong influence on the mass loss of the naphthalene plume, as demonstrated by a mass loss increase of 2.7 times with the increased biokinetics. The addition of limiting nutrients (N and P) in Phase IIA had made a moderate positive effect on biodegradation compared to in Phase I, consistent with the determination that biokinetics were one of the overall rate-limiting processes.

Chapter 7 Conclusions and Recommendations

7.1 Summary and Conclusions

This research investigated the impact of substrate heterogeneity and the relevant hydro-geochemical interfaces on *in situ* bioremediation. The scales of heterogeneities and associated interfacial processes were utilized as an organizational tool, and dimensionless numbers were used to capture the complexity of the interactions between these subsurface physical, chemical and biological processes. It was hypothesized that a quantitative framework using the scales of heterogeneities as an organizing principle and based on a set of dimensionless numbers could be developed to define the limits of *in situ* bioremediation. The overall goal of this study was to refine and evaluate such a quantitative framework under different simulated scenarios relevant to the subsurface.

To accomplish the overall goal, the developed quantitative framework was evaluated under three scenarios relevant to the subsurface: a macro-scale dispersion limited scenario, a micro-scale biokinetics limited scenario and a meso-scale sorption/desorption limited scenario. In each scenario, the quantitative framework was used to predict the overall limiting process and what engineering actions, if any, would positively impact the *in situ* biodegradation rates.

This integrated modeling and experimental investigation had three major specific objectives and corresponding activities. First, the quantitative framework based on the systematic comparison of a set of dimensionless numbers was developed to compare the phenomena occurring at different scales and to predict the overall rate-limiting process for a given simulated scenarios. Second, the two-layered ISFC was built to represent a realistic, yet experimentally tractable natural subsurface system for evaluating the

physical, chemical, and microbiological processes occurring at heterogeneous interfaces. Three, the bioremediation simulation experiments were conducted for three specifically selected scenarios. The mathematical model, RT3D/VMOD, was chosen to verify the independently estimated hydro-geological and biological parameters and to simulate the experimentally investigated scenarios in the ISFC.

A critical component of the experimental evaluation of the quantitative framework was the independent parameter estimation experiments that were conducted to measure the kinetic parameters describing groundwater flow and contaminant fate and transport in the simulated subsurface system of the ISFC. Specifically, the hydraulic conductivity, dispersivity within each layer and between the two layers, sorption/desorption kinetics and biodegradation kinetics parameters were estimated. The independently determined hydrogeologic parameters summarized when used in RT3D/VMOD were able to accurately describe the experimental data obtained in the Control Bioremediation Simulation Experiments (Section 6.2.1), verifying the use of these parameters for modeling of the bioremediation simulation experiments. Although there were some discrepancies between the experimental and modeling data, these could be explained. The control experimental data also demonstrated the interlayer mass transfer phenomena and were used to fit the interlayer mass transfer coefficient, α'_z, which signifies the importance of interlayer mass transfer that resulted from the *K* heterogeneities. The control experiment also demonstrated there was no biodegradation of naphthalene in the ISFC prior to inoculation and the naphthalene transport in the ISFC responded as expected when excess of N and P were added or when the flow rate was increased.

The first bioremediation simulation experiment, Scenario #1 simulated dispersion-limited *in situ* bioremediation. The hydraulic mixing at the interface of the dissolved contaminant plume and "clean" groundwater that is induced by subsurface hydraulic conductivity heterogeneities is a key interfacial process that has been observed to impact *in situ* bioremediation (Barker et al. 1987; MacIntyre et al. 1993; Molz and Widdowson 1988; Sutton and Barker 1985). Further, laboratory (MacQuarrie and Sudicky 1990; Szecsody et al. 1994) and modeling (MacQuarrie and Sudicky 1990; Odencrantz 1991; Wood et al. 1994; Yang et al. 1994) studies have demonstrated increased microbial activity and, thus, enhanced biodegradation near the two-layer interface where hydraulic mixing between waters carrying different substrates occurs due to vertical transverse dispersion. Therefore, in Scenario 1, the experimental conditions were established such that the dimensionless numbers were as follows, $Pe_T >> 1$, $Sh'_2 >> 1$ and $Da_6 >> 1$. Correspondingly, the vertical transverse dispersion was successfully identified experimentally as the overall rate-limiting process based on the quantitative framework. Based on this analysis, increased advection, and thereby increased vertical transverse dispersion was selected as the appropriate system perturbation and was observed to increase the biodegradation of naphthalene by ~ 2.7 times. Specifically, the increased flow rate (3 times), increased the vertical transverse dispersion, which probably resulted in a greater mixing of electron donor (naphthalene) and electron acceptor (oxygen) across the interface and, thus, an enhanced amount and rate of biodegradation.

The second bioremediation simulation experiment represented biokinetics-limited *in situ* bioremediation. Although it is often the rate of advective transport and dispersive

mixing (macro-scale) of the contaminants and other substrates (e.g., DO) and the sorption (meso-scale) of the organics that have a greater influence on the actual mass loss by biodegradation (MacQuarrie and Sudicky 1990), as demonstrated in Scenario #1, the conditions in Scenario #2 represented a case with slow biokinetics, e.g., due to inhibitory conditions or difficult-to-biodegrade organic contaminants. For the experimental conditions of Scenario #2 Phase I, with high salinity, the dimensionless numbers were such that $Pe_T >> 1$, $Sh'_2 >> 1$ and $0.2 < Da_6 < 5$, indicating that both the dispersion and the slow biokinetics were the overall rate-limiting processes. The engineered remedial strategy to alleviate the limits of dispersion was investigated in Scenario #1. Therefore, the engineered perturbation to alleviate the slow biokinetics was studied in Scenario #2. Removal of the high salinity in Phase IIB of Scenario #2 illustrated that the kinetics of biodegradation have a strong influence on the mass loss of the naphthalene plume, as demonstrated by a mass loss increase of 2.7 times with the increased biokinetics. The addition of limiting nutrients (N and P) in Phase IIA had made a moderate positive effect on biodegradation compared to in Phase I, consistent with the determination that biokinetics were the overall rate-limiting process.

Finally, in conclusion, this research evaluated the developed quantitative framework and confirmed via an integrated modeling and experimental investigation that it could be used successfully to predict the rate-limiting process for *in situ* bioremediation and to aid in selecting appropriate engineered perturbation(s) to enhance the rate of biodegradation. This represents the first step toward the development of a useful quantitative decision-making tool for practitioners in the field that does not require sophisticated numerical modeling tools but can be used to make decisions based on the

systematic comparison of dimensionless numbers calculated using parameters obtained in field and laboratory testing.

7.2 Recommendations for Future Work

As discussed above, the developed quantitative framework was successfully evaluated in the laboratory in the ISFC for two different scenarios: a macro-scale dispersion-limited scenario, and a micro-scale biokinetics-limited scenario. However, due to time limitation, the proposed third sorption/desorption-limited scenario was not accomplished completely, with only the sorption/desorption kinetics parameter estimation experiments and model predictions implemented so far. Therefore, given the importance of sorption limitations on bioavailability in the field, it is recommended that the unfinished Scenario #3 be completed to further evaluate the application of the quantitative framework under different conditions. This experimental investigation is currently in progress, with the work primarily performed by Ms. Eunyoung Hong, with some assistance from the author in setting up the experiments and analyzing samples. It is also recommended that the quantitative framework be evaluated in the laboratory using the ISFC under other key conditions that are relevant *in situ* bioremediation of the natural subsurface, in particular when NAPL dissolution is the overall rate-limiting process (Seagren et al. 1994), or when oxygen supply to the saturated zone is the rate-controlling factor (Borden and Bedient 1986; Borden et al. 1986).

With respect to the laboratory-scale evaluation of the quantitative framework, one of the key aspects of the testing is the parameter estimation. Two of the parameter estimation techniques that needed be improved are the biokinetics and dispersivity determinations. As discussed in Section 5.3.4, Monod kinetic parameters estimated using

non-steady-state batch analysis are subject to large uncertainties. These uncertainties are a function of the initial experimental conditions, the values of the parameters, the type and magnitude of the measurement errors, and the number of samples (Liu and Zachara, 2001). Careful manipulation of experimental conditions was required to reduce the correlations between Monod parameters allowing for the estimation of unique parameters with the lowest degree of uncertainty. The estimation of unique biokinetics parameters in this study was made challenging due to the above mentioned uncertainties. For example, only few sets of respirometry experimental results proved to be valid, based on the initial estimation techniques used by Brown, et al. (1990). Thus, more replicate experiments need to be performed and more efforts are required for better manipulation of the experimental conditions for the respirometry studies and the model fitting techniques in order to obtain unique biokinetics parameters.

In addition, as indicated by the results of the Bioremediation Simulation Experiments, Section 6.2-6.4, the hydro-geological parameters probably evolved slowly in the ISFC due to the slow development of biomass distributed in the flow cell over time (Taylor and Jaffe 1990). This may have contributed to some discrepancies between the model simulations and experimental data, which, in turn, could negatively affect the evaluation of the quantitative framework. Therefore, it is suggested that a tracer study (dispersivity within each layer) and a control experiment (dispersivity between two layers) be performed at appropriate time intervals in between scenarios to investigate the effect of biomass distribution on these parameters.

The final step in the evaluation of the application of the quantitative framework is to test its application in the field. Of course, the field scale is expected to be more

complex than the ISFC experiments of this work. Furthermore, given the heterogeneities in the field and possible changes in mass-transfer and biokinetic parameters over time, the assessment of the rate-limiting phenomenon at field scale will need to be checked spatially and temporally (Ramaswami and Luthy 1997; Sturman et al. 1995). One way to perform a field-scale evaluation is to examine well-studied sites, such as the Canadian Forces Base (CFB) Borden sites, e.g., (Schirmer and Barker 1998; Schirmer et al. 1999; Schirmer et al. 2000), that are well documented with sufficient data, including the hydro-geological and biokinetics parameters needed to evaluate the quantitative framework. In addition, research is currently underway at field site investigation to evaluate the quantitative framework at the field scale. That study is being performed by Matt Wheaton, a M.S. student in the Civil and Environmental Engineering Department, University of Maryland, College Park. Successful implementation of this study at the field scale would contribute greatly to the evaluation of the quantitative framework. Testing of the quantitative framework using compiled field data, represents another step toward the development of a useful quantitative tool for defining in the field when *in situ* bioremediation will work, and when an engineered or intrinsic approach is best.

Appendix

Appendix 1: Materials and Parts for ISFC

Materials:

1. Glass plates (untempered): ½" think,

   2 plates $16\frac{3}{4}" \times 52\frac{1}{4}"$;

   2 plates $5" \times 16\frac{3}{4}"$;

   1 plate $5" \times 52\frac{1}{4}"$;

   1 plate $5" \times 53\frac{1}{4}"$;

Cart material:

2. 4 Thermoplastic rubber wheels, cushion-load cold forged caster swivel, 6" × 2";

   McMaster-Carr Supply Company, Part number: 2703T61

3. 4 Brakes for 6" Diameter thermoplastic rubber wheel,

   McMaster-Carr Supply Company, Part number: 2703T33

Screen material:

4. Type 316 Stainless Steel Woven Wire Cloth 150 ×150 Mesh, .0026" Wire Dia, 12" × 24" Sheet;

   McMaster-Carr Supply Company, Part number: 9319T52

5. Type 316 Stain Steel Sheet With #2B Finish .075" Thick, 12" × 24";

   McMaster-Carr Supply Company, Part number: 88885K25

6. 40 Machine screw nuts (Hex, 18-8 stainless-steel), 6-32 coarse;

Physics Shop, University of Maryland, College Park

Tubing and Fittings:

7. 1 Bulkhead Unions (Teflon PFA), Tubing O.D.: $\frac{3}{8}$";

   Cole-Parmer Instrument Company, Catalog No: A-06482-34

8. 2 White Teflon Flat Washer, $\frac{1}{2}$" screw size, 0.500" ID, 1.003" OD, 0.057" thick;

   MacMaster-Carr Supply Company, Part number: 95630 A248

9. Teflon PTFE tubing, I.D.: $\frac{19}{64}$", O.D.: $\frac{3}{8}$";

   Cole-Parmer Instrument Company, Catalog No: A-06407-46

10. 1 Union Reducing, $\frac{3}{8}"\times\frac{1}{4}"$;

    Cole-Parmer Instrument Company, Catalog No: A-06373-72

11. Teflon PTFE tubing, I.D.: $\frac{3}{16}$", O.D.: $\frac{1}{4}$";

    Cole-Parmer Instrument Company, Catalog No: A-06407-44

Sampling port:

12. 1 Branch Tee, Teflon PFA, Male $\frac{1}{4}"\times\frac{1}{8}"$;

    Cole-Parmer Instrument Company, Catalog No: A-06374-52

13. 1 Mininert Valve $\frac{1}{8}$" Female NPT to Mininert Septum,

    Alltech Associate, Inc., Part Number: 631204

14. Pump, Mflex, L/S, PTFE-Tubing, 115 V,

    Cole-Parmer Instrument Company, Catalog No: A-77912-00

15. 3 Valves (PTFE teflon), Tubing O.D.: $\frac{1}{4}$";

    Cole-Parmer Instrument Company, Catalog No: A-06373-55

16. 3 Bulkhead Unions (Teflon PFA), Tubing O.D.: $\frac{1}{8}$";

    Cole-Parmer Instrument Company, Catalog No: A-06357-32

17. 2 White Teflon Flat Washer, $\frac{3}{8}$" screw size, 0.406" ID, 1.00" OD, 0.057" thick;

    MacMaster-Carr Supply Company, Part number: 95630 A248

18. 1 Union crosses (Teflon PTFE), Tubing O.D.: $\frac{1}{4}$";

    Cole-Parmer Instrument Company, Catalog No: A-06399-11

19. 3 Male pipe adapter, Teflon PFA, $\frac{1}{4}$"×$\frac{1}{4}$";

    Cole-Parmer Instrument Company, Catalog No: A-06374-03

20. Headtank material: Extruded acrylic sheet 12" x 24", 0.230" thick,

    McMaster-Carr Supply Company, Part number: 8589K82

21. Silicone caulking

    Aquarium Sealant 100% Silicone, Home Depot, College Park, Maryland, U.S.A

Sampling Parts:

22. Laboratory Pipetting Needles, Stainless steel hub with 304 stainless steel tubing, 20 Gauge, O.D.: 0.035", I.D.: 0.023", 4" long;

    Popper and Sons, Cat. No. for VWR: 20068-696

23. Mininert syringe valves, push-button operations; To fit any standard luer tip syringes;

    Alltech Associate, Inc., Part No.: 6540

Appendix 2 FORTRAN Program "trafit3d"

```
      PROGRAM trafit3d


      USE numerical_libraries

    THIS IS A FORTRAN PROGRAM THAT CALCULATES THE SUM OF THE SQUARES
OF EITHER THE ABSOLUTE OR RELATIVE RESIDUALS BETWEEN THE
NORMALIZED EXPERIMENTAL CONSERVATIVE TRACER DATA AND THE
NORMALIZED FLUX- AVERAGED CONCENTRATION CALCULATED USING THE
CONTINUOUS POINT SOURCE MODEL AT STEADY STATE AS DESCRIBED BY
ROBBINS (1989) AND THE BEST FIT HYDRODYNAMIC DISPERSION COEFFICIENT,
DH, AND AVERAGE PORE WATER VELOCITY, V (WHICH IS USED TO CALCULATE
THE BEST FIT PORO-SITY).  THE BEST FIT PARAMETERS ARE OBTAINED USING A
MODIFIED LEVENBERG-MARQUARDT METHOD TO MINIMIZE THE SUMS OF THE
SQUARES OF THE RESIDUALS BETWEEN OBSERVED AND CALCULATED
CONCENTRATIONS.  THE EXPER- IMENTAL DATA ARE FROM A SAND FLOW TANK
WITH A SQUARE CROSS-SECT.
     THE MAIN PROGRAM CALLS FIVE SUBROUTINES:
     INPUT:  READS INPUT FROM A DATA FILE CALLED INDAT1D.
     DUNLSF: AN IMSL SUBROUTINE THAT SOLVES A NONLINEAR LEAST SQUARES
PROBLEM USING A MODIFIED LEVENBERG-MARQUARDT ALGORITHM AND A
FINITE-DIFFERENCE JACOBIAN.
     FCN: CALCULATES EITHER THE ABSOLUTE OR RELATIVE RESIDUAL VECTOR.
     EXER:   CALCULATES EXP(A) ERFC(B)
     VARIABLES:
     AREA - COLUMN CROSS SECTIONAL AREA (CM^2).
     BSTPOR - BEST FIT FOR POROSITY; CALCULATED FROM VELOCITY BEST FIT.
     CEX(I) - NORMALIZED EXPERIMENTAL EFFLUENT CONCENTRATION AT EACH
SAMPLING TIME.
     CMOD(I) - CALCULATED NORMALIZED FLUX-AVERAGED EFFLUENT
CONCENTRATION AT EACH SAMPLING TIME, USING OPTIMUM FIT PARAMETER
VALUES.
     DATPTS - NUMBER OF EXPERIMENTAL OBSERVATIONS.
     VD(I) - ESTIMATED VALUES FOR AVERAGE PORE WATER VELOCITY AND
HYDRODYNAMIC DISPERSION COEFFICIENT, RESPECTIVELY.
     FJAC(I,J) - FINITE DIFFERENCE APPROXIMATE JACOBIAN AT SOLUTION.
     FLOW - EXPERIMENTALLY DETERMINED BULK FLOW RATE (ML/HR).
     FSCALE(I) - DIAGONAL SCALING MATRIX FOR FUNCTION.
     LENGTH - LENGTH OF COLUMN (CM);(DISTANCE BETWEEN SAMPLING PORTS).
     N - NUMBER OF PARAMETERS TO BE ESTIMATED.
     PGUESS(I) - INITIAL GUESS FOR AVERAGE PORE WATER VELOCITY (CM/HR)
AND HYDRODYNAMIC DISPERSION COEFFICIENT (CM^2/HR) , RESPECTIVELY.
     PSCALE(I) - DIAGONAL SCALING MATRIX FOR VARIABLES.
     RESID(I) - ABSOLUTE OR RELATIVE RESIDUALS.
     RPARAM(I) - PARAMETER VECTOR FOR OPTIMIZATION SUBROUTINE.
     SUMSQ - SUM OF SQUARES OF ABSOLUTE OR RELATIVE RESIDUALS.
     TIME(I) - TEST SAMLING TIMES (HR).
     DECLARATION OF VARIABLES
```

```
      DOUBLE PRECISION TIME (70), CEX(70), CMOD(70), RESID(70), VD(2),
     *RPARAM (7), FJAC(70,2), PSCALE(2), PGUESS(2), FSCALE(70)
      DOUBLE PRECISION EXER, SUMSQ, LENGTH, FLOW, AREA, BSTPOR, STDDEV
      INTEGER SSE, DATPTS, I, LDFJAC, IPARAM(6), N
      COMMON/OBS/LENGTH, TIME, CEX, CMOD, SSE
      EXTERNAL FCN, INPUT
C OPEN FILES
      OPEN (5, FILE='INDAT1D', STATUS='OLD')
      OPEN (6, FILE='BSTFIT1D', STATUS='UNKNOWN')
C READ INPUT VARIABLES
      CALL INPUT (LENGTH, FLOW, AREA, PGUESS, SSE, DATPTS, TIME, CEX)
C INITIALIZE OPTIMIZATION SUBROUTINE ARGUMENTS
      N=2
      DO 90 I=1,N
        PSCALE(I)=1.0
   90 CONTINUE
      DO 100 I=1,70
        FSCALE(I)=1.0
  100 CONTINUE
      IPARAM(1)=0
      LDFJAC=70
C CALL THE OPTIMIZATION SUBROUTINE TO SOLVE FOR THE BEST-FIT
PARAMETERS
      CALL DUNLSF(FCN, DATPTS, N, PGUESS, PSCALE, FSCALE, IPARAM,
     *RPARAM, VD, RESID, FJAC, LDFJAC)
C CALCULATE THE SUM OF THE SQUARES OF THE RESIDUALS
      SUMSQ=0.0D0
      DO 120 I=1,DATPTS
        SUMSQ=SUMSQ+RESID(I)**2
  120 CONTINUE
C CALCULATE THE STANDARD DEVIATION OF THE ABSOLUTE OR RELATIVE
RESIDUALS
      STDDEV=DSQRT(SUMSQ/DFLOAT(DATPTS-2))
C CALCULATE THE BEST FIT POROSITY FROM THE BEST FIT AVG. PORE
WATER VELOCITY, FLOW, AND CROSS-SECTIONAL AREA
      BSTPOR=FLOW/(AREA*VD(1))
C WRITE RESULTS TO OUTPUT FILE
      WRITE (6, 130)
  130 FORMAT (8X, 'THE BEST-FIT PARAMETERS ARE:')
      WRITE (6, 140) VD(1), BSTPOR, VD(2)
  140 FORMAT (10X, 'VELOCITY =', X, F6.3, 4X, 'POROSITY =', X, E12.3, 4X
     *, 'DH =', X, F6.3,/)
      IF(SSE.EQ.1) THEN
      WRITE (6, 150)
  150 FORMAT (10X, 'TIME', 8X, 'C/C''(exp)', 4X, 'C/C''(model)',
     *4X, 'ABS RESIDUAL', /)
        ELSE
      WRITE (6, 160)
  160 FORMAT (10X, 'TIME', 8X, 'C/C''(exp)', 4X, 'C/C''(model)',
     *4X, 'REL RESIDUAL', /)
      ENDIF
```

```
          DO 200 I=1, DATPTS
            WRITE (6, 190) TIME(I), CEX(I), CMOD(I), RESID(I)
       190    FORMAT (8X, F6.2, 8X, F6.4, 9X, F6.4, 8X, E10.4)
       200 CONTINUE
          WRITE (6,*)
          WRITE (6, 210) SUMSQ
       210 FORMAT (18X, 'THE SUM-OF-SQUARED RESIDUALS IS: ', G10.4)
          WRITE (6, 220) STDDEV
       220 FORMAT (7X, 'THE STANDARD DEVIATION OF THE RESIDUALS IS: ', G10.4)
          STOP
          END
          SUBROUTINE INPUT (LENGTH, FLOW, AREA, PGUESS, SSE, DATPTS, TIME,
CEX)
     C THIS SUBROUTINE READS INPUT FROM A DATA FILE CALLED INDAT1D
     C IF SSE=1, THE ABSOLUTE LEAST SQUARES (ALS) CRITERION IS USED;
     C IF SSE=2, THE RELATIVE LEAST SQUARES (RLS) CRITERION IS USED.
          DOUBLE PRECISION TIME(70), CEX(70), PGUESS(2)
          DOUBLE PRECISION LENGTH, FLOW, AREA
          INTEGER SSE, DATPTS, I
          READ (5,*) LENGTH, FLOW, AREA, PGUESS(1), PGUESS(2)
          write (6, *) length, flow, area, pguess(1), pguess(2)
        2 FORMAT(F6.3)
          READ (5,*) SSE, DATPTS
          write (6, *) sse, datpts
        4 FORMAT(I2)
          DO 10 I=1, DATPTS
            READ (5,6) TIME(I), CEX(I)
            write(6,*) time(i), cex(i)
        6 FORMAT(F7.4, X, F6.4)
       10 CONTINUE
          RETURN
          END
     SUBROUTINE FCN(DATPTS, N, VD, RESID)
     C THIS SUBROUTINE COMPUTES THE ANALYTICAL SOLUTION TO THE NON-
REACTIVE SOLUTE TRANSPORT EQUATION AT STEADY STATE (ROBBINS 1989).
THE POSITION (X), TIME (T), PORE WATER VELOCITY (VD(1)), AND THE
DISPERSION COEFFICIENT (VD(2)) ARE INPUTS. THE OUTPUT IS THE
NORMALIZED(OVER STEADY STATE) FLUX-AVERAGED CONCENTRATION (C/C')
AT THE GIVEN POSITION AND TIME. THIS
REQUIRES AN EXTERNAL FUNCTION EXER(A,B), WHICH COMPUTES THE VALUE
OF EXP(A)*ERFC(B). THE SUBROUTINE USES THESE VALUES TO THEN CALCULATE
EITHER THE ABSOLUTE OR RELATIVE RESIDUAL VECTOR.
     C DECLARE VARIABLES
          DOUBLE PRECISION TIME(70), CEX(70), CMOD(70), VD(2), RESID(70),
         *LENGTH
          INTEGER DATPTS, N, SSE, I
          COMMON/OBS/LENGTH, TIME, CEX, CMOD, SSE
     C DECLARE LOCAL VARIABLES
          DOUBLE PRECISION A(70), EXER
     C COMPUTE THE VALUES OF THE LOCAL VARIABLES
          DO 300 I=1,DATPTS
```

```
          A(I)=(LENGTH-VD(1)*TIME(I))/(2.0D0*DSQRT(VD(2)*TIME(I)))
        300 CONTINUE
      C COMPUTE THE NORMALIZED(STEADY ST.) FLUX-AVERAGED
CONCENTRATION AT THIS REQUIRES AN EXTERNAL FUNCTION EXER(A,B) WHICH
COMPUTES THE VALUE OF EXP(A)*ERFC(B).
          DO 310 I=1,DATPTS
          CMOD(I)=0.5D0*EXER(0.0D0,A(I))
        310 CONTINUE
      C CALCULATE EITHER THE ABSOLUTE OR RELATIVE RESIDUALS VECTOR
          DO 320 I=1,DATPTS
            RESID(I)=CEX(I)-CMOD(I)
            IF(SSE.EQ.2) RESID(I)=RESID(I)/CEX(I)
        320 CONTINUE
          RETURN
          END
          DOUBLE PRECISION FUNCTION EXER(A,B)
      C THIS SUBROUTINE IS FROM VAN GENUCHTEN AND ALVES (1982)
      C PURPOSE: TO CALCULATE EXP(A)*ERFC(B)
      C DECLARE DUMMY VARIABLES
          DOUBLE PRECISION A, B
      C DECLARE LOCAL VARIABLES
          DOUBLE PRECISION C, X, T, Y
          EXER=0.0D0
          IF ((DABS(A).GT.170.).AND.B.LE.0.0) RETURN
          IF (B.NE.0.0) GOTO 100
          EXER=DEXP(A)
          RETURN
        100 C=A-B*B
          IF ((DABS(C).GT.170.).AND.(B.GT.0.0)) RETURN
          IF (C.LT.-170.) GOTO 130
          X=DABS(B)
          IF (X.GT.3.0) GOTO 110
          T=1.0D0/(1.0D0+0.3275911D0*X)
          Y=T*(0.2548296D0-T*(0.2844967D0-T*(1.421414D0-T*(1.453152D0-
         *1.061405D0*T))))
          GOTO 120
        110 Y=0.5641896D0/(X+0.5D0/(X+1.0D0/(X+1.5D0/(X+2.0D0/(X+2.5D0/(X+
          *1.0D0))))))
        120 EXER=Y*DEXP(C)
        130 IF (B.LT.0.0) EXER=2.0*DEXP(A)-EXER
          RETURN
          END
      ***************************************************************
```

Appendix 3: FORTRAN Program "nvolma"

```
      PROGRAM MAIN

* ----------------------------------------------------------------
*                  PROGRAM 'NVOLMA'
*
*     This program fits a curve to batch oxygen consumption data
*     using Monod or Andrews kinetics to describe the removal of a non-volatile
*     substrate.  The best values for the parameters Um, Ks, Ki, and
*     X0, are found using a least sum of squares estimator to
*     determine the best fit for a given set of experimental data.
*     The complex search routine of Box (Kuester, J.L. and Mize,
*     J.H., "Optimization Techniques with Fortran", McGraw-Hill,
*     pp 368-385, 1973.) is used to find the best fit.
*
*     You have the choice of having the program find the initial
*     cell concentration, X0 or having X0 stay at a fixed value
*     which you input and therefore only search for Um and Ks, Ki.
*     You also have the choice of fitting to the Monod or Andrews equation
*
*      This program is a modification of volma.for wich was written for
*     volatile components and any updates to volma.for must be included
*     in this program
*     Version 3.1
*     Last Edited 7 JULY 1994
*
* ----------------------------------------------------------------

      INTEGER I,J,II,SIGN,FINDX,INDX,tnpts,cma
      REAL T(500),AOU(500),MUMUB,MUMLB,KSUB,KSLB,X0UB,X0LB,S0,
     1     Y,YP,B,TN,PAOU(500),MUM,KS,X0,F(9),X(4,9),XN(4,9),
     2     XC(4),FMAX,FMIN,XUB(4),XLB(4),Ki, KiLB, KiUB
      COMMON /BLOCKA/ T,AOU,S0,Y,YP,B,TN,PAOU,IIMAX
      COMMON /BLOCKB/ X,F,XUB,XLB,NN
      COMMON /BLOCKC/ XN,XC
      COMMON /BLOCKD/ FINDX,cma
      CHARACTER W1*3,W2*2,W3*3,W4*2,W5*3,W6*3,W7*3,W8*4,W9*9,
     1          W10*9,W11*10,W12*1,W13*2,W14*3,W15*2,W16*5,
     2          W17*3,W18*2,W19*2,W20*2,W22*5, W23*5, W21*10
      CHARACTER*15 DATAIN, VOLPARAMSIN,RESULTSOUT
* ----------------------------------------------------------------
*                   INSTRUCTIONS
*
*     The batch oxygen consumption data will be read in from
*     a separate file, call "DATAIN". Parameter estimates,
*     limits, and fitting criteria are read in from a seperate
*     file called "VOLPARAMSIN".
*
```

```
*
* ---------------------------------------------------------------
      WRITE (6,*)'This program Copyright of ESE Department'
      WRITE (6,*)'Clemson University, 1994'
      WRITE (6,*)'ENTER THE NAME OF YOUR DATA INPUT FILE'
      READ (5,'(A15)') DATAIN
      WRITE (6,*) ' DATAIN= ',DATAIN
      WRITE (6,*)'ENTER THE NAME OF YOUR PARAMETER INPUT FILE'
      READ (5,'(A15)') VOLPARAMSIN
      WRITE (6,*) 'VOLPARAMSIN=', VOLPARAMSIN
      WRITE (6,*)'ENTER THE NAME OF YOUR RESULTS OUTPUT FILE'
      READ (5,'(A15)') RESULTSOUT
      WRITE (6,*)'RESULTSOUT=', RESULTSOUT


      OPEN (UNIT=7,FILE= DATAIN, STATUS='OLD')
      open (UNIT=10,FILE= VOLPARAMSIN, STATUS='OLD')
      OPEN (UNIT=8,FILE = RESULTSOUT, STATUS='UNKNOWN')



* ---------------------------------------------------------------
*             DEFINITIONS OF INPUT DATA FOR PARMS.IN
*
*      S0 = initial substrate conc. if all the substrate were in
*           the liquid phase.          MUMLB = Um lower boundary
*      Y  = bacterial cell yield       MUMUB = Um upper boundary
*      YP = product yield coefficient  KSLB  = Ks lower boundary
*      B  = decay coefficient          KSUB  = Ks upper boundary
*      KiLB= Ki lower boundary         X0LB  = X0 lower boundary
*      KiUB = Ki upper boundary        X0UB  = X0 upper boundary
*      ALFA = best fitting criterion   X0 = initial biomass conc
*      BETA = converge factor          KI = Andrews coeff
*      ITK  = maximum iteration times  KS = Monod coeff
*      SEED = for random No. generation, 0.0<SEED<1.0
*      FINDX = 1 if you want the program to find X0, 0 otherwise
*      CMA = 1 if you want the program to fit to Andrews eqn, 0 otherwise
* ---------------------------------------------------------------

      read (10,*) S0, X0,Y, YP, B, MUM, KS, Ki
      read (10,*) MUMLB, MUMUB, KSLB, KSUB, X0LB, X0UB,KiLB, KiUB
      read (10,*) ALFA, BETA, ITK, SEED
      read (10,*) FINDX, cma

* ---------------------------------------------------------------
*          ADDITIONAL INPUT DATA DUE TO VOLATILE COMPOUND
*
*      HS = Dimensionless Henry's Law Constant for Substrate
*     VL = Volume of Liquid, mL.
*     VG = Volume of Gas, mL.
*     aMW = Molecular weight of substrate.
```

```
*     CODr = mg COD/mg Mass for substrate.
*       TempC = Temperature of Experiment, Celcius.
* ---------------------------------------------------------------

*       read (10,*) HS, VL, VG, aMW, CODr, TempC

* ---------------------------------------------------------------
*  This section for input of experimental data.
* ---------------------------------------------------------------

      II=1
 203    READ(7,*,end=205) T(II),AOU(II)
        II=II+1
          GO TO 203

 205    IIMAX=II-1
     tnpts=iimax

       IF (FINDX .EQ. 0) THEN
         NN=3
       ELSE
         NN=4
       END IF

* ---------------------------------------------------------------
*       This part is for rearranging data
* ---------------------------------------------------------------

       X(1,1)=MUM
       X(2,1)=KS
       X(3,1)=Ki
       X(4,1)=X0
       XUB(1)=MUMUB
       XUB(2)=KSUB
       XUB(3)=KiUB
       XUB(4)=X0UB
       XLB(1)=MUMLB
       XLB(2)=KSLB
       XLB(3)=KiLB
       XLB(4)=X0LB
* ---------------------------------------------------------------
*       This part is for generating 8 new starting points
* ---------------------------------------------------------------

       RAND=SEED
       DO 30 J=2,9
         DO 20 I=1,NN
         CALL RANDOM(RAND)
         X(I,J)=XLB(I)+RAND*(XUB(I)-XLB(I))
20         CONTINUE
         IF (cma .EQ. 0) THEN
```

```
          X(4,J)=KI
        END IF
        IF (FINDX .EQ. 0) THEN
          X(4,J)=X0
        END IF
30     CONTINUE

* ---------------------------------------------------------------------
*       This part is for calculation the objective function
* ---------------------------------------------------------------------
       W17='RSS'
       W18='Um'
       W19='Ks'
       W20='X0'
       W22='Ki'
       WRITE(8,*) '         ** Starting Points **'
      WRITE(8,*) '-------------------------------------------------'
       WRITE(8,5) W17,W18,W19,W22,W20

       DO 40 J=1,9
         CALL RKT(X(1,J),X(2,J),X(3,J),X(4,J),F(J))

       WRITE(8,6) F(J),X(1,J),X(2,J),X(3,J),X(4,J)
40     CONTINUE
       WRITE(8,*) '         '

* ---------------------------------------------------------------------
*       This part is for executing of Box search routine
* ---------------------------------------------------------------------
       FMIN=1.0
      DELT=1.0
      SIGN=1
       ITR=0

  206  IF (SIGN .EQ. 0 .OR. FMIN .LT. ALFA .OR. DELT .LT. BETA
     1        .OR. ITR .EQ. ITK) GO TO 207
       FMAX=AMAX1(F(1),F(2),F(3),F(4),F(5),F(6),F(7),F(8),F(9))
       DO 50 J=1,9
         IF (F(J) .EQ. FMAX) THEN
           INDX=J
         END IF

50     CONTINUE

       IF (SIGN .EQ. 1) THEN
         CALL EXCBOX(INDX,Y1,Y2,Y3,Y4,YF,SIGN)
         X(1,INDX)=Y1
         X(2,INDX)=Y2
         X(3,INDX)=Y3
         X(4,INDX)=Y4
         F(INDX)=YF
```

```
        FMIN=AMIN1(F(1),F(2),F(3),F(4),F(5),F(6),F(7),F(8),F(9))
        FMAX=AMAX1(F(1),F(2),F(3),F(4),F(5),F(6),F(7),F(8),F(9))
      END IF

      DELT=FMAX-FMIN
      ITR=ITR+1
      GO TO 206
     CONTINUE

207   IF (FMIN .LT. ALFA) THEN
      WRITE (8,*) 'Curve fitting criterion alpha was met'
      END IF
      IF (DELT .LT. BETA) THEN
      WRITE (8,*) 'Curve fitting criterion beta was met'
      END IF
      IF (ITR .EQ. ITK) THEN
      WRITE (8,*) 'Did not converge within preset iteration steps'
      END IF
      IF(SIGN .EQ. 0) THEN
      WRITE (8,*) 'No further search is possible.'
      WRITE (8,*) 'Try a different start point or seed.'
      END IF
      WRITE(8,*) '    '

      DO 60 J=1,9
        IF (F(J) .EQ. FMIN) THEN
        INDX=J
        END IF
60    CONTINUE

* ---------------------------------------------------------------
*      This part for output of curve fitting results
* ---------------------------------------------------------------

      W1='S0='
      W2='Y='
      W3='Yp='
      W4='b='
      W5='Um='
      W6='Ks='
      W7='X0='
      W23='Ki='
      W8='RSS='
      W9='RSS<'
      W10='RSSmax - RSSmin='
      W11='Iteration='
      W12='T'
      W13='AOU'
      W14='PAOU'
      W15='to'
      W16='SEED='
```

```
W21='# of data points ='

 IF (FINDX .EQ. 0) THEN

   WRITE(8,*) 'Xo was given by the user.'
 else
  WRITE(8,*) 'This program searched for Xo.'
 END IF

 If(cma.eq.0) then
  write(8,*)'This program fit to the Monod Equation'
 else
  write(8,*)'This program fit to the Andrews Equation'
 endif

 WRITE(8,*) '-------------------------------------------'
 WRITE(8,*) '  KNOWN PARAMETERS AND INITIAL CONDITIONS'
 WRITE(8,*) '-------------------------------------------'
 WRITE(8,*) '         '

 WRITE(8,*) '           ** Known Parameters **'
WRITE(8,*) '-------------------------------------------------'
 IF (FINDX .EQ. 0) THEN
   WRITE(8,1) W1,S0,W2,Y,W3,YP,W4,B,W7,X0
 ELSE
   WRITE(8,1) W1,S0,W2,Y,W3,YP,W4,B
 END IF
 WRITE(8,4) W21,tnpts

 WRITE(8,*) '        '
 WRITE(8,*) '           ** Boundary Conditions **'
WRITE(8,*) '-------------------------------------------------'
 WRITE(8,2) W5,MUMLB,W15,MUMUB
 WRITE(8,2) W6,KSLB,W15,KSUB
 write(8,2) W23,KiLB,W15,KiUB
 IF (FINDX .EQ. 1) THEN
   WRITE(8,2) W7,X0LB,W15,X0UB
 END IF

 WRITE(8,*) '           ** Searching Criterions **'
WRITE(8,*) '-------------------------------------------------'
 WRITE(8,31) W9,ALFA
 WRITE(8,31) W10,BETA
 WRITE(8,32) W11,ITK
 WRITE(8,31) W16,SEED
 WRITE(8,*) '        '
 WRITE(8,*) '            ** Best Fit Results **'
WRITE(8,*) '-------------------------------------------------'
 WRITE(8,32) W11,ITR
 WRITE(8,31) W10,DELT
 IF (FINDX .EQ. 0) THEN
```

```
        WRITE(8,7) W8,F(INDX),W5,X(1,INDX),W6,X(2,INDX),W23,X(3,INDX)
      ELSE
        WRITE(8,7) W8,F(INDX),W5,X(1,INDX),W6,X(2,INDX),
     1            W23,X(3,INDX),W7,X(4,INDX)
      END IF
      WRITE(8,*) '       '

      BASE=0.0

c     Call the Runge Kutta a final time with the values of umax, Ks,
c     Xo, and Ki that yield the lowest residual SS

      CALL RKT(X(1,indx),X(2,indx),X(3,indx),X(4,indx),F(indx))

      WRITE(8,5) W12,W13,W14
      DO 70 I=1,IIMAX
       WRITE(8,8) T(I),AOU(I),PAOU(I)
70     CONTINUE


1     FORMAT (A5,E10.2,2X,A5,F7.4,2X,A5,F7.4,2X,A5,F7.4,2X,
     1        A5,F10.2)
2     FORMAT (2X,A5,F12.4,2X,A2,F12.2)
3     FORMAT (2X,A10,F7.4,2X,A2,2X,F7.4)
4     FORMAT (2X,A20,I7,2X,A2,2X,I7)
5     FORMAT (3X,A8,3X,A8,3X,A8,3X,A8)
6     FORMAT (E15.5,3F11.4)
7     FORMAT (A5,E15.5,2X,A5,F7.4,2X,A5,F12.4,2X,A5,F12.4)
8     FORMAT (4F11.4)
9     FORMAT (2X,A10,E15.5)
31    FORMAT (2X,A15,E16.2)
32    FORMAT (2X,A15,8X,I5)
c234567
      STOP
      END

* ---------------------------------------------------------------
*     Subroutine RKT calculating the 'rss' for every set of (Um,
*     Ks,Ki).  A 4th order universal Runge-Kutta was written to
*     generate theoretical curve
* ---------------------------------------------------------------
      SUBROUTINE RKT(MUM,KS,Ki,X0,RSS)
      REAL AOU(500),MUM,KS,Ki,T(500),S0,B,TN,X0,YP,PAOU(500),R,RSS,Y,
     1  coeff,sub1, sub2, sub3, sub4
      DOUBLE PRECISION CVR(5),VR(5),H(3,5),CF(3)
      INTEGER J,NE,N,IIMAX,cma,findx
      COMMON /BLOCKA/ T,AOU,S0,Y,YP,B,TN,PAOU,IIMAX
      COMMON /BLOCKD/ FINDX,cma

      N=3
      R=0.0
```

```
      PAOU(1)=0.0

        CVR(1)=S0
        CVR(3)=0.0
        CVR(2)=X0
       TT=T(1)

      DO 500 II=2,IIMAX
         DO 550 JJ=1,10
            VR(1)=CVR(1)
            VR(2)=CVR(2)
            VR(3)=CVR(3)
            TT=T(II)-T(II-1)
            TN=TT/10
         DO 400 NE=1,N
            H(NE,1)=0.0
400        CONTINUE

         DO 300 J=2,5

            CK=0.5*INT((J-1)/2)

              SUB1=MUM*(VR(1)+CK*H(1,J-1))*(VR(2)+CK*H(2,J-1))
              SUB2=KS+VR(1)+CK*H(1,J-1)
     1          + real(cma)*(VR(1)+CK*H(1,J-1))**2./(Ki)
              coeff=  real(cma)*(VR(1)+CK*H(1,J-1))**2./(Ki)
              SUB3=KS*B*(VR(2)+CK*H(2,J-1))
              SUB4=KS+VR(1)+CK*H(1,J-1)
c               write(6,*)'coeff=', coeff
c               write(6,*)'sub1=', sub1
c               write(6,*)'sub2=', sub2
c               write(6,*)'sub3=', sub3
              CF(1)=-SUB1/(Y*SUB2)
              CF(2)=(SUB1/SUB2)-(SUB3/SUB4)
              CF(3)=YP*SUB1/(Y*SUB2)
c               write (6,*) 'cf(1) =',cf(1)
c               write (6,*) 'cf(2) =',cf(2)
c               write (6,*) 'cf(3)=',cf(3)

            DO 200 NE=1,N
            H(NE,J)=TN*(CF(NE))
200           CONTINUE
300           CONTINUE

        DO 100 NE=1,N
        CVR(NE)=VR(NE)+(H(NE,2)+2.0*H(NE,3)+2.0*H(NE,4)+H(NE,5))/6
100       CONTINUE
        IF (CVR(1) .LT. 0.0) THEN
          CVR(1)=0.0
        END IF
```

```
550       CONTINUE

          PAOU(II)=(S0-CVR(1))-(CVR(2)-X0)-CVR(3)
c         write(8,*) PAOU(II)

          R=R+(PAOU(II)-AOU(II))**2

500     CONTINUE
        RSS=R

        RETURN
        END

* ----------------------------------------------------------------
*       Subroutine RANDOM for generating radom numbers.
* ----------------------------------------------------------------

        SUBROUTINE RANDOM(SEED)
        REAL A,B,C,SEED

        A=65536
        B=25173
        C=13849
        SEED=((A*SEED+B)/C)-INT((A*SEED+B)/C)
        RETURN
        END

* ----------------------------------------------------------------
*       Subroutine EXCBOX for execute Box search routine
* ----------------------------------------------------------------

        SUBROUTINE EXCBOX(INDX,Y1,Y2,Y3,Y4,YF,SIGN)
        INTEGER SIGN,findx,cma
        REAL XC(4),XCN,XN(4,9),X(4,9),F(9),FN(9),XUB(4),XLB(4)
        COMMON /BLOCKB/ X,F,XUB,XLB,NN
        COMMON /BLOCKC/ XN,XC
        COMMON /BLOCKD/ FINDX,cma
        FMAX=AMAX1(F(1),F(2),F(3),F(4),F(5),F(6),F(7),F(8),F(9))
        DO 1010 I=1,NN
          CALL CENTRD(I,INDX,XCN)
        XC(I)=XCN
1010    CONTINUE
        DO 1020 I=1,NN
        XN(I,INDX)=XC(I)+1.3*(XC(I)-X(I,INDX))
        IF (XN(I,INDX) .GT. XUB(I)) THEN
          XN(I,INDX)=XUB(I)
        END IF
        IF (XN(I,INDX) .LT. XLB(I)) THEN
        XN(I,INDX)=XLB(I)
        END IF
```

```
1020    CONTINUE
        IF (cma .EQ. 0) THEN
          XN(3,INDX)=X(3,INDX)
        end if
        IF (FINDX .EQ. 0) THEN
          XN(4,INDX)=X(4,INDX)
        END IF
        CALL RKT(XN(1,INDX),XN(2,INDX),XN(3,INDX),XN(4,INDX),FN(INDX))
        IF (FN(INDX) .GE. F(INDX)) THEN
        CALL GOLDEN(INDX,XN(1,INDX),XN(2,INDX),XN(3,INDX),XN(4,INDX),
     1            FN(INDX),SIGN)
        END IF
        Y1=XN(1,INDX)
        Y2=XN(2,INDX)
        Y3=XN(3,INDX)
        Y4=XN(4,INDX)
        YF=FN(INDX)

        RETURN
        END

* ----------------- ----------------------------------------------------
*       Soubroutine CENTRD for calculation of centroids of
*       remaining points.
* ---------------------------------------------------------------------

        SUBROUTINE CENTRD(I,INDX,XCN)
        INTEGER I,INDX
        REAL X(4,9),SIGMA,XCN,XN(4,9),XC(4),F(9),XUB(4),XLB(4)
        COMMON /BLOCKB/ X,F,XUB,XLB,NN
        COMMON /BLOCKC/XN,XC
        SIGMA=0.0
        DO 2010 J=1,9
        SIGMA=SIGMA+X(I,J)
2010    CONTINUE
        XCN=(SIGMA-X(I,INDX))/8
        RETURN
        END


* ---------------------------------------------------------------------
*       Subroutine GOLDEN for execute golden section search.
* ---------------------------------------------------------------------

        SUBROUTINE GOLDEN(INDX,Y1,Y2,Y3,Y4,YF,SIGN)
        REAL Y1,Y2,Y3,Y4,YF,X(4,9),F(9),XUB(4),XLB(4),P(4,4),PF(4)
        INTEGER SIGN,INDX
        COMMON /BLOCKB/ X,F,XUB,XLB,NN

        G=0.618
        IT=1
```

```
      P(1,1)=X(1,INDX)
      P(2,1)=X(2,INDX)
      P(3,1)=X(3,INDX)
      P(4,1)=X(4,INDX)
      PF(1)=F(INDX)
      P(1,4)=Y1
      P(2,4)=Y2
      P(3,4)=Y3
      P(4,4)=Y4
      PF(4)=YF

      DO 3010 I=1,4
        P(I,2)=P(I,1)+(1-G)*(P(I,4)-P(I,1))
        P(I,3)=P(I,1)+G*(P(I,4)-P(I,1))
3010   CONTINUE
      CALL RKT(P(1,2),P(2,2),P(3,2),P(4,2),PF(2))
      CALL RKT(P(1,3),P(2,3),P(3,3),P(4,3),PF(3))

      PFMIN=AMIN1(PF(1),PF(2),PF(3),PF(4))
      IF (PFMIN .LT. F(INDX)) THEN
        SIGN=1
        DO 3020 J=2,4
          IF (PF(J) .EQ. PFMIN) THEN
          JG=J
          END IF
3020    CONTINUE
        Y1=P(1,JG)
        Y2=P(2,JG)
        Y3=P(3,JG)
        Y4=P(4,JG)
        YP=PF(JG)
      ELSE
209      IF (PFMIN .LT. F(INDX) .OR. IT .EQ. 10) GO TO 208
         IT=IT+1
         IF (PFMIN .EQ. PF(1)) THEN
           DO 3030 I=1,4
             P(I,4)=P(I,2)
             P(I,2)=P(I,1)
             P(I,1)=P(I,2)-(1-G)*(P(I,4)-P(I,2))
             P(I,3)=P(I,1)+G*(P(I,4)-P(I,1))
3030          CONTINUE
           PF(4)=PF(2)
           PF(2)=PF(1)
           CALL RKT(P(1,1),P(2,1),P(3,1),P(4,1),PF(1))
           CALL RKT(P(1,3),P(2,3),P(3,3),P(4,3),PF(3))
         END IF

         IF (PFMIN .EQ. PF(2)) THEN
           DO 3040 I=1,4
             P(I,4)=P(I,3)
             P(I,3)=P(I,2)
```

```
            P(I,2)=P(I,1)+(1-G)*(P(I,4)-P(I,1))
3040          CONTINUE
            PF(4)=PF(3)
            PF(3)=PF(2)
            CALL RKT(P(1,2),P(2,2),P(3,2),P(4,2),PF(2))
          END IF

          IF (PFMIN .EQ. PF (3)) THEN
            DO 3050 I=1,4
              P(I,1)=P(I,2)
              P(I,2)=P(I,3)
              P(I,3)=P(I,1)+G*(P(I,4)-P(I,1))
3050          CONTINUE
            PF(1)=PF(2)
            PF(2)=PF(3)
            CALL RKT(P(1,3),P(2,3),P(3,3),P(4,3),PF(3))
          END IF

          IF (PFMIN .EQ. PF(4)) THEN
            DO 3060 I=1,4
              P(I,1)=P(I,3)
              P(I,3)=P(I,4)
              P(I,4)=P(I,3)+(1-G)*(P(I,3)-P(I,1))
              P(I,2)=P(I,4)-G*(P(I,4)-P(I,1))
3060          CONTINUE
            PF(1)=PF(3)
            PF(3)=PF(4)
            CALL RKT(P(1,2),P(2,2),P(3,2),P(4,2),PF(2))
            CALL RKT(P(1,4),P(2,4),P(3,4),P(4,4),PF(4))
          END IF
        GO TO 209
 208    CONTINUE

          IF (IT .EQ. 10 .AND. PFMIN .GE. F(INDX)) THEN
            SIGN=0
            Y1=X(1,INDX)
            Y2=X(2,INDX)
            Y3=X(3,INDX)
            Y4=X(4,INDX)
            YF=F(INDX)

          ELSE
            DO 3070 J=1,4
              IF (PF(J) .LT. F(INDX)) THEN
                JG=J
              END IF
3070          CONTINUE
            Y1=P(1,JG)
            Y2=P(2,JG)
            Y3=P(3,JG)
            Y4=P(4,JG)
```

```
        YF=PF(JG)
        SIGN=1
      END IF
END IF

RETURN
END
```

Bibliography

Alexander, M. (1994). *Biodegradation and Bioremediation*, Academic Press, San Diego.

Alexander, M. (1995). "How toxic are toxic chemicals in soil?" *Environmental Science & Technology*, 29, 2713-2716.

Anderson, M. P., and Woessner, W. W. (1992). *Applied Groundwater Modeling: Simulation of Flow and Advective Transport*, Academic Press, Boston, MA.

Angley, J. T., Brusseau, M. L., Miller, W. L., and Delfino, J. J. (1992). "Nonequilibrium sorption and aerobic biodegradation of dissolved alkylbenzenes during transport in aquifer material: column experiments and evaluation of a coupled-process model." *Environ. Sci. Technol.*, 26(7), 1404-1410.

APHA, AWWA, and WEF. (1995). *Standard Methods for the Examination of Water and Wastewater*, American Public Health Association, American Water Works Association, and Water Environment Federation, Washington, D.C.

Appert-Collin, J. C., Dridi-Dhaouadi, S., Simonnot, M. O., and Sardin, M. (1999). "Nonlinear sorption of naphthalene and phenanthrene during saturated transport in natural porous media." *Physics and Chemistry of the Earth Part (B)- Hydrology Oceans and Atmosphere*, 24(6), 543-548.

ASTM-D2434. (2000). *Standard Test Method for Permeability of Granular Soils (Constant Head)*, ASTM International.

Bae, W., and Rittmann, B. E. (1996). "A structured model of dual-limitation kinetics." *Biotechnology and Bioengineering*, 49, 683-689.

Barker, J. F., Patrick, G. C., and Major, D. (1987). "Natural attenuation of aromatic hydrocarbons in a shallow sand aquifer." *Ground Wat. Monitor. Rev.*, 7(1), 64-71.

Barkley, W. E., and Richardson, J. H. (1994). *Methods for General and Molecular Bacteriology*, American Society for Microbiology, Washington, D. C.

Bath, G. R., Hill, M. C., Illangasekare, T. H., and Rajaram, H. (2001). "Predictive modeling of flow and transport in a two-dimensional intermediate-scale, heterogeneous porous medium." *Water Resources Research*, 37(10), 2503-2512.

Baveye, P., and Valocchi, A. (1989). "An evaluation of mathematical-models of the transport of biologically reacting solutes in saturated soils and aquifers." *Water Resources Research*, 25(6), 1413-1421.

Beck, A. J., Wilson, S. C., Alcock, R. E., and Jones, K. C. (1995). "Kinetic constraints on the loss of organic chemicals from contaminated soils: Implications for soil-quality limits." *CRC Critical Reviews in Environmental Science and Technology*, 25, 1-43.

Behrens, H. "Water tracer chemistry: a factor determining performance and analytics of tracers." *5th Int. Symp. on Undergound Water Tracing*, Insitute of Geology and Mineral Exploration, Athens, Greece, 121-133.

Blake, G. R., and Hartge, K. H. (1986). *"Particle density." Methods of soil analysis, Part 1, Physical and mineralogical methods*, Am. Soc. of Agronomy, Madison, Wis.

Borden, R. C., and Bedient, P. B. (1986). "Transport of dissolved hydrocarbons influenced by oxygen-limited biodegradation. 1. Theoretical development." *Water Resour. Res.*, 22(13), 1973-1982.

Borden, R. C., Bedient, P. B., Lee, M. D., Ward, C. H., and Wilson, J. T. (1986). "Transport of dissolved hydrocarbons influenced by oxygen-limited biodegradation. 2. Field application." *Water Resour. Res.*, 22(13), 1983-1990.

Bosma, T. N. P., Middeldorp, P. J. M., Schraa, G., and Zehnder, A. J. B. (1997). "Mass transfer limitation of biotransformation: quantifying bioavailability." *Environmental Science & Technology*, 31, 248-252.

Bouwer, E., Durant, N., Wilson, L., Zhang, W., and Cummingham, A. (1994). "Degradation of xenobiotic compounds in situ: Capabilities and limits." *Microbiology Review*, 15, 307-317.

Brock, T. D. (1977). "The Poisoned Control in biogeochemical Investigations." Environmental Biogeochemistry and Geomicrobiology, Ann Arbor Science, Ann Arbor, MICH., 717-725.

Brockman, F. J., and Murray, C. J. (1997). *Microbiological heterogeneity in the terrestrial subsurface and approaches for its description*, Lewis Publishers, Boca Raton, FL.

Brown, M. J., and Burris, D. R. (1996). "Enhanced organic contaminant sorption on soil treated with cationic surfactants." *Ground Water*, 34(4), 734-744.

Brown, S. C., Grady Jr., C. P. L., and Tabak, H. H. (1990). "Biodegradation kinetics of substituted phenolics: Demonstration of a protocol based on electrolytic respirometry." *Water Research*, 24(7), 853-861.

Brusseau, M. L. (1991). "Application of a multi-process non-equilibrium sorption model to solute transport in a stratified porous-medium." *Water Resources Research*, 27(4), 585-595.

Brusseau, M. L. (1992). "Transport of rate-limited sorbing solutes in heterogeneous porous media." *Water Resources Research*, 28, 2485-2497.

Brusseau, M. L. (1994). "Transport of reactive contaminants in heterogeneous porous-media." *Review of Geophysics*, 32(3), 285-313.

Brusseau, M. L., Jessup, R. E., and Rao, P. S. C. (1991). "Non-equilibrium sorption of organic chemicals: Elucidation of rate-limiting processes." *Environmental Science & Technology*, 25, 134-142.

Brusseau, M. L., and Rao, P. S. C. (1989). "Sorption nonideality during organic contaminant transport in porous media." *CRC Critical Reviews in Environmental Control*, 19, 22-99.

Brusseau, M. L., and Rao, P. S. C. (1991). "Influence of sorbate structure on non-equilibrium sorption of organic-compounds." *Environmental Science & Technology*, 25(8), 1501-1506.

Brusseau, M. L., and Zachara, J. M. (1993). "Transport of CO32- in a physically and chemically heterogeneous porous-medium." *Environmental Science & Technology*, 27(9), 1937-1939.

Burris, D. R., and Antworth, C. (1992). "In situ modification of an aquifer material by a cationic surfactant to enhance retardation of organic contaminants." *Journal of Contaminant Hydrology*, 10, 325-337.

Calvillo, Y. M., and Alexander, M. (1996). "Mechanism of microbial utilization of biphenyl sorbed to polyacrylic beads." *Applied Microbial Biotechnology*, 45, 383-390.

Carrera, J. (1993). "An overview of uncertainties in modeling groundwater solute transport." *Journal of Contaminant Hydrology*, 13(1-4), 23-48.

Chang, H. T., and Rittmann, B. E. (1987). "Verification of the model of biofilm on activated carbon." *Environmental Science & Technology*, 21, 280-288.

Clement, T. P. (1998). "RT3D Tutorials for GMS users." *PNNL-11805*, Pacific Northwest National Laboratory Report.

Clement, T. P., Sun, Y., Hooker, B. S., and Petersen, J. N. (1998). "Modeling multi-species reactive transport in ground water." *Groundwater Monitoring and Remediation Journal*, 18(2), 79-92.

Dand, J. S., Harvey, D. M., Jabbagy, A., and Grady, C. P. L. J. (1989). "Evaluationof biodegradation kinetics with repirometric data." *Research of Journal of the Water Pollution Control Federation*, 61(11-12).

David, F., Sandra, P., Stafford, S. S., and Slavica, B. (1993). "Analysis of polynuclear aromatic hydrocarbons using pressure-pulsed splitless injection." *Application Note 228-224*, Hewlett Packard Company, Germany.

Davis, S. N. (1969). *Flow through porous materials*, Academic Press, New York.

Desai, J. D., and Banat, I. M. (1997). "Microbial production of surfactants and their commercial potential." *Microbiology and Molecular Biology Reviews*, 61(1), 47-64.

Domenico, P. A., and Schwartz, F. W. (1998). *Physical and Chemical Hydrogeology*, John Wiley & Sons, New York, NY.

Efroymson, R. A., and Alexander, M. (1991). "Biodegradation by an Arthrobacter species of hydrocarbons partitioned into an organic solvent." *Applied Environmental Microbiology*, 57, 1441-1447.

Eguchi, M., Kitagawa, M., Suzuki, Y., Nakamuara, M., Kawai, T., Okamura, K., Sasaki, S., and Miyake, Y. (2001). "A field evaluation of in situ biodegradation of trichloroethylene through methane injection." *Water Research*, 35(9), 2145-2152.

Falatko, D. M., and Novak, J. T. (1992). "Effects of biologically produced surfactants on the mobility and biodegradation of petroleum-hydrocarbons." *Water Environment Research*, 64(2), 163-169.

Famisan, G. B., and Brusseau, M. L. (2003). "Biodegradation during contaminant transport in porous media: 6. Impact of sorption on coupled degradation-transport behavior." *Environmental Toxicology and Chemistry*, 22(3), 510-517.

Fetter, C. W. (2001). *Applied Hydrogeology*, Prentice-Hall, Inc., Upper Saddle River, New Jersey.

Feuerstein, D. L., and Selleck, R. E. (1963). "Fluorescent tracers for dispersion measurements." *J. Sanit. Eng. Div., Proc. Am. Soc. Civ. Eng.*, 89(SA 4), 1-21.

Fritz, J. S., and Schenk, G. H. (1979). *Quantitative Analytical Chemistry*, Allyn and Bacon, Inc., Boston, MA.

Fry, V. A., and Istok, J. D. (1994). "Effects of Rate-limited Desorption on the Feasibility of in-situ Bioremediation." *Water Resources Research*, 30(8), 2413-2422.

Gelhar, L. W., Welty, C., and Rehfeldt, K. R. (1992). "A critical review of data on field-scale dispersion in aquifers." *Water Resources Research*, 28(7), 1955-1974.

Ghoshal, S., and Luthy, R. G. (1998). "Biodegradation Kinetics of Naphthalene in Nonaqueous Liquid-Water Mixed Batch Systems: Comparson of Model Predictions and Experimental Results." *Biotechnology and Bioengineering*, 57(3), 356-366.

Ghoshal, S., Ramaswami, A., and Luthy, R. G. (1996). "Biodegradation of naphthalene from coal tar and heptamethylnonane in mixed batch systems." *Environmental Science & Technology*, 30(4), 1282-1291.

Grady Jr., C. P. L., Smets, B. F., and Barbeau, D. S. (1996). "Variability in kinetic parameter estimates: A review of possible causes and a proposed terminology." *Water Research*, 30(3), 742-748.

Grblic-Galic, D. (1988). "Anaerobic Microbial Transformation of Aromatic Hydrocarbons and the Relevance to Regeneration of Contaminated Ground Waste Aquifers," Stanford University.

Gu, M. B., and Chang, S. T. (2001). "Soil biosensor for the detection of PAH toxicity using an immobilized recombinant bacterium and a biosurfactant." *BIOSENSORS & BIOELECTRONICS*, 16(9-12), 667-674.

Guerin, W. F., and Boyd, S. A. (1992). "Differential bioavailability of soil sorbed naphthalene to 2 bacterial species." *Applied Environmental Microbiology*, 58, 1142-1152.

Guerin, W. F., and Boyd, S. A. (1997). "Bioavailability of naphthalene associated with natural and synthetic sorbents." *Water Research*, 31(6), 1504-1512.

Haggerty, R., and Gorelick, S. M. (1994). "Design of multiple contaminant remediation: Sensitivity to rate-limited mass transfer." *Water Resources Research*, 30(2), 435-446.

Harayama, S. (1997). "Polycyclic aromatic hydrocarbon bioremediation design." *Current Opinion in Biotechnology*, 8, 268-273.

Harms, H., and Zehnder, A. J. B. (1995). "Bioavailability of sorbed 3-chlorodibenzofuran." *Applied Environmental Microbiology*, 61, 27-33.

Harvey, R. W., Smith, R. L., and George, L. (1984). "Effect of organic contaminant upon microbial distribution and heterotrophic uptake in a Cape Co. Mass. aquifer." *Applied Environmental Microbiology*, 48(5), 1197-1202.

Head, I. M. (1998). "Bioremediation: towards a credible technology." *Microbiology-UK*, 144(3-4), 599-608.

Hornberger, G. M., Mills, A. L., and Herman, J. S. (1992). "Bacterial transport in porous media: Evaluation of a model using laboratory observations." *Water Resources Research*, 28(3), 915-938.

Hughes, J. B., Beckles, D. M., Chandra, S. D., and Ward, C. H. (1997). "Utilization of bioremediation processes for the treatment of PAH-contaminated sediments." *Journal of Industrial Microbiology and Biotechnology*, 18, 152-160.

Johnson, C. R., and Scow, K. M. (1999). "Effect of nitrogen and phosphorus addition on phenanthrene biodegradation in four soils." *Biodegradation*, 10, 43-50.

Johnson, J. A. (2004). "A quantitative framework for understanding the compex interactions of competing interfacial processes and in situa biodegradation," Master of Science, University of Maryland, College Park.

Kent, D. B., Davis, J. A., Anderson, L. C. D., Rea, B. A., and Waite, T. D. (1994). "Transport of chromium and selenium in the suboxic zone of a shallow aquifer: Influence of redox and adsorption reactions." *Water Resources Research*, 30(4), 1099-1114.

Kibbey, T., and Hayes, K. F. (1993). "Partitioning and UV absorption studies of phenanthrene on cationic surfactant-coated silica." *Environmental Science & Technology*, 27, 2168-2173.

Kissel, J. C., McCarty, P. L., and Street, R. L. (1984). "Numerical-simulation of mixed-culture biofilm." *Journal of Environmental Engineering-ASCE*, 110(2), 399-411.

Klonis, N., and Sawyer, W. H. (1996). "Spectral properties of the prototropic forms of fluorescein in aqueous solution." *J. Fluoresc.*, 6(3), 147-157.

Klotz, D., Seiler, K. P., Moser, H., and Neumaier, F. (1980). "Dispersivity and velocity relationship from laboratory and field experiments." *Journal of Hydrology*, 45(3-4), 169-184.

Kono, T., and Asai, T. (1969). "Kinetics of continuous cultivation." *Biotechnology and Bioengineering*, 11, 19-36.

Kramer, W. H., and Hayes, T. J. (1987). "Water Soluble Phase of Gasoline: Results of a Laboratory Mixing Experiment." *New Jersey Geological Survey Technical Memorandum 87-5*, New Jersey Department of Environmental Protection, Trenton, NJ.

Kuester, J. L., and Mize, J. H. (1973). *Optimization Techniques with Fortran*, McGraw-Hill.

Lapidus, L., and Amundson, N. R. (1952). "The rate-determining steps in radial adsorption analysis." *Journal of Physical Chemistry*, 56(3), 373-383.

MacIntyre, W. G., Boggs, M., Antworth, C. P., and Stauffer, T. B. (1993). "Degradation kinetics of aromatic organic solutes introduced into a heterogeneous aquifer." *Water Resour. Res.*, 29(12), 4045-4051.

MacQuarrie, K. T. B., and Sudicky, E. A. (1990). "Simulation of biodegradable organic contaminants in groundwater. 2. Plume behavior in uniform and random flow fields." *Water Resour. Res.*, 26(2), 223-239.

Macrae, J. D., and Kenneth, J. H. (1998). "Biodegradation of polycyclic aromatic hydrocarbons (PAH) in marine sediment under denitrifying conditions." *Water Science Technology*, 38(11), 177-185.

Major, D. W., McMaster, M. L., Cox, E. E., Edwards, E. A., Dworatzek, S. M., Hendrickson, E. R., Starr, M. G., Payne, J. A., and Buonamici, L. W. (2002). "Field demonstration of successful bioaugmentation to achieve dechlorination of tetrachloroethene to ethene." *Environmental Science & Technology*, 36(23), 5106-5116.

Manilal, V. B., and Alexander, M. (1991). "Factors affecting the microbial degradation of phenanthrene in soil." *Applied Microbiology and Biotechnology*, 35, 401-405.

McCarty, P. L. (1987). "Bioengineering issues related to in-situ remediation of contaminated soils and groundwater." Environmental Biotechnology, G. S. Omenn, ed., Plenum Press, New York, 143-162.

McMahon, P. B., and Chapelle, F. H. (1991). "Microbial production of organic acids in aquitard sediments and its role in aquifer geochemistry." *Nature*, 349(6306), 233-235.

Metcalf & Eddy Inc. (1991). *Wastewater Engineering: Treatment, Disposal, and Reuse*, McGraw-Hill Inc., New York, NY.

Mihelcic, J. R., and Luthy, R. G. (1991). "Sorption and microbial degradation of naphthalene in soil-water suspensions under denitrification conditions." *Environmental Science & Technology*, 25(1), 169-177.

Miller, C. T. (1984). "Modeling of sorption and desorption phenomena for hydrophobic organic contaminants in saturated soil environments," The University of Michigan.

Miller, C. T., and Weber, W. J. (1988). "Modeling the sorption of hydrophobic contaminant by aquifer material 2. column reactor systems." *Water Research*, 22(465-474).

Miller, M. E., and Alexander, M. (1991). "Kinetics of bacterial degradation of benzylamine in a montomorilllonite suspension." *Environmental Science & Technology*, 24, 240-245.

Molz, F. J., and Widdowson, M. A. (1988). "Internal inconsistencies in dispersion-dominated models that incorporate chemical and microbial kinetics." *Water Resources Research*, 24, 615-619.

Mukherji, S., Peters, C. A., and Weber Jr., W. J. (1997). "Mass transfer of polynuclear aromatic hydrocarbons from complex DNAPL mixtures." *Environmental Science & Technology*, 31(2), 416-423.

Mulder, H., Breure, A. M., Andel, J. G. V., Grotenhuis, J. T. C., and Rulkens, W. H. (2000). "Effect of mass-transfer limitations on bioavailability of sorbed naphthalene in synthetic model soil matrices." *Environmental Toxicology and Chemistry*, 19(9), 2224-2234.

Mulder, H., Breure, A. M., and Rulkens, W. H. (2001). "Application of a mechanistic desorption-biodegradation model to describe the behavior of polycyclic aromatic hydrocarbons in peat soil aggregates." *Chemosphere*, 42, 285-299.

Murphy, E. M., Ginn, T. R., Chilakapati, A., Resch, C. T., Phillips, J. L., Wietsma, T. W., and Spadoni, C. M. (1997). "The influence of physical hetergeneity on microbial degradation and distribution in porous media." *Water Resources Research*, 33(5), 1087-1103.

National Research Council. (1993). *In situ Bioremediation: When Does it Work?*, National Academy Press, Washington, D.C.

Odencrantz, J. E. (1991). "Modeling the biodegradation kinetics of dissolved organic contaminants in a heterogeneous two-dimensional aquifer," University of Illinois at Urbana-Champaign.

Ogram, A. V., Jessup, R. E., Qu, L. T., and Rao, P. S. C. (1985). "Effects of sorption on biological degradation rates of (2,4-dichlorophenoxy) acetic acid in soils." *Applied and Environmental Microbiology*, 49(3), 582-587.

Oliviera, I. B., Demond, A. H., and Salehzadeh, A. (1996). "Packing of sands for the production of homogeneous porous media." *SOIL SCIENCE SOCIETY OF AMERICA JOURNAL*, 60(1), 49-53.

Oya, S., and Valocchi, A. J. (1998). "Transport and biodegradation of solutes in stratified aquifers under enhanced in situ bioremediation conditions." *Water Resources Research*, 34(12), 3323-3334.

Park, J. H., Zhao, X. D., and Voice, T. C. (2002). "Development of a kinetic basis for bioavailability of sorbed naphthalene in soil slurries." *Water Research*, 36(6), 1620-1628.

Pearce, A. E., Voudrias, E. A., and Whelan, M. P. (1994). "Dissolution of TCE and TCA pools in saturated subsurface systems." *Journal of Environmental Engineering*, 120(5), 1191-1206.

Peters, C. A., and Luthy, R. G. (1993). "Coal tar dissolution in water miscible solvents: Experimental evaluation." *Environmental Science & Technology*, 27(13), 2831-2843.

Peyton, B. M., Skeen, R. S., Hooker, B. S., Lundman, R. W., and Cunningham, A. B. (1995). "Evaluation of bacterial detachment rates in porous media." *Applied Biochemistry and Biotechnology*, 51, 785-797.

Phanikumar, M. S., and McGuire, J. T. (2004). "A 3D partial-equilibrium model to simulate coupled hydrogeological, microbiological, and geochemical processes in subsurface systems." *Geophysical Research Letters*, 31(11), Art. No. L11503.

Ramaswami, A., and Luthy, R. G. (1997). "Measuring and modeling physicochemical limitations to bioavailability and biodegradation." Manual of Environmental Microbiology, C. J. Hurst, G. R. Knudsen, M. J. McInerney, L. D. Stetzenbach, and M. V. Walter, eds., ASM Press, Washington DC, 721-729.

Rhykerd, R. L., Weaver, R. W., and McInnes, K. J. (1995). "Influence of salinity on bioremediation of oil in soil." *Environmental Pollution*, 90(1), 127-130.

Riis, V., Kleinsteuber, S., and Babel, W. (2003). "Influence of high salinities on the degradation of diesel fuel by bacterial consortia." *Canadian Journal of MIcrobilogy*, 49, 713-721.

Rijnaarts, H. M., Bachmann, A., Jumelet, J. C., and Zehnder, A. J. B. (1990). "Effect of desorption and intraparticle mass transfer on the aerobic biominerilization of hexachlorocyclohexane in a contaminated calcareous soil." *Environmental Science & Technology*, 24, 1349-1354.

Rittmann, B. E. (1993). "The significance of biofilms in porous media." *Water Resources Research*, 29(7), 2195-2202.

Rittmann, B. E., and McCarty, P. L. (1980). "Model of steady-state-biofilm kinetics." *Biotechnology and Bioengineering*, 22(22), 2343-2357.

Rittmann, B. E., Seagren, E. A., Wrenn, B. A., Valocchi, A. J., Ray, C., and Raskin, L. (1994). *In situ bioremediation*, Noyes Publishers, Park Ridge, NJ.

Rittmann, B. E., Valocchi, A. J., Seagren, E. A., Ray, C., and Wrenn, B. (1992). "A critical review of in situ bioremediation." *Gas Res. Inst., Top. Rep.*

Robbins, G. A. (1989). "Methods for determining transverse dispersion coefficients of porous media in laboratory column experiments." *Water Resources Research*, 25(6), 1249-1258.

Rockne, K. J., Chee-Sanford, J. C., Sandford, R. A., Hedlund, B. P., Staley, J. T., and Strand, S. E. (2000). "Anaerobic naphthalene degradation by microbial pure

cultures under nitrate-reducing conditions." *Applied and Environmental Microbiology*, 66(4), 1595-1601.

Rockne, K. J., and Strand, S. E. (1998). "Biodegradation of bicyclic and polycyclic aromatic hydrocarbons in anaerobic enrichments." *Environmental Science & Technology*, 32, 2962-2967.

Rockne, K. J., and Strand, S. E. (2001). "Anaerobic biodegradation of naphthalene, phenanthrene, and biphenyl by a denitrifying enrichment culture." *Water Research*, 35(1), 291-299.

Rumer, R. R., Jr. (1962). "Longitudinal dispersion in steady and unsteady flow." *J. Hydraulics Div., Proc. Amer. Soc. Civil Eng.*, 88, 147-172.

Salanitro, J. P., Johnson, P. C., Spinnler, G. E., Maner, P. M., Wisniewski, H. L., and Bruce, C. (2000). "Field scale demonstration of enhanced MTBE bioremediation through aquifer bioaugmentation and oxygenation." *Environmental Science & Technology*, 34(19), 4152-4162.

Schafer, W., and Kinzelbach, W. (1992). "Stochastic modeling of in situ bioremediation in heterogeneous aquifers." *Journal of Contaminant Hydrology*, 10(1), 47-73.

Scheibenbogen, K., Zytner, R. G., Lee, H., and Trevors, J. T. (1994). "Enhanced removal of selected hydrocarbons from soil by Pseudomonas aeruginosa UG2 biosurfactants and some chemical surfactants." *Journal of Chemical Technology and Biotechnology*, 59(1), 53-59.

Schicke, C. (1996). "Innovative evaluation methods for bioremediation: flow-cell construction and tracer analyses," Northwestern University, Evanston, IL.

Schirmer, M., and Barker, J. F. (1998). "A study of long-term MTBE attenuation in the Borden Aquifer, Ontario, Canada." *Ground Wat. Monitor. Remed.*, 18(2), 113-122.

Schirmer, M., Butler, B. J., Barker, J. F., Church, C. D., and Schirmer, K. (1999). "Evaluation of biodegradation and dispersion as natural attenuation processes of MTBE and benzene at the Borden field site." *Phys. Chem. Earth (B)*, 24(6), 557-560.

Schirmer, M., Molson, J. W., Frind, E. O., and Barker, J. F. (2000). "Biodegradation modeling of a dissolved gasoline plume applying independent laboratory and field parameters." *Journal of Contaminant Hydrology*, 46, 339-374.

Schwartz, F. W., and Zhang, H. (2002). *Foundamentals of Ground Water*, John Wiley & Sons, Inc., New York.

Seagren, E. A. (1994). "Quantitative evaluation of flushing and biodegradation for enhancing in situ dissolution of nonaqueous phase liquids," Ph.D. Dissertation, University of Illinois, Urbana-Champaign.

Seagren, E. A., and Moore, T. O. (2003). "Nonaqueous phase liquid pool dissolution as a function of average pore water velocity." *JOURNAL OF ENVIRONMENTAL ENGINEERING-ASCE*, 129(9), 786-799.

Seagren, E. A., Rittmann, B. E., and Valocchi, A. J. (1994). "Quantitative evaluation of the enhancement of NAPL-pool dissolution by flushing and biodegradation." *Environmental Science & Technology*, 28(5), 833-839.

Shan, C., and Stephens, D. B. (1994). "Recommendations for usage of SURFER to gridding model results." *Ground Water*, 32(3), 503-506.

Sheng, G. Y., X.R.Wang, Wu, S. N., and Boyd, S. A. (1998). "Enhanced sorption of organic contaminants by smectitic soils modified with a cationic surfactant." *Journal of Environmental Quality*, 27(4), 806-814.

Silliman, S. E., Zheng, L., and Conwell, P. (1998). "The use of laboratory experiments for the study of conservative solute transport in heterogeneous porous media." *Hydrogeology Journal*, 6, 166-177.

Sims, R. M., and Overcash, M. R. (1983). "Fate of polynuclear aromatic compounds (PNAs) in soil-plant systems." *Residue Review*, 88, 1-68.

Singleton, I. (1994). "Microbial metabolism of Xenobiotics: fundamental and applied research." *Journal Chemical Technology and Biotechnology*, 59(1), 9-23.

Smets, B. F., Chandran, K., and Riefler, R. G. (2001). "Estimation of biokinetics parameters. Section 3-3-2." Environmental Engineering Process Laboratory Manual, S. E. Powers, J. J. Biosgni, Jr., J. G. Burken, and K. Pagilla, eds.

Smith, S. A., and Pretorius, W. A. (2002). "The conservative behavior of fluorescein." *Water SA*, 28(4), 403-406.

Smith, S. C., Ainsworth, C., Traina, S. J., and Hicks, R. J. (1992). "Effect of sorption on the biodegradation of quinoline." *Soil Science Society of America Jounral*, 56, 737-746.

Speitel, G. E., and DiGiano, F. A. (1987). "The bioregeneration of GAC used to treat micropollutants." *Journal American Water Works Association*, 79, 64-73.

Sturman, P. J., Stewart, P. S., Cunningham, A. B., Bouwer, E. J., and Wolfram, J. H. (1995). "Engineering scale-up in situ bioremediation processes: a review." *Journal of Contaminant Hydrology*, 19, 171-203.

Sudicky, E. A., Gillham, R. W., and Frind, E. O. (1985). "Experimental investigation of solute transport in stratified porous media. 1. The nonreactive case." *Water Resources Research*, 21, 1035-1041.

Sun, Y., Pertersen, J. N., and Clement, T. P. (1999). "Analytical solutions for multiple species reactive transport in multiple dimensions." *Journal of Contaminant Hydrology*, 35(4), 429-440.

Sutherland, J. B., RafII, F., Khan, A. A., and Cerniglia, C. E. (1995). "Mechanisms of polycylic aromatic hydrocarbon degradation." Microbial Transformation and Degradation of Toxic Organic Chemicals, Wiley-Liss, Inc., 269-306.

Sutton, P. A., and Barker, J. F. (1985). "Migration and attenuation of selected organics in a sandy aquifer-A natural gradient experiment." *Ground Water*, 23(10-16).

Szecsody, J. E., and Bales, R. C. (1989). "Sorption kinetics of low-molecular-weight hydrophobic organic compounds on surface-modified silica." *Journal of Contaminant Hydrology*, 4, 181-203.

Szecsody, J. E., Brockman, F. J., Wood, B. D., Steile, G. P., and Truex, M. J. (1994). "Transport and biodegradation of quinoline in horizontally stratified porous media." *Journal of Contaminant Hydrology*, 15, 277-304.

Taylor, S. W., and Jaffe, P. R. (1990). "Substrate and biomass transport in a porous medium." *Water Resources Research*, 26(2153-2159).

Tchobanoglous, G., and Burton, F. (1991). *Wastewater engineering: treatment, disposal, and reuse*, Metcalf & Eddy, Irwin/Mcgraw-Hill.

Thornton, S. F., Quigley, S., Spence, M. J., Banwart, S. A., Bottrell, S., and Lerner, D. N. (2001). "Processes controlling the distribution and natural attenuation of dissolved phenolic compounds in a deep sandstone aquifer." *Journal of Contaminant Hydrology*, 53(3-4), 233-267.

Trevor, J. T. (1996). "Sterilization and inhibition of microbial activity in soil." *Journal of Microbiological Methods*, 26, 53-59.

Volkering, F. (1996). "Bioavailability and biodegradation of polycyclic aromatic hydrocarbons," Ph.D thesis, Agricultural University of Wageningen, Wageningen, The Netherlands.

Volkering, F., Breure, A. M., and Van Andel, J. G. (1993). "Effect of microorganism on the bioavailability and biodegradation of crystalline naphthalene." *Applied Microbiology and Biotechnology*, 40, 535-545.

Voudrias, E. A., and Yeh, M. F. (1994). "Dissolution of a toluene pool under constant and variable hydraulic gradients with implications for aquifer remediation." *Ground Water*, 32(2), 305-311.

Wang, Y. L., Banziger, J., Dubin, P. L., Filippelli, B., and Nuraje, N. (2001). "Adsorptive partitioning of an organic compound onto polyelectrolyte-immobilized micelles on porous glass and sand." *Environmental Science & Technology*, 35, 2608-2611.

Weber, W., Jr, McGinley, P., and Katz, L. (1991). "Sorption phenomena in subsurface systems: concepts, models and effects on contaminant fate and transport." *Water Research*, 25, 499-528.

Weber, W. J., and Miller, C. T. (1988). "Modeling the sorption of hydrophobic contaminants by aquifer materials. 1. rates and equilibria." *Water Research*, 22(4), 457-464.

Weber, W. J., and Smith, E. H. (1987). "Simulation and design models for adsorption processes." *Environmental Science & Technology*, 21, 1040-1050.

Weiner, R. W., Seagren, E., Arnosti, C., and Quintero, E. (1999). "Bacterial survival in biofilms: Probes for exopolysaccharide and its hydrolysis and measurement of interphase mass fluxes." *Methods in Enzymology*, 310, 403-426.

Welty, J. R., Wicks, C. E., and Wilson, R. E. (1984). *Fundamentals of Momentum, Heat, and Mass Transfer*, John Wiley & Sons, Inc., New York, NY.

Whelan, M. P., Voudrias, E. A., and Pearce, A. (1994). "DNAPL pool dissolution in saturated porous media: Procedure development and preliminary results." *Journal of Contaminant Hydrology*, 15(3), 223-237.

Whitman, B. E., Lueking, D. R., and Mihelcic, J. R. (1998). "Naphthalene update by a Pseudomonas fluorescens isolate." *Canadian Journal of Microbiology*, 44, 1086-1093.

Willumsem, P. A., and Arvin, E. (1999). "Kinetics of degradation of surfactant-solubilized fluoranthene by a Sphingomonas paucimobilis." *Environmental Science & Technology*, 33, 2571-2578.

Wilson, L. P., D'Adamo, P. C., and Bouwer, E. J. (1997). "Bioremediation of BTEX, naphthalene, and phenanthrene in aquifer material using mixed oxygen/nitrate electron acceptor conditions." National Risk Management Research Laboratory, USEPA.

Wood, B. D., Dawson, C. N., Szecsody, J. E., and Streile, G. P. (1994). "Modeling contaminant transport and biodegradation in a layered porous media system." *Water Resources Research*, 30, 1833-1845.

Woozinski, R. S., and Johnson, M. V. (1968). "Yields of baterial cells from hydrocarbons." *Applied Environmental Microbiology*, 23, 1077-1081.

Yang, X., Erickson, L. E., and Fan, L. T. (1994). "Dispersive-convective characteristics in biorestoration of contaminated soil with a heterogeneous formation." *Journal of Hazardous Materials*, 38(163-185).

Zeng, Y. M. (2004). "Naphthalene Pathway Map." University of Minnesota. http://umbbd.ahc.umn.edu/naph/naph_map.html.

Zhang, X., Sullivan, E. R., and Young, L. Y. (2000). "Evidence for aromatic ring reduction in the biodegradation pathway of carboxylated naphthalene by a sulfate reducing consortium." *Biodegradation*, 11, 117-124.

Zhang, Y. M., and Miller, R. M. (1992). "Enhanced Octadecane Dispersion and Biodegradation by a Pesudomonas Rhamnolipid Surfactant (Biosurfactant)." *APPLIED AND ENVIRONMENTAL MICROBIOLOGY*, 58(10), 3276-3282.

Zheng, C. (1990). "MT3D. A modular three-dimensional transport model for simulation of advection, dispersion and chemical reactions of contaminants in groundwater systems." U.S.E.P.A. report.